CRANFIELD UNIVERSITY

ENNIO CAPRIA

ELECTROSTATIC MANIPULATION OF PIEZOELECTRIC FIBRES USING A SHARP PROBE ELECTRODE IN A DIELECTRIC LIQUID:

ANALYSIS OF THE ELECTROHYDRODYNAMIC PHENOMENA

SCHOOL OF APPLIED SCIENCES

PhD THESIS

CRANFIELD UNIVERSITY

SCHOOL OF APPLIED SCIENCES

PhD THESIS

Academic Year 2006-2007

E. CAPRIA

Electrostatic Manipulation of Piezoelectric Fibres Using a Sharp Probe Electrode in a Dielectric Liquid: Analysis of the Electrohydrodynamic Phenomena

Supervisor: S A Wilson

May 2007

Ai miei genitori
per il loro amore sincero ed incondizionato,
da sempre punto di riferimento,
di partenza e di arrivo.

A Marie-Pierre,
avec qui j'ai appris beaucoup,
et avec qui j'ai maintenant envie
de découvrir le monde.

> In the temple the man said, "I am going to tell you something that you will never forget." And then he said, "To every man is given the key to the gates of heaven. The same key opens the gates of hell."
>
> And so it is with science […] and we do not have any instruction as to which is which gate. Shall we throw away the key and never have a way to enter the gates of heaven? […] That is, of course, a very serious question, but I think that we cannot deny the value of the key to the gates of heaven

Feynman, R. (1999), *The meaning of it all*, ed. Penguin, London

Abstract

Micro-assembly techniques have been identified as a major technology ‘pillar’ that will underpin further advancements in integrated micro-and nano-systems. In practice, there is a generic requirement for component parts that are often fragile, or that have been prepared by mutually incompatible processes, to be brought together to make a complete working system. This thesis discusses an electrostatic positioning technique for micro-scale elements that could form the basis of an industrial process.

A highly non-uniform field generated between a needle-like upper electrode and a bottom flat electrode can be used to electrostatically capture, displace, and relocate elements into a predefined spatial configuration. The very intense field at the needle tip can facilitate the collection of the material at a precise point. However charge injection and local dielectric breakdown must also be considered as they can induce instability near the tip, and consequently interfere with any picking up action.

The principal physical phenomena and potential benefits are analysed and discussed, considering three different configurations to achieve the pick and place operation for a micro-fibre in the needle-plane configuration. The first two are operated on an isolated single fibre lying on a flat bottom electrode, applying respectively a DC or an AC voltage. The third case is that of a group of fibres, and it exploits a dielectrophoretic chain structuring effect to assist in the micro-manipulation technique. Experimentation has focussed on the importance of the charge transfer mechanisms, leading to a model which provides good agreement with the observed behaviour. Moreover, an analysis of the forces exerted on the fibres showed that they arise not only from a polarisation effect, but that there is also an electrophoretic contribution.

The viability of the proposed technique has been demonstrated using lead zirconate titanate (PZT rods and carbon fibres).

Acknowledgements

I could not start these pages without expressing a huge thank you to Liz for her friendship and her precious help in the writing up of this thesis.

Very special thanks to Dr. Steve Wilson for his invaluable help during these years of intense and hard work.

I would like to thank Professor Roger Whatmore, who gave me the possibility to work on this project accepting me in the group, and moreover, who gave me his support, his enthusiasm and a very friendly reception.

Special thanks to EPSRC and DSTL for their financial support under the Joint Grants Scheme and to Ceranova Corp. for providing the piezoelectric fibres.

Also, I would like to thank all the people I met in the Nanotechnology group who put every effort to assist me in my task, senior staff, technicians and all the colleagues. A particular thank for Chris Shaw and Rob Wright.
Many thanks also to Enza for her professionalism and her friendly smile.

Thanks go to Professors Atten P. and Zahn M. for their valuable advice.

Thanks also to Dr. Kazilas, for his important help in the first months of my work, to Dr. Nick Lawson and Dr. Martin Hyde for the support on the PIV and to Dr. Oswald for the support with FEM.

Thanks to colleagues Cristina Bertoni for our passionate discussions about any aspect of life and Alberto Venturi for the most fruitful discussions during the most important moment: the coffee break.

Thanks also to Florent and Michel, two very special friends.

Thank you very much also to all the special friends of the “Italians in Cranfield Association” (Itaca), for the nice time we spent together, for the advice and for the opportunity to learn from them.

Thank you very much to Vivian and Nadia.

Many thanks to Angela’s ice-creams: a fundamental source of life energy!

For those who still don’t know it, I am going to become one of the most famous guitar players in the UK, but not without my special friend Amar! Many thanks boss, for the unforgettable jam sessions.

Zia Enza, zio Nino, zia Maria and zio Donato are the special suppliers of the olive oil I used in my experiments. Many thanks to you.

List of contents

Chapter 3: THE ELECTROHYDRODYNAMICS OF RIGID BODIES: A REVIEW

Chapter 4: THE EXPERIMENTAL SETUP - DESCRIPTION OF THE PROCESS UNIT

Chapter 5: MATERIAL CHARACTERISATION AND PRELIMINARY INVESTIGATIONS

Chapter 6: CONDUCTION AND ELECTROHYDRODYNAMICS OF AN HOMOGENEOUS DIELECTRIC FLUID IN A NEEDLE-PLANE ELECTRODES CONFIGURATION

Chapter 7: ELECTROHYDRODYNAMICS OF A SINGLE MICRO-FIBRE EXPOSED TO A UNIFORM AND DIVERGENT ELECTRIC FIELD

Chapter 10: OVERALL DISCUSSION

List of figures

List of tables

Nomenclature

K_n	the Knudsen number
θ	angular acceleration
a	acceleration
A	adimensioned factor; area
a,b	minor and major axes of an ellipsoidal particle
β	Clausius-Mossotti factor
B	magnetic induction
χ	Polarisability
C_D	drag coefficient
c_i	integration constant
c_s	velocity of the sound in the fluid
d	distance between a particle and a zero-potential surface
D	displacement vector
D	diffusion coefficient for the ionic species
$d\gamma/dt$	shear rate
$\Delta l/l$	mechanical strain
D_n	normal component of the **D** vector
E	electric field
E_0	externally applied electric field
Ec	critical field
E_{gap}	electric field in the interparticle gap
E_m	measured lift-off electric field
E_{max}	electric field near the tip; breakdown electric field
E_{RMS}	root mean square value of the electric field
E_{th}	theoretical lift-off electric field; threshold electric field
ε'	real part of the complex permittivity of the material
ε''	imaginary part of the complex permittivity of the material
ε_s	value of ε at low frequency
ε_∞	value of ε at high frequency, after relaxation
ε_l	permittivity of the fluid
ε_p	permittivity of the particle
ε_r	relative permittivity
ε_{rp}	relative permittivity of the particle
ε_{rl}	relative permittivity of the liquid
$\tan\delta$	dielectric loss coefficient
Φ	electric potential
ϕ	particle diameter

$\mathbf{p_{eff}}\times\mathbf{E}$	orientational torque
f	frequency of the signal
$\mathbf{F_C}$	Coulomb force
$\mathbf{F_D}$	drag force
$\mathbf{F_{DEP}}$	dielectrophoretic force
$\mathbf{F_w}$	weight force considering the buoyancy
$\mathbf{F_{int}}$	interparticle force
$\mathbf{F_{adh}}$	adhesion force
$\mathbf{F_{up}}$	cohesion force between the element in a fibre group
$\mathbf{F_{down}}$	the sum of the weight of the elements below the surface and the adhesion in a fibre group
$\mathbf{f}$	force per unit volume
$\mathbf{f_e}$	electric forces on an infinitesimal volume
$\mathbf{f_s}$	force per unit area acting on S
$\kappa'\boldsymbol{\omega}$	viscous torque
η	dynamic viscosity
η_b	Bingham viscosity
h	distance between the electrodes
$\mathbf{H}$	magnetic intensity field
h_c	height of superposition between two cylindrical particles
h_{max}	maximum height
h_{inc}	inception height
$\mathbf{I}$	Current
$\mathbf{J}$	current density
$\mathbf{J}$-	flux of negative carriers
$\mathbf{J'}$	current density with respect to a non-inertial observer
$\mathbf{J}$+	flux of positive carriers
$\underline{K}$	coefficient of shape
K	complementary drag coefficient
k	mobility of charge carriers
k_-	mobilities of the negative carriers
k_+	mobilities of the positive carriers
k_H	hydrodynamic turbulent mobility
k_F	friction coefficient describing damping
k_S	“spring” coefficient or constant; describing the restoring force
K_R	Intrinsic mean curvature
L	elongated particle length
Λ	the characteristic length scale of the system
λ_c	spatial scale of variation of the charge concentration
λ_d	the free path of the molecules
L_{mol}	intermolecular length

L_{ion}	ions maximum travel distance
μ	magnetic permeability
N	number of dipoles each m^2
P	polarization
p	polar moment
$\mathbf{p_{eff}}$	polar moment induced on the particle itself by the electric field E
p	Pressure
θ	angle between the vectors **n** and **E**
Q	particle charge
Qs	particle suface charge
Q_{Fh}	theoretical charge acquired by induction by an horizontal cylindrical conducting particle
Q_{Fv}	theoretical charge acquired by induction by a vertical cylindrical conducting
Q_w	minimum value of the particle charge necessary for lift-off at E_m
Q_i	measured particle charge during its first lift-off
Q_d	measured particle charge during its downwards motion
Q_u	measured particle charge during its upwards motion
Q_{max}	saturation value for a mono-ionised field case
Q_{mF}	theoretical charge that the particle should assume for a field equals to E_m
q	volume density of free charge; distributed load
q_p	volume density of bounded charge, and
qs	surface charge
ρ_m	density
ρ_p	particle density
ρ_l	liquid density
R	Resistance
G	Conductance
r	particle radius
R	position vector in polar coordinates
r_0	tip radius
Re	Reynolds number
S	surface
S	distance between particles and electrode
sign(u_r)	function returning a number with module 1 and sign opposite to u_r
K_s	surface conductivity of the interface
σ	Conductivity
σ_p	particle conductivity
σ_l	particle conductivity
σ_{ij}	overall stress tensor
σ^M_{ij}	mechanical stress tensor

σ^{E}_{ij}	electrical stress tensor
T^{E}_{ij}	electrostatic part of the Maxwell stress tensor
t	Time
T	Temperature
t_0	transient time characteristic at which saturation occurs
t_i	incubation time
t_t	transit time
τ_y	yield stress
τ	generic time constant
$\mathbf{U}$	fluid speed
$\mathbf{u_{EHD}}$	EHD instability motion velocity
u_n	normal speed of the interface
$\mathbf{u_p}$	speed of the particle
$\mathbf{u_r}$	relative speed of the body respect to the fluid
V	generic volume
V	applied voltage
V_{th}	threshold voltage
W	electrostatic energy
ω	angular frequency
ω^*	conjugate value of the complex angular frequency
w_{fi}	work function
$\mathbf{z}$	vertical coordinate
z_c	value of the averaged asperity height
ν_p	volume fraction of the dispersed phase
ϕ_v^{max}	maximum volume fraction of the dispersed phase
φ	signal phase
p	Pauthenier coefficient; pyroelectric coeficient
Y_i	Young's modulus
G_i	torsion modulus
m	mass; Poisson's module = dy/dx =dz/dy
m_i	inertial mass
m_p	particle mass
M_{mol}	molar mass,
χ_z	shear module
I_i	axial moment of inertia, and in our specific case
D	diameter
S_i	static moment
$\Delta y(L)$	beam deflection

Mathematical operators, symbols and physical constants

e	elementary charge = 1.6×10^{-19} C
ε_0	permittivity of the free space = 8.8542×10^{-12} F/m
$\mathbf{g}$	gravity acceleration = 9.81 m/s^2
N_A	Avogadro's constant = 6.022×10^{23} M^{-1}
π	3.141592…
k_B	Boltzmann's constant = 1.3807×10^{-23} J/K
c	speed of light in vacuum = 2.99×10^{8} m/s
Ψ	Euler's constant = 0.577

cS	centistokes	it is the cgs physical unit for kinematic viscosity: 1cS=1mm²/s (kinematic viscosity is normally indicated with ν and it is defined as: $\nu = \eta/\rho_m$)

$\mathbf{i}$	unitary vectors in the cartesian coordinate system parallel to x axis
$\mathbf{j}$	unitary vectors in the cartesian coordinate system parallel to y axis
$\mathbf{k}$	unitary vectors in the cartesian coordinate system parallel to z axis
$\mathbf{e_\theta}$	unitary vectors in the polar coordinate system
$\mathbf{e_r}$	unitary vectors in the polar coordinate system
$\mathbf{n}$	unitary vector normal to the surface S
$\mathbf{t}$	unitary vector tangent to the surface S
∇	nabla operator $\nabla=(\partial/\partial x; \partial/\partial y; \partial/\partial z)$
∇^2	laplacian operator $\nabla^2 f=(\partial^2 f/\partial x^2+\partial^2 f/\partial y^2+\partial^2 f/\partial z^2)$
∇_s	$\nabla_\sigma = \nabla - \mathbf{n}(\mathbf{n}\nabla\cdot)$
δ_{ij}	Kronecher tensor
$\partial\imath$	tensorial expression of the operational ∇
$\times$	vectorial product
$\cdot$	scalar product
$\int_S dS$	surface integral
$\int_v dv$	volume integral
[f]i	generical function
$[f]_{ij}$	jump function
Δ	difference
j	imaginary number ($j^2 = -1$)
$\langle\ \rangle$	average

Abbreviations

EFS	electric field structuring
DC	direct current
AC	alternating current
PZT	lead zirconate titanate
POPD	poly-oxypropylene-diamine
BA	butyl-alcohol
IPA	iso-propyl-alcohol
TBATBP	tetrabutyl-ammonium-tetraphenylborate
PTFE	poly-tetra-fluoro-ethylene
MEMS	micro-electro-mechanical-system
PIV	particle-image-velocimetry
EHD	electro-hydro-dynamics
FEM	finite element modelling
FEA	finite element analysis
FDM	finite difference modelling
EP	electrophoresis
DEP	dielectrophoresis
MWS	Maxwell-Wagner-Sillar model
IDD	interpretation of the dielectric data
RAM	random access memory
MPB	morphotropic phase boundary
ER	electro-rheology
RMS	root mean square
ROT	electro-rotation
IAF	ideal alignment frequency
CMOS	complementary metal–oxide–semiconductor
CAD	computer assisted design
PWM	pulse-width modulation
DRIE	deep reactive-ion etching
GITL	gas insulated transmission lines
PUA	pick-up angle
PDE	partial differential equation

Chapter 1

INTRODUCTION

The present chapter shall give a description of the context of the thesis and the declaration of the objectives.

1.1 BACKGROUND AND CONTEXT OF THE RESEARCH

There is an increasing interest in sensors and actuators based on fine-scale arrays of individual elements. These devices are applied in different sectors. Lab on a chip for biological application (Cheung et al.,1999; Gray et al., 2004; Zeng et al., 2004), devices for pyroelectric imaging (Whatmore, 1986), and metamaterials (Smith et al., 2004) are just a few examples.

1D and 2D arrays are usually made by precision machining (dicing) of a bulk ceramic material (Guillon et al. 2002), which places restrictions on the sizes and geometry of the components that can be made. There are problems related to micro-cracking or ceramic grain pull-out, with a consequent unreliability of the electrical properties of individual array elements. Alternatively the piezoelectric ceramic can be injection moulded to take the required form (Bowen et al. 1993). The injection moulding of components is a more flexible technique, but the tooling costs are very high, limiting the commercial exploitation to devices with element diameter of around 100nm.
Rapid prototyping (e.g. exploiting modified ink jet printers) (Tay and Evans, 2003) techniques are being explored as alternatives for making composite structures. These techniques tend to be slow processes and usually the final material exhibits some loss of performance.

An alternative, approach that can be considered, is micro-positioning of the fibres. The fibres already produced with the desired size and shape, could be captured, displaced, and relocated following a predefined spatial configuration.

The suggested process opens the discussion about all micro-manipulation problems and the picking-up of small objects to achieve the required placement precision.

The mechanical way using remotely controlled micro-tweezers (Dechev et al., 2004), or other micro-mechanical manipulation technologies (Feddema et al., 2001; Li et al., 2004a; Malyan and Balachandran, (2001)), reach a serious limit when the dimensions of the objects decrease below a hundred micrometers, and so need more and more expensive technology. For this range of dimensions, a non-mechanical driving force should be considered. Electrostatic force seems to be an interesting alternative.

Electrostatic manipulation, it is now operated at nanoscale, e.g. exploiting the useful properties of the scanning probe microscopy (Rougeot et al., 2005; Terris et al., 1989), or, at bigger, scale in the electrokinetic positioning of particle and cells (Hunt and Westervelt, 2006; Pethig et al., 1992). Both techniques mainly use dielectrophoresis as driving force. Nevertheless, in principle, electrostatic picking up and positioning could be achieved using both electrophoresis and dielectrophoresis.

Long range interactions typical of the electrostatic field give evident advantages in collecting the particular object. For example, if a mechanical pick, instead of tweezers is positioned on the object to manipulate it, using an electrostatic field, it is enough to place the tweezers in the vicinity of the object and it will be attracted. Complementarily the precision in controlling the pickup place is directly related to the sharpness of the collection tip.

It is possible to say that two conditions are essential for carrying out an electrostatic manipulation:

a) To have an electromagnetic force strong enough to make the manipulation possible.
b) To have a spatial gradient of the electrostatic force, with a maximum localised in an area as small as possible. The more localised is the force, the higher is the power of selection of the technique.

A physical system which satisfies those two requirement particularly well is the tip-plane system. Considering the geometry of the electric field between a needle-like vertical upper electrode, and a plane, it is possible to create the desired force localisation. The precision and the selectivity of the micro-manipulation are directly related to the sharpness of the collection tip.

Unfortunately, a very sharp tip has the unwanted consequence of generating charge injection and local dielectric breakdown that considerably corrupts the stability in proximity to the tip and consequently the stability of any picking up action in DC. Moreover, if the body has a finite conductivity (as is always the case in practice), the pickup has a certain decay time, because the body discharges through the electrode.

1.1.1 THE ELECTRIC FIELD STRUCTURING TECHNIQUE USING THE TECHNIQUE OF THE UPPER MOVABLE ELECTRODE

S.A.Wilson et al. (2003) firstly observed the possibility to generate a structuring on piezoelectric fibre in a divergent electric field. They obtained a chain-like structuring of short rods PZT5A (2-3mm) in poly-oxypropylene-diamine (POPD), using the electric field generated between a needle-like top electrode and a plate bottom electrode.
The process was believed to have a commercial potential for the production of novel composites materials and it was patented (Wilson and Whatmore, 2001).
This new micromanipulation process, very general in nature, has a wide potential range of applications in terms of different materials and geometries. In conjunction with adhesive bonding, it could be used to produce a large variety of hybrid structures and MEMS devices. It is an inherently low-temperature process and there is, therefore, a possibility of using this method to address some of the complex issues surrounding the integration of micro-mechanical components with device electronics.

A schematic diagram in figure 1.1 presents a process description.
An electric field is applied across an array of needle-like top electrodes and a grounded bottom flat electrode. A bunch of piezoelectric fibres is supported by the bottom electrode. The whole system is immersed in a dielectric fluid.
Under suitable conditions of electric field topology and frequency, the fibres polarise themselves and exhibit a mutually attractive force. Due to this force, a columnar structure is generated between the needle-like top electrode and the bottom electrode permitting the structuring effect. Withdrawing the needle array through the holes of a template, it is possible to position the polarised rods to form a pre-determined spatial array.

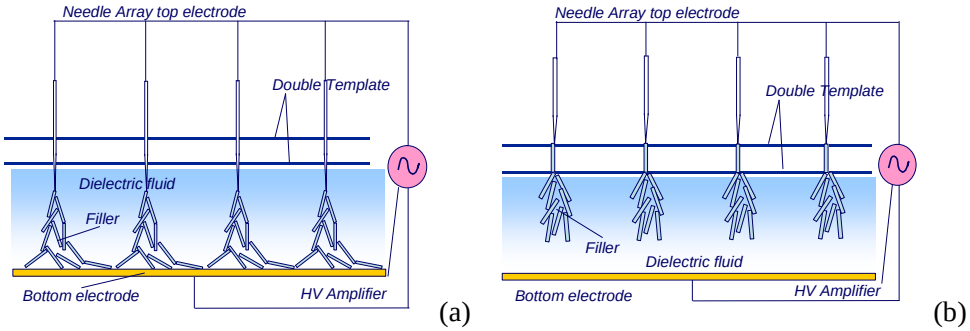

Figure 1. 1: Schematic of the novel technique. The needle drags a chain-like structure (a) The fibre is positioned exploiting the template (b)

On the achievement of the array based composites structure the template can subsequently be fixed in place to complete the composite structure (figure 1.2).

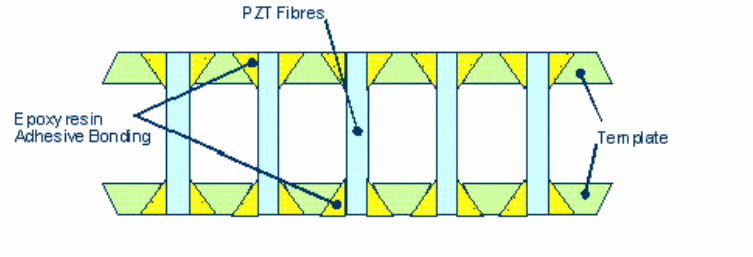

Figure 1. 2. Novel MEMS structure achievable by electric field structuring

For the first time the experiment was conducted with a needle-like top electrode and a plate bottom electrode. The studied materials were short rods PZT5A (2-3 mm) in poly-oxypropylene-diamine (POPD).

When an electric field of magnitude 1kV and frequency 3 kHz was applied, a concentration of the PZT rods into a small area was instantly observed. The needle electrode was withdrawn in a controlled manner (with a speed of 10 mm/min) and an individual polarisation of the rods occurred. The polarisation phenomenon generated a dielectrophoretic attraction between the nearest neighbours. As the gap between electrodes increased, then more rods were attracted to fill it and an extending, concentrated column of rods, was formed. All fibres were aligned in the field direction.

The pictures in fig.1.3 shows the evolution of the achieved process:

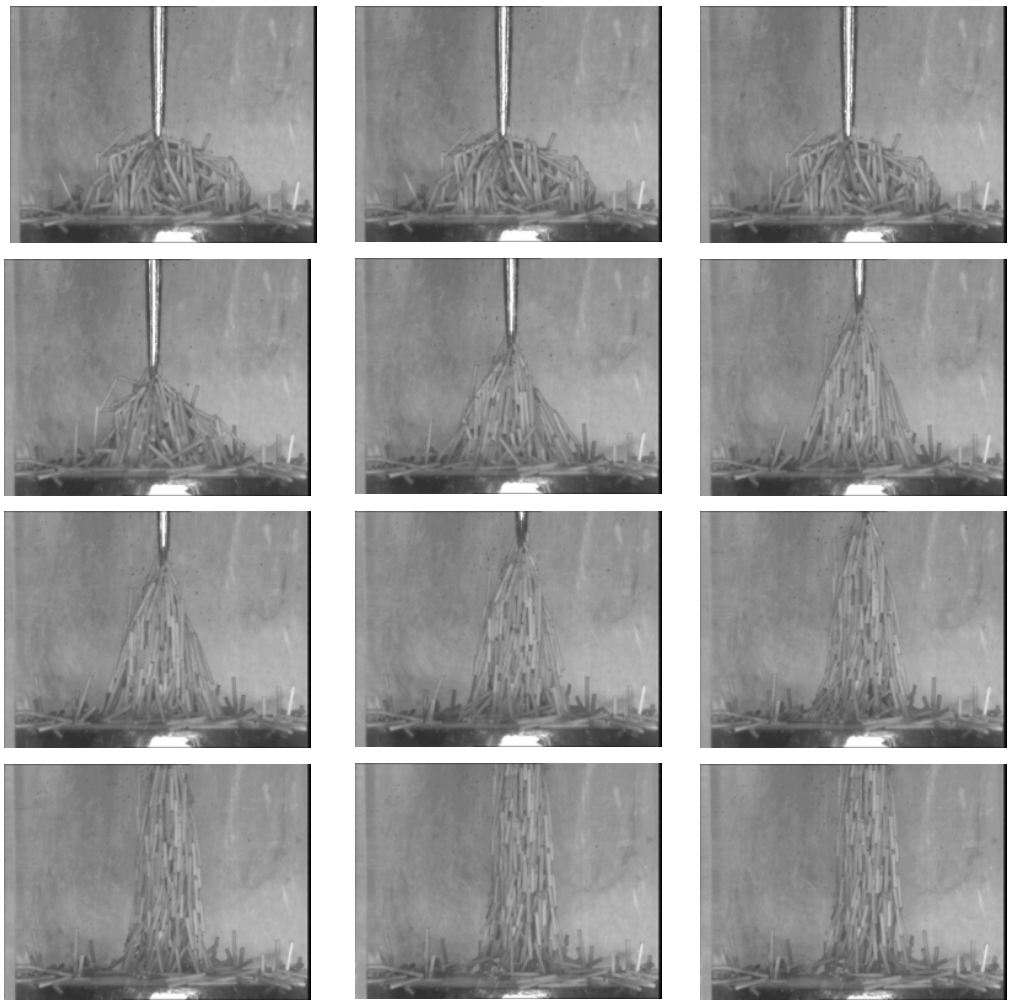

Figure 1. 3 Dielectrophoretic alignment of 130μm diameter PZT fibres in poly-oxypropylene-diamine (Wilson, 2003)

1.2 THESIS OBJECTIVES

The main aim of this study is to investigate the process of electrostatic micro-manipulation operated using a non-uniform electric field generated between a sharp probe electrode and a flat one.

The study shall evaluate the potential, the qualities and the critical points of the technique. The investigation shall supply a set of variables and experimental evidence

allowing the formulation of a procedure, and also permitting a practical exploitation of the process in the production of devices.
Considering the scientific and technological interest, and in agreement with Ceranova Corp., our industrial partner who supplied the material, we decided to focus our attention more on the structuring of piezoelectric fibres. Specifically, our main objectives would be to:

1) Investigate the main mechanisms and physical phenomena involved in the process of electrostatic capture of micro-rods
2) Show the viability of the electrostatic micro-manipulation in a particular case of PZT micro-rods
3) Establish a set of macroscopic indicators able to describe the characteristics of the process with particular attention to the practical industrial applications, providing the best experimental conditions to optimise the structuring process.

In relation to the understanding of the physical mechanisms involved in the electrostatic capture of micro-rods, one of the main difficulties to describe it is the very high number of critical factors:

- powder characteristic (density, shape, permittivity, conductivity)
- fluid characteristic (viscosity, permittivity, conductivity)
- electric field topology (electrodes materials, electrodes shape, electrode position)
- frequency
- alignment drag speed

A quick calculation shows it is possible to find at least 14 variables playing an active role in the phenomenon. Where possible, attempts were made to understand the role played by each factor in the dynamics of the process. However, the analysis is more oriented to achieve the optimum of performance, rather than making an extensive study of all the possible combinations of all these values.

To achieve the objectives declared above, a methodology has been followed. This can be summarised in a series of milestones, listed below:

1. Build up a remotely controlled process unit to operate the experiment of micro-manipulation safely, on which an optical access could allow a real time monitoring of the structuring process.
2. To measure the properties of the materials..To be able to understand the process model, and to derive a model, it was necessary to have a direct measure of the fibres properties. However, considering the dimension of the fibres, standard characterisations were not adequate. A particular measuring setup has been requested.
3. To analyse the effects of the divergent field in absence of any filler. The EHD instabilities have been characterised via PIV.
4. To analyse the behaviour of a single particle in DC. This activity was particularly interesting to understand the potential of the micromanipulation technique on a single, small body exposed to a DC field and, moreover, to characterise the charge exchanges between the fibres and the system.
5. To analyse the single particle behaviour in AC. In this case the micromanipulation behaviour has been characterised in terms of frequency, in a way to try to eliminate any EP contributions due to charge exchanges.
6. To analyse the behaviour of a group of particles. Once the dynamic was understood in the case of a single particle, it was interesting to extend the concepts to micromanipulation operated on a group of fibres.
7. To construct relevant FEM and analytical models.

Figure 1.4 shows a scheme of the logical path followed in this experimental study, and detailed in this chapter.

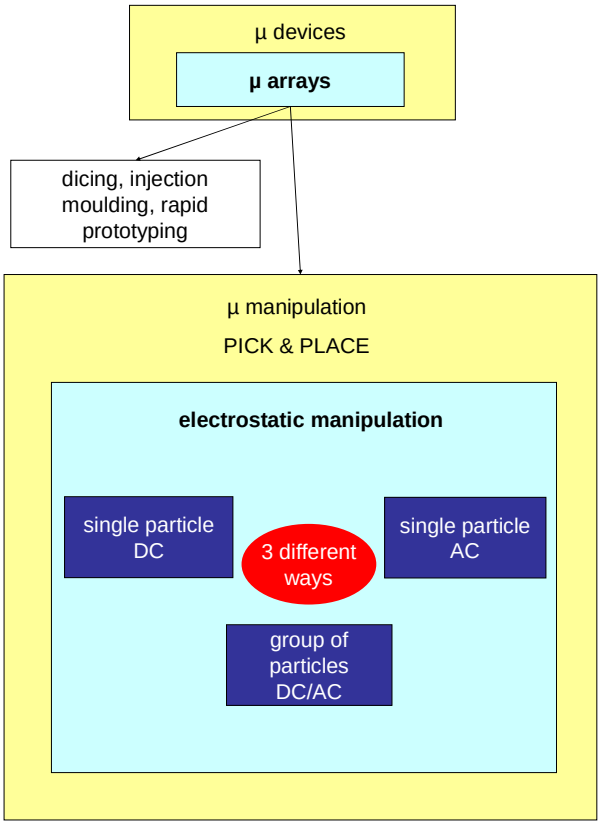

Figure 1. 4: Context and objective of the present research work

1.3 THESIS STRUCTURE

In this section a brief list containing a short summary of the main contents of each chapter is provided.

Chapter 1: In this chapter there is an initial description of the context of the thesis and the declaration of the objectives.

Chapter 2: This chapter is entirely dedicated to the expression of the physical models related to the Electrohydrodynamics. In this chapter the reader will be able to find a summary of all the theoretical background and the definitions that are necessary to understand the phenomena treated in the subsequent chapters. In certain cases, some

concepts have also been presented more broadly than necessary for the simple application to the present research project. This choice was made by the author so that a consistent level of insight would be provided across all the branches of theory presented, without reducing the theoretical introduction to purely a list of formulas disconnected from any physical context. The theoretical background in chapter 2 also gives the basic concepts necessary for understanding the solvers employed in the FEM simulations.

Chapter 3: This is another chapter part of the literature review. It contains all the principles relative to the behaviour of a particle, or a system of particles, in an electric field. The chapter reports a detailed description of the previous work with a critical organisation of the most important concepts.

Chapter 4: In this chapter the experimental setup is presented. A detailed description of the process unit, made specifically for the present research work, is reported.

Chapter 5: This chapter focuses on describing the materials utilised in this study. All the characteristics of the fluid and the particles have been reported. Where the characterisation of the material was presented, all the details related to such a characterisation have been provided.

Chapter 6: In this chapter the behaviour of the fluid exposed to a highly divergent electric field when no particles have been inserted into it is studied. Considering that in these conditions a fluid instability can be generated, an analysis via particle imagery velocimetry (PIV) has been proposed.

Chapter 7: This chapter reports the results related to the electrohydrodynamic behaviour of a single fibre exposed to an electric field. The behaviour of conducting and insulating PZT fibres in different configurations of electric field has been analysed. A discussion of the most important results has been provided at the end of the chapter.

Chapter 8: In this chapter is the description of the behaviour of different kinds of fibres exposed to both divergent and non-divergent, non-uniform electric fields in AC. Also in this case the discussion of the results is reported at the end of the same chapter.

Chapter 9: This chapter it is the longest, the most complex and the most important of the chapters of the experimental results. This chapter considers the behaviour of a group of fibres when exposed to a non-uniform electric field in both conditions of divergent and non-divergent. The dependence of the phenomenon on the characteristics of the electric field, and on the dielectric liquid, and the particles characteristics have been considered. Moreover an evaluation of the influence of the drag speed on the structuring process has been made. Once more, the discussion of the most important result has been proposed at the end of the chapter.

Chapter 10: This chapter offers an overview of the whole research work. An overall discussion and an overview of all the results are presented. All the main results which have emerged during the course of the thesis are here presented in a homogeneous manner. Moreover, this chapter includes a list of the main achievements and the conclusion, as well as a list of suggested further work and a critical view of the possible practical applications that the present research work can originate.

1.4 NOVELTY IN THE PRESENT EXPERIMENTAL WORK

Since Faraday's (1838) time , several researchers have tried to study and exploit the electromechanical effect applied on differently shaped small bodies, for many different applications (Tilmatine et al., 2004). Some of them also tried to use these forces in non-uniform configuration to operate a capture of tiny objects (Li et al., 2004b).
However nobody, before the author of this thesis, carried out an extensive study on the electrohydrodynamics of piezoelectric rods, in the range of dimensions presented here.

In the most typical configuration used in this work, the fibres are at rest on a bottom flat electrode and are immersed in an insulating oil. Then a capture of the fibres is attempted

by applying a divergent electric field between a movable upper needle and a bottom flat electrode. The use of a movable upper needle is a new configuration.

Before the present work, other researchers analysed the phenomena of charge transfer on a small body (Felici, 1966; Asano et al., 1997a; Choi et al., 2000;2001; Dascalescu, 1996; Yatsuzuka et al., 1995). However, the majority of the studies have been concentrated on the conducting particle, or, more occasionally on the insulating particle, but never on piezoelectric particles.

In summary, at present there is no other study that supplies such an extensive description of the phenomenon of electrostatic manipulation, and investigates such a high number of variables.

Chapter 2

EQUATIONS IN ELECTROHYDRODYNAMICS

This chapter is entirely dedicated to the expression of the physical models related to the Electrohydrodynamics. In this chapter the reader will be able to find a summary of all the theoretical background and the definitions that are necessary to understand the phenomena treated in the subsequent chapters. In certain cases, some concepts have also been presented more broadly than necessary for the simple application to the present research project. This choice was made by the author so that a consistent level of insight would be provided across all the branches of theory presented, without reducing the theoretical introduction to purely a list of formulas disconnected from any physical context. The theoretical background in chapter 2 also gives the basic concepts necessary for understanding the solvers employed in the FEM simulations.

2.1 INTRODUCTION TO THE ELECTROHYDRODYNAMIC MODEL

Electrohydrodynamics (EHD) is the discipline which studies the motion and the forces acting on a fluid when exposed to an electric field. When characteristic speeds are negligible compared to the speed of light and the scale of the phenomena are large enough to neglect any quantum effects, classical mechanics can be used to model a physical system. Additionally, in cases where each phase of the system can be modelled as a continuous medium (i.e. small Knudsen number, see section 2.1.1 for a definition), continuum mechanics can offer a set of solutions.

A set of equations to describe the forces applied to an elementary element of volume of the continuous medium is constituted by:

- conservation of mass (considered reliable, because no mass-energy transformations should occur)
- conservation of momentum
- conservation of charge
- Maxwell's equations
- universal gravity law

together with:

- the mechanical and electrical constitutive equations of the materials
- the mechanical and electrical boundary conditions

When two or more phases are present, it is recommended to write the equilibrium of the interfaces taking into account the effect due to surface tension.

Considering the present physical model, there are at least two notable solutions which received much attention due to their manifold applications:

1. the solution where the constitutive equations of the fluid are the ones of a Newtonian, incompressible, isothermal fluid
2. the solution where at least one phase of the system is represented by an un-deformable body, which can be assimilated to a rigid body

The solution of the first problem is given by the famous Navier-Stokes equation. This equation enables the calculation of the deformation rate of any infinitesimal element of the fluid. The solution can be written as a sum of different terms relating to:

- viscosity
- pressure
- gravity
- electric field (this term corresponds to the Maxwell's stress tensor in a dielectric)

The solution of the second case is obtained analysing the equilibrium of the un-deformable phase, using the mechanics of rigid bodies. In this case, the analysed body is considered to be "as a whole", and the problem is no more considered in terms of deformation rate, but is reduced to the equilibrium of the body forces. However, the solution of this problem does not differ much the Newtonian fluid solution:

- considering that the body is moving in a fluid, it is still necessary to calculate the viscous resistance using Navier-Stokes equation

- considering that the body is exposed to an electric field, it is necessary to solve the electrical boundary problem calculating the electrostatic body force using Maxwell's stress tensor

Nevertheless, if the body has a simple shape, some notable solutions exist for the viscous and electromechanical forces and the solution of the problem can be reduced to a simple equation of equilibrium.

It is important to say that when the number of bodies in the system increases and when the system becomes stochastic, the rigid body solution can become very computational-costly. In this case, it may be more advantageous to define some "equivalent constitutive equations" and to consider the system of many rigid bodies randomly disposed as a continuous phase. The smaller the dimension of the single solid phase in comparison with the characteristic dimensions of the system, the more accurate the approximation is.

An understanding of the electrohydrodynamic (EHD) mathematical model is crucial to explain all the phenomena observed in the present study, which can be seen as a particular case of the general solution. Moreover, the understanding of the EHD model is fundamental because it is the basis of the Finite Element Modelling solvers, widely employed in the present study.

2.1.1 THE HYPOTHESIS OF CONTINUUM

All materials discussed in this work are treated as continuous and isotropic. However, considering the length scale of the investigated particles, this hypothesis could be questioned. The Knudsen number, K_n, defines the deviation from the hypothesis of continuity (White,1991):

$$K_n = \lambda_d / \Lambda \qquad (2\text{-}1)$$

where λ_d and Λ are the free path of the molecules and the characteristic length scale respectively. For liquids, λ_d is approximately the intermolecular length L_{mol} (bond length) is defined as:

$$L_{mol} = (M_{mol} / \rho_m N_A)^{1/3} \quad (2\text{-}2)$$

where M_{mol} is the molar mass, ρ_m is the density, and N_A is Avogadro's constant (an adimensioned number equal to 6.022×10^{23}) .

For instance, for water λ_d= 0.31nm, and for a silicone oil (polydimethylsiloxane, PDMS) with a chain of 100 monomers, i.e. a M_{mol}= 7532 g, and a density 0.95g/cm^3, λ_d= 2.4 nm.
In PZT, λ_d could be identified with the length of the elementary lattice cell.

2.1.2 ABOUT THE NOTATION

All the formulae involving tensor quantities have been written using the Einstein compacted notation. However, to facilitate the reading, all formulae in which only vector or scalar quantities are involved, the vectorial notation has been preferred; each vector quantity is indicated in bold and the scalar quantity as normal text.

2.2 ELECTRICAL EQUATIONS

The electrical charge is a fundamental property of elementary particles constituting material bodies, and is responsible for any electromagnetic interaction. The elementary unit charge is the electron charge $e = 1.6\times10^{-19}$ C. Charges can be free or bounded if they can move distances either larger or of the same dimension as the molecules or the atoms constituting the body. This is translated through Gauss's law stating:

$$\varepsilon_0 \nabla\cdot\mathbf{E} = q + q_p \quad (2\text{-}3)$$

where ε_0=8.8542×10^{-12} F/m is the permittivity of the free space, q the volume density of free charge, q_p the volume density of bounded charge, and **E** the electric field.

Since for any body inside the volume v:

$$\int_v q_p dv = 0 \tag{2-4}$$

it is possible to define a vector **P**, called polarisation that, except when it equals zero outside the body, can be written as:

$$q_p = -\nabla \cdot \mathbf{P} \tag{2-5}$$

P is directly proportional to the electric field through χ, called polarisability:

$$\mathbf{P} = \chi \mathbf{E} \tag{2-6}$$

Defining the displacement vector **D** as:

$$\mathbf{D} = \varepsilon_0 \mathbf{E} + \mathbf{P} = \varepsilon \mathbf{E} \tag{2-7}$$

where $\varepsilon = \varepsilon_0 \varepsilon_r$, and $\varepsilon_r = 1 + \chi$ is called relative dielectric constant.

Gauss' law can be written as:

$$\nabla \cdot \mathbf{D} = q \tag{2-8}$$

The non existence of magnetic charge imposes that there is not scalar source of the magnetic field:

$$\nabla \cdot \mathbf{B} = 0 \tag{2-9}$$

where **B** is the magnetic induction.

Faraday's law states that a time dependent magnetic field generates an electric field through:

$$\nabla \times \mathbf{E} = -\partial \mathbf{B} / \partial t \tag{2-10}$$

where *t* is the time.

Finally, the fourth law tells us that the vector sources of the magnetic field are the current density due to the motion of charge carriers, either free or bounded, and that the magnetic field induced by a time varying field:

$$\nabla \times \mathbf{H} = \mathbf{J} + \partial \mathbf{D} / \partial t \tag{2-11}$$

where **J** is the current density, and **H** is the magnetic intensity field.

The ratio between electrostatic energy and magnetic energy can be expressed as:

$$\frac{\varepsilon E^2/2}{B^2/2\mu} = \frac{E^2}{c^2 B^2} \tag{2-12}$$

where μ is the magnetic permeability, and c is the speed of light.

It is possible to show that when this ratio is greater than, equal to, or less than one, we have an electrically dominated system, a radiation field, or a magnetically dominated field respectively.

In the first case, called electro-quasistatic, and the last one, named magnetoquasistatic, it is possible to considerably simplify the Maxwell's equations. In both cases, any intricacies related to radiation phenomena and electromagnetic waves can be disregarded, thus leading towards greater simplification. Moreover, in these two cases, it is possible to consider the limit $c \to \infty$, consequently obtaining two Galilean limits to the electromagnetic field.

The case treated in this work is the electro-quasistatic case, where the electric energy is more significant than the magnetic one (Castellanos et al., 1998)

$$\frac{\varepsilon E^2/2}{B^2/2\mu} = \frac{E^2}{c^2 B^2} > 1 \tag{2-13}$$

It is possible to show that, in this–electro-quasistatic field, the electric field is irrotational, and the third Maxwell equation becomes:

$$\nabla \times \mathbf{E} = 0 \tag{2-14}$$

equals to:

$$\mathbf{E} = -\nabla \Phi \tag{2-15}$$

where Φ is the electric potential.

This means that the electric field can be derived from a potential function.

The Maxwell equations can then be reduced to:

$$\nabla \cdot \mathbf{D} = q \tag{2-16}$$

$$\nabla \cdot \mathbf{B} = 0 \tag{2-17}$$

$$\nabla \times \mathbf{E} = 0 \tag{2-18}$$

$$\nabla \times \mathbf{H} = \mathbf{J} + \partial \mathbf{D}/\partial t \tag{2-19}$$

plus the charge conservation law:

$$\partial q/\partial t + \nabla \cdot \mathbf{J} = 0 \tag{2-20}$$

2.2.1 JUMP CONDITIONS AT THE INTERFACE

In this chapter, to explain the jump conditions across an interface between two different media, 1 and 2, we will refer to a jump function $[f]_{21,}$ defined as:

$$[f]_{21} = [f]_2 - [f]_1 \tag{2-21}$$

where $[f]_i$ is a generical function, describing a characteristics of the system, which assumes a real value in each medium (each medium is described by the subscript *i*).
Considering **n** as the normal vector directed from medium 2 into medium 1, we can write the known boundary conditions:

$$\mathbf{n} \times [\mathbf{E}]_{21} = E_{t2} - E_{t1} = 0 \tag{2-22}$$

$$\mathbf{n} \cdot [\mathbf{D}]_{21} = D_{n2} - D_{n1} = -q_s \tag{2-23}$$

expressing the continuity of the tangential component of the electric field, and the jump in the normal component of the electric displacement due to the surface charge density. The indices *n* and *t* are referred respectively to the normal value and the tangent value with respect to the surface. These conditions together with the specification of the potential on the electrodes, enable us to solve the partial differential equations to calculate the electric field distribution.

The equation for the distribution of charge on a boundary can be written by imposing the condition of charge conservation on the boundary:

$$\frac{\partial q_s}{\partial t} + u_n \mathbf{n} \cdot \nabla q_s + 2K u_n q_s + \nabla_s \cdot K_s + \mathbf{n} \cdot [\mathbf{J'}]_{21} = 0 \tag{2-24}$$

where q_s is the surface charge, u_n is the normal speed of the interface, K_s is the surface conductivity of the interface, **J'** is the current density with respect to a non-inertial

observer moving solely with the interface. ∇_s is defined as the ∇ operator minus its projection onto the normal direction:

$$\nabla_s = \nabla - \mathbf{n}(\mathbf{n}\cdot\nabla) \tag{2-25}$$

For a general surface, the three dimensional divergences of the normal vector are associated to the intrinsic mean curvature K_R (r_1 and r_2 are the radii of curvature following the two mean tangent unit vectors) through:

$$\nabla\cdot\mathbf{n} = (1/r_1 + 1/r_2) = 2K_R \tag{2-26}$$

The first three terms of the equation are related to the rate of change in q_s while the interface is moving, while the last two terms are related to the divergence of the current density.
It is important to see how, for a fixed flat interface with zero conductivity, the equation reduces to:

$$\frac{\partial q_s}{\partial t} + \mathbf{n}\cdot[\mathbf{J}']_{21} = 0 \tag{2-27}$$

2.2.2 THE ELECTRIC FIELD BETWEEN A NEEDLE-LIKE UPPER ELECTRODE AND A FLAT PLANE BOTTOM ELECTRODE

When an electric field is generated across a needle-like electrode, and a flat electrode, the electric field around the needle tip becomes very intense. An analytical expression of the electric field, in the ideal case of a dielectric perfect insulator, was established by Durand (1966) assuming that the upper electrode shape is the approximate to a rotational hyperboloid. This approximation also works well in the case of real needles. Durand calculated an expression for the electric field using the prolonged ellipsoid coordinates. After him different researchers (Radu, 2004) obtained different expressions for the value of the electric field between the needle tip and the bottom flat electrode on the needle axis. The relative differences between values calculated using these different methods are always less than 0.5%. The relation given by Bamji et al.(1993) is:

$$E(z)=(E_{max}\, hr_0)/(hr_0+2hz-z^2) \quad (2\text{-}28)$$

where the electric field near the tip E_{max} is:

$$E_{max}=2V/(\, r_0 \ln(1+4h/r_0) \quad (2\text{-}29)$$

knowing that h is the distance between the electrodes, z is the vertical coordinate with origin on the needle tip centre, r_0 is the tip radius and V is the applied voltage. E_{max} is normally not very sensitive to h and r_0. In the graph below the relationship between E_{max} and h for a tip with r_0=6.5 μm is shown.

Considering the high values of the field around the tip, an injection could be generated and a free charge can be generated. This can activate an EHD instability (see section 2.5.3.1), and a jet-like charged liquid motion (i.e. a charged plume) is observed (see section 2.5.3.2).

Considering the work conditions reported in this study, the field dependence for h=6mm, V=10kV and r_0=6.5 μm was reported in figure 2.1. The horizontal line reports, as a matter of comparison, the electric field value in a parallel flat electrodes system at the same distance and voltage.

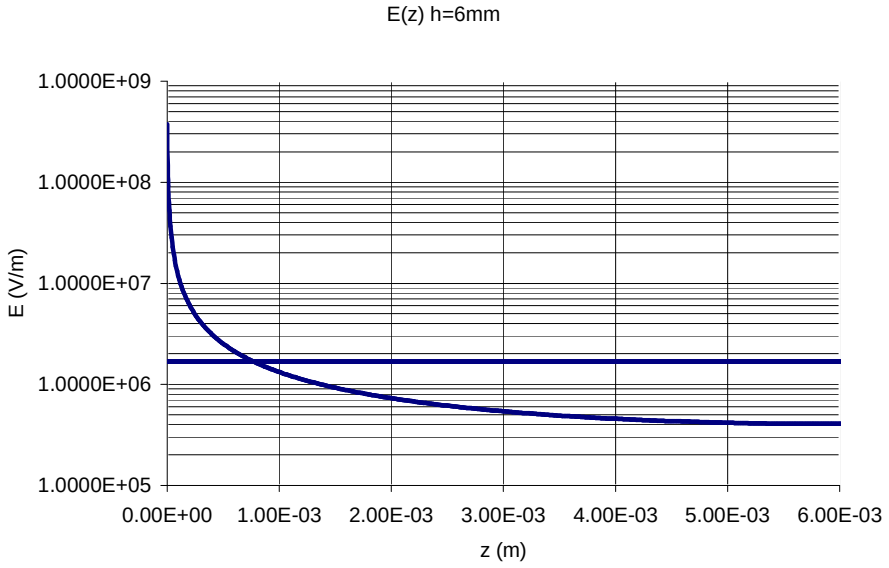

Figure 2. 1: Electric field as a function of the position between the electrodes as calculated with (2-28)

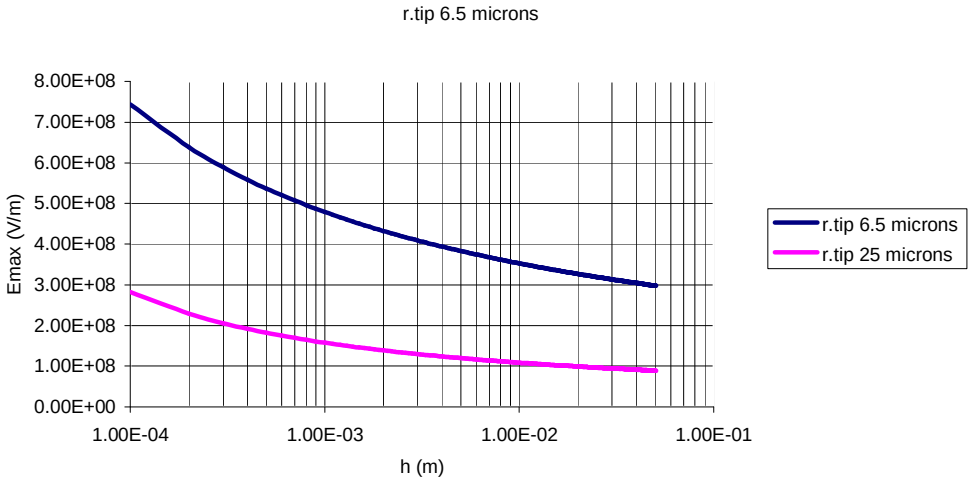

Figure 2. 2: Electric field on the tip as a function of the distance between the electrodes as calculated with (2-29)

2.3 POLARISATION OF MATTER

2.3.1 THE COMPLEX PERMITTIVITY

The notation utilised in this section describes the polarisation phenomena using a complex permittivity:

$$\varepsilon^* = \varepsilon' - j\varepsilon'' \tag{2-30}$$

In this notation ε' indicates the electrostatic energy stored by the material and ε'' indicates the energy loss per cycle. Following some simple circuital considerations (Pohl, 1978) it can be demonstrated that:

$$\varepsilon'' = \sigma / \varepsilon_0 \omega \tag{2-31}$$

where σ is a conductivity term, and ω is the angular frequency, defined as $\omega=2\pi f$, with f being the frequency of the signal. It is important that σ takes into account the contribution due to the free charge motion (ionic conductivity), normally important only at very low frequency, and of what is called dielectric conductivity, due to all the

"internal frictions" and loss mechanisms that dissipate energy during the material polarisation.

Dielectric losses can also quantified using another indicator:

$$\tan\delta = \varepsilon''/\varepsilon' \qquad (2\text{-}32)$$

This subject has been extensively addressed in the literature (Stratton, 1941).

2.3.2 REVIEW OF THE PRINCIPAL MECHANISMS OF POLARISATION IN MATTER

In the following section the main mechanisms of polarisation operating in nature are listed.

Electronic polarisation (also called atom or atomic polarisation)

This mechanism is typical of any material, because it is a direct consequence of the atomic structure. When an electrical field is applied, the centre of charge of the electrons is no more centred on the nucleus. This results in an induced dipole. ε_r has a typical value of 1.00008.

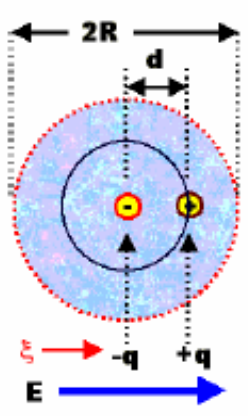

Figure 2. 3: Electronic polarisation mechanism (Foll, 2006)

Ionic polarization

Any ionic material has naturally lots of internal dipoles, due to the characteristics of the ionic bond. In field free conditions, these are internal dipoles, and there is no macroscopic effect. If an external field is acting, then net dipoles are induced as a consequence of the slight displacement of the ions from their equilibrium position.

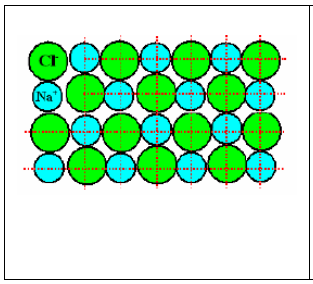

Figure 2. 4: structure of a ionic material (Foll, 2006)

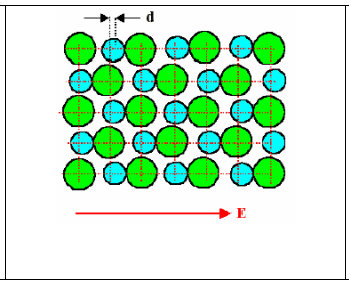

Figure 2. 5: showing the electric field on a ionic material (Foll, 2006)

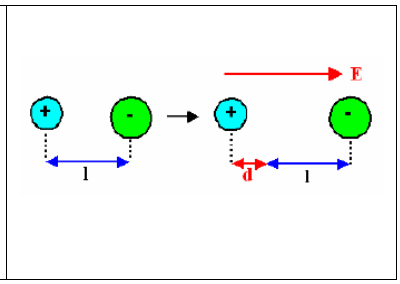

Figure 2. 6: dipole formation in a ionic material under an electric field action (Foll, 2006)

The polarisability is also related to the Young's modulus. The higher it is, the more rigid the material (i.e. less easy to polarise).

Orientation polarisation.

This mechanism of polarisation in material (usually liquid or gaseous) can be found in natural dipoles which can rotate freely. In the case of thermal equilibrium, the dipoles are randomly oriented and produce no net polarisation. The application of an external field aligns these dipoles and induces a polarisation. The notable example is H_2O, in its liquid form.

Without field With field

Figure 2. 7: Orientation polarisation mechanism in a dipolar permanent fluid material (Foll, 2006)

Such a mechanism of polarisation is always in competition with thermal energy, and therefore has the tendency to be less effective in increasing the temperature.

Effects due to migrating charges

The transport of charges is a purely dissipative process. In terms of complex permittivity, only the dielectric loss is influenced by the presence of migrating charges (Senturia and Sheppard, 1986):

$$\varepsilon'_{ion} = 0 \tag{2-33}$$

$$\varepsilon''_{ion} = \frac{\sigma}{\omega\varepsilon_0} \tag{2-34}$$

where, ω is the angular frequency and ε_0 is the permittivity of free space. The above equations show that whenever migrating charges dominate the dielectric signal, the product $\omega\ \varepsilon_0\ \varepsilon''$ is frequency independent and equal to the conductivity σ.

The relation above is, in practice, used to measure the value of conductivity in systems where the losses are governed by conductivity.

Interface polarisation

The action of an electric field can achieve a migration charge by:

1) bulk transport of charge carriers within the higher conductivity phase
2) surface migration of charge carriers

As a consequence surfaces, grain boundaries, interphase boundaries (including the surface of precipitates) may charge. Charges "blocked" at the interface between two phases with different conductivity give a contribution to the net polarisation of the body exposed to the electric field.

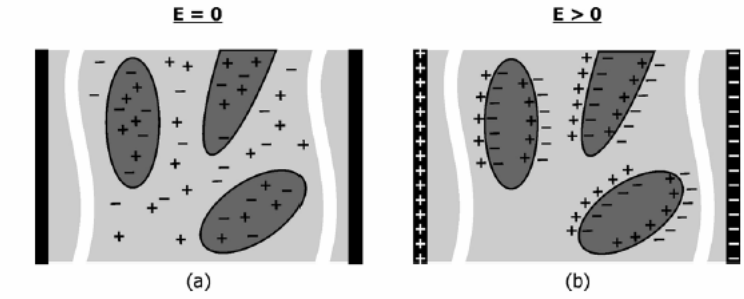

Figure 2. 8: Maxwell Wagner Sillar polarisation mechanism (Kazilas, 2003)

The Maxwell–Wagner–Sillars (MWS) model (Maxwell, 1954; Sillars, 1937) is conventionally used for the description of interfacial polarisation phenomena. For a two phase system, the relaxed and unrelaxed permittivity and the relaxation time of the interfacial polarisation are:

$$\varepsilon_{r,i} = \varepsilon_l\left(\frac{2\sigma_l + \sigma_p + 2v_p\Delta\sigma}{2\sigma_l + \sigma_p - v_p\Delta\sigma}\right) + 3v_p\sigma_l\left(\frac{(2\sigma_l + \sigma_p)\Delta\varepsilon - (2\varepsilon_l + \varepsilon_p)\Delta\sigma}{(2\sigma_l + \sigma_p - v_p\Delta\sigma)}\right)$$

$$\varepsilon_{u,i} = \varepsilon_l\left(\frac{2\varepsilon_l + \varepsilon_p + 2v_p\Delta\varepsilon}{2\varepsilon_l + \varepsilon_p - v_p\Delta\varepsilon}\right) \qquad (2\text{-}35)$$

$$\tau_i = \varepsilon_0\left(\frac{2\varepsilon_l + \varepsilon_p - 2v_p\Delta\varepsilon}{2\sigma_l + \sigma_p - v_p\Delta\sigma}\right)$$

In those relationships, v_p is the volume fraction of the dispersed phase, ε_l and ε_p are the real permittivities of the bulk and the dispersed phase; σ_l and σ_p are the conductivities and $\Delta\varepsilon = \varepsilon_p - \varepsilon_l$, $\Delta\sigma = \sigma_p - \sigma_l$ and ε_0 is the permittivity of free space. The model is valid for $v_p < 0.2$ (Maxwell, 1954; Sillars, 1937).

If the majority phase is a fluid, another polarisation phenomenon can be active at interfacial level: the migration of charge carriers within the double layer of a liquid phase.

In reality filler immersed in a liquid medium develops a charged surface. To balance that charge a layer of counterions forms immediately. A redistribution of ions in the surrounding fluid, which generates a diffuse electrical double layer, also occurs. This layer has finite thickness (Debye length) and there is an osmotic pressure associated with the local ions redistribution. In the presence of an applied electric field the symmetry of this double layer can be distorted (Morgan and Green, 2003).

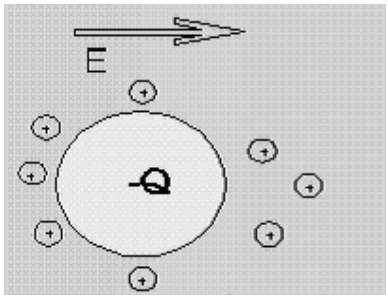

Figure 2. 9: Double layer distortion typical of a filler dispersion that undergoes an electric field (Pethig, 2006)

Electrode polarisation
The phenomenon is described by Adamec (1972) and Adamec and Calderwood (1989), as being the result of a difference between the flux of charges across the electrode interface (slower) and the one inside the bulk material (faster) when an electric field is present. Due to that difference, charges accumulate in the vicinity of the sensor electrodes generating an increase of the measured permittivity. The model is a three layer capacitor (blocking electrodes model).
Electrode polarisation is a free charge induced phenomenon which relaxes at very low frequencies,.as in the case of the polarisation effect due to double layer displacement.

2.3.3 FREQUENCY DEPENDENCE OF THE DIELECTRIC CONSTANT

2.3.3.1 General Remarks

All dielectric materials polarise in the presence of an electric field. All those polarisation mechanisms involve a displacement of masses. As a consequence of the inertia, it is therefore expected that the polarisation phenomena depend on the frequency of the electrical field.

Considering the polarisation mechanisms discussed before, there is a fundamental difference in the dynamics of the mechanisms with regard to their characteristic polarisation mechanisms:

- In electron and ionic polarisation there is the electrostatic force, against a restoring force that is approximated as being directly proportional to the separation distance of the dipole charges. It is, in mechanical terms, an oscillator. The characteristic property of an oscillating system is the phenomenon of resonance at the proper frequency of the system.

- In the case of the orientation and interfacial polarisation, there is no direct mechanical force, only a series of statistical events whose the zero average can be displaced by an electrical field. The reaction to the electric field is not instantaneous, but follows the diffusion laws, and is thermally activated. Then if the electric field disappears, the dipoles will assume random distribution within a characteristic time known as relaxation time. The process it is characterised by its relaxation time instead of a resonance frequency.

2.3.3.2 Resonance for Ionic and Electronic Polarization

A driven oscillating system with a linear force law and some damping is the mathematical description of the frequency dependence of the electronic and ionic polarization mechanisms. An oscillating system driven by a force with a sin(ωt) time dependence is described by:

$$m\frac{d^2\mathbf{x}}{dt^2} + k_F m\frac{d\mathbf{x}}{dt} + k_s\mathbf{x} = q\mathbf{E_0}e^{i\omega t} \qquad (2\text{-}36)$$

with:

m = mass

k_F = friction coefficient describing damping

k_S = "spring" coefficient or constant; describing the restoring force

qE_0 = Coulomb force

$E = E_0\, e^{i\omega t}$ is the time dependence of electrical field in complex notation.

The conservative solution given that the resonance frequency ω_0 is equal to:

$$\omega_0 = \sqrt{\frac{k_s}{m}} \tag{2-37}$$

After development of the equations the following value for the dielectric constant is identified:

$$\varepsilon' = \varepsilon_0 + \frac{Nq^2}{m}\frac{\omega_0^{\,2} - \omega^2}{\left(\omega_0^{\,2} - \omega^2\right)^2 + k_F^{\,2}\omega^2} \tag{2-38}$$

$$\varepsilon'' = \frac{Nq^2}{m}\frac{k_F\omega}{\left(\omega_0^{\,2} - \omega^2\right)^2 + k_F^{\,2}\omega^2} \tag{2-39}$$

Where N is the number of dipoles per m^2.

The functions are represented graphically in the figure 2.10.

For the electronic polarisation mechanism a resonance occurs in the ultraviolet region at around 5×10^{16} Hz. Therefore, the dielectric constant at frequencies higher than the UV part of the spectrum is always 1.

For the ionic polarisation mechanism, the masses are several thousand times higher. The resonance frequency is then considerably lower: in the order of 10^{12}-10^{14} Hz range (infrared range).

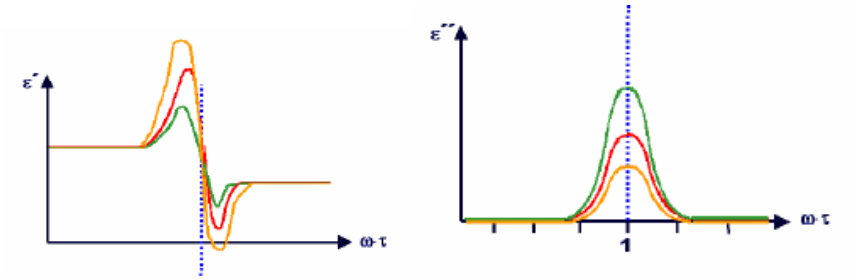

Figure 2. 10: Permittivity frequency dependence in a material with a resonant polarisation behaviour (Foll, 2006)

2.3.3.3 Dipole Relaxation

If an electric field has been constant for a sufficiently long time to obtain an equilibrium distribution of dipoles and it is suddenly switched off, the dipoles will randomize and the polarisation will go to zero. This phenomenon cannot occur instantaneously. A specific dipole can change orientation only by some interaction with other dipoles or, in a solid, with phonons. It needs a characteristic time, dependent to the time between collisions, before the dipole moment will have disappeared. This time is called the relaxation time of the system.

The smooth change over from the polarisation with field to zero within the relaxation time t, follows behaviour as shown in figure 2.11:

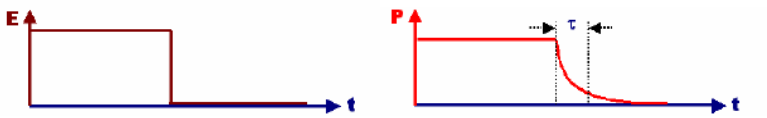

Figure 2. 11: polarisation relaxation behaviour (Foll, 2006)

P decays after the switch-off according to:

$$P(t) = P_0 \, e^{-t/\tau} \tag{2-40}$$

In Debye approximation we can calculate ε', the real part of a complex amplitude, the amplitude of the response in phase with the driving force, and ε", the imaginary part the amplitude of the response phase-shifted by 90°.

$$\varepsilon' = \varepsilon_\infty + \frac{\varepsilon_s - \varepsilon_\infty}{1 + \left(\omega / \omega_0\right)^2} \tag{2-41}$$

$$\varepsilon'' = \frac{\left(\omega / \omega_0\right)\left(\varepsilon_s - \varepsilon_\infty\right)}{1 + \left(\omega / \omega_0\right)^2} \tag{2-42}$$

Where ε_s is the value of ε at low frequency, before relaxation, and ε_∞ is the value of ε at high frequency, after relaxation.

The distortions of the electrical double layer have a finite relaxation time and become negligible above about 50 kHz. For a frequency bigger than 50 kHz the dipole moments associated with Maxwell-Wagner interfacial polarisations are the only ones that can exert their influence.

2.3.3.4 Complete Frequency Dependence of a Model Material

The relationship between permittivity and frequency is the superposition of the various polarisation mechanisms seen before. In the idealised case of a model material containing all four basic bulk dipole displacement mechanisms in their pure form, the curves in figure 2.12 would be expected.

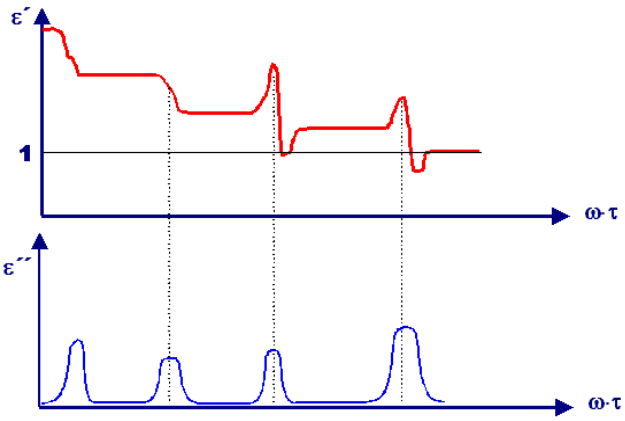

value.

Figure 2. 12: Idealised case of a model material containing all four basic bulk dipole displacement mechanisms in their pure form. Starting from the right side, it is possible to individuate the resonance for the electronic and the ionic polarisation, a Debye-like dipole relaxation and an interfacial relaxation. (Foll, 2006)

It is a general property of complex functions describing physical reality, the fact that under certain very general conditions, the real and imaginary part are directly related. The relation is called Kramers-Kronig relation.

For any complex function, e.g. $\varepsilon^*(\omega) = \varepsilon'(\omega) + j\varepsilon''(\omega)$, the Kramers-Kronig relation can be written as follows:

$$\varepsilon'(\omega) = \frac{-2\omega}{\pi}\int_0^{\infty}\frac{\omega^* \cdot \varepsilon''(\omega^*)}{\omega^{*2} - \omega^2}\,d\omega^* \tag{2-43}$$

$$\varepsilon''(\omega) = \frac{2\omega}{\pi}\int_0^{\infty}\frac{\varepsilon'(\omega^*)}{\omega^{*2} - \omega^2}\,d\omega^* \tag{2-44}$$

Where ω is a complex angular frequency and ω^* is its conjugate

PIEZOELECTRICITY, FERROELECTRICITY AND THE LEAD ZIRCONATE TITANATE (PZT)

All crystal structures can be classified into one of 32 possible forms of crystal symmetry. Eleven of these forms are centrosymmetric. Out of the remaining 21 non-centrosymmetric groups, 20 are known to be piezoelectric. A piezoelectric is a material that produces a deformation if exposed to an electric field (direct effect), and that generates a polarisation in response to applied mechanical stress (inverse effect). The polarisation P is directly proportional to the mechanical strain $\Delta l/l$:

$$P = \text{const} \cdot (\Delta l/l) \tag{2-45}$$

Piezoelectricity should not be confused with electrostrictive effect, an effect usually much weaker than the piezoelectric effect, where $(\Delta l/l)$ depends on the square of the electrical field:

$$\Delta l/l = \text{const} \cdot E^2 \tag{2-46}$$

In contrast to piezoelectricity, due to the quadratic dependence, the sign of the field is irrelevant. Moreover, no converse effect exists in electrostriction, i.e. a deformation does not produce an electric field.

There is a permanent electric dipole in 10 of the 20 piezoelectric crystal groups. The equilibrium of the electrostatic potential caused by this dipole can be distorted by either mechanical stress or temperature change, generating respectively piezoelectricity or pyroelectricity. The pyroelectricity is the polarisation of a material generated by a

temperature change. Ferroelectric materials are a particular category of pyroelectric materials.

In physics, the ferroelectric effect is an electrical phenomenon whereby certain ionic crystals and piezoelectric polymers may exhibit a spontaneous dipole moment, which can be reversed by the application of an electric field. The term ferroelectricity is used in analogy to ferromagnetism, in which a material exhibits a permanent magnetic moment and the curve P = P (E) manifests as a hysteresis cycle (see section 5.3.1 for an example).
Ferroelectric crystals often show several Curie points and domain structure hysteresis, much as do ferromagnetic crystals. By analogy to magnetic core memory, this hysteresis can be used to store information in ferroelectric RAM, which has ferroelectric capacitors as memory cells. The nature of the phase transition in some ferroelectric crystals is still not well understood.

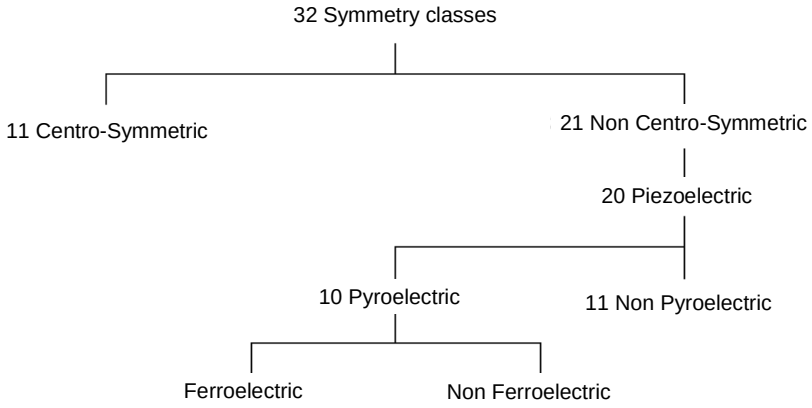

Figure 2. 13: Summary of the different symmetry classes in crystals and relationship with piezoelectricity

Ferroelectrics often have very large dielectric constants, and thus are often used as the dielectric material in capacitors. They also often have unusually large nonlinear optical coefficients.

Lead zirconate titanate ($Pb[Zr_xTi_{1-x}]O_3$) presents a very large dielectric constant at the morphotropic phase boundary (MPB) near x = 0.52. The increase in piezoelectric response and poling efficiency in proximity of x = 0.52 derive from the augmentation of the number of allowable domain states at the MPB. At MPB limit, 6 possible domain states come from the tetragonal phase <100> and 8 other possible domain states from the rhombohedral phase <111>. Considering that these two phases are equally favourable energetically, it results in a maximum of 14 possible domain states.

For these properties, PZT-based compounds are between the most prominent and useful electroceramics. PZT normally is not in used commercially in its pure form. Instead it is doped with either acceptor dopants, which create oxygen (anion) vacancies, or donor dopants, which create metal (cation). In general, acceptor doping generates *hard* PZT, and donor doping creates *soft* PZT. In general, *soft* PZT has a higher piezoelectric constant, but larger losses in the material. The losses are due to internal friction. In *hard* PZT, domain the wall motions are blocked by the impurities. This generates a decrease in the material loss, but at the expense of a reduced piezoelectric constant.

PZT is commonly employed in the production of acoustic transducers, other sensors, actuators, high performance capacitors and FRAM components.

Table 2. 1: Room temperature (25°C) dielectric, ferroelectric, and piezoelectric properties of PZT based ceramics (Morgan Electro Ceramics, Bedford, Ohio, US).

Property	Units	PZT-4	PZT-5A	PZT-5H	PLZT-9/65/35
K (1 kHz)	---	1400	1600	3400	5000
tan δ (1kHz)	---	0.05	0.02	0.02	0.06
E_C	kV/cm	14.4	11.8	5.5	2.5
P_R	μC/cm^2	31.0	23.0	12.9	1.1
P_{SAT}	μC/cm^2	40.1	27.7	19.5	20.8
k_{eff}	---	0.49	0.50	0.53	---
k_p	---	0.54	0.56	0.59	---
d_{33} ($x10^{-12}$)	m/V	225	350	585	---
g_{33} ($x10^{-3}$)	Vm/N	8.5	16.6	12.5	---
k_{33}	---	0.35	0.53	0.59	---
d_{31} ($x10^{-12}$)	m/V	-85	-190	-265	---
g_{31} ($x10^{-3}$)	Vm/N	-7.5	-13.7	-8.5	---
k_{31}	---	0.22	0.40	0.36	---
Density	g/cm^3	7.6	7.7	7.4	7.3

All the subjects related to ferroelectricity, has been extensively addressed in the literature (Xu, 1991).
In the table 2.1 some characteristic properties for a PZT 5A and PZT 5H - the two products we used in this study – are reported.

Here K is the relative dielectric constant, tanδ the loss factor, E_c the coercitive field, P_R the residual polarisation, P_{SAT} the saturation polarisation, and all the other the piezoelectric coefficients.
The resistivity and the dielectric constant are particularly interesting in the context of applications related to this research:

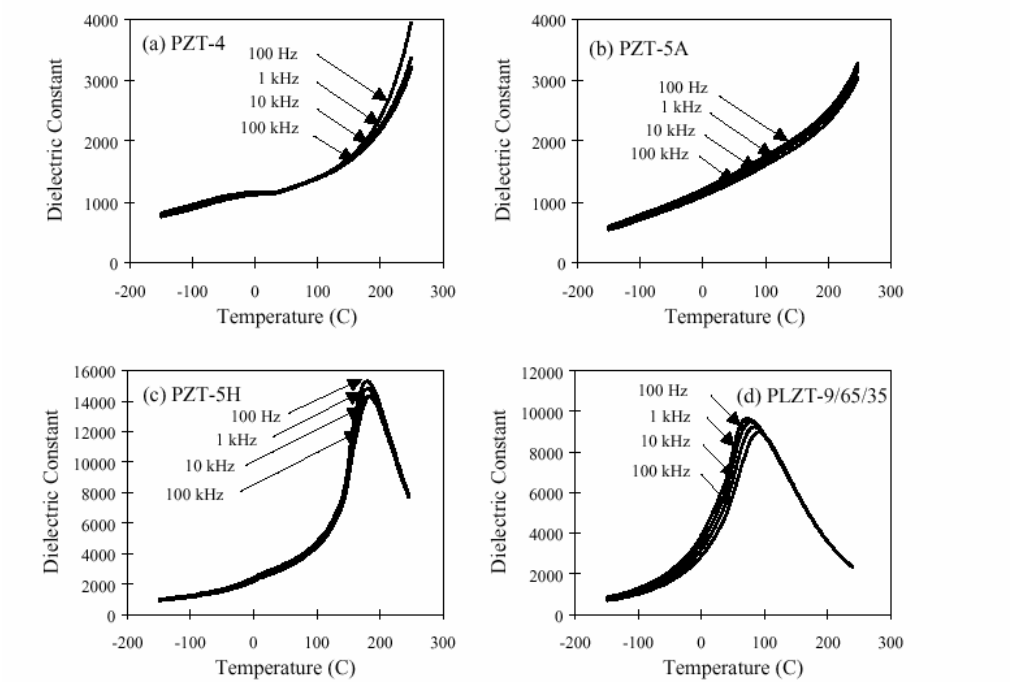

Figure 2. 14: Dielectric constant versus temperature data for (a) PZT-4, (b) PZT-5A, (c) PZT-5H, (d) PLZT-9/65/35 (Hooker, 1998).

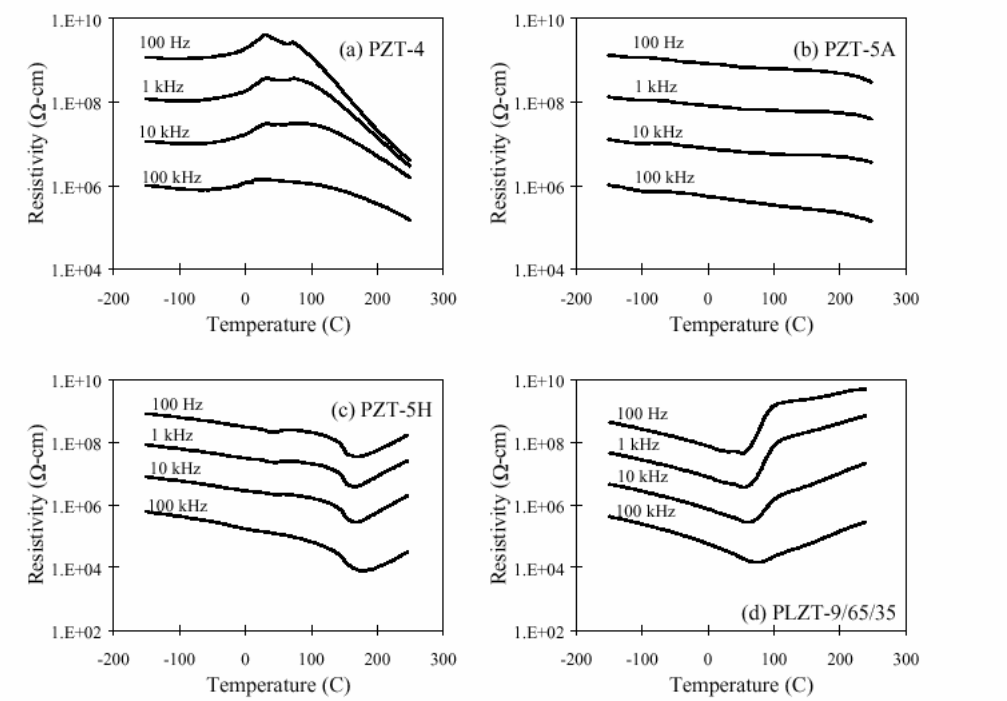

Figure 2. 15: Resistivity versus temperature for (a) PZT-4, (b) PZT-5A, (c) PZT-5H, (d) PLZT-9/65/35 (Hooker, 1998).

2.4 CONDUCTIVITY OF MATTER

2.4.1 OHMIC REGIME

Where the electrical transport is the result of the flow in both directions of charged species of both sign, the system follows the Ohm's law (i.e. is called an ohmic regime):

$$\mathbf{J} = \sigma \mathbf{E} \tag{2-47}$$

The ability of a material to conduct electric current, if exposed to an electric field, is expressed by the electrical conductivity σ, that relates the current density **J** to the electric field **E**. The conductivity is expressed as:

$$\sigma = \sum k_i q_i \tag{2-48}$$

with q_i the volume charge density, and k_i the carrier mobility. The mobility is the constant of proportionality between carrier speed **u** and electric field **E**:

$$\mathbf{u} = k\mathbf{E} \tag{2-49}$$

The Ohm's law is always respected when the material is in condition of thermodynamic equilibrium. It means that the charge concentration and the mobility do not change as a consequence of interfacial phenomena, electroconvection, or any other equilibrium displacement phenomena. When the system moves away from the equilibrium condition σ can became dependent from the electric field. However, it can be assumed that Ohm's law is respected, but σ is no more a constant.

When analysing the electric transport phenomena, if the fluid has a certain liquid speed **u**, the speed must be taken into account and the law becomes:

$$\mathbf{J} = \sigma\,\mathbf{E} + q\,\mathbf{u} \tag{2-50}$$

2.4.2 UNIPOLAR REGIME

Under certain experimental conditions, some unipolar (all of the same sign) charges can be injected into the conduction media through the electrode. Supposing that the injection happens in a perfectly insulating liquid (σ=0), and that the injected charges are positive, the behaviour can be expressed as:

$$\mathbf{J} = qk\mathbf{E} - D\nabla q + q\mathbf{u} \tag{2-51}$$

Considering λ_c the spatial scale of variation of the charge concentration, and Λ the characteristic dimension of the system, it can be demonstrated that the molecular ionic diffusion term will be generally negligible with respect to the drift term, unless the potential drop is of the order of 25mV for $\lambda_c \sim \Lambda$, or a very high gradient of charge density exists, or $\lambda_c << \Lambda$.

2.4.3 PHYSICAL ORIGIN OF CONDUCTIVITY

Depending on the transport mechanisms, charge carriers can be electrons, ions and electronic or ionic holes. The most common model describing electronic conduction in solid materials is the band model. In this model electrons can lie in two possible energetic bands, separated from a certain energy gap. At the lower energy is the valence band, in which the electrons are bonded to atoms, and at the higher is the conduction band, in which the electrons are free to move.

In metals, the two bands are superimposed, consequently, a significant number of electrons is always available to conduct. In this case $\sigma > 10^5$ S/m. In semiconductors, the energy gap is in the order of k_BT (where k_B is the Boltzmann's constant, equal to 1.3806503×10^{-23} m^2 kg s^{-2} K^{-1}) and a certain number of electrons can leave the valence band to reach the conduction band only exploiting their thermal energy. The electron hopping leaves a hole in the valence gap, and conduction arises from the electrons in the conduction band and the holes in the valence band.
Some impurities, added as dopants, can contribute to increase the conductivity, by increasing either the number of electrons (n-type), or the number of holes (p-type).
In electronic semiconductors, the conduction, e.g. in silicon, or silicon carbide, equates to $\sigma \approx 10^2$ S/m.
When increasing the gap energy, the number of electrons in the conduction band decreases. Consequently, the conductivity decreases too. When the energy gap becomes larger than 6eV, the material is defined as an insulator ($\sigma < 10^{-20}$ S/m), because electronic conduction is practically impossible, although the presence of impurity can allow a certain conductivity.
Ionic conduction is permitted in solids by impurities and lattice vacancies. Ionic conductors usually have a lower σ, and quite often the ionic mechanism of conduction is superimposed to a certain electronic conductivity (Boukamp et al., 2004). Ions can be due to the diffusion of impurity, to self-diffusion of ions constituting the ceramic, or to charged holes coming from oxygen vacancies, for instance. Ceramics characterised from a high ionic conductivity are called solid electrolytes ($\sigma \approx 1$ S/m).

Even far from any kind of breakdown phenomena, ionic conductivity also is the main conducting mechanism in liquids and gases.

2.4.4 CONDUCTIVITY IN A DIELECTRIC LIQUID

2.4.4.1 Ohmmic conduction in a dielectric liquid and dependence of the conductivity on the electric field

The conductivity of a dielectric fluid increases with the permittivity. This is known as the Nernst-Thompson rule, and was formulated in qualitative form in the 19th century. Sharbaug and Baker (1965) then made an extensive survey resulting in the chart below. A relationship between resistivity and permittivity can be derived applying the law of mass action to the equilibrium between the dissolved impurities and the dissociated ions.

The result can be summarised by:

$$-\log\sigma \approx a/\varepsilon + b \tag{2-52}$$

where a and b are constants.

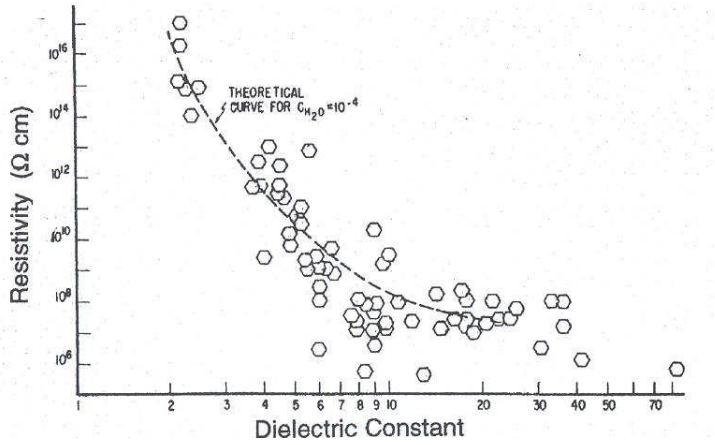

Figure 2. 16: Published values for DC volume resistivity vs dielectric constant. The dashed lines shows the theoretical trend for ρ versus ε', assuming that water is a common contaminant at a level of 10^{-4} M/l (Sharbaugh and Barker, 1965)

Water is partially soluble in any dielectric. A reasonable assumption is therefore that some water is present as a contaminant. To give an order of dimension the curve shown in the chart is relative to a water content of 10^{-4} M/l (the solubility in hexane is 10^{-3}). Water seems to be the main actor of the conductivity phenomena in dielectrics (Whatson, 1998).

As extensively explained by Felici (1971), they are four main kinds of dielectric fluids:

a) Non-polar: ε_r=2 $\sigma>10^{-12}$ S/m; few examples are silicone oil, transformer oil, paraffin oil, carbon tetra-fluoride, castor oil, mineral oil, benzene, kerosene, fluorocarbons
b) Mildly polar: ε_r=4-6 $\sigma>10^{-11}$ S/m; an important example of this category are the PCBs (Polyclorinated biphenyls) also known with the commercial name of Arochlor and Pyralene, once widely employed as transformer oils, now illegal
c) Highly-polar not associated (H-bond, etc.): ε_r=30-80 $\sigma>10^{-9}$ S/m; an important examples are nitrobenzene and sulfolanes
d) Highly-polar not associated: ε_r=30-200 $\sigma>10^{-8}$ S/m; this category includes water, alcohols, and all the amines

If these are the order of dimension for pure dielectrics, interesting fluid with original interesting characteristics can be made by doping or creating some mixtures of different pure dielectrics.
Sometimes, mixtures of oils can be used to change the characteristics (silicone oil-butylalcohol to change conductivity and dioxane-water to change epsilon from 2.2 to 80). The sensitivity to impurities of the fluid conductivity increases when the permittivity rises.
The conductivity of water can be raised up to 5 S/m by adding salts. Also the conductivity of non polar oils can be increased a thousand times by adding organic salts (Boissy et al., 1995).
In the electrorheological ER fluid technology (see section 3.4), the choice of the oil is very varied and depends upon factors such as density, viscosity, manipulating without fume hood, flammability, injection.

Leaving aside any effect due to solid impurity, barrier energy on the electrodes and field emission, the electric transport in a dielectric liquid derives from the presence of ions or ionic complex into the fluid. The ions derive only in a very small quantity, from natural radiation. In non self-ionised liquids with weak permittivity, carriers are mainly generated from the spontaneous dissociation of some ionisable impurities. In self-ionised liquids even with higher permittivity the molecules of the liquid itself dissociate. At room temperature the transition takes place at $\varepsilon_r \approx 2$. Conduction by electrons is not permitted at normal impurity concentrations. Electrons are easily trapped by electron-acceptor species dissolved in the liquid, and they have a short lifetime (0.1ms).

The conductivity in non-self-ionised liquids arises from the dissociable species. They have a certain concentration in the fluid resulting in an equilibrium of dissociation and recombination. When applying a weak field (<0.1MV/m), the equilibrium does not notably modify, and the conduction becomes ohmmic. When the electric field increases, so does the dissociation coefficient, despite the recombination rate, which remains practically constant. As a result of the ion concentration and the conductivity increases too. This behaviour is well explained by the theory of Onsager. Felici et al. (1994) derived a useful formula to describe the conductivity of a dielectric liquid following the Onsager theory:

$$\sigma_l = \sigma_l(0)(1 - A + A \exp((E / E_c)^{1/2})) \qquad (2\text{-}53)$$

where A is an adimensioned factor, E_c is the critical field and $\sigma_l(0)$ the liquid ionic conductivity at low field. In a liquid, following the Onsager's theory, when a field is bigger than $10E_c$, the fluid starts to increase its conductivity, and when $E>100E_c$, it practically becomes a conductor.

If the dissociation and recombination rate remains the same, by increasing the voltage the current saturation can be obtained. All the ions generated are immediately collected at the electrode, and no recombination can occur.

2.4.4.2 Unipolar injection in a dielectric liquid

Apart from the dissociation-recombination mechanism, another ion generation mechanism plays a role in the liquid conductivity: ion injection through the electrode. Injection consists of an electrochemical reaction where, via an electronic transfer across the electrode surface, an electroneutral species acquires a homocharge (charge of the same sign of the electrode). The generated ions are strongly repelled from the electrode by columbic force, and injected into the liquid bulk. In the upper limit condition of strong injection, the current density at steady-state is space-charge limited (SCL), and varies of the square of the field. The formula in the hypothesis of E=0 has been derived by Thompson (Von Hippel, 1954):

$$j_i = 9\varepsilon k V^2/8h^3 \qquad (2\text{-}54)$$

Where h is the distance between the two electrodes.
Injection normally happens when the field overcomes a certain threshold.
A particularly interesting case of injection, analysed in this research, is the injection through the needle tip in a needle-plane electrode configuration.
Coelhot and Debeaus (1971) calculated an expression for the current derived from the electric charge injection through the needle tip roughly approximating that the electric field on the tip was equal to 0:

$$I = 4\varepsilon k(V^2/s) \qquad (2\text{-}55)$$

One of the ways to measure electrical mobility in a dielectric fluid is to inject some charge from an electrode and observe how the current changes. In the experiments in which a tip is used as emitter, this gives a useful relationship between the current and the mobility. This method revealed very useful to measure the mobility.

2.4.4.3 The charge equilibrium near the electrode

To understand the charge distribution and the structure of the electrical double layer in proximity to the electrode surface, in a dielectric oil, is key to understanding the particle

electrification phenomena (see chapter 7), and moreover, to understand any eventual EHD effects. Although an extensive review on this subject is out of the scope of the present section, a basic introduction would be useful to understand the discussion to the phenomena presented in chapters 7,8 and 9.

In a low or moderate field (E>0.1 MV/m) a layer of charge is physically adsorbed in proximity to the electrode surface, mainly due to the image charge. The thickness of this adsorbed layer ς_{ad} can be calculated from the balance between the diffusion current and the current due to short range forces:

$$\varsigma_{ad} = ek/16\pi\varepsilon D = e^2/16\pi\varepsilon k_B T \qquad (2\text{-}56)$$

Where D is the diffusion coefficient for the ionic species, *e* is the elementary charge and T is the temperature:

$$D=\Phi_0 k \qquad \Phi_0=k_B T/e$$

However, there is also a diffused electric layer issued from the balance of diffusion and migration currents. The length of this diffused layer ς_{el} can be calculated as:

$$\varsigma_{el} = \Phi_{0/}E_v \qquad \Phi_0=k_B T/e \qquad (2\text{-}57)$$

where E_v is the field at the boundary with the adsorbed layer. It is important to remark that this case is quite different to the one in water based systems where the Debye length ($\lambda_D=(\varepsilon k_B T/Ne^2)$ determines the diffusion length of the electrical double electric layer.

At high electric fields the diffused layer disappears and the condition $\varsigma_{ad} > \varsigma_{el}$ is verified. In this condition the diffusion layer is followed by a non-equilibrium layer $\varsigma_{d,}$ in which the dissociation-recombination reaction are not in equilibrium. This layer has a characteristic length equal to:

$$\varsigma_d = \varepsilon E_0/en_0 = \varepsilon(k_+ + k_-)E_0/\sigma \qquad (2\text{-}58)$$

Where k_+ and k_- are the ionic mobilities of the positive and negative carriers respectively. The boundary problem to evaluate the electric intensity inside the non-equilibrium layer has been proposed by Zhakin (1998). A solution is presented in figures 2.17 and 2.18. The importance played by the injection and by the ratio between

the mobility of the homo-charge and hetero-charge is clear. Without injection the field is always decreasing, moving apart from the electrode. On the contrary, in presence of strong injection the trend can be reversed.

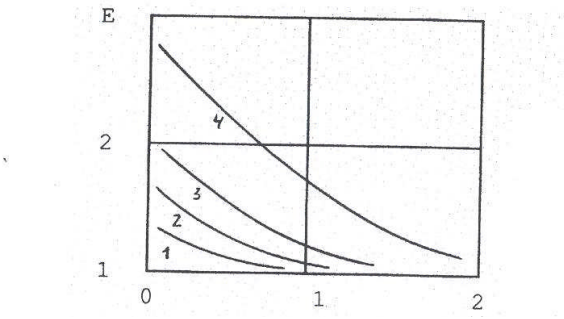

Figure 2. 17: Distribution of the electric intensity in non-equilibrium layer near cathode in absence of the charge injection $\sigma_c = 0$ and various mobilities of homoions (k_+) and heteroions (k_-). Curves 1-4 are correspondent to k_+/k_-=0.5; 1; 2; 5 accordingly (Zhakin, 1998).

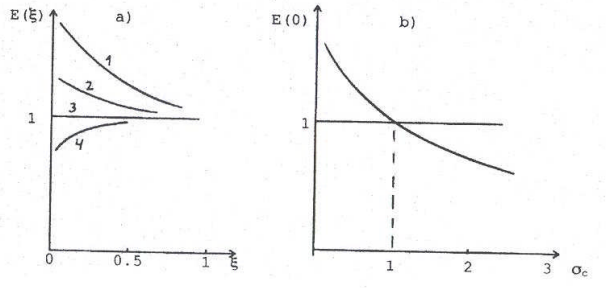

Figure 2. 18: a) Distribution of the electric intensity in non-equilibrium layer at various level of charge injection and equal mobilities $k_+ = k_-$. Curves 1-4 are correspondent to $\sigma_c = 0$; 0.5; 1; 2. b) Dependence of the electric intensity on the cathode surface versus injection parameter σ_c at equal mobilities (Zhakin, 1998).

In conclusion, it is worth highlighting that in classical electrochemistry the discharge rate at the electrode is considered to have a very high value due to the strong intensity of the field inside the double layer (around 1 MV/cm), and the discharging mechanism is considered practically instantaneous. Unfortunately the field outside the adsorbed layer is far below 1 MV/cm and for this range of field the ions would not discharge. However, the discharge of an ion on an electrode is an ordinary effect. This apparent incoherence can be explained by considering the microscopic roughness of the electrode. On highly polished surfaces, they are around 10^{12} micro-asperities/m^2 with a

dimension in the order of 2μm and with an amplification factor for the electric field of 100-1000.

Taking these factors into account, the real model can still be reliable, but only by introducing a virtual smooth surface S, where the conditions are stated, that acts on behalf of the electrode surface. The real distribution of charge in proximity to an electrode is summarised in the picture in figure 2.19.

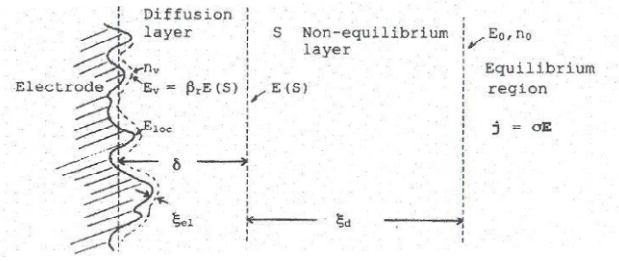

Figure 2. 19: Structure of the electrical double layer near a real electrode when immerged into a dielectric liquid (Zhakin, 1998).

Before to conclude this section it is important to say that some groups reported the generation of a waxy coating on the electrodes for periods relatively long of exposition of a dielectric liquid to an electric field. These structures have been associated to some possible electro-polymerisation phenomena (Briere and Gaspard, 1968; Gallagher, 1975).

2.4.4.4 The breakdown in dielectric fluids

The charge transport in gases is always due to free electrons and ions generally originated by external radiation. The electrical conductivity is very small, and of the order of 10^{-16} – 10^{-15} S/cm. Nevertheless, if these carriers are exposed to a strong electric field, they acquire a strong kinetic energy, so strong as to be able to ionize the neutral gas molecules. Furthermore, the newly charged particles ionise other molecules, and this generates an avalanche-like process leading to formation, across the electrodes, of the so called “streamers”, which are channels of conducting plasma, with an electrical resistance of virtually zero.

If a liquid is pure, its breakdown mechanism is very close to that of a gas. If a liquid contains some impurities, which are liquid in the form of droplets, with a permittivity greater than that of the main liquid, the breakdown is caused by the generation of ellipsoids issued from these drops. For particularly strong fields and a high conductivity path, these elongated droplets can coalesce. At that point, an increase in the current, and consequently of the temperature in the channel, is measurable. This causes the liquid to boil, and it would be then the current through the steam canal that causes the breakdown. Such a formation of conductive channels is also observed in liquids contaminated with solid impurities. Breakdown can also result from gas impurities in the form of small bubbles. These can generate a localised heating of the fluid due to a local increase of the current density. This can bring the liquid to the boil. Then the size of the gas bubbles increases, they can merge, and a gaseous channel can form. At that point the breakdown medium is once more the gas plasma (Von Hippel, 1954).

2.5 THE MECHANICAL EQUATIONS

2.5.1 THE CONSERVATION OF MASS

The principle of mass conservation states that the decrease over time of the mass in the volume enclosed by the surface must be equal to the flux of mass through the surface:

$$\int_v \frac{\partial \rho_m}{\partial t} dv + \int_S \rho_m u \cdot n dS = 0 \tag{2-59}$$

Where **n** is the unitary vector normal to the surface S, *v* is the volume, **u** is the fluid speed and ρ_m is the fluid density. Applying Gauss's theorem, the expression for every control volume become:

$$\frac{\partial \rho_m}{\partial t} + \nabla \rho_m \cdot u = 0 \tag{2-60}$$

For isentropic flows, pressure and density variations are related as:

$$\frac{d\rho_m}{dt} = \left(\frac{\partial \rho_m}{\partial p} \right)_s \frac{dp}{dt} = \frac{1}{c_s^2} \frac{dp}{dt} \tag{2-61}$$

where p is the pressure, c_s is the velocity of the sound in the fluid and the ratio $(\partial\rho_m/\partial p)_S$ indicates compressibility of the fluid in iso-entropic conditions. Taking $\rho_m(l/\tau)^2$ as the scale for the pressure, we have $\Delta\rho_m/\rho_m \approx (u/c_s)^2$. As consequence, if the fluid speed is much smaller than the sound speed ρ can be considered as a constant and the mass conservation reduces to:

$$\nabla\cdot\mathbf{u} = 0 \tag{2-62}$$

2.5.2 THE CONSERVATION OF MOMENTUM AND THE NAVIER-STOKES EQUATION

The example of a closed surface through which the fluid is flowing shall be examined. The decrease with time of linear momentum must be equal to the flux of momentum dragged by the fluid through the interface plus the rate of change of momentum due to volume and surface acting upon the fluid. This is another way to express the symmetry with respect to the space of the Newton's second principle:

$$\int_v \frac{\partial \rho_m u}{\partial t} dv + \int_S \rho_m u(u\cdot n)dS = \int_v f dv + \int_S f_s dS \tag{2-63}$$

where **f** is the force per unit volume and $\mathbf{f_s}$ is the force per unit area acting on S.
The surface force $\mathbf{f_s}$ can be calculated expressing a mechanical tensor σ^M_{ij} with:

$$f_{si} = \sigma^M_{ij}\, n_j \tag{2-64}$$

the surface force density.
The majority of fluids are characterised by the constitutive equation:

$$\sigma^M_{ij} = -p\delta_{ij} + \sigma'_{ij} \tag{2-65}$$

where p is the hydrostatic pressure, which in the case of the fluid does not depend on the particular orientation of dS; δ_{ij} the Kronecher tensor, that is always equal to 0 except when i=j, when it is equal to 1. For a Newtonian fluid:

$$\sigma'_{ij} = \eta\,[\partial_j u_i + \partial_i u_j] + (\lambda - 2/3\,\eta)\,\partial_l u_l\,\delta_{ij} \tag{2-66}$$

with η and λ the first and second coefficient of viscosity, and ∂_i the tensorial expression of the operational ∇.

Applying Gauss's theorem, and applying mass conservation theorem, the equation can finally be written as:

$$\rho_m \, \partial_t u_i = \partial_j \, \sigma^M_{ij} + f_i \, \delta_{ij} \tag{2-67}$$

where $\partial_t u_i$ corresponds to $\partial \mathbf{u}/\partial t$ in vectorial notations, and $\partial_j \, \sigma^M_{ij}$ is a vector representing the divergence of the tensor σ^M_{ij}. Substituting the constitutive equation of the fluid into the expression above, and deriving, supposing η and λ constants, the Navier-Stokes equation is obtained.

The equation for incompressible fluids reduces to:

$$\rho_m \, \partial \mathbf{u}/\partial t = -\nabla \mathbf{p} + \eta \nabla^2 \mathbf{u} + \mathbf{f} \tag{2-68}$$

Where **f** is the ensemble of all the external volume forces. In electrohydrodynamics it can be expressed as:

$$\mathbf{f} = \mathbf{f_e} + \rho_m \, \mathbf{g} \tag{2-69}$$

Where $\mathbf{f_e}$ is the electric forces on an infinitesimal volume and $\rho_m \mathbf{g}$ the gravity force, with g the gravity acceleration (9.81 m/s^2).

2.5.3 THE MAXWELL'S STRESS TENSOR AND THE ELECTROSTATIC FORCES ACTING ON A BODY EXPOSED TO AN ELECTRIC FIELD

A force $\mathbf{f_e}$ acting on a finite volume V can be represented as a stress applied to the surface S of the volume. This consideration is a direct consequence of the conservation of linear momentum that imposes that the rate of change of momentum inside a volume is represented as the momentum flowing through its surface.

Considering a system of stationary charges inside a volume V, placed in an electrostatic field, in vacuum, and assuming that no free neutral dielectric materials exist in the volume, the following identity (written in tensorial notation) has been demonstrated (Goranovic, 2003):

$$f_{ei} = \int_v q E_i \, dv = \int_S T^E_{ij} \, n_i \, ds \tag{2-70}$$

Where f_{ei} is the resultant force applied on the volume v, q is the free charge, E_i is the electric field, and T^E_{ij} is the electrostatic part of the so called Maxwell stress tensor, that can be specified, in Einstein notation as:

$$T^E_{ij} = \varepsilon_0 E_i E_j - 1/2\ \varepsilon_0 E^2 \delta_{ij} \tag{2-71}$$

The electrical force acting on a unit area of the unit area of the volume in vector notation then becomes:

$$\mathbf{f_s^e} = \varepsilon_0 (\mathbf{n}\cdot\mathbf{E})\mathbf{E} - 1/2\ \varepsilon_0 E^2 \mathbf{n} \tag{2-72}$$

Expressing the field in terms of normal and tangential components with respect to the surface:

$$\mathbf{E} = E \cos\theta\ \mathbf{n} + E \sin\theta\ \mathbf{t} \tag{2-73}$$

where θ is the angle between the vectors **n** and **E**, and **t** is the unitary vector tangent to the surface S. It is possible to demonstrate that:

$$\mathbf{f_s^e} = 1/2\ \varepsilon_0 E^2 (\cos 2\theta\ \mathbf{n} + \sin 2\theta\ \mathbf{t}) \tag{2-74}$$

The equation shows that **E** always bisects the angle between the stress and the normal.
The interactions calculated above, as we have seen, are only appropriate in the free space. Consequently, as discussed by Goranovic (2003), it is an important aspect worthy of attention. In the early days of electromagnetism, Maxwell and Faraday considered these stresses as associated to the ether deformation. It has since been demonstrated that the electric fields are primary quantities, and that electromagnetic waves do not need any media to propagate in, because it is the electromagnetic field itself that vibrates supporting the electromagnetic wave propagation. In that sense, this stress formula became more a mathematical convenience than an (essential) physical reality.
A similar approach can be considered when evaluating the electrostatic stress acting on a real dielectric. As in the free space case, the electrostatic force on a volume of dielectric can be equalised to the surface force acting on the boundary surface of the volume and can be calculated integrating an analogous stress tensor.

$$\int_v f_i\, dv = \int_S \sigma_{ij}\, n_i ds \tag{2-75}$$

In this formulation it can also be proved that:

$$f_i = \partial_i \sigma_{ij} \tag{2-76}$$

There are several approaches to determine the stress tensor σ_{ij} in dielectrics. The most general method is described by Landau and Lifshitz (1960) in the following expression:

$$\sigma_{ij} = -P_0(\rho_m,T)\delta_{ij} - 1/2\ \varepsilon_r\varepsilon_0\ [1 - \rho_m/\varepsilon_r\ (\partial\varepsilon_r/\partial\rho)_T]\ E^2\ \delta_{ij} + \varepsilon_r\varepsilon_0 E_i E_j \tag{2-77}$$

where $-P_0(\rho,T)$ is the pressure exerted on the dielectric when E=0. Therefore the electrostatic part of the tensor results in:

$$\sigma^E_{ij} = -1/2\ \varepsilon_r\varepsilon_0\ [1 - \rho_m/\varepsilon_r\ (\partial\varepsilon_r/\partial\rho_m)_T]\ E^2\ \delta_{ij} + \varepsilon_r\varepsilon_0 E_i E_j \tag{2-78}$$

Considering ε=1, it is possible to recover the Maxwell's stress tensor in vacuum T^E_{ij}. Differentiating the upper equation for uncompressible fluids, it is possible to get the force for unit volume:

$$\mathbf{f} = -\nabla[P_0 - 1/2\varepsilon_0 E^2 \rho_m\ (\partial\varepsilon_r/\partial\rho_m)_T] - 1/2\varepsilon_0 E^2 \nabla\varepsilon_r + q\mathbf{E} = -\nabla P_0 + \mathbf{f^e} \tag{2-79}$$

The first term is a pressure term, which considers any external pressure acting on the fluid and the electrostriction effect, which can be considered, for an uncompressible fluid, as an additional pressure term. The last two terms describe the only two effects able to create continuous motion in a fluid, a gradient in permittivity (often associated with thermal gradient) and the presence of a free charge density q in the dielectric.
The electromechanic force results then in:

$$\mathbf{f^e} = q\mathbf{E} - 1/2\varepsilon_0 E^2 \nabla\varepsilon_r + \nabla P_{st} \tag{2-80}$$

with ∇P_{st} the electrostrictive contribution.
And the Navier-Stokes equation, take the final form, for EHD systems (Castellano, 1998):

$$\rho_m\ \partial\mathbf{u}/\partial t = -\nabla p + \eta\nabla^2\mathbf{u} + q\mathbf{E} - 1/2\varepsilon_0 E^2 \nabla\varepsilon_r + \nabla P_{st} + \rho_m\mathbf{g} \tag{2-81}$$

2.5.3.1 Heuristical explanation of the Maxwell's stress tensor in a dielectric

When a fluid is exposed to an electric field, a net motion can arise in the bulk when an unbalanced net charge exists (Melcher and Taylor, 1969). As seen in section 2.5.3, the force exerted on an elementary volume can be calculated as:

$$f_e = qE - \frac{1}{2}E^2\nabla\varepsilon_l + \frac{1}{2}\nabla\left(\rho_m \frac{\partial\varepsilon_l}{\partial d_l}E^2\right) \qquad (2\text{-}82)$$

where q is the volume charge density, E is the actual electric field, ε_l is the dielectric constant of the fluid, d_l is the density of the fluid. The first term is the force exerted on the free charge, and the second is the force due to a gradient of permittivity (normally associated with a gradient in temperature, composition or density). The third term considers an electrostrictive contribution and can be neglected in non-compressible fluids. These first two force terms can generate a continuous motion of the fluid.

A physical description of the first term can be given pointing out that any free charge in a liquid experiences a Coulomb force. This force imposes a charge drift characterised by a given mobility. Due to the viscous interaction in the fluid, the drifting ions can transfer a given kinetic energy to the fluid. This results in an electromechanical force acting on the liquid, with a consequent motion generation. What is important to obtain a movement is to have a net flux of charge in a preferential direction. In electrolysis for example, despite a huge amount of ions moving, no liquid motion is observable. This is due to the absence of a net free charge flux (Felici, 1971).

The second term becomes very important when thermal gradients exist in the fluid, and it is the basics of electrothermal motion. In the present study this term has not been considered, because it was irrelevant for comparison with the effects due to the first term.

When paying more attention to the first term of the equation (2-82), the free space charge necessary to generate a liquid instability can be originated at least in two ways: a double layer (DL) or a charge injection.
The double layer is very often exploited in the electromechanical activation of a dielectric liquid. The phenomenon is called electro-osmosis, and is a common phenomenon in DC in uniform and non-uniform electric fields and in AC only in non-uniformly electric fields. The injection is a phenomenon introduced in section 2.4.2 and is particularly interesting in the present study. In some circumstances and particularly for high levels of electric field it is possible to have an injection of charge through one

or both of the electrodes. This generates a free space homocharge, in the vicinity of a very high electric field area of the electrode which results in a liquid motion.
The electrohydrodynamic instabilities have seen interesting technological applications (e.g. Atten 1996b; Lacroix et al., 1975; Jacobson et al., 1999; Studer et al., 2002).

2.5.3.2 Instabilities due to charge injection through a needle tip: the electric wind and the EHD plume

As a result of the application of a voltage in a dielectric fluid, between a tip and an opposite plane electrode, if the field is high enough, ions can be injected into the liquid through the needle electrode. If the phenomenon happens in air such an injection is also called "corona" injection. The Coulomb force q**E** applied by the electric field **E** on the injected space charge q, can generate an instability, and consequently a fluid motion (Adamiak and Atten, 2004; Atten et al., 2002; 2004; Honma and Ohyama, 2000).

This effect can be quantified introducing the parameter M, which is defined as the ratio between the hydrodynamic turbulent mobility $k_H=(\varepsilon/\rho_m)^{1/2}$ (obtained from the balance between electrostatic energy density $(1/2)\varepsilon E^2$ and kinetic energy density $(1/2)\rho_m u^2$) and the true mobility k of charge carriers:

$$M=(1/k)(\varepsilon/\rho_m)^{1/2}= k_H/k \qquad (2\text{-}83)$$

In gases the normal condition at atmospheric pressure is M<<1 (for example, in air k_H = 2.6cm^2/(Vs) and k ≈ 2cm^2/(Vs), while in liquid M is always larger or much larger than 3 (Atten et al., 1996a; 1997a).

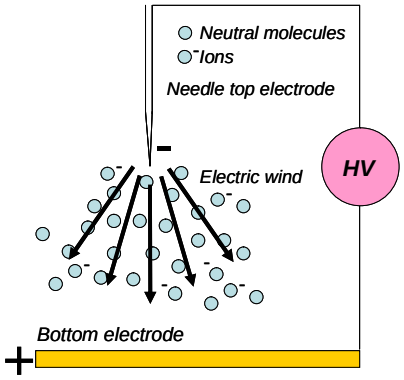

Figure 2. 20: Schematic representation of a corona injection

As a consequence, in a gas the ions created have a drift velocity k**E** (with k the ion mobility) considerably higher than the air velocity (electric wind) induced by the force q**E**. In that case the problem can be divided into two simpler problems, because the boundary electrical problem is completely uninfluenced by the aerodynamic motion, and the aerodynamic problem can be solved only by considering the force distribution q**E**, derived from the solution of the electric problem.

The problem in the case of the liquid is more complicated. The velocity of the fluid is considerably higher than the drift velocity of the ions. In this configuration the hydrodynamic problem can not be separated from the electrostatic one. The ions do not move anymore following the field lines, but a plume-like jet instability is generated. Injection is characterised by a transient:

$$t_i = 0.787 t_0 \tag{2-84}$$

where t_0 is the transient time characteristic at which saturation occurs, and it is calculated using the following expression:

$$t_0 = h^2/kV \tag{2-85}$$

where h is the distance between the electrode, and V it is the applied voltage (Tobazeon, 1984).

Experimental observation showed that injection starts above a certain threshold voltage V_{th} (Coelhot and Debeau, 1971), and the injection follows a law like:

$$I = A\,(V-V_{th})^2 \tag{2-86}$$

A major issue in the characterisation and modelling of the plumes is the knowledge of the electric field inside. When a plume exists, the electric field distribution is no more the one predicted by the Durand (1966) formula. Considering that an extensive discussion related to this argument is beyond the scope of this thesis, as an initial approximation, it makes sense to assume that the field in the presence of a plume would be reduced to a threshold value lower than E_{max} near the tip, and that the field would be bigger with respect to that predicted by Durand near the bottom flat electrode. This because reasonably, the big amount of charge sprayed through the tip on the bottom electrode does not discharge instantly on the bottom electrode. Then a heterocharge accumulation can build on the bottom electrode, with a resulting local increase in the electric field.

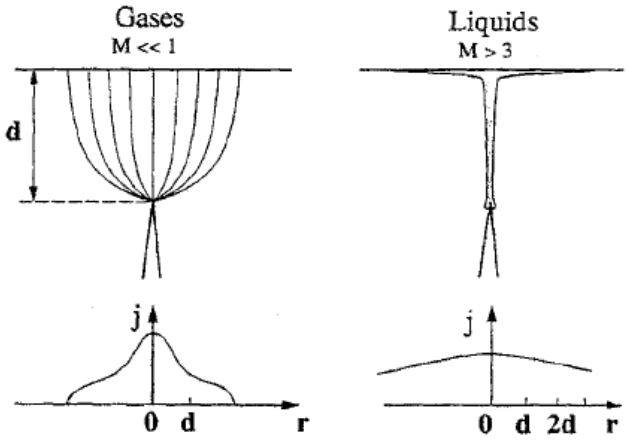

Figure 2. 21: (a) Gases: the ions follows practically the field lines and the current density is concentrated on a finite area of the flat electrode. (b) Liquids: the liquid flow takes the configuration of a plume and the ions are transported by the liquid around the axis of symmetry of the needle. When the ions reach the flat electrode the plume spreads out (Atten et al., 1997a)

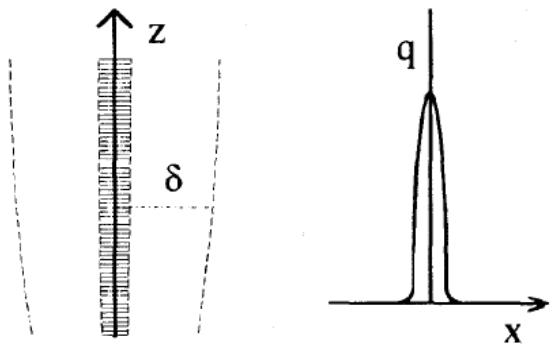

Figure 2. 22: Charge density profile for a laminar EHD plume (Atten et al., 1997a)

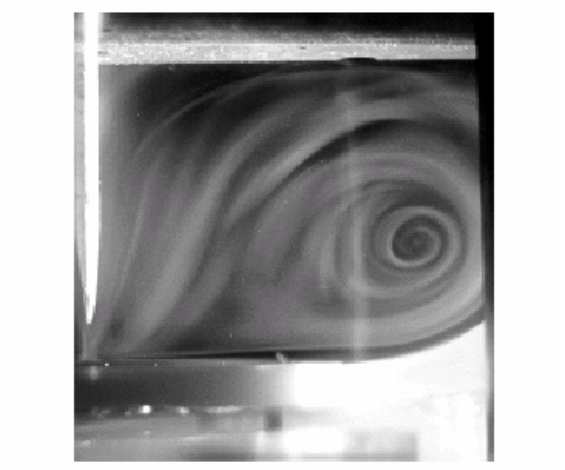

Figure 2. 23: Steady structure of the velocity field of the electric wind occurring in air when a corona injection exists. The photograph reports the incense smoke repartition in a vertical slice of the vessel V=5kV I=6μA (Batina et al., 2001).

2.5.4 JUMP CONDITIONS AT THE INTERFACE

From the tensor equations (2.77) and (2.78), already written in section 2.5.3, the electromechanical equilibrium of the interface can be written.

The forces at the two sides of the interface are equal and opposite. The following can be stated in terms of stress tensor σ^{M}_{ij}:

$$[\sigma^{M}_{ij}]_{21}\, n_j = 0 \qquad (2\text{-}87)$$

Considering an unified general pressure term P_0', containing all the effects opposite to the electrostatic forces, including in this generalised pressure also the electrostrictive term, and finally splitting **E** into the two components tangent (E_t) and normal (E_n):

$$P_0' = -P_0(\rho_m,T)\delta_{ik} - 1/2\ \varepsilon_r\varepsilon_0\ [1 - \rho_m/\varepsilon_r\ (\partial\varepsilon_r/\partial\rho_m)_T]\ E^2\ \delta_{ik} \qquad (2\text{-}88)$$

it is possible to get the normal stress as (Goranovic, 2003) :

$$[P_0']_{21} = [1/2\ \varepsilon\ (E_n^2 - E_t^2)]_{21} = 1/2\ [\varepsilon E_n^2]_{21} - 1/2\ E_t^2[\varepsilon]_{21} \qquad (2\text{-}89)$$

and the tangential stress (Goranovic, 2003):

$$[E_t D_n]_{21} = E_t\ [D_n]_{21} = -E_t\ q_s \qquad (2\text{-}90)$$

Where D_n is the normal component of the **D** vector. Spliting the P_0' into its different components, for the normal direction the general expression can be derived:

$$n_i\ [2\eta e_{ij}]_{21}\ n_i - [p]_{21} - [P_{st}]_{21} + 1/2\ [\varepsilon E_n^2]_{21} - 1/2\ E_t^2[\varepsilon]_{21} = \gamma\ (1/R_1 + 1/R_2) \qquad (2\text{-}91)$$

and for the tangent:

$$s_{Ii}\ [2\eta e_{ij}]_{21}\ n_i + q_s\ s_{Ii}\ E_{ti} = 0 \qquad I = 1,2 \qquad (2\text{-}92)$$

where $e_{ij} = 1/2\ (\partial u_i/\partial x_j + \partial u_j/\partial x_i)$, it is the deformation rate of the infinitesimal element, and s_{Ii} is the unitary tensor containing the informations relatives to the tangential directions respect to the element of surface.

In order to have a complete set of equations to model the EHD system, also the kinematic conditions of the interface should be specified:

$$v_n\mathbf{n} \cdot \nabla F + \partial F/\partial t = 0 \qquad (2\text{-}93)$$

where $F(\mathbf{r},t) = 0$ is the implicit function defining the interface shape, and u_n is the normal speed. Such a definition excludes cavitation at the interface, and does not take into consideration eventual tangential speed of the particles at the interface.

2.6 FINITE ELEMENT ANALYSIS

Due to the difficulty of solving the Poisson equation in an analytical way, to solve the electrical boundary problem, a series of finite elements analyses was conducted. To carry out the computation two different codes were used.

2.6.1 FEMLAB

FEMLAB 3.1 is a code written and commercialised by Comsol, able to design and solve complete three-dimensional (3D) problems. This code, written in Java, has the advantage of being very user friendly and very versatile in terms of post processing treatment of the simulations. This code was used as a tool to solve partial differential equations. The user has the opportunity to define the system of differential equations he wants to solve, and the code, using the finite element modelling (FEM) calculation method, calculates the solution. Unfortunately, the matrix inversion uses up a great deal of memory, and the code becomes unreliable for problems involving a lot of elements, in particular if in 3D. Moreover, this code has a very low ability to "parallelise" the solution process.
FEMLAB also proposes a multi-physics approach that allows users to evaluate very heterogeneous problems, in conditions very close to reality, having a pre-designed set of equations for some canonical physical problems.

2.6.2 MAXWELL

Maxwell SV is a bi-dimensional (2D) electric field solver, able to solve problems with planar or axial symmetry. The code is distributed by Ansoft free of charge (Ansoft Corp., US). The numerical methods and algorithms used by the program are not in the public domain. Although the program has been termed a FEM solver, some extra-routines would be probably be needed to allow some boundary conditions, such as the "balloon" condition, which assumes a boundary placed at infinity. In contrast to FEMLAB, this program is not a multi-physics solver and the user does not have the

possibility of inserting a user defined equations system. Maxwell SV is only a solver of electric fields, and the user can only choose between a few different solver modes:

- *Electrostatic*: gives the solution of the Laplace's equation:

$$\nabla^2\Phi = 0 \qquad (2\text{-}94)$$

  Where ∇^2 is the Laplacian operator and ϕ is the function potential. This means that we have a solution to electrostatic problems only considering the dielectric properties of materials and charge distribution; it is the solution in the hypothesis of no free charge. This solution gives the limit for infinite frequency, once any conduction phenomena are relaxed.
- *Conduction*: solves the DC case only with respect to the materials conductivity.
- *Other solvers*: give solutions related to magnetostatic fields, and Eddie's current computation, related to a time varying field with frequency high enough to invalidate the hypothesis of electroquasistatic field (see section 2.2); these solvers are less interesting for applications required for this thesis.

Maxwell uses an adaptive mesh generation to make the space discretisation, where the program determines automatically how to increase the mesh density, trying to minimise the total potential energy error. Moreover the system is able to calculate the matrix of impedance and to execute a series of post-processing operations to calculate, for example, the Maxwell stress tensor. However, the electrostatic force can also be computed using the principle of virtual works. In the electrostatic solver, at the same time that the adaptative meshing process progresses, the force on a specified object is calculated as a derivative of the electrostatic energy in respect to the displacement ds:

$$F = dW/ds \qquad W = 1/2 \int_v E \cdot D \, dv \qquad (2\text{-}95)$$

Where W is the electrostatic energy.

This calculation is correct if we suppose the absence of any dissipative mechanisms due to current flow.

A 3D version of Maxwell (Maxwell 11) has also been used to solve some 3D geometry questions. Some tests, carried out on canonical problems, showed absolute correspondence between the solutions achieved with the 2D and 3D versions.

Chapter 3

THE ELECTROHYDRODYNAMICS OF RIGID BODIES: A REVIEW

This chapter contains all the principles relative to the behaviour of a particle, or a system of particles, in an electric field. The chapter reports a detailed description of the previous work with a critical organisation of the most important concepts.

3.1. THE EHD MODEL AND ITS APPLICATION TO THE DYNAMICS OF PARTICLES

The present chapter shall illustrate the dynamic of an isolated single particle, or a group of particles in an electric field.

As already introduced in section 2.1, all the electrohydrodynamic models described in chapter 2 are still reliable in the solution of the forces acting on particles exposed to an electric field. The body force can be calculated as:

$$F = \int_S \sigma_{ij}\, n_j\, dS = \int_S (\sigma^M_{ij} + \sigma^E_{ij})\, n_j\, dS \qquad (3\text{-}1)$$

where σ_{ij} is a tensor having a mechanical (σ^M_{ij}) and an electrostatic (σ^E_{ij}) component.

Nevertheless, the fact that the analysis is focused on non-deformable particles allows us to treat each particle as a rigid body, and their dynamics can be described by solving the equilibrium of forces and moments.

The main forces involved in the equilibrium of a rigid body are:

- gravity
- viscous interactions
- electrostatic interactions

In general the viscous interactions can be calculated by solving the Navier-Stokes equation.

The electrostatic forces can be calculated by solving the boundary problem, calculating the field distribution and then integrating the surface force using the Maxwell's stress tensor as:

$$\int_S \sigma^E_{ij}\, n_j\, dS = \mathbf{f_s^e} = \varepsilon_0\, \varepsilon_l \int_S [(\mathbf{n}\cdot\mathbf{E_l})\mathbf{E_l} - 1/2\, E_l^2 \mathbf{n}]\, dS \qquad (3\text{-}2)$$

When a particle is immersed in a surrounding medium without space discontinuities, for distances considered long relative to the particle dimensions, the electrostatic interaction can be considered in terms of:

a) Single particle Coulomb forces.
b) Single particle polarisation forces.
c) Orientation torque, in the case of elongated particles.

Moreover, if the particle is in proximity of a space discontinuity (e.g. an electrode, or another particle), other interactions appear, which can be modelled in terms of image forces.

If the bodies under examination have a simple canonical shape (e.g. sphere, ellipsoid, cylinder), some established solutions for the viscous and electrical problem are already available, and the equilibrium of the rigid body can be solved without having to solve a partial differential equation. Such a solution was extensively used in the present study, except when an analytical solution to the electrical problem was not available, in which case the electrostatic interactions was calculated by finite element modelling.

3.2. INTRODUCTION

The present chapter presents some fundamental concepts on the behaviour of particles exposed to an electric field. This knowledge is introduced to understand the experimental results presented in chapters 7 to 9, where the objective is to investigate the physical phenomena involved in the electrostatic micromanipulation technique introduced in chapter 1.

Trying to relate the electric field structuring (EFS) phenomenon to the most up-to-date knowledge on structuring and micromanipulations, it is possible to consider the process as an intermediary case between two limit cases:

1. the micromanipulation of a single particle (also correlated with the most general subject of the electrokinetics)

2. the pearl-chain forming and structuring of particles in suspension in a liquid (also correlated with the electrorheological effect)

In both cases the electric field induces a deterministic force able to break the isotropy (i.e. to induce a space organisation) of some heterogeneous systems in which at least one of the phases is a solid.

In the case of the manipulation of a single particle, the body control depends only on the electric field geometry, and the electric properties of the system. The particle is manipulated to obtain a relatively precise positioning, without any interaction with other particles. The driving force could be either the electrophoresis (DC), or the dielectrophoresis (AC, DC), or both (DC).

In the case of the structuring of a suspension of dielectric particles in a fluid. The system is dominated only by the mutual interactions between the particles. These interactions determine the formation of chain-like structures in the dispersion. Conversely to the case of micromanipulation, in this instance, the field promotes some asymmetries of the system (i.e. there is a breaking of the isotropy of the particle dispersion), but no control of the particle position can be achieved. A large part of the experimental work on this subject is related to the electrorheological (ER) effect.

The picture 3.1 shows finally that the EFS technique under development as part of the studies for this work is a hybrid case between the manipulation of a single fibre and the structuring of an ER suspension.

A needle-like electrode is used as a probe on a group of particles. As a result the filler is arranged to form a chain-like structure, as in the case of the ER suspensions, but now operating a precise control of the position, as in the case of the micromanipulation. The procedure described up to this point can be described as “micro-manipulation assisted by structuring”. Only one example of electric field structuring using a needle-plane configuration could be found in literature. Tang et al. (2003) used the dielectrophoretic structuring to align some carbon nanotubes to form fibre-like structures (figure 3.2).

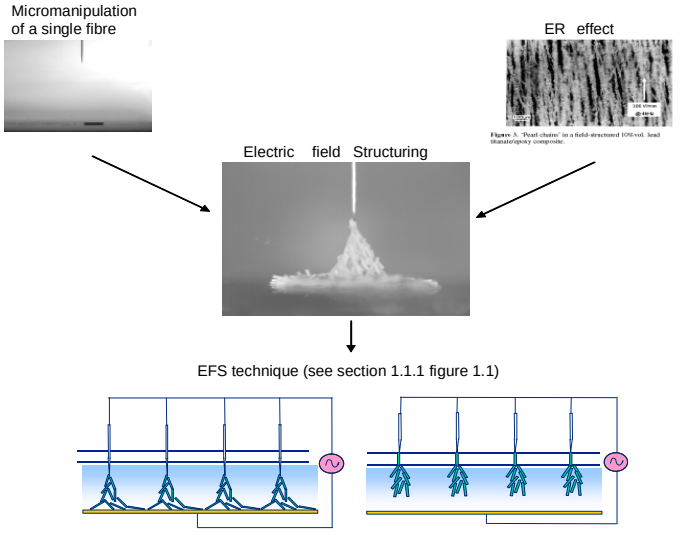

Figure 3. 1: This outline shows that the electric field structuring technique proposed by Wilson et al. (2000) is a hybrid configuration between the micromanipulation of a single fibre and an ER fluid

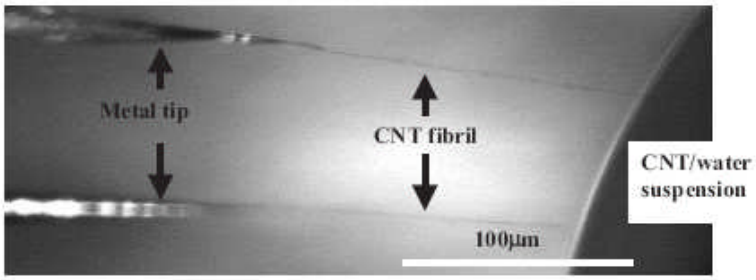

Figure 3. 2. CNT fibrils structures achieved by Jie Tang et al. (2003) using a needle like electrode

3.3. BEHAVIOUR OF A SINGLE PARTICLE IN AN ELECTRIC FIELD

3.3.1. INTRODUCTION

The motion of solid particles and small bodies exposed to an electric field has been observed for a long time, and it would be very difficult to define a starting date for the related studies. Although this phenomenon has been considered as a mere physical curiosity for many years, in the past 35 years the motion of solid particles in a uniform electric field, has been thoroughly studied, particularly in air, but also in vacuum and in dielectric oil (Felici, 1971). Many various branches of engineering are interested by these studies.

One particular focus is related to all high voltage applications involving the use of dielectric liquid or gas as insulator. The presence of solid particles in fluid dielectrics is responsible for a reduction of an order of dimension of the breakdown resistance, and for a consistent increase in the conductivity of the fluid.

Other important applications are the many techniques of granular material separation. Those techniques have been used for a long time in mineral elaboration and purification and are becoming more and more important in the treating and recycling of waste. All the separation techniques use an electric field to select and separate the materials on the basis of their electrical properties. The simplest kind of separator is based on the principle of charge induction (Cross, 1987). The granular material resting on a bottom flat electrode is exposed to an electric field. As a consequence of the electric field application, the metallic particles, only able to charge by induction on the electrode, move toward the opposite electrode and can be separated. In particular when the waste is mainly polymers, the mixture can be melted (Choi et al., 1999), and the conducting inclusions can be collected. Another electrostatic separator described by a different working principle is the corona electrostatic separator (Dascalescu et al., 1995; 1998; Delon, 1966). Waste, supported on a grounded electrode, is sprayed with charge via a corona injector. In this case, after the “charge-shower”, the insulator material becomes electrified and can be collected.

The other electrostatic technologies that can benefit from the knowledge of the particle trajectory in an electric field are printing, coating, filtering and electrostatic micromanipulation (see chapters 8 and 9) (Cross, 1987).

3.3.2. MECHANISM OF ELECTRIFICATION OF SMALL BODIES AND PARTICLES

3.3.2.1. Charging by contact potential difference

Contact electrification is a field free charging phenomenon happening when two metals are in contact. Thermodynamic equilibrium and solid band theory are used to explain this behaviour. Soon after two metals are put in contact, their Fermi levels line up and a contact voltage V_c is generated:

$$V_c=(w_{f1}-w_{f2})/e \qquad (3\text{-}3)$$

Where w_{fi} is the work function, and $e=1.6\times10^{-19}$ C is the elementary charge of the electron. The metal with the larger work function charges negatively. The contact potential for Cu and stainless steel is 0.2V.

When the two surfaces are separated, a tunnelling current is generated, so as to discharge the particle and to maintain a constant V_c on the particle. After a distance $z_{c,}$ in the order of nanometers (Lowell and Truscott, 1986c), the current interrupts, and the charge on the particle reaches a final value: $Q= V_cC(z_c)$.

The force acting on the particle can be evaluated using the expression considered by Russel (1909) (see section 3.3.4.1).

The description of the phenomenon is very similar for rough surfaces. The sphere/plane capacitance is of the same order of $C(z_c)$ between a smooth sphere and a smooth plane, but they are separated by a gap z_c , where z_c is the value of the averaged asperity height (Sternovsky et al., 2001).

3.3.2.2. Charging by contact between a metal and an insulator

The charge acquired from an insulator in contact with a metal is normally bigger than the one acquired by a metal, because no tunnelling effect exists. It can reach a value of between 10^{-5} and 10^{-3} C/m^2 (Lowell, 1986a; 1986b). The charge is normally motionless around the contact area. The electric field above an area of localised charge can reach a value of:

$$E=Q_S/\varepsilon_0(\varepsilon_r+1) \qquad (3\text{-}4)$$

This value can be bigger than the breakdown resistance of the dielectric medium (Harper, 1967).

Although in an insulator the conduction band is empty (i.e. it is almost equal to the vacuum level) and no charge transfer should be possible. Some localised electrons energy level can exist, due to lattice defects, impurities, and the presence of the surface. These defects are supposed to be at the origin of the insulators electrification. Experimental evidences showed the possibility to define an "effective" work function for insulators too. Triboelectric series have been made in this way Moore (1973).

A comprehensive theory of electrification mechanism is not available yet. Electron motion seems to be the charge mechanism in vacuum. The ionic charging has also been considered. Charge transfer times of ≈1s were observed in most of the cases. Repeated contacts can enhance the tribocharge (Lowell, 1984), probably because consecutive contacts increase the contact area (Lowell, 1986c;1988).

When two materials are in contact with each other, the more polarisable becomes positively charged. This statement is called the Cohen's law, and it is an empirical law that was proposed analysing a series of triboelectric series. Nevertheless, some exceptions exist to the general behaviour (Jonassen, 1998).

Considering the numerous experimental validations of the consideration that triboelectricity on solid is mainly due to electrons exchange, Cohen's law could be explained in terms of the Debye length. Considering that Debye length is inversely proportional to the permittivity means that an electrical perturbation created by the subtraction of an electron in a more polarisable material can be relaxed on a shortest space than one with a smaller permittivity. Therefore the increase of potential energy

induced by an unbalanced electron hole in a more polarisable material is smaller. Consequently, a more polarisable material can stabilise an electron hole better than a less polarisable one.

3.3.2.3. Charging by induction

Any particle having a finite conductivity and being at rest on an electrode affected by an electric field, acquires the potential of the electrode becoming charged by induction. The induction charge acquired by objects of different shape has been calculated by Felici (1966).

In the case of a particle with a resistivity ρ_p negligible comparing with the one of the hosting fluid and a permittivity ε_p considerably bigger than that of the fluid, the charging phenomenon has a time constant $\tau=\varepsilon/\sigma$ (Moore, 1973). For example, τ is about 20s for Alumina. In a real case scenario, any contact resistance can dramatically influence the charging time.

In a non uniform electric field, the charge acquired should be corrected multiplying by a factor K_Q depending from the field non uniformity ($K_Q<1$).

Table 3. 1 Expression of the induced charged (Q) on a conducting particle exposed to an electric field E, of the adhesion force (F_{adh}), and of the lift-off electric field (E_{th}), as calculated by Felici (1966), for different particles geometries.

	Sphere	**Cylinder**	
		Horizontal	*Vertical*
Q	$(2\pi^3/3)\varepsilon r^2 E$	$2\pi\varepsilon LrE$	$\pi[\ln(2L/r)-1]^{-1}\varepsilon L^2 E$
$\mathbf{F_{adh}}$	$0.168QE$	$0.285QE$	$(1-[\ln(L/r)-0.5][\ln(2L/r)-1]^{-1})QE$
$\mathbf{E_{th}}$	$0.494[R(\rho_p-\rho_l)g/\varepsilon]^{1/2}$	$0.836[r(\rho_p-\rho_l)g/\varepsilon]^{1/2}$	$[1-F_{adh}/(QE)]^{-1}[\ln(L/r)-0.5]^{0.5}[r(\rho_p-\rho_l)g/(L/r)\varepsilon]^{1/2}$

3.3.2.4. Charge acquired in a mono-ionised field

When a particle is immersed in a media characterised by a space charge, the particle acquires some charge from the mono-ionised field, and gets charged. Pauthenier (1932) calculated the maximum charge acquired by a sphere in this condition:

$$Q_{max} = 4\pi\varepsilon_l E_0 p\, r^2 \quad (3\text{-}5)$$

where p=3 (conductive particle), $p=(3\varepsilon_p/(\varepsilon_p+2\varepsilon_l))$ dielectric particle, E_0: externally applied electric field

Pautenier's computation of the maximum charge Q_{max} was calculated as the equilibrium between the charges attracted on the particle from the external field and the repulsion given by the charge already present on the particle. Pauthenier considers that conductive and dielectric particles charge in the same way, and that differences were only due to the electric field modification.
Following the same assumptions for a horizontal cylinder:

$$Q_{max}/L = 2\pi\varepsilon_l E_0 p\, r \quad (3\text{-}6)$$

p=2 (conductive particle), $p= (2\varepsilon_p/ (\varepsilon_p+\varepsilon_l))$ dielectric particle

and for a conducting vertical cylinder (approximating the cylinder with an ellipsoid) (Dascalescu et al., 1996):

$$Q_{max}= 4\pi\varepsilon_l E_0 r^2 e^3 \{(L/2r)\ln[(L/2r)+e_f]-e_f\}^{-1} \quad (3\text{-}7)$$

$$e_f = [(L/2r)^2-1]^{1/2}$$

To give an order of magnitude, if L=1.3mm and r = 96μm:
$Q_{max\ vertical} = 3.85\ Q_{max\ horizontal}$.

The rate at which the particle charges is expressed by the formula (Pauthenier, 1932):

$$dQ/dt= (Q-Q_{max})^2/(\tau\, Q_{max}) \quad (3\text{-}8)$$

where $\tau=4\varepsilon_l/(qk)$, q is the space charge density, and k the charge mobility.

3.3.2.5. Charge acquired in a bi-ionised field

Using the same assumptions, Pauthenier (1956) calculated the charge acquired by a particle in a bi-ionised electric field. In this case, if the flow of carriers of different signs

has the same magnitude, no net charge is deposed on the particle. On the contrary, when a mismatch exists in the carrier flux, it is possible for a particle to become charged. The particle charge at the equilibrium can be calculated as:

$$Q_{equilibrium} = Q_{max}\,[(1-f)/(1+f)] \qquad (3\text{-}9)$$

where Q_{max} is the saturation value for the mono-ionised field case (see section 3.3.2.4) and $f = (J-/J+)^{1/2}$, being J- and J+ the flux of negative and positive carriers respectively.

Moore calculated the charge time relationship:

$$Q = Q_{equilibrium}(1-e^{-\alpha t})/(1-[(1-f)/(1+f)]\,e^{-\alpha t}) \qquad (3\text{-}10)$$

where $\alpha = (J+J-)^{1/2}/(\varepsilon_l)$.

3.3.3. ELECTROHYDRODYNAMICS OF THE MOTION OF A PARTICLE IN A DIELECTRIC FLUID EXPOSED TO AN ELECTRIC FIELD

The first model for the electrostatic induced motion of a conducting spherical particle moving in a dielectric liquid, was proposed by Krasucki (1968). He claimed good agreement between his model and the current measured by House (1957) in n-hexane.

Birlasekaran and Darveniza (1972) examined the motion of an 800 μm diameter metallic sphere in transformer oil. Their results indicated that the charge was not proportional to the electric field. This observation was in conflict with the Krasucki (1968) model and Dakin and Hughes (1968) measures, although it confirmed those of Felsenthal and Vonnegut (1967).

Rhodes and Brignell (1971, 1972) examined the transport in test cell where “natural fibres” were observed. The particles were moderately insulating. The average speed was 10m/s, and the “dwell” time on each electrode was greater than 100ms. Birlasekaran and Darveniza (1972) measured the same “dwell” time on a glass sphere.

Felsenthal and Vonnegut (1967) measured the current due to conductive particles (diameter between 200 μm and 2mm) in a fluorinated liquid. They pointed out that the speed was directly proportional to the electric field E. They assumed that the charge

acquired by the particle Q', remained constant as the field changed. Moreover, the ratio Q'/r was constant. Felsenthal and Vonnegut defined a maximum effective potential:

$$V_0 = Q'/4\pi\varepsilon r \qquad (3\text{-}11)$$

for a spherical particle. They measured V_0 =16V in Freon 113. On the other hand, from their measures in n-hexane and transformer oil, it seemed that V_0 was dependent on R. Rhodes and Brignell (1972) measured V_0=12V in n-hexane. This value was taken, in contrast to the direct measure of charge they made, with an electrometer.

Bislasekaran (1991) published a study on the measurement of the charge on a single spherical particle. Although there was not much correspondence between experiments and theoretical predictions, Bislasekaran's study was particularly interesting because he was the first to consider a non linear variation between the drag coefficient and the Reynolds number. Unfortunately only the case of a conductive sphere of 1mm of diameter for a single gap is considered in this paper.

Tobazeon (1996) conducted a very exhaustive study of the electrohydrodynamic of metallic particles in a uniform electric field in an insulating white oil (see chapter 7). He evaluated two kinds of geometry, spherical particles and elongated particles. For both he measured the lift-off electric field. The measured values were in agreement with the ones predicted by Felici (1966) and with the one calculated using the "Charge Simulation Program" (a boundary finite element charge calculation code, developed by Levin and co-workers (1993)). Tobazeon characterised the dynamic of the particles' motion and modelled the behaviour with respect to the relationship between drag coefficient and Reynold's number. In particular Tobazeon showed that the directly proportional relationship between the speed and the electric field verified firstly by Vonnegut, and confirmed by other researchers, could be due to a variation of the drag coefficient, more than to a constant charge on the particle connected to a maximum effective potential. Tobazeon showed that because that series of data was obtained in an intermediate regime (Re=several hundreds), the Stokes formula was not valid anymore.

Tobazeon also analysed in depth the apparent charge of the particles, and the microdischarges produced by the particles approaching the electrode, and compared the results with experiments. Contrary to Bislasekaran, Tobazeon concluded that the particle does not lose a significant amount of charge during the travelling, i.e. no appreciable space charge effect was observed.

More recently, Asano et al.(1997a, 2000a) observed the motion of conductive spheres in silicone oil. They characterised the motion, using a high speed camera and monitoring the current at the same time. They observed that the charging phase on the electrodes was characterised by a certain "dwell" time. Some measures of acceleration showed an acceleration when the particle was detaching, and a deceleration approaching the arrival electrode. The charge acquired by the particle was also measured, and reported to be around 40-60% of the theoretical value. Unfortunately, the charge values Asano reported in were calculated using the Stokes formula, though the motion did not occur in a viscous regime.
Yatsuzuka et al.(1999) also calculated the charge integrating the current signal, but with no satisfying results. It is possible to identify at least two possible reasons:

a)as pointed out by Tobazeon after a series of simple fundamental theoretical analyses, the apparent charge measured integrating the current is physically only a fraction of the total charge carried by the particle;

b)following the draft of the experimental setup shown in their paper, the current was measured reading the voltage with an oscilloscope across a resistance of 1MΩ. This is also the value of the internal resistance of the oscilloscope. Therefore this value can be affected by a current partition error.

3.3.3.1. The force equilibrium

The equilibrium of the forces acting on a charged particle in motion in a dielectric fluid and exposed to a uniform electric field can be written as:

$$\mathbf{F_C} - \mathbf{F_D} \pm \mathbf{F_w} = m_i\mathbf{a} \qquad (3\text{-}12)$$

Where F_w is the weight force considering the buoyancy ($F_w = (m_p - \rho_l v)\, g$), F_D the drag force, F_C the Coulomb force ($\mathbf{F_C} = Q\mathbf{E}$), and $m_i\mathbf{a}$ the inertial force, where $\mathbf{a}$ is the acceleration, and m_i is the inertial mass. The inertial mass takes into account both, the body mass, and the mass of the fluid dragged into motion by the particle. Normally:

$$m_i = v(\rho_p - \underline{K}\,\rho_l) \tag{3-13}$$

where v is the particle volume, ρ_p the particle density, ρ_l the liquid density, and $\underline{K}$ a coefficient of shape. $\underline{K}$=0.5 for a sphere, $\underline{K}$=1 for a cylinder moving perpendicular to its axis, and $\underline{K}$<0.2 for a cylinder moving parallel.

The drag force is generally expressed as:

$$F_D=(1/2)C_D S\rho_l\, sign(u_r)u_r^2 \tag{3-14}$$

where C_D is the drag coefficient, S the resistant section (a circle for the sphere and the cylinder moving parallel to its axis, and a rectangle for a cylinder moving perpendicular to its axis), u_r the relative speed of the body in respect to the fluid, and $sign(u_r)$ a function assuming returning a number with module 1 and sign opposite to u_r.

In presence of EHD motion:

$$u_r=u_{EHD}-u_p \tag{3-15}$$

where u_p is the speed of the particle, and u_{EHD} is the EHD motion speed.

The drag coefficient depends on the shape of the body and on Reynold's number ($Re=\rho_l u_r \phi/\eta$). It is possible to define three main behaviour regimes: a) a viscous regime (Re<1); b) an intermediate regime (1<Re<1000); c) an inertial regime (Re>1000). Only the viscous regime has been considered in this study since all the observed phenomena run at low Reynold's number.

For a sphere in viscous regime, $C_D=24/Re$, and drag force described by the Stokes formula:

$$F_D=6\pi\eta r u_r \tag{3-16}$$

For a cylinder moving perpendicular to its axis, it is possible to extrapolate from the experimental data in viscous regime $C_D=8/Re$ (Munson et al., 1996), and consequently:

$$F_D=4\eta L u_r \tag{3-17}$$

For a cylinder moving parallel to his axis:

$$F_D=(2\pi\eta L u_r)/[\ln(L/2r)+0.193] \tag{3-18}$$

In general, in the viscous regime F_D is directly proportional to the speed:

$$F_D=\kappa\, u_{r.} \tag{3-19}$$

Solving the differential equation of the equilibrium of a particle in the viscous regime, it is possible to express the instantaneous speed as:

$$u_p(t) = (\alpha\tau)[1-e^{-t/\tau}] \qquad \tau = m_i/\kappa \qquad \alpha=(QE \pm m_p g)/m_i \qquad (3\text{-}20)$$

When the transit time is a lot lower than the time constant τ, the particle moves linearly, increasing its speed with time. On the contrary if, as in the case of the present study, the transit time is a lot bigger compared with the time constant, the particle moves at the limit speed, practically on the whole gap.

These computations are exact only on the first excursion of the particle. After that the rebound effect should also be taken into account. The reader may learn more about this subject Tobazeon (1996), but one can say that in the condition in which the transit time $t_t >> \tau$, the rebound does not substantially modify the equilibrium.

Another fluid-dynamic effect that has been identified among the fluid-dynamic phenomena is a "history" effect that considers the previous disturbances in the fluid when a particle is moving. This could become important especially after the particle rebound. This effect will be not considered in this study (Clift et al., 1978).

3.3.3.2. The dielectrophoretic force (DEP)

When a particle is exposed to an electric field, it acquires a net polarisation. This happens both if the particle has a net charge or if it is neutral. As a consequence, if the field is not uniform, another interaction has to be taken into account: the dielectrophoretic force (DEP).

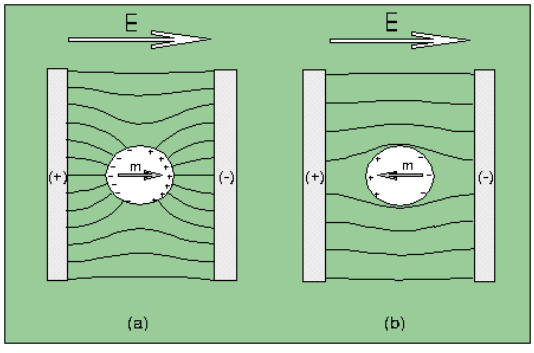

Figure 3. 3: Polarisation effect on matter in uniform electric field (Pethig, 1996)

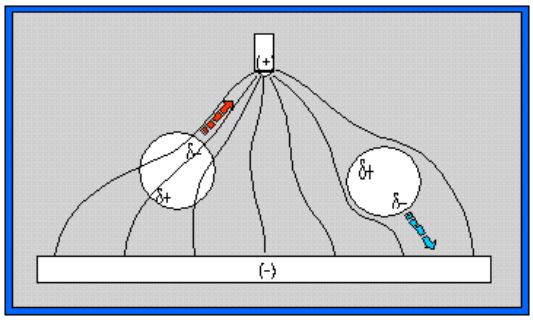

Figure 3. 4: Polarisation effect on matter in non-uniform electric field and dielectrophoretic effect. The two particles experience positive (left) and negative (right) dielectrophoresis. The difference is given by a positive (left) and a negative (right) value of Re[β].(Pethig, 1996)

As any other electrostatic interactions, also DEP force acting on a homogeneous particle immersed in a dielectric medium and exposed to a spatially non-uniform electric field can be calculated using the Maxwell-Stress tensor (see section 2.5.3). Obviously, to solve the integral it is necessary to know precisely the electric field, and consequently to solve the system of linear partial differential equations (PDE).

The effective dipole moment (Pohl, 1951; 1978) is a useful approach that gives a good approximation of DEP when the particle dimension is negligible compared to the distance from the electrodes, and the gradient of the field is so small that it can be considered constant across the particle dimension. With these approximations DEP can be calculated as the force exerted by the field E on $\mathbf{p}_{\mathbf{eff}}$, that is the polar moment induced on the particle itself by the electric field E:

$$\mathbf{DEP} = (\mathbf{p}_{\mathbf{eff}} \cdot \nabla)\mathbf{E} \qquad (3\text{-}21)$$

The simplification in the calculation arises from the fact that the moment $\mathbf{p}_{\mathbf{eff}}$, is calculated assuming that the field is uniform, and then, its value is inserted into the equation 3-21 to evaluate the force.

As already mentioned in section 2.3.1 which introduces the concept of complex permittivity, if a dielectric has some losses, the polarisation is not instantaneous. Consequently, the dipolar moment has to be expressed as the sum of a real and an imaginary part. Thereby, the most general expression for the DEP exposed to a periodic external field becomes:

$$\mathbf{DEP(t)} = (\mathrm{Re}[\mathbf{p_{eff}}e^{j\omega t}\cdot \nabla])\mathrm{Re}[\mathbf{E_0}e^{j\omega t}] \tag{3-22}$$

This expression results in a time dependent force. For a spherical particle of radius r and permittivity ε_p and conductivity $\sigma_{p,}$ immersed in a fluid of permittivity ε_l and conductivity σ_l, exposed to an external electric field E_0 the force can be expressed by:

$$\mathbf{DEP(t)} = 2\pi\varepsilon_l r^3 \nabla E_0^2 \left[\left(\frac{\sigma_p - \sigma_l}{\sigma_p + 2\sigma_l} \right) (1 - e^{-\frac{t}{\tau}}) + \left(\frac{\varepsilon_p - \varepsilon_l}{\varepsilon_p + \varepsilon_l} \right) e^{-\frac{t}{\tau}} \right] \tag{3-23}$$

Where τ is a relaxation time and depends from the interfacial polarisation:

$$\tau = \frac{\varepsilon_p + 2\varepsilon_f}{\sigma_p + 2\sigma_f} \tag{3-24}$$

This expression (Jones, 1995) can be decomposed into an oscillatory term at frequency the half of the external one (for fluid with normal conductivities and particles with dimension between 1μm and 1mm this term is practically always relaxed), and in the average term written below:

$$\langle \mathbf{DEP(t)} \rangle = 2\pi r^3 \mathrm{Re}[\beta(\omega)] \nabla E^2_{RMS} \tag{3-25}$$

Where E_{RMS} is the root mean square value of the electric field and β is the Clausius-Mossotti factor, calculated using the complex permittivities (see section 2.30):

$$\beta = \frac{\varepsilon_p^* - \varepsilon_f^*}{\varepsilon_p^* + 2\varepsilon_f^*} \tag{3-26}$$

and where the real part of this factor is:

$$\mathrm{Re}[\beta] = \frac{(\sigma_p - \sigma_f)}{(1 + \omega^2\tau^2)(\sigma_p + 2\sigma_f)} + \frac{\omega^2\tau^2(\varepsilon_p - \varepsilon_f)}{(1 + \omega^2\tau^2)(\varepsilon_p + 2\varepsilon_f)} \tag{3-27}$$

When Re [β] > 0 there is a positive dielectrophoresis, and the particle moves in the region where the electric field is stronger, the opposite when Re [β] < 0 and we have negative dielectrophoresis.

In the graphic below (figure 3.5) we show the plot of Re [β] for a PZT powder in deionised water.

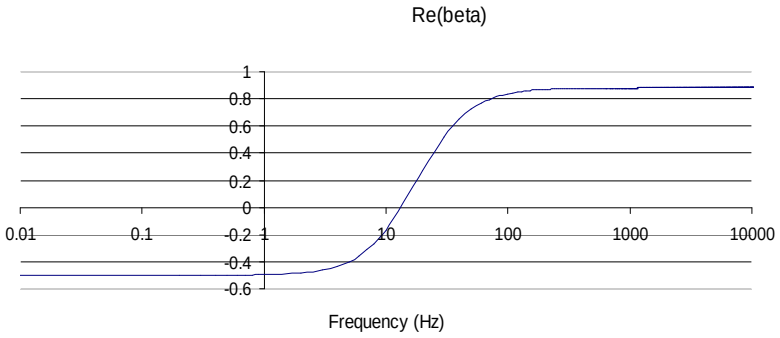

Figure 3. 5. Plot of Re [β] for a PZT powder in deionised water

When analysing the expressions for Re [β], one immediately notes the importance of the electrical characteristics of both the filler and the fluid, and how key it is to measure these properties with precision. This is a necessary condition to have a good prediction of the dielectrophoretic force.

Let us consider how the expression of the DEP changes if there is a lack in spatial uniformity in the phase factor (Xujing et al., 1997). This condition can be written, in spherical coordinates, as:

$$\mathbf{E_0} = \mathbf{E_i}(\mathbf{r})e^{j(\omega t+\varphi(\mathbf{r}))} \tag{3-28}$$

which ,using the Maxwell's stress tensor, becomes:

$$\langle \mathbf{DEP(\varphi_i)} \rangle = 2\pi r^3 \varepsilon_l \left(\mathrm{Re}[\beta]\nabla E^2_{RMS} + \mathrm{Im}[\beta](E_x^2\nabla\varphi_x + E_y^2\nabla\varphi_y + E_z^2\nabla\varphi_z)\right) \tag{3-29}$$

Where r is the position vector in polar coordinates, Ei the amplitude of the electric field and φ is the signal phase. This result can be particularly useful in analysing some anomalous behaviour where dielectrophoretic chaining of particles occurs (see section 9.3.4).

For the sake of completeness at the end of this review the expression of DEP in the case of elongated particles is reported. For a horizontal cylindrical particle the effective dipole solution neglecting any end effect is given by (Pohl, 1978):

$$\mathbf{DEP} = \pi r^2 L \varepsilon_l \mathrm{Re}[\beta_{pr}]\nabla E_{RMS}^2 \tag{3-30}$$

Where $\beta_{pr} = (\varepsilon_p^* - \varepsilon_f^*)/(\varepsilon_p^* + \varepsilon_f^*)$.

Moreover, for a prolate ellipsoid particle positioned with its major axis parallel to the electric field gradient, the force is given by (Jones, 1995):

$$\mathbf{DEP_z} = \frac{2}{3}\pi ab^2 \varepsilon_f \, \mathrm{Re}[\beta] \frac{\partial E_{z\,RMS}^{\;2}}{\partial z} \tag{3-31}$$

where a and b are the minor and major axis respectively, $\beta=(\varepsilon_p^*-\varepsilon_f^*)/[\varepsilon_p^*+(\varepsilon_p^*-\varepsilon_f^*)L_{\|}]$, and $L_{\|} \approx (b^2/a^2)[\ln(2a/b)-1]$

3.3.3.3. The orientation of a dielectric rod exposed to an electric field

In this section the orientation of an isotropic perfectly insulating fibre-like dielectric particle, exposed to an electric field is introduced. The orientation of an elongated particle should not be not confused with particle's rotation (ROT) in an electric field. Orientation torque also arises in ideal dielectrics, while rotation requires the material to have a conductivity. Sometimes both orientation and rotation can influence the motion of a real elongated particle, which produces the interesting orientation spectra of lossy elongated particles (Jones, 1995; Xujing et al., 1997).

A fibre-like dielectric particle can be modelled as an ellipsoidal particle with a major axis L, and the two minor axes equal to 2R. If this kind of particle is exposed to an electric field, it has the tendency to align with its major axis, in the same direction as the external field. This is due to the fact that normally the field inside the ellipsoid and the net dipole moment $\mathbf{p_{eff}}$ induced inside the particle is not aligned with the external field, unless one of the particle's symmetry axes is aligned with the external field. This means that the particle would experience a torque:

$$\mathbf{T} = \mathbf{p_{eff}} \times \mathbf{E} \tag{3-32}$$

that would tend to align the particle's lunger axis with the external electric field vector.
The dynamic problem presents at least two equilibrium positions. The first is the horizontal one. Is a position of unstable equilibrium, any minimum perturbation from the horizontal position induces a particle rotation. The second is the vertical position, which is a position of stable equilibrium. On the basis of these considerations we can say that a fibre-like dielectric particle, when exposed to an electric field, is in a stable

equilibrium under the condition that it is aligned following the flux line of the electric field.

For a fibre-like particle the torque expression can be expressed as (Jones, 1995):

$$T^e \approx \frac{2\pi r^2 L}{3}\varepsilon_1 E_0{}^2 \sin 2\theta \left[\frac{(\varepsilon_p - \varepsilon_1)^2}{[\varepsilon_1 + (\varepsilon_p - \varepsilon_1)L_\parallel](\varepsilon_p + \varepsilon_1)}\right]$$
$$L_\parallel \approx \frac{4r^2}{L^2}\left[\ln\left(\frac{L}{r}\right) - 1\right] \qquad (3\text{-}33)$$

where L is the particle length and θ is the angle between the major axis and the ground plane.

When the ellipsoid reaches the equilibrium position, the horizontal components of the field are zero, and the field is vertical.

The orientation phenomena in lossy particles and electro-rotation have not been considered in the present study, because in the range of frequencies analysed the material did not present any orientation phenomena deviating from the ideal behaviour.

The reader can find an extensive description of electro-rotation and orientation of lossy particle in (Jones, 1995; Asano et al.,1997b). These phenomena are normally related to the interaction between the imaginary part of the dipolar moment and the electric field.

3.3.4. BEHAVIOUR OF A SINGLE PARTICLE IN CONTACT WITH ONE OF THE ELECTRODES

3.3.4.1. Field free

When a particle rests on a surface, adhesion forces are generated. Van der Waals forces, surface tension forces, mechanical deformation of both the particle and the surface and chemical interactions are normally the main components of a phenomenon commonly called stiction. Moreover, as shown in section 3.3.2, due to different causes, a particle is normally not electroneutral. Consequently, an electrostatic term needs to be added to stiction.

The most common way to calculate the electrostatic adhesion between a particle carrying a certain charge and a metallic substrate, is to consider the charge concentrated in the centre of gravity, and the particle attracted by a symmetrical image charge of the opposite sign. Unfortunately, if the particle is a conductor, and the distance particle-plane reduces, this simplification fails. The charge on the particle is going to polarise, the charge barycentre moving toward the plane, and the hypothesis of circular potential lines is flawed. This problem was solved by Russel (1909) who calculated the capacitance between a plane and a sphere, and derived an expression of the force as the energy derivative rate of change in stored energy when the surfaces are separated:

$$F = (d/dz)\,(1/2\ CV^2) = (\pi\varepsilon r V^2)/d = Q^2/\{16\pi\varepsilon r d\,[\Psi + 0.5\ \ln(2r/d)]^2\} \qquad (3\text{-}34)$$

where d is the separation gap and Ψ is the Euler's constant (=0.577).

To give an order of magnitude, when a spherical particle of chromium (r=70μm) is 1μm far from a stainless steel plane (contact potential 0.25V) in silicone oil, the charge acquired by contact would be $Q=1.48\times10^{-14}$C (considering that the medium does not contribute to the contact potential). If the force were calculated considering a point charge in the centre the force would result 40.1pN, otherwise, if calculated with the Russel's formula, the force results 304 pN. A Maxwell FEM simulation of the force carried out an adhesion force value 247pN, very close to the Russel one. The simulation also showed that the electric field in the narrower part of the gap near the particle is of the order of 0.3MV/m.

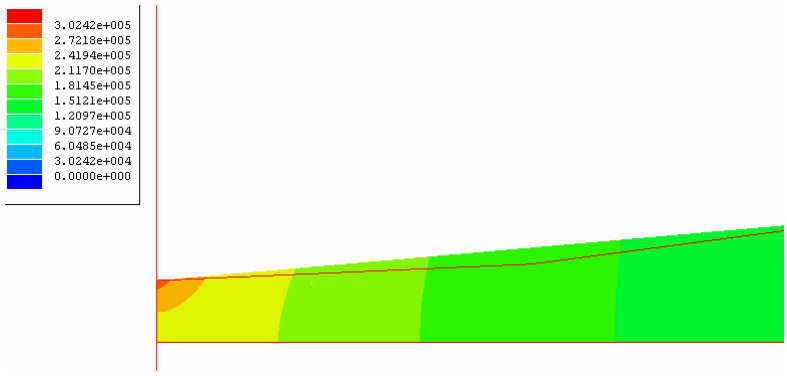

Figure 3. 6: Electric field distribution in the gap between a chromium particle and a stainless steel plane derived by the contact potential difference

The charge has also been FEM computed using FEMLAB, and the resulting value, 1.35×10^{-14}C, is very close to the theoretical one.

Even if the particle is an insulator, it is difficult to define a centre of charge of the particle. The tribocharge concentrates preferably in patches around the contact zone. Consequently, if the history of the particle is characterised by many contacts, its surface charge distribution (and consequently the charge centre) becomes too difficult to assess with precision.

Davis (1969) calculated the adhesion force on conducting and dielectric spheres, calculating the electric field around the sphere solving the Laplace equation in bispherical coordinates. He considered the case of a charged and of an uncharged sphere. He assumed that conducting and insulating spheres acted in the same way except for the different shapes of the electric field affected by the dielectric constant.

3.3.4.2. Applying an electric field

In this section the problem of the electrostatic adhesion of a particle resting on a flat electrode under the application of an electric field is discussed. The main models to evaluate the adhesion force and the electric field in the gap have been described for the most common cases of conducting and dielectric particles, with and without failure of the dielectric in the gap.

The research work in this thesis is focused on cylindrical rods at rest on a substrate, exposed to an electric field. Despite the great practical interest of such a problem, the case of a dielectric cylindrical particle has been given less attention than the sphere, as many analytical models are available. For this reason, this section reviews the models relevant to the spherical case. The results will be used to validate the series of FEM simulations carried out in section 7.1 to calculate the adhesion in the cylindrical case.

3.3.4.2.1. Conducting particles

As discussed in section 3.3.2.3, when a metallic particle is resting on an electrode affected by an electric field, the particle get charged by induction. As a consequence the particle experiences a Coulombic lifting force, and an image adhesion force. Felici (1966), using the images method, and other transformation methods, achieved a

numerical computation of the electrostatic force on small conductive objects of different shape (see table 3.1). In particular, the charge he calculated for the conductive sphere, was the same evaluated by Maxwell and confirmed by Jones (1985). Lebedev and Skal'skaya (1962) obtained the same results solving the problem in bi-spherical coordinates, and integrating the Maxwell stress tensor. It is interesting to observe that, in the case of the sphere, the image force is twice that experienced in a scenario where charge concentrated in the particle centre.

3.3.4.2.2. Dielectric particles perfectly insulating

If an uncharged perfectly insulating dielectric particle is at rest on an electrode affected by an electric field, the particle becomes polarised without acquiring any charge by induction. For this reason, there is no columbic lift force, only an image interaction due to the image multipoles. Despite its great practical interest and due to the mathematical complexity of the boundary problem, the problem of a dielectric sphere at a certain distance d from a grounded plane (or the equivalent problem of two spheres at a distance 2d from each other) exposed to an electric field, received much less consideration than the one of the perfect conductor. However the solution of two isolated conductive particles not carrying any net charge can give some useful indications. In fact, this solution is still available with standard methods and represents the upper limit of particle polarisability ($\varepsilon_p/\varepsilon_l \to \infty$). PZT and a metal can be considered as the two limit cases for the problem of the adhesion force. In the case of a metallic particle, the model is the one of isopotential perfectly conducting particles, and in the case of PZT, the model is the one of perfectly insulated conductor spheres (Jones, 1985).

An approximate solution for a dielectric particle was given by Jones using multipolar expansion. Davis (1969), Love (1975), Godin and Zil'bergleit (1986) analytically solved the problem in bispherical coordinates. Chen (1991) calculated the interparticle force using an expansion of spherical harmonics. Klingenberg et al. (1989) calculated the parallel and normal components of the interparticle forces as a function of permittivity ratios between the particle and the fluid. His calculation used the exact

solution from a multipole expansion solution to Laplace's equation. As expected no force exists for a permittivity ratio equal to 1, and with large values of that ratio, the force rapidly saturates to 80-90% of the value expected for conducting particles. Tao et al. (1995) used the FEM to calculate the interaction between two particles in an infinite chain aligned parallel to the electric field. Considering that there is no problem of convergence with the FEM, Tao et al. also calculated the result for two dielectric spheres in contact. This result was not achievable in the traditional analytical way due to the divergence of the solution to the boundary problem. Chaumet and Dufour (1998) solved the problem considering two conducting spheres of different size. Other important contributions belong to Robinson and Jo (1984) and Sanchis et al. (2004).

For the purpose of comparison, in table 3.2 a series of values of the adhesion force, calculated for a PZT spherical particle (r = 70μm) in silicone oil, and exposed to a field of 1.666MV/m for different gap values, is reported. It is remarkable as the Jones et al. (1995) multipolar expansion model gives a value of interaction bigger than the one calculated with the FEM by Tao et al. The values are both compared with the dipole-dipole approximation.

Table 3. 2 Comparison between the adhesion force acting on a PZT particle (R=70μm) in silicone oil, E=1.666MV/m, calculated using a dipole-dipole approximation, an analytical model (Jones, 1995), and a FEM model (Tao et al, 1995)

Model	d (μm)	F (μN)
Dipole-dipole (Coulson,1948)	0.5	1.38
	0.05	1.41
	0 (contact)	1.42
Jones (1995)	0.5	28.40
	0.05	170
Tao et al. (1995)	0.5	10.4
	0.05	105
	0 (contact)	8650

The dipole-dipole (Coulson, 1948) approximation is expressed by the formula:

$$\mathbf{F} = 12\pi\varepsilon r^2\beta^2\{[R/2(r+d)]^4[(3\cos^2(\theta)-1)\mathbf{e_r} + \text{sen}(2\theta)\mathbf{e_\theta}\} \qquad (3\text{-}35)$$

Where d is the gap between the particles, θ is the angle between the line joining the particles centres and the electric field vector, r is the particles radius, $\mathbf{e_r}$ and $\mathbf{e_\theta}$ are the unitary vectors in the polar coordinate system.
It represents the interparticle force without taking into account multipolar contributions. As expected, the dipole-dipole approximation appears to be underestimated for small gaps.
Opportunely substituting β with an appropriate β_e, normally depending on the ellipsoid eccentricity, this formula can also be applied to ellipsoids. As in the case of the sphere, the estimated force is correct only when the elongated particles are far from each other.

3.3.4.2.3. Dielectric particle with finite conductivity: current-controlled interparticle forces

The computation of the electrostatic adhesion of a dielectric particle on a substrate is a problem that can easily become divergent. If the gap dimension decreases and if the particle permittivity is very big, the electric field in the gap rapidly diverges, reaching values for which the hypothesis of perfect insulation of the dielectric fluid is no longer reliable. In this case a current pulse through the gap is established and a charge is deposited on the particle surface. This will reduce the electric field in the gap and the electric stress on the insulator. The particle can acquire a net charge and a lifting Coulomb force can be generated. If these mechanisms are suitable, the models considered in the previous section are no longer reliable for the description of the force acting on the particle. An image adhesion force still exists but has to be calculated using a current controlled adhesion model.

Some current controlled interparticle models have been created to calculate the interparticle force in electrorheological (ER) fluids exposed to a DC field. They provide the interparticle force between particles inserted in an infinite chain bridging the gap across the electrodes. Therefore, these models do not give any information about the charge acquired by the particle and its additional image, because the modelled structure is percolating and cannot retain any net charge. Nevertheless, these models deserve

consideration as they can give an example of how the interaction varies from the hypothesis of perfect insulator to the one of current controlled interparticle gap.

Arp and Mason (1977) gave an empirical expression for the electric field in the upper limit case of two insulated conducting spheres ($\varepsilon_p/\varepsilon_l \to \infty$):

$$E_{gap}/E_0 = (-2\pi^2/3)/\{(2d/r)\ln[(2d/r)/12.69]\} \tag{3-36}$$

In order to give an order of magnitude, if r =70μm, 2d=1 μm, E_0=1.666MV/m, the field in the gap would be: E_{gap}=113 MV/m (see fig.7.2).

McLean (1977) calculated the field across the interface assuming that there was a conduction current around the particle, and that the phenomena was controlled by a surface conductivity. The equations were solved numerically, taking into consideration a deformation of the interface according to Hertz's law. Dietz and Melcher (1978) recalculated the expression by analytical method. The results of the adhesion force were:

$$F \approx (0.415)\, 4\pi\varepsilon\, r^2 E_{max}^{\ 0.8}\, E_0^{\ 1.2} \tag{3-37}$$

Where E_{max} is the breakdown electric field.

Moslehi and Self (1984) carried out an analysis including volume and surface conductivity. They assumed that any non linear conduction process will tend to limit the gap field and weaken the dependence of the mutual force on E_0. A simple relationship like $F \propto E_0^{\lambda_{DM}}$ with $1.1 < \lambda_{DM} < 1.4$ was revealed to be a good prediction of the interaction (Robinson and Jones, 1984).

Wu and Conrad (1996; 1997) formulated a model considering that the fluid conductivity follows (2-53). In this model at low field the force increases with the electric field, but when the field in the gap reaches a value almost two orders bigger than E_c, the gap becomes conduction controlled, and the field becomes constant. The model shows good agreement with the experiments when $\sigma_p/\sigma_l > 10^3$.

The force is expressed by:

$$\begin{gathered} F = \pi\varepsilon\beta E_0^{\ 2} r^2 f \\ f = D_s(\Gamma/A)^{0.1}(E_c/E_0)^n \qquad \Gamma=\sigma_p/\sigma_l \end{gathered} \tag{3-38}$$

where D_s and n are two coefficients depending from the experimental conditions (e.g. for the case analysed in chapter 7: $D_s = 66$, $n = 0{,}92178/E_c^{0.05868}$)

The field in the gap:

$$E_f/E_0 = 1 + r/d \tag{3-39}$$

and the saturation field:

$$E_m = 30(\Gamma/A)^{0.1}E_c^{0.9}E_0^{0.1} \tag{3-40}$$

Two other conductivity models have been elaborated by Atten et al. (1993; 1994) and by Boissy et al. (1996). A first model that only considers an Onsager behaviour for the fluid conductivity is described by two expressions, respectively for low and high fields. These expressions showed a good agreement with a series of interparticle force measures, that the authors carried out at big scale (sphere diameter in the order of the mm), for values of σ_p/σ_l up to 10^3. Then the authors proposed a second model for σ_p/σ_l bigger than 10^3, giving more attention to the liquid conduction mechanisms. They considered two possible regimes of conduction in the limited gap area. The first, supposing a saturation current, and particularly valid for big scale phenomena, and the other, considering injection as the predominant conduction mechanism, for smaller scale.

As a matter of comparison, in this case too the adhesion force has been calculated for a spherical particle of PZT with radius 70 μm, in silicone oil, with an external field E=1.666MV/m, at different gaps, and different values of particle conductivity (see table 3.3). For the Wu and Conrad (1996) model, the values that the field and the force would have if the spheres were always equipotential are reported in squared brackets.

For the Dietz and Melcher (1978) model a range of values is proposed for different values of the exponent λ_{DM}. Finally, for the Atten et al. (1994) model, the formula used was the one for low conductivity ratio (σ_p/σ_l up to 10^3) and high fields:

$$F=2\pi r^2\varepsilon E_c E_0\{\ln[10\Gamma/\pi)(2E_0/E_c)^{1/2}]\}^2 \qquad \Gamma = \sigma_p/\sigma_l \tag{3-41}$$

The Atten et al. model is always underestimated in respect to Wu and Conrad's, though considering that the two models are established for two different windows of conductivity ratios, a comparison does not have a real physical meaning. Considering

that, there is a current flowing in the gap, the conductivity models are not sensitive to the gap width. A comparison of these conductivity models with the dielectric models shows that for low values of conductivity and small gaps, the force is normally lower for the conductivity model. Conversely, for higher values of conductivity or higher gaps, it is the opposite. However, it is important to emphasise that the values are always in the same order of dimension.

Table 3. 3: Comparison of the adhesion force and the electric field in the gap, acting on a PZT particle (R=70μm) in silicone oil, E=1.666 MV/m, calculated using different current controlled interparticle models, for different values of the gap. The values in brackets are the one calculated in the hypothesis of no current across the gap.

Model	d (μm)	F (μN)	E_{gap} (MV/m)	
Wu and Conrad (1996)	**0.5**	**68.21 [68.21]**	**40.97 [71]**	$\sigma_p=10^{-8}$
	0.05	**127.22 [682.1]**	**40.97 [710]**	$\sigma_p=10^{-8}$
	0.5	68.21 [68.21]	32.55 [71]	$\sigma_p=10^{-10}$
	0.05	80.27 [682.1]	32.55 [710]	$\sigma_p=10^{-10}$
	0.5	63.76 [68.21]	20.49 [71]	$\sigma_p=10^{-11}$
	0.05	63.76 [682.1]	20.49 [710]	$\sigma_p=10^{-11}$
Dietz and Melcher (1978) (E_{max}=30MV/m)	0.5	3.8	-	λ_{DM} = 1.1
	0.05	3.8	-	λ_{DM} = 1.1
	0.5	15.9	-	λ_{DM} = 1.2
	0.05	15.9	-	λ_{DM} = 1.2
	0.5	278	-	λ_{DM} = 1.4
	0.05	278	-	λ_{DM} = 1.4
Atten et al. (1994)	0.5	30.7	-	$\sigma_p=10^{-8}$
	0.05	30.7	-	$\sigma_p=10^{-8}$
	0.5	**10.4**	-	$\sigma_p=10^{-10}$
	0.05	**10.4**	-	$\sigma_p=10^{-10}$
	0.5	**4.3**	-	$\sigma_p=10^{-11}$
	0.05	**4.3**	-	$\sigma_p=10^{-11}$

The Dietz and Melcher (1978) model shows how, by changing the value of λ it would be possible to cover practically all the ranges of conductivity ratios, even if the value 1.2 seems to be the more reasonable in our case.

3.4. BEHAVIOUR OF A DISPERSION OF PARTICLES IN AN ELECTRIC FIELD

3.4.1. FIELD FREE INTERACTIONS

3.4.1.1. The microscopic view: the interaction between particles

The forces acting on particles in suspension in a dielectric fluid are the same as those that commonly act on a single particle extensively described in section 3.3 and to which should be added the interaction between neighbouring particles. These forces can be classified as: field free proximity forces, and image forces arising from the electric field exposition.

The field free interparticle proximity forces (Israelachvili, 1992) are effective for distances between the particles smaller than about 100nm and could be strong enough to activate the irreversible aggregation of particles. The main interactions of this kind are listed below.

Van der Waals forces increase with the particle size and can be classified as:

1. *Keesom forces*, the attractive forces between permanent dipole molecules, that decrease with $1/r^3$
2. *Debye forces*, the attractive forces between a permanent dipole molecule and an induced dipole molecule. An induced dipole molecule is a nonpolar molecule which was made (induced) to become a dipole molecule by the attractive force of another dipole molecule. Decrease with $1/r^6$
3. *London forces*, the attractive force between two induced dipoles, which decrease with $1/r^6$

Ion-dipole forces are attractions between ions and permanent dipoles. Their character is similar to ionic bond but with fractional charges and such forces decrease with 1/r.

Ion-Induced dipole forces are attractions between ions and induced dipoles decreasing with $1/r^4$

Hydrogen bonds are also weak forces of attraction arising from the interaction between a hydrogen atom and a strong electronegative atom such as oxygen, fluorine, or nitrogen.

Electrostatic repulsion: decrease follow $1/r^n$ with n = 5÷12

Solvation/hydration forces => short range repulsive force (1nm) associated with hydration cells of surface-adsorbed ions (Israelachvili, 1992). Those forces are against Van der Waals forces, but are normally negligible. Only on particles of nanometric size is it possible to appreciate these kinds of interferences.

3.4.1.2. The macroscopic view: the rheological response of a dispersion of particles

If no electric field exists, a suspension of solid particles in a Newtonian fluid behaves as a Newtonian fluid and obeys:

$$\tau = \eta \, d\gamma/dt \tag{3-42}$$

where τ is the shear stress, η is the viscosity and $d\gamma/dt$ is the shear rate (Halsey, 1992).
The addition of a certain volume fraction (ϕ_v = particle volume/total volume) of filler into a liquid induces an increase in viscosity. Such a phenomenon is due to the fact that the molecules of the fluid are forced to move around the particles. This process dissipates some energy within the fluid by viscous friction. After the proposition of a first model from Einstein (1906) which was reliable only for very dilute dispersions (ϕ_v < 0.03), Mooney (1951) proposed a solution which is also reliable for bigger particles volume fractions:

$$\eta = \eta_0 \exp\left(\frac{5v_p / 2}{1 - v_p / v_p^{max}} \right) \tag{3-43}$$

ν_p^{max} is the maximum packing fraction tolerable by the fluid. Though in an ideal case of hexagonal close packing ν_p^{max} = 0.74, in situations where the powder consists of randomly shaped particles, ν_p^{max} is lowered in the region 0.5.

3.4.2. FORCES ARISING FROM THE APPLICATION OF AN ELECTRIC FIELD AND THE CHAINING EFFECT

3.4.2.1. The microscopic view: the electrostatic interparticle force

When an isolated neutral spherical particle is immersed in a uniform electric field it does not experience any net force. The field gradient is zero and the dielectrophoresis is impossible. If another particle is located in close proximity it generates a local field modification generating a reciprocal attraction that can drive the particles to the contact. Once in contact, the two of particles can be considered as an elongated object. The small chain then experiences an orientation torque that aligns the couple parallel to the external field. The same behaviour repeated for more particles can result in the formation of chain-like structures and in the so called electrorheological effect (Zukoski, 1993).

3.4.2.1.1. The effect of the dielectric constant

A series of models has been proposed, considering the perfectly insulating particles arranged in different configurations. These models, called “dielectric models”, express very well the influence of the dielectric properties of the materials on the interparticle force, and are particularly reliable in the AC case, for frequency high enough to relax any contribution due to conduction (Blackwood et al., 1994).

Model of a couple of particles at a certain distance and tilted at a certain angle

This kind of models is very useful to understand the interaction between the particles when they are going to come close and therefore to model the first phases of the so called electrorheological effect. All the models presented in section 3.3.4.2.2 to calculate the adhesion between the dielectric particle and a grounded electrode refer to this category. In particular, the Klingenberg et al. (1989) model has been very useful in the progress of the ER fluid understanding. Klingenberg et al. calculated the long-range forces associated with the dipoles and the forces between two identical ideal dielectric spheres assuming perfect dielectric spheres. These forces are a function of the diameter, the distance between the particles, the dielectric constants of the hosting fluid and of the

particles and the electric field, in magnitude and frequency. In particular Klingenberg et al. (1989) discovered that the interparticle force F_{int} is directly proportional to the factor:

$$F_{int} \alpha (1/\varepsilon_l) (\beta E_0)^2 \quad (3\text{-}44)$$

However, the most important result of this study is that the force relies also on the angle between the electric field vector and the line connecting the two centres of the particles. The force is repulsive if the angle is 90°, and attractive if it is 0. Where the line joining the particle centres is at angle of less than 55° in respect to the field vector, the particles experience a torque which attempts to align the centres with the field. This explains the tendency for particles to form "pearl chains" in dilute suspension. Further improvements in the knowledge have been made by Feng (2000) who calculated the interaction between two spheres carrying a certain amount of net charge.

The dielectrophoretic interparticle force between two particle has been calculated also by Washizu and Jones (1996), using the equivalent multipole-moment method.

A chain of spherical particles of different length

Klingenberg et al. (1989) demonstrated that in a dispersion of particles exposed to an electric field the chaining effect is a condition of stable equilibrium (see section 3.3.4.2.2); to improve the understanding of ER fluid it was necessary to make some models close to reality. A first improvement was to extend the calculation of the interparticle forces to a chain, and not only to a cluster of two particles. These models, considering a certain tilting, would also give the relationship between shear stress and shear rate inside the ER dispersion.

Jones (1995) calculated the polar moment of chains of different length, for different polarisation mismatches between particles and fluids. He then carried out an average moment for each particle, a result which can be put in relation with the interparticle force. Finally he compared these results with the results achieved with the method of images. Two important considerations derive from Jones' calculations: a) the longer the chain, the bigger its own polar moment is; b) due to the truncation of the higher order terms, the calculation is reliable for low a mismatch in polarisation, but it gradually fails as the particle polarisation increases.

Nakajima and Matsuyama (2002) calculated the interparticle force for chains from 2 up to 80 particles inclusive and calculated the force between each couple of particles inside

the chain. They showed that the force is bigger inside the chain and that it reduces near both ends of the chain, even if it is still much stronger than the one between two particles. The force inside increases with the number of particles, and it reaches a saturation value for chains of more than a few dozen of particles. For $\beta=1$ and a chain of 80 particles, the saturation force was 4 times the one in the case of only two particles.

Clercx and Bossis (1993) proposed a general method based on a multipole expansion theory to calculate the interaction and the permittivity of a system of particles. They compared their results with the Klingenberg et al. (1989), which matched closely. Then they computed the interparticle force on chains of three particles. Such a force was 1.3 times the one calculated by Klingenberg et al. for a particle with $\varepsilon_r = 10$, and doubled, if $\varepsilon \to \infty$, in line with what was expected.

Chen et al. (1991) solved the problem finding a potential expansion satisfying the Laplace equation, and they considered the solution employing 25 multipole terms and considering 40 particles. For a value of $\beta=1$ they calculated a force 3 times bigger than the one for the case of two particles. Considering the interpolated value of the force calculated by Nakajima and Matsuyama (2002) the two computations are in a good agreement.

An infinite particle chain

These models are normally realised considering two particles in contact with two isopotential planes, and they simulate an infinite chain exploiting the image charge symmetry. Tao et al. (1995) used this geometry to calculate the interparticle force using the finite difference method (FDM), a numerical method alternative to the FEM. Davis (1992a) used an FEM method to calculate the force on a particle chain and he derived the shear module from shear dependence. Techaumnat et al. (2004) carried out a simulation of an infinitely long isolated chain, to derive the rheological response of a dispersion.

A bundle containing a different number of chains and arranged in a different way.

Klingenberg et al. (1989) simulated numerically the dynamics of an electrorheological fluid, starting from a randomly distributed dispersion of dielectric particles in a dielectric liquid. He showed that only when the interaction force is approximated to an

expression that takes into account the short ranges interaction, the structure simulated agrees well with the real one. Such a simulation shows that in a real ER fluid, the chains are not arranged as independently isolated chains, but more as clusters of chains. The formation of clusters has been frequently observed experimentally in non-diluted dispersion. Moreover, it is at present a strong belief that such arrangements are a bct-like (body centred tetragonal). For this reason, to really simulate the interaction inside an ER fluid, it would be necessary to consider some arrays, or clusters of chains.

Shih et al. (1994) showed that for a low concentration of particles a single chain arrangement was energetically more stable than a columnar arrangement. The trend inverts as the particle concentration increases. Shih et al. also calculated the interaction in a two chain rectangular and hexagonal array, making the distinction between a case in which there was polarisation rotation and a case where there was none. From their calculation, no difference in the shear force strength occurred in a two chain system compared with a one chain system, in both the arrangements. If a polarisation rotation was assumed the force was generally smaller. Some experiments they conducted on particular arrangement of soda glass spheres in silicone oil showed that the strength of a chain array increases more than linearly increasing the number of chains above 2.

3.4.2.1.2. The effect of the conductivity

As already explained in section 3.3.4.2 the polarisation model fails when the conductivity effects stop being negligible. Some authors (Anderson, 1991; Wu and Conrad, 1996; Davis, 1992b; 1995) tried to take into account the effect of the ohmmic conductivity, introducing the use of the complex permittivity into the polarization model. These models showed good agreement with the results for electric field small enough not to have any non-ohmmic conduction effect.

When the interparticle field is higher some electric field enhanced conductions are observed. In this case, another kind of model should be considered to describe the phenomenon. The conductivity models of Atten et al. (1994; 1997b) and Wu and Conrad (1996), already introduced in section 3.3.4.2.3, are the main models belonging to this category.

Particularly worth mentioning is the behaviour of metallic particle dispersed in a dielectric fluid. Rattray (1994) reports that when the particle conductivity is too big, complete chains do not form, and there is a decrease of the ER effect.

Jones (1995) reports that, according to the static theory, two metallic particles should not form a chain but should be pulled apart. Nevertheless, in AC, dynamic viscosity limits the separation rate between the particles. Consequently, if the polarity change is too rapid for any particle motion a chain can form.

3.4.2.1.3. The effect of frequency

It has been observed that the ER effect decreases when the frequency increases, especially in the region between 100Hz and 10kHz. A similar reduction is exhibited as well by the permittivity of the ER fluid.

A large scale direct measure of interparticle force has been carried out by Atten et al. (1993). They measured the attraction between two half spheres of polyamide of 0.7 cm radius, having $\sigma = 1.7\times10^{-8}$ S/m, immersed in a transformer oil $\sigma = 3\times10^{-13}$ S/m and $\varepsilon_r = 2.2$. The interaction has been tested on a field between 1kV/cm and 4kV/cm. Polyamide has an ε_r of 35 at 10Hz and 12 at 100kHz, and also the particle-interaction follows the same trend being maximum in DC and decreasing with frequency. However, partially hidden by the relaxation of the polyamide, a relaxation due to the mismatch in conductivity is expected around 100Hz.

Wang et al. (2003; 2005) conducted a series of direct measurements of the interparticle force between two spheres of 6.3mm in diameter of different materials, immersed in different dielectric fluids, exposed to electric fields of intensity up to 220 V/mm and frequencies ranging from zero to 3kHz, and finally with different spaces gap with an accuracy of 1μm. All the systems they analysed do not relax in the range of frequencies analysed. They observed that the forces, though having the same trend as the one predicted by the FDM (finite difference model) simulation of Tao et al.(1995), always have a bigger magnitude. They deeply analysed the force between two particles of $SrTiO_3$, a ferroelectric material with $\varepsilon_r=294$ and $\sigma=2\times10^{-8}$ S/m. The force in castor oil is slightly bigger than the one in silicone oil (due to the bigger dielectric constant). Forces are always smaller in more conducting fluids like ethyl benzoate. The force

normally has a quadratic dependence on the field and the particle dimension. The force measured between 25 and 61 V/mm increases with frequency, even if β^2 was constant. Such a behaviour could be explained considering a phenomenon of enhanced dissociation inside the particle gap. A similar behaviour has been confirmed by some measures of shear stress dependence from field frequency and magnitude of a dispersion of $Ba_{1-x}Sr_xTiO_3$ in silicone oil operated by Misono et al. (2004) and by Miller et al., (1993). They showed that the ER effect in this dispersion is almost independent of the frequency for a field of 0.5 MV/m, and has a tendency to slightly increase with frequency for field of 1 MV/mm. For a field of 2 MV/m a net increase with frequency is observed. Such a behaviour is consistent with the measures of Wang et al. and with the hypothesis that a phenomenon of enhanced dissociation inside the particle gap. Nevertheless, Wang et al. conducted their measures in conditions of smaller electric field.

3.4.2.2. The macroscopic view: the Electrorheological effect

ER fluids are sometimes called “electroviscous fluids”. However such a definition is inappropriate because electroviscosity is an increase in viscosity in a pure fluid (and not a dispersion), induced by an electric field. Therefore, electroviscosity is not related to the chaining effect. Excluding liquid crystals, this increase in viscosity has been associated to an EHD instability (Atten and Honda, 1982) and, except for the particular case of the liquid crystals, it is normally only few times that of the fluid at rest.

Winslow discovered the electrorheological effect in 1949. He thoroughly investigated the phenomenon with the aim of identifying some promising practical applications. After Winslow, Klass and Martinek (1967) gave a further extensive contribution to the subject. They noted that viscosity increases continuously when the electric field increases, until electric breakdown, saturation or irreversible solidification appears.
Arp and Mason (1977), working on ER fluids containing conducting particles, observed that a breakdown always happens before particles touch. At that point they observed that particles bonded together by small amount of polymerized dielectric liquid.

When an ER fluid is exposed to an electric field, it behaves like a Bingham fluid, and its dynamic in a direction perpendicular to the field is described by the constitutive equation:

$$\tau(E) = \tau_y(E) + \eta_b \, d\gamma/dt \qquad (3\text{-}45)$$

According to this equation, where η_b is termed the Bingham viscosity, motion only occurs when $\tau(E)$ is bigger than the yield stress τ_y. η_b shown to be either invariant or slightly variant with the electric field. Below τ_y the fluid behaves as a gel or a solid, even if, as pointed out by Block and Kelly (1990), the constitutive equation of that solid phase has not yet been established.

Many studies (Rattray, 1994) at low to moderate electric field (below 1 MV/m) showed a dependence described by:

$$\tau_y = E^a \qquad \text{where } 1.8 < a < 2.4 \qquad (3\text{-}46)$$

Other groups (Rattray, 1994) reported a linear trend after exceeding a threshold field. Both the threshold value and the gradient in the linear phase turn out to be system dependent.

A sigmoidal behaviour has also been detected by several groups (Rattray, 1994). It seems to be the most suitable, as otherwise the fluid would become infinitely rigid, which is clearly impossible. The high field roll off could be caused by the non-ohmic effects of increase in conductivity in the interparticle gap.

To conclude, at fixed field and temperature, τ_y seems to be a monotone increasing function of the concentration, and that function can be parabolic or sigmoidal.

In some cases, τ_y showed some sensitivity to the shear rate too. It has been shown by some charts that for $\tau = \tau(d\gamma/dt)$, calculated increasing the shear rate from 0 to 1200 N $/m^2$ and then decreasing it to 0, the initial τ_y starting from a shear rate 0 it is bigger than the returning point. In other words, it is possible to define two values for τ_y, a static and a dynamic one, the first of the two being the bigger one (Rattray, 1994).

Some visual observations showed that as the electric field increased, the formed structures change their morphology from “pearl-chains” to “fibrils” and finally to “columns”. Halsey (1992) affirmed that the force between neighbouring chains inside a

column has a different nature with respect to the inter-particle force. He ascribes the observed formation of columns to fluctuations in electric field inducing some phase delays.

3.4.3. THE ELECTRIC FIELD STRUCTURING TECHNIQUE

An important application of the ER effect is the structuring of composites materials (Wilson et al., 2005; Randall et al., 1993; 1994). As introduced above, when a suspension of ceramic particles in an insulating electric fluid is exposed to an electric field, the particles polarise and under suitable conditions they can assemble into chains. If the fluid is a resin pre-polymer, this can then be cured and the new-formed structures frozen into place to form a composite material with anisotropic properties. Wilson (1999) conducted an extensive study of this manufacturing technique working on dispersion of PZT powders in epoxy-resin.

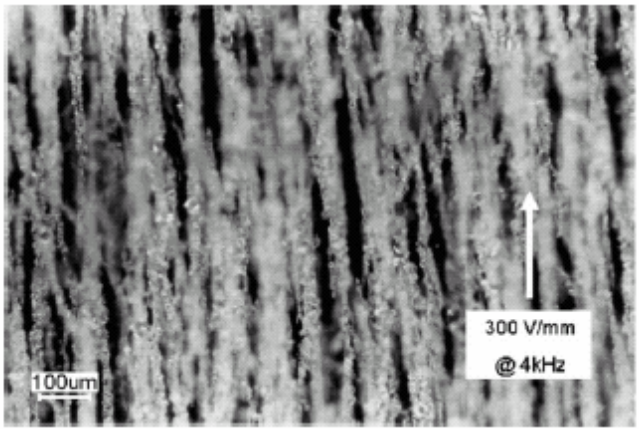

Figure 3. 7: "Pearl chains" in a field-structured 10% vol. lead titanate/epoxy composite (Wilson, 1999)

Kim et al. (2004; 2005a) using the structuring power of the electric field have been able to make some oriented composites in epoxy matrix and with 3M Zeosphere ceramic microspheres, graphite and glass fibres. Kim (2005b) characterised also the thermophysical properties of these composites.

3.4.3.1. Ideal alignment frequency and electric field threshold

Khusid and Acrivos (1995; 1996) postulate that there is a critical threshold for the electric field strength which is required to trigger the aggregation of particles and which depends upon the particle size. In dilute suspension: $E_{th}^2 \sim 1/\phi_v$ where ϕ_v is the particle volumetric fraction. Tao (1992) calculates this threshold in more detail by an energy balance taking into consideration thermal motion too. He proposed the equation 3-48.

$$E_{th}^2 = [8\pi kT(1-\Phi)] / [\beta^2 \nu_p \Phi \varepsilon_l] \quad (3\text{-}47)$$

where ϕ_v is the volume fraction of particles.

Bowen et al. (1994), studying the electric field structuring of different materials, was the first to observe:

- A critical field frequency maximising the formation of fibril, which he called the Ideal Alignment Frequency (IAF)
- A critical field magnitude to have formation of fibrils

If the frequency is higher than the IAF there could be a relaxation in interfacial polarisation and a decrease of the dielectric force.

3.4.4. PARTICLES IN A NON UNIFORM ELECTRIC FIELD

Khusid and Acrivos (1995;1996) elaborated a statistical theory to describe the behaviour of low conducting colloidal suspensions exposed to a DC field and to a non uniform AC electric field. The theory predicts chain formation in a positive polarisation case, the formation of “disk-like aggregates” in negative polarisation case, and the possible non aggregation of particles when $\beta \sim 0$.

Kadaksham et al. (2004a) conducted a dynamic simulation of an ER suspension in the condition of non uniform electric field.

3.4.5. NON SPHERICAL PARTICLES

To have a precise description of the phenomenon it is necessary to know how it is related to particle geometry, particle orientation and surface irregularity. Some useful generalisations regarding particle shape were made. About fibres and platelets S.A. Wilson (1999) observed the general behaviour that in positive dielectrophoresis high aspect ratio particles align with their major axis parallel to the applied field. The volume required to achieve that was much greater than the one of the individual fibres.

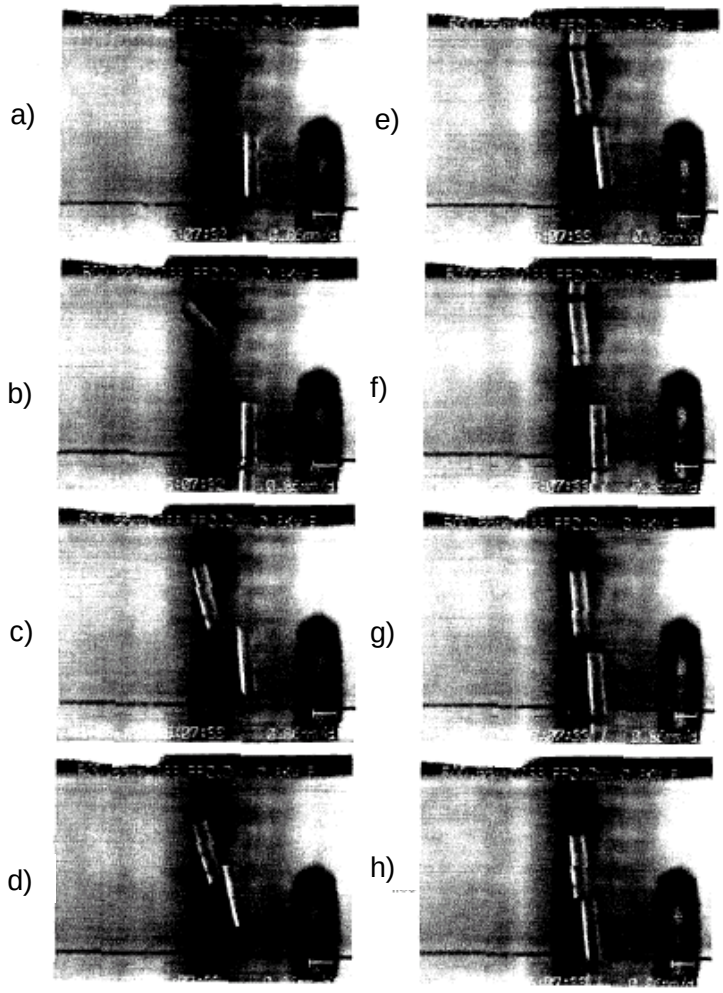

Figure 3. 8: This sequence of pictures shows the behaviour of two polymer particles (PP particles) exposed to a uniform electric field (Yatsuzuka et al. (1995). The particles moved up and down across the gap between the two electrodes. Once the particles made contact with each other they started to move together, constituting a small chain (d-h). This structure is very similar to observations made in the present research work , shown in chapter 9

Miller and Jones (1987) have analysed the torque components due to the dielectrophoresis force for ellipsoidal particles and their frequency dependence. They have shown that alignment parallel to the field and also perpendicular to the field are both possible. Again the polarisability parameter is the principal controlling factor. Finally Sanchis et al. (2004) calculated the attraction between particles of different shape and size.

An interesting study was carried out by Yatsuzuka et al. (1995) who analysed the motion of a couple of cylindrical polymer particles placed inside the gap separating two parallel plate electrodes. The two fibres oriented and moved across the gap and they also attracted each other forming some clusters as visible in the picture 3.8.

3.4.6 DISCUSSION ON THE FORCES IN A DISPERSION OF PARTICLES

A summary of all the forces introduced in this section is represented in figure 3.9.

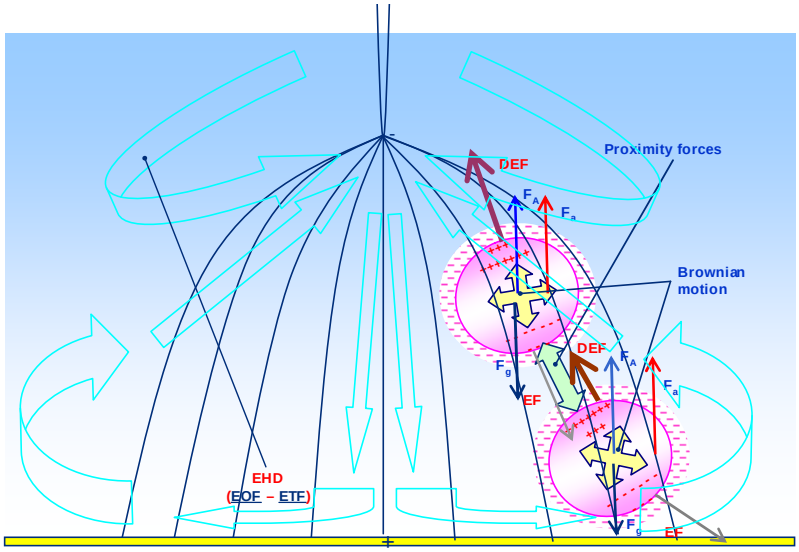

Figure 3. 9. Review of the main interactions involved in the alignment phenomenon

The polarisation force overshadows field free interparticle forces and at separation equivalent to or less than Debye length. Gast and Zukoski (1989) estimated the relative magnitudes of the interparticle interactions for a typical ER fluid and concluded that the induced polarisation and viscous forces totally overshadow the field-free interparticular

forces (10000:1). If the dimension of the body is bigger than 0.5 μm, Brownian motion, relatively small, is also overshadowed by polarisation forces.

The distance between strongly polarised particles is uncertain, but 4-7 nm was estimated (Block, 1999). The adsorbed ions layer prevents direct normal contact. In that phenomenon separation particle shape and surface roughness are important. If an electric current is established between the particles, either by direct contact or by ion surface migration the polarising field is disturbed. Local temperature gradient, field-induced ionisation and tunnelling are factors to consider. The basic polarisation model can be refined to incorporate variations in particle size, shape and spatial distribution. In the very small interparticle separation, a number of additional effects are likely to be in competition. EP force can be neglected above a certain frequency threshold depending on the particle. This frequency is inversely connected with the inertia of the particle.

Chapter 4

THE EXPERIMENTAL SETUP: DESCRIPTION OF THE PROCESS UNIT

This chapter supplies a detailed description of the process unit, made specifically for the present research work.

A block diagram of the experimental system is featured above. The diagram indicates each instrument employed in the Process Unit with all the connections characteristics.

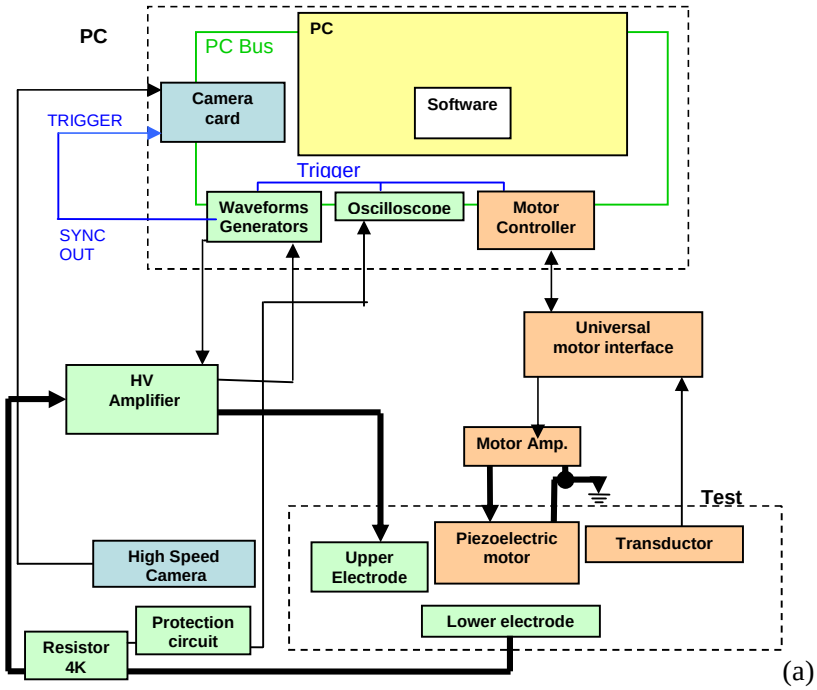

(a)

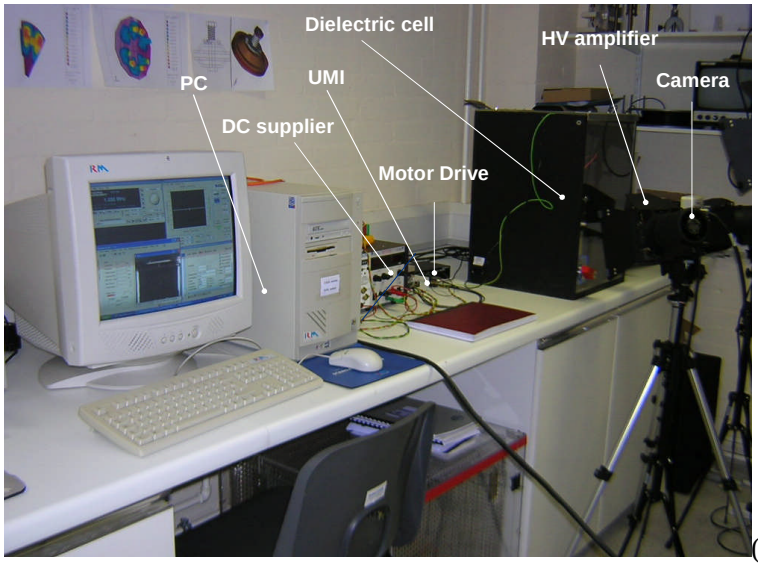

(b)

Figure 4. 1: Experimental setup. (a) A block diagram (b) The ensemble

4.1 THE PC CARDS AND THE SYSTEM SYNCRONISATION

The system is driven by a computer using Labview 3.1. Four boards are plugged into a PC: an oscilloscope card (NI 5112), a waveform generator (NI 5401), a motion controller (NI 7344) and a video-camera acquisition card. The oscilloscope card DC accuracy is 2.5% of the range setting, while the clock accuracy is 50 ppm. The waveform generator has an accuracy of 5mV and frequency resolution of 9.31 mHz. The motion controller has a 62μs PID loop update rate (National Instruments, US).

The three National Instruments boards are connected by a RTSI trigger bus that enables the synchronisation on these cards. However, the video-camera acquisition card is synchronised by a SYNC signal generated by the waveform generator. The trigger event used to synchronise all parts of the system is the waveform generation.

The other element synchronised with the waveform generator is the motion controller. It is connected to both the motor drive and the linear transducer via a Universal motor interface (UMI 7764). The UMI needs to be powered by a 5V DC, which is supplied by a Thurlby PL310 DC generator.

4.2 THE HIGH SPEED CAMERA

A high-speed CMOS video camera is connected and driven to the camera acquisition card. It is a Red Lake Motion Pro, characterised by a definition of 1280×1024 pixels at low speed and a recording speed between 500 and 10,000 frames per second (fps). No information has been found about the uncertainty on the frame duration. It is reasonable to consider an uncertainty below 50ppm (Rudeforth, 2003). The camera is mounted on a tripod. The light necessary for the observation is provided by 3 halogen lamps (1250 W each). The optic objective installed on the camera is a Sigma 50mm macro-objective. The camera allows a real-time observation of the dielectric cell. Recording is enabled when the signal generation starts via the SYNC output of the NI 5401. A high-speed video-camera became necessary for the observations, due to the very quick rod motion when exposed to an electric field.

Because of heat generated by the halogen lamps, monitoring of the temperature of the dielectric cell was carried out, ensuring control on the experimental conditions. Moreover, monitoring of the temperature was also necessary to ensure that all the electronic equipment was still working within standard operational conditions.

The cell temperature was monitored by a FLIR ThermaCAM SC3000, a thermal camera supplied by the EPSRC Engineering Instrument Pool. The thermal camera had an uncertainty of ±1%. Figure 4.2 shows some thermal pictures of the area of the experimental system closest to the dielectric cell.

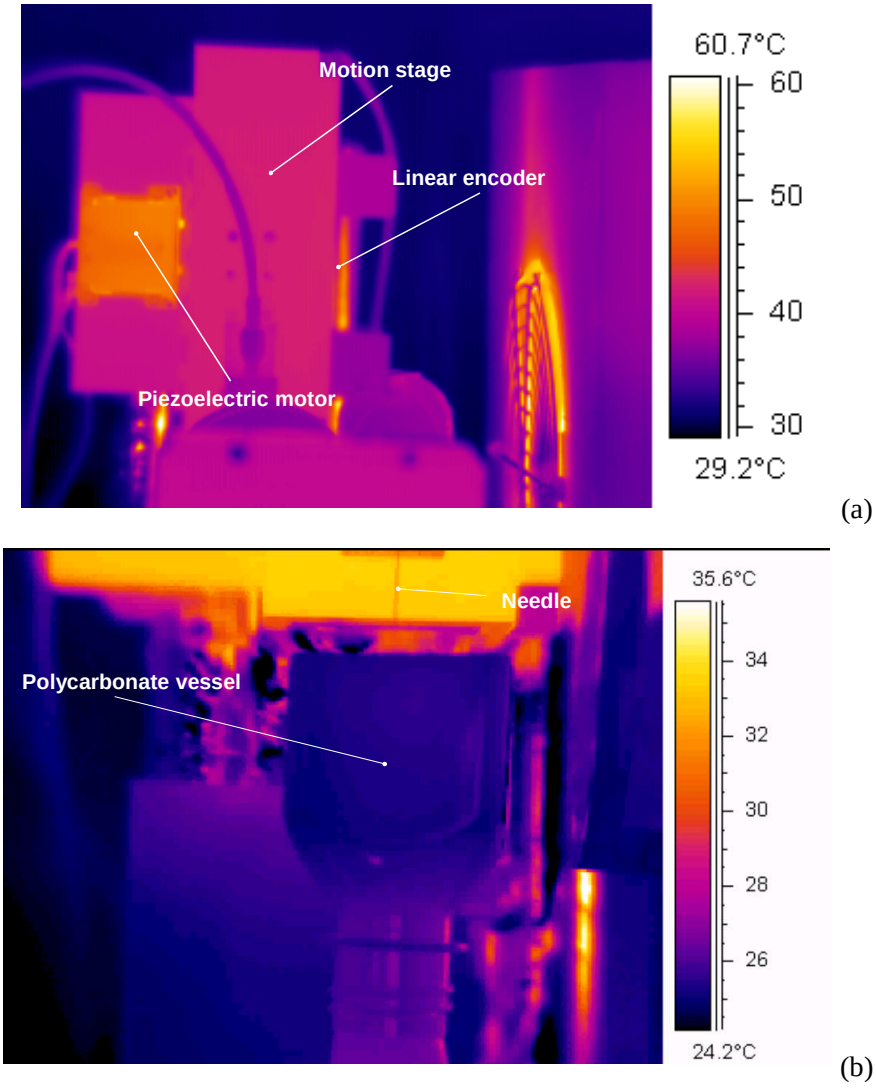

Figure 4. 2: Images showing the temperature distribution in the dielectric cell. (a) The motion setup (see figure 4.3. (b) The polycarbonate vessel (see figure 4.11)

4.3 THE MOTION SETUP AND THE FEEDBACK SYSTEM

The piezoelectric motor and the reading head of the linear transducer are mounted on a fixed support. The ceramic strip and the transducer are mounted on a moving part. The mobile part consists of a mobile support fixed on a linear bearing. The linear bearing is also mounted on the fixed support.

The design below shows the mounting configuration. Two other supports are designed to fix the motion system to the chassis. The four supports shown in figure 4.3 were designed by the 3D CAD Solid Edge (see appendices designs).

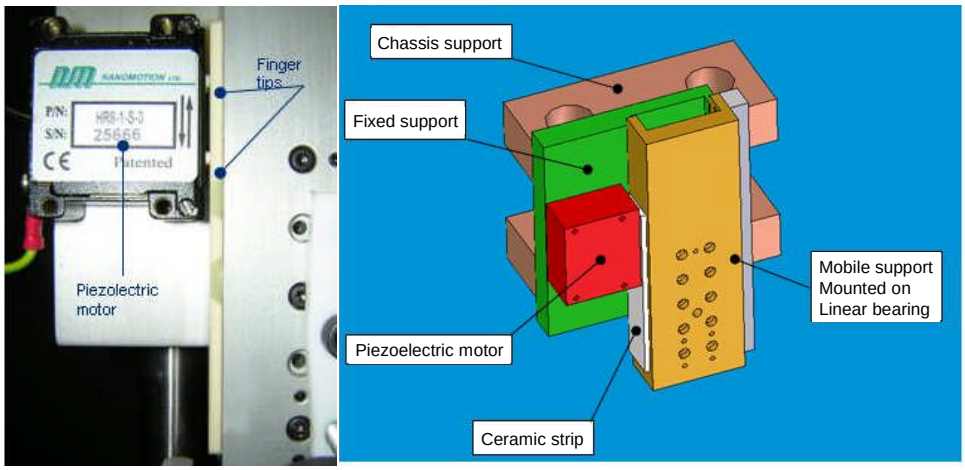

Figure 4. 3: Detail of the designed movement system. The linear bearing is hidden by the mobile support

4.3.1 THE MOTOR AND THE MOTOR DRIVE

The motor selected to carry out the displacement of the needle-like upper electrode is a Nanomotion piezoelectric motor HR8. This motor was chosen since it operates in a way that excludes any generation of intrinsic electromagnetic field (Karasikov and Ganor, 2000). When the driving voltage is not applied, the ceramic plate is stationary and generates a holding force on the stage. Even if no other braking device is employed, the holding force of the Nanomotion motor is big enough to prevent any position shift even when the motor is switched off.

This motor works by exploiting the deformation of a little piezoceramic rod excited in a transverse bending vibration mode at close frequency proximity to the longitudinal mode (Timoshenko et al., 1990). The simultaneous excitation of the two above-mentioned modes creates a small elliptical trajectory of the ceramic edge (Uchino, 1997; Ueha and Tomikawa, (1993). Under these conditions, if the rod is pushed on a surface, it can be transformed into finger-like elements and so be able to climb onto the surface. This surface is normally a ceramic strip bonded to the moving part.

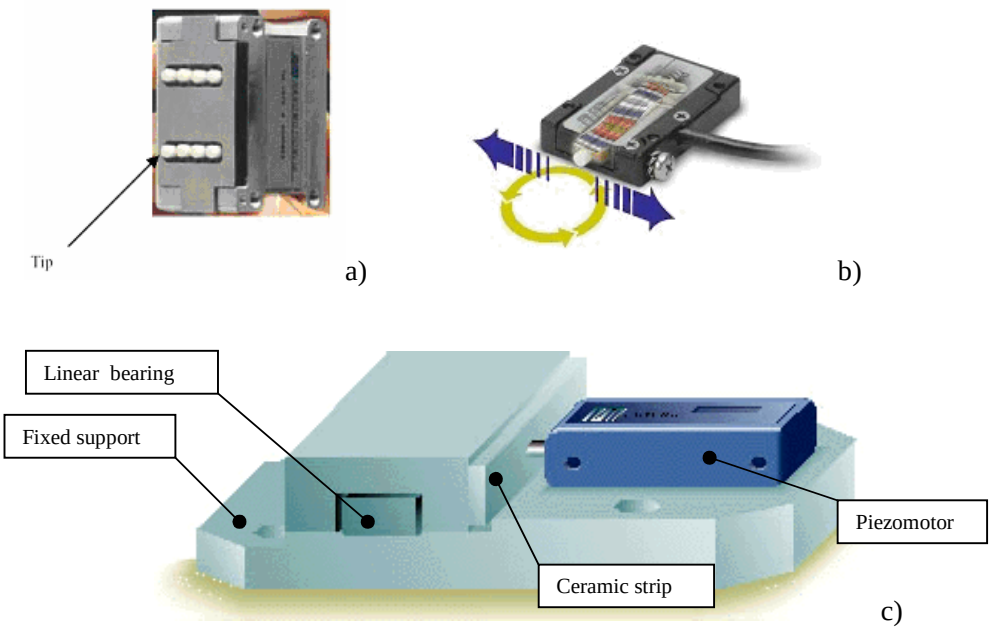

Figure 4. 4: Review of Nanomotion piezoelectric motor picture. In picture a) tips disposition in a HR8 type. In picture b) the tip movement that permit the motion generation is put in evidence. Picture c) is a representation of the mounting mode by a ceramic strip, a linear bearing and a fix support (Nanomotion Ltd., Israel)

Typical piezomotor force/velocity performance is shown in the curve below:

The current Nanomotion technology allows velocities bigger than 1 m/sec and as low as a few μm/sec to be achieved, while maintaining dynamic forces of tenths of a Newtons. The motor is driven in current like a common servomotor using an AB5 drive. The drive is DC powered with 24V using a Thurlby PL310 DC generator.

The drive receives 3 signals from the controller. The first of these signals is a PWM (Pulse Wave Modulation) signal, and it is the effective command signal for the motor. The second is the earth reference level and the third is the enabler signal. This last signal is normally on "active low", but has been switched on to "active high" due to compatibility problems with the controller.

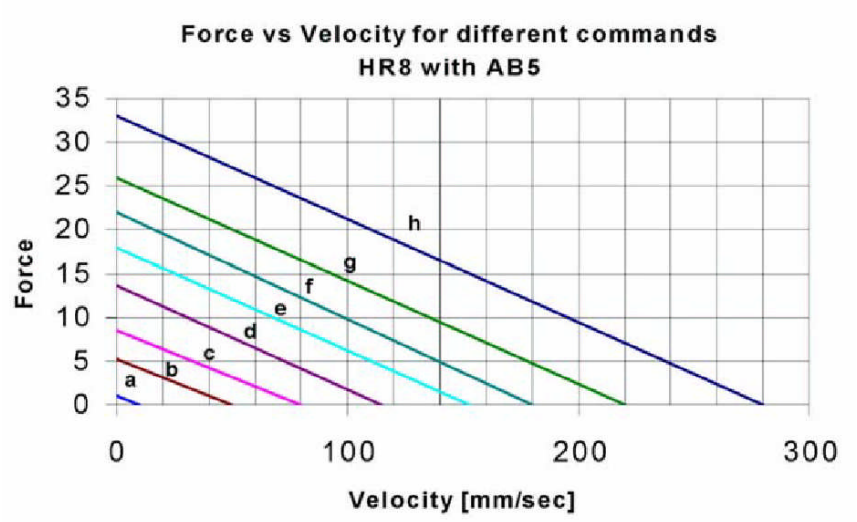

Figure 4. 5: Graphic of a series of typical piezoelectric motor response curves for different values of duty cycle (Nanomotion Ltd., Israel)

4.3.2 THE LINEAR ENCODER

A necessary element to complete the feedback loop is the linear transducer: RSF Elektronic MSA 170.83. It is composed of two pieces, a support containing the glass scale and a reading head.

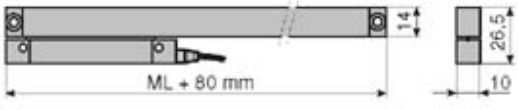

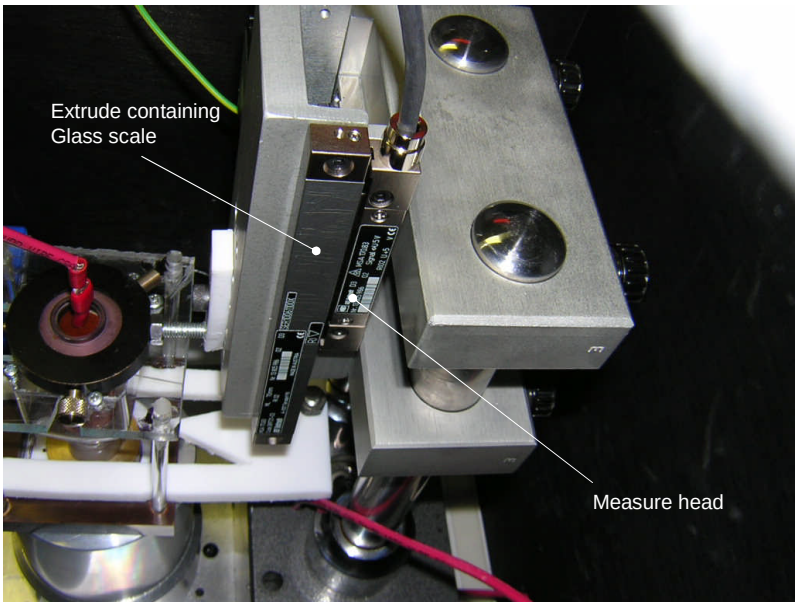

Figure 4. 6*:* Linear transducer (Heidenhain Corp, US)

This transducer has a resolution of 0,1 μm. The transducer exchanges 8 signals with the UMI. These signals are a 5V signal and a ground signal to permit the transducer to function. The 6 remaining signals are the quadrature signals. Incremental encoders provide two sinusoidal or square-waves, 90° phase-shifted measuring signals and one reference mark signal (Heidenhain Corp, US).

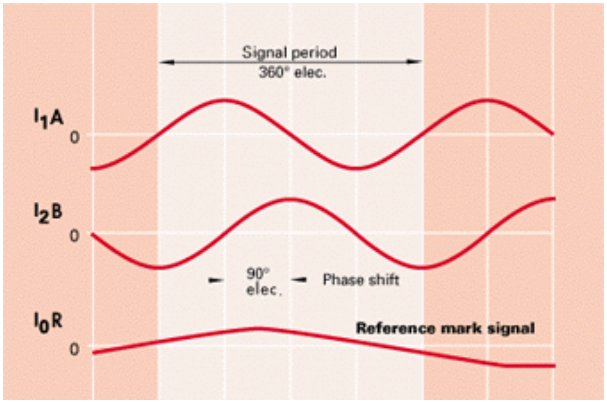

Figure 4. 7: A typical incremental encoder sinusoidal measuring signals (Heidenhain Corp, US)

The sinusoidal signals are digitised and evaluated 4-fold in the subsequent electronics, which results in a measuring step 1/4 the signal period of the encoder (a transparent and a black sector on the glass scale).

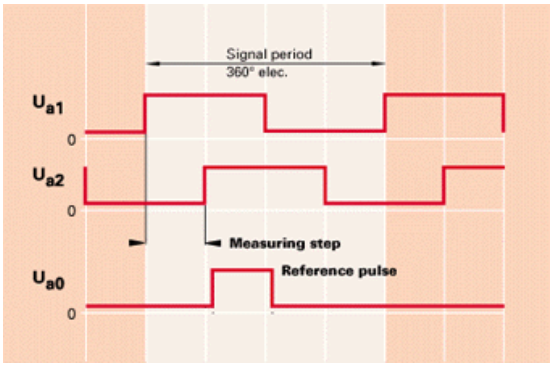

Figure 4. 8: A typical incremental encoder measuring signals after digitising (Heidenhain Corp, US)

To attain smaller measuring steps the sinusoidal signals are interpolated before digitizing.

The most common type of incremental encoder uses two output channels (A and B) to sense position. Using two code tracks with sectors positioned 90˚ out of phase, the two output channels of the quadrature encoder indicate both the position and direction of displacement. Some quadrature encoders also include a third output channel, called a zero or index or reference signal, which supplies a single pulse per revolution. This single pulse is used for precise determination of a reference position.

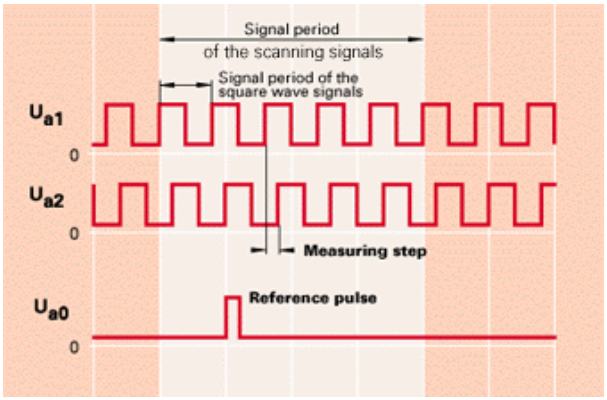

Figure 4. 9: A typical incremental encoder Measuring signals after 5-fold interpolation (Heidenhain Corp, US)

4.4 THE DIELECTRIC CELL AND THE ELECTRODES

A dielectric cell has been assembled, as shown in the picture 4.10.

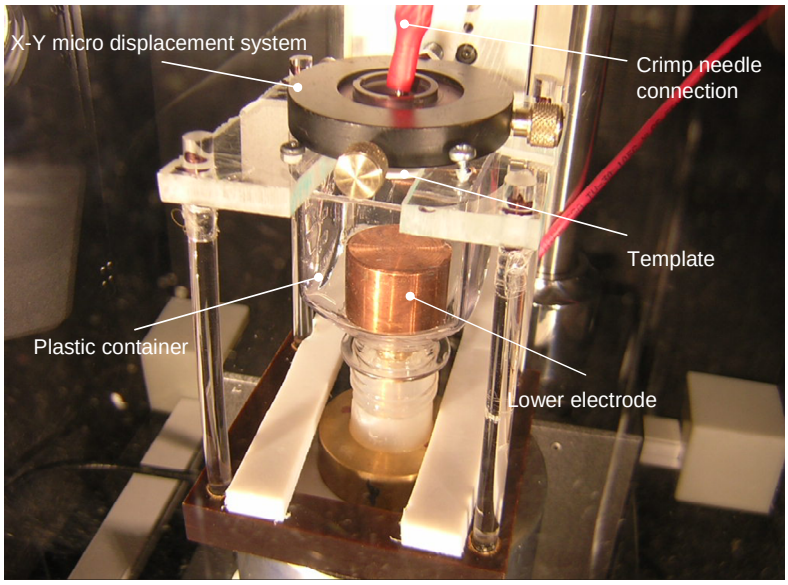

Figure 4. 10: Experimental dielectric cell

The vessel of the dielectric cell is a square transparent polycarbonate vessel allowing optical access. The cell is filled with the dielectric oil. In the cell different electrodes are positioned. The bottom one is a rectangular (30x35mm) stainless steel mirror finished flat plate. It can be coated (or not) with a layer of PTFE 0.5mm thick, depending on the

experiments. The top electrode can have a different shape, and depending on the experiment will be chosen from the list below.

a) Another rectangular (30x35mm) stainless steel mirror finished flat plate; this configuration is used to analyse the behaviour in injection free experiment with no gradient of the electric field.

b) A stainless steel needle with a diameter of 120μm, and a tip radius of 6.5μm; this configuration is used to analyse the behaviour in regime of unipolar injection; the needle diameter has been chosen considering that in the EFS technique presented in section 1.1.1; the diameter of the needle has to be smaller than that of the PZT fibre.

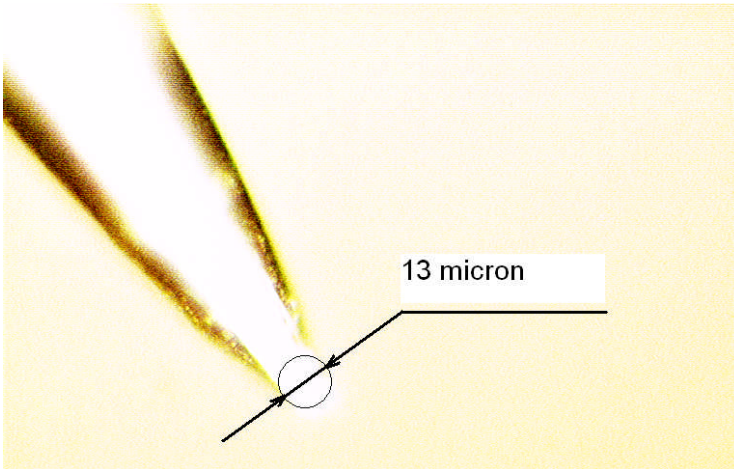

Figure 4. 11: Detail of the tip of the acupuncture needle we used in our experiments. The needle has a diameter of 120μm

c) The same needle, but coated with a bubble of epoxy resin (diameter 1.4mm) on the tip, and glass coated (external diameter 1mm and thickness 0.45mm) on the side; this configuration is used to inhibit both the charge transfer through the needle and the electrochemistry on the tip, in experiments with non-uniform electric fields and no injection.

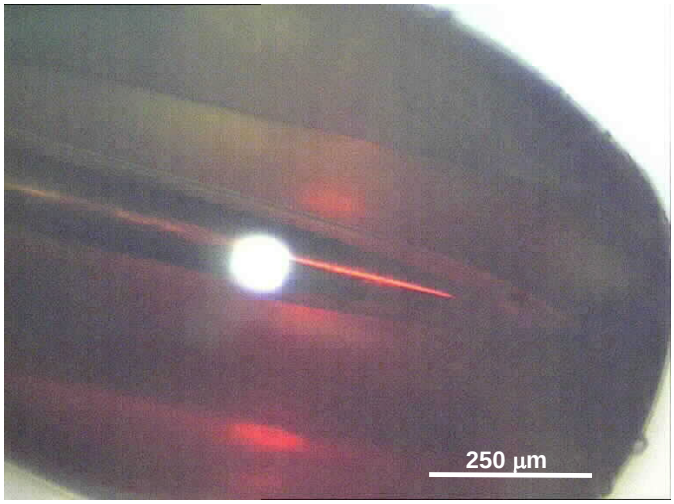

Figure 4. 12: Detail of the tip of the insulating coated acupuncture needle.

d) A stainless steel needle with a diameter of 750µm, and a tip radius of 25 µm; this configuration is used to analyse the behaviour in a regime of unipolar injection without lateral corona (see chapter 6).

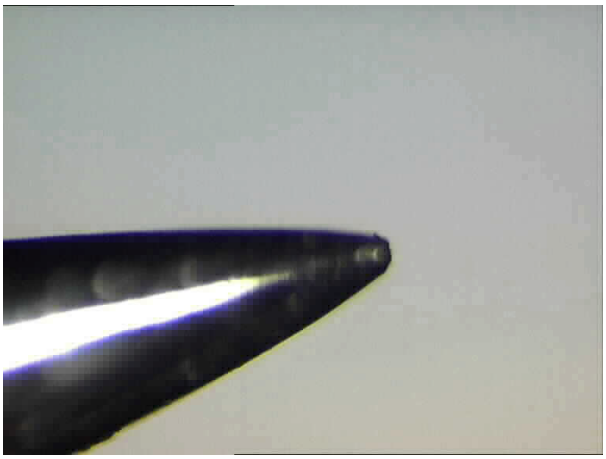

Figure 4. 13: Detail of the tip of the needle we used in our experiments. The needle has a diameter of 750µm and a tip radius of 25 µm

e) A stainless steel sphere with a diameter of 8mm, mirror finished; this configuration was used to analyse the behaviour in injection free experiment with a gradient of the electric field.

4.5 THE HIGH VOLTAGE AMPLIFIER

The electrodes are connected to a high voltage amplifier (TREK 610 C) which can amplify the signal sent by the waveform generator up to a thousand times.

A characteristic response in frequency of the amplifier is shown in the following diagram (figure 4.14). $V_{max\ in}$ represents the voltage supplied by the waveform generator and $V_{max\ out}$ represents the voltage supplied by the amplifier as shown by the monitor output. The output uncertainty is better than 0.1% of the full scale, the offset is less than 5mV, and the noise is less than 20mV peak to peak.

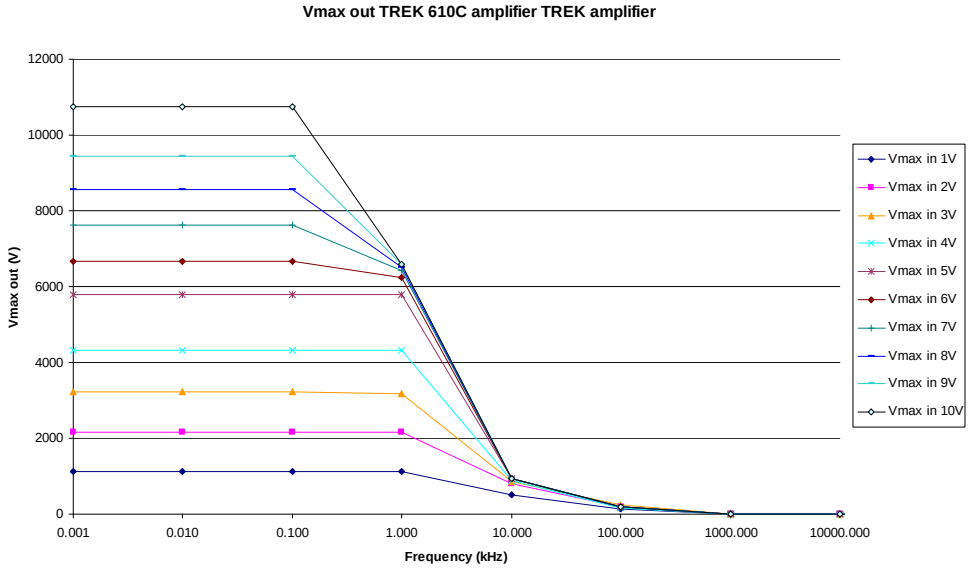

Figure 4. 14. Bode diagram of the Trek Amplifier used in the experimental setup

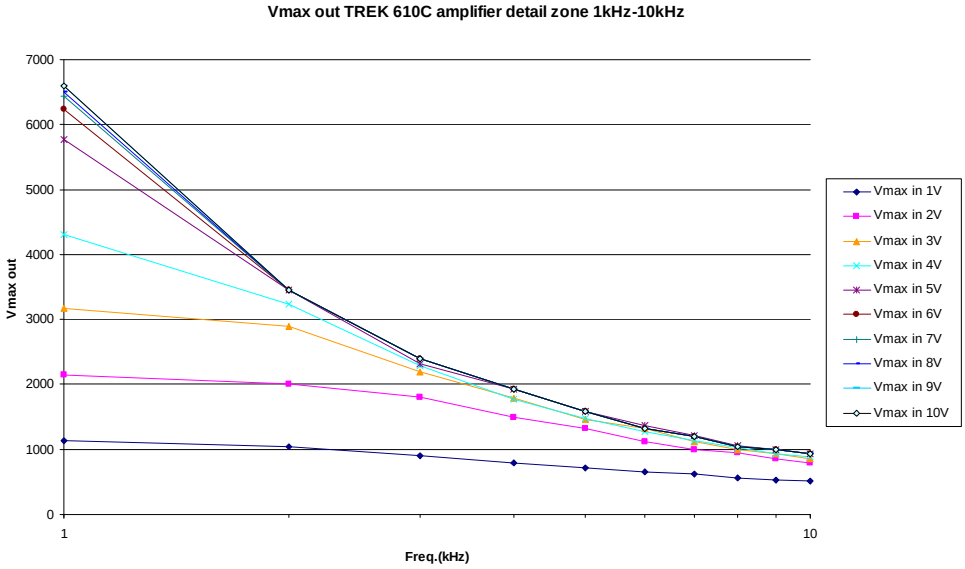

Figure 4. 15. Bode diagram of the Trek Amplifier used in the experimental setup (detail 1-10 kHz).

Chapter 5

MATERIAL CHARACTERISATION AND PRELIMINARY INVESTIGATIONS

This chapter focuses on describing the materials utilised in this study. All the characteristics of the fluid and the particles have been reported. Where the characterisation of the material was presented, all the details related to such a characterisation have been provided.

5.1 FEM SIMULATION OF THE ELECTRIC FIELD IN VARIOUS NEEDLE-PLANE ELECTRODES CONFIGURATIONS

This chapter collects a series of FEM simulations of the theoretical electric field in the different needle-plane electrodes configurations considered in our study. The simulations have been carried out considering 4mm spacing between the electrodes, and a voltage of 10kV.

5.1.1 THE 120μm NEEDLE

To find the shape of the electric field in a needle-plane configuration, it is necessary to solve the Laplace equation (see chapter 2.6.2).
Applying the distribution theory, Durand (1966) proposed an analytical result approximating the needle with a hyperboloid. The result is shown in section 2.2.2.
The result of a FEM simulation is represented in figure 5.1.

The FEM simulation carried out a value of E_{max} of 3.4 MV/mm, slightly lower than the 3.94 MV/mm calculated analytically. The chart in figure 5.1 shows how the field has a significant gradient in the first 0.2mm near the tip, and how it decreases, becoming almost homogeneous. For this reason one can expect the dielectrophoretic manipulation to be limited to the area close to the tip.

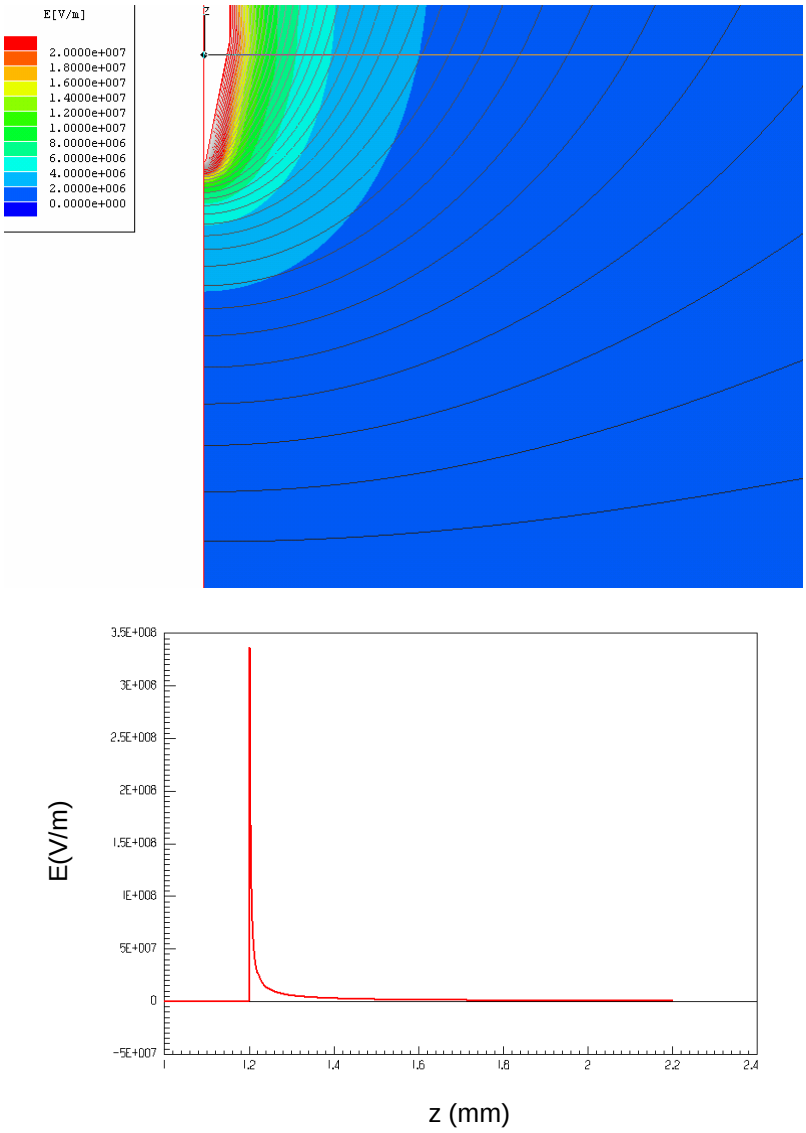

Figure 5. 1: Electric field in a system with a parallel flat bottom electrode and a needle-like top electrode, calculated by FEM simulation. The distance between the electrodes is 0.5mm, the needle diameter is 120µm the tip radius 6.5µm.

5.1.2 THE INSULATOR COATED 120µm DIAMETRE NEEDLE

The solution proposing an insulator coated needle is particularly interesting because, as shown by the FEM chart, below, the field is always contained below 5.5 MV/m. In this configuration, then, even if the field continues to be highly non-uniform, no charge injection can appear. However, the simulation would be only a simplification of the

reality because the field around the tip is still too big, and an ionisation of the air film close to the needle can be expected. At this moment the interior wall of the capillary could acquire a different potential to the one predicted by FEM. Moreover, if some phenomena of electric field enhanced conductivity are generated inside the glass or the resin, this can modify the field distribution too.

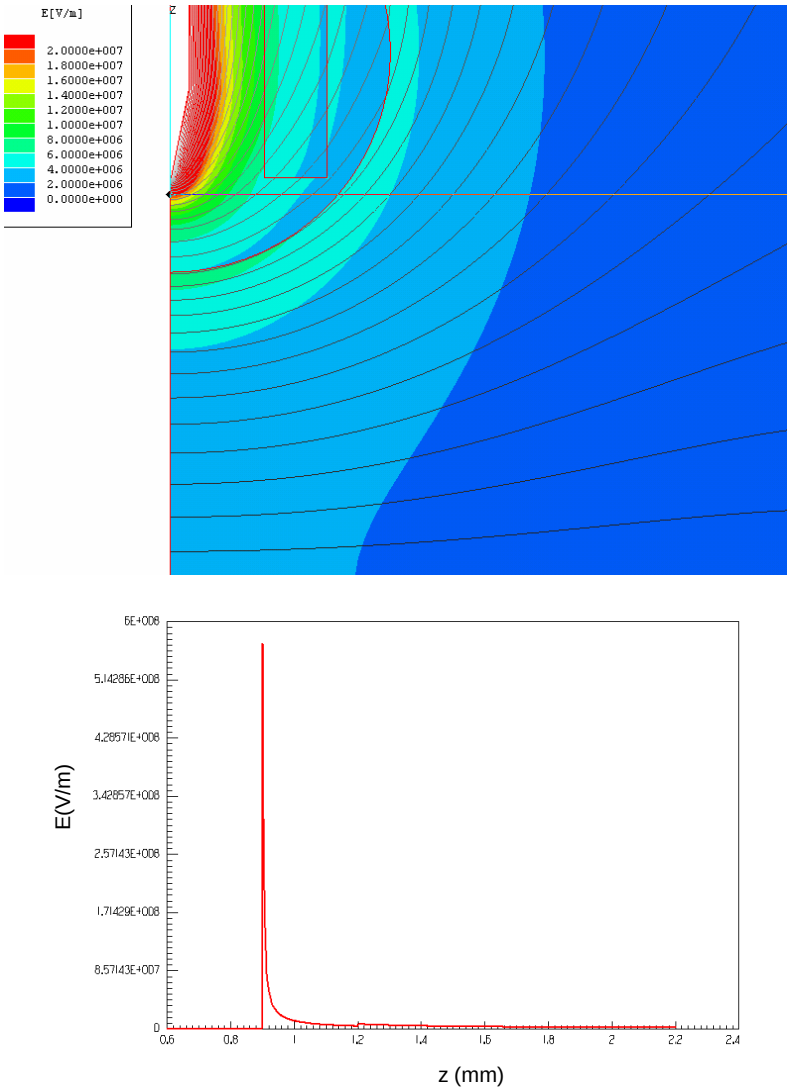

Figure 5. 2: Electric field in a system with a parallel flat bottom electrode and an insulator coated needle-like top electrode by FEM simulation. The distance between the electrodes is 0.5mm and the tip radius 10µm.

5.1.3 THE 750µm DIAMETER NEEDLE

In this case the FEM simulation gives a value of E_{max} of 1.8 MV/mm, slightly bigger than the 1.24 MV/mm calculated analytically. The chart has a smoother shape than in the case of a thinner needle with a shallower gradient near the needle tip.

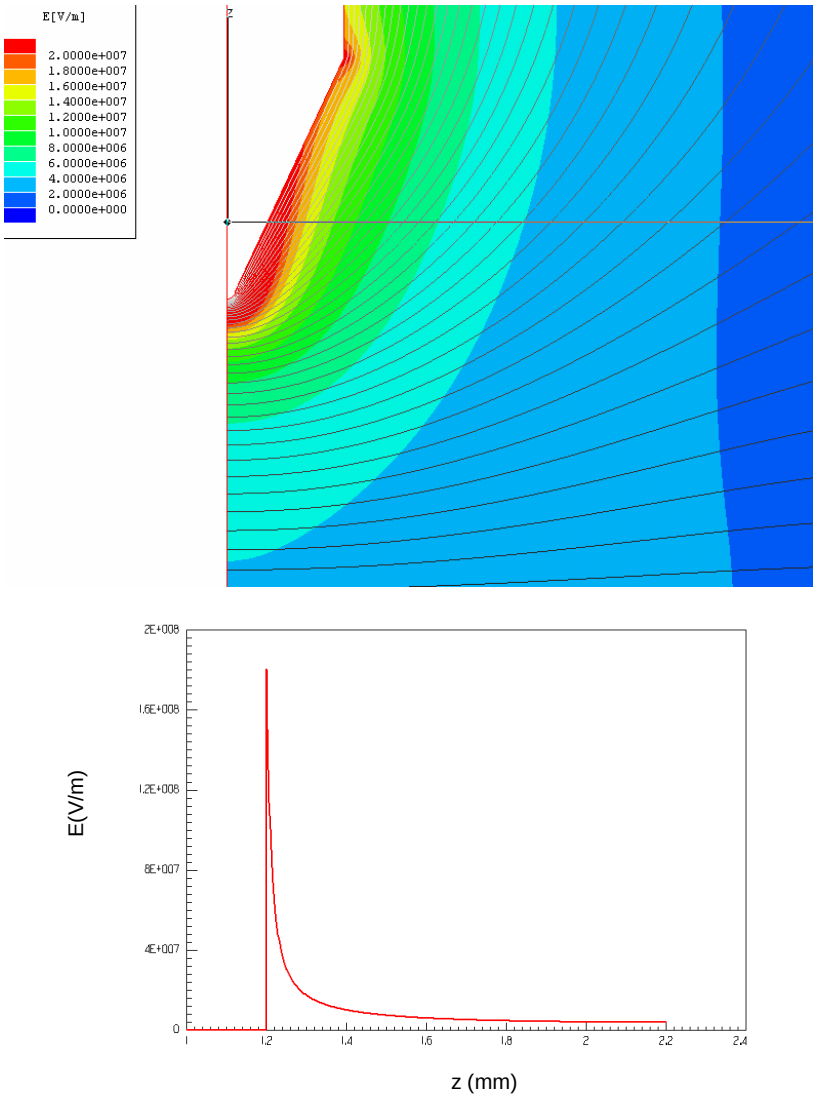

Figure 5. 3: Electric field in a system with a parallel flat bottom electrode and a needle-like top electrode, calculated by FEM simulation. The distance between the electrodes is 0.5mm, the needle diameter is 750µm the tip radius 25µm.

5.2 THE DIELECTRIC FLUID

5.2.1 ELECTRICAL PROPERTIES OF DIELECTRIC FLUIDS

Given what was reported about the dielectrophoretic force, in section3.3.3, it is clear that the measure of the permittivity and the ionic conductivity of the fluid are fundamental to the understanding of the phenomenon under analysis.

The permittivity of the fluid has been calculated using an HP 4192A impedance analyser with an interdigitated electrode exploiting a technique extensively applied to the cure monitoring of resins (Kazilas, 2003). The capacitance measured by the HP 4192A has an uncertainty of 0.15% and Kazilas evaluated an uncertainty of the measurement of $\varepsilon_r' < 3\%$.

The ionic conductivity has been measured applying a DC voltage on a a parallel plate capacitor of dimensions W=49±1mm x L=38±1mm x h=200±50μm and filled with the fluid. Its value corresponds to the ratio between the applied voltage and the consequent current, measured by using a Keithley 6517A.

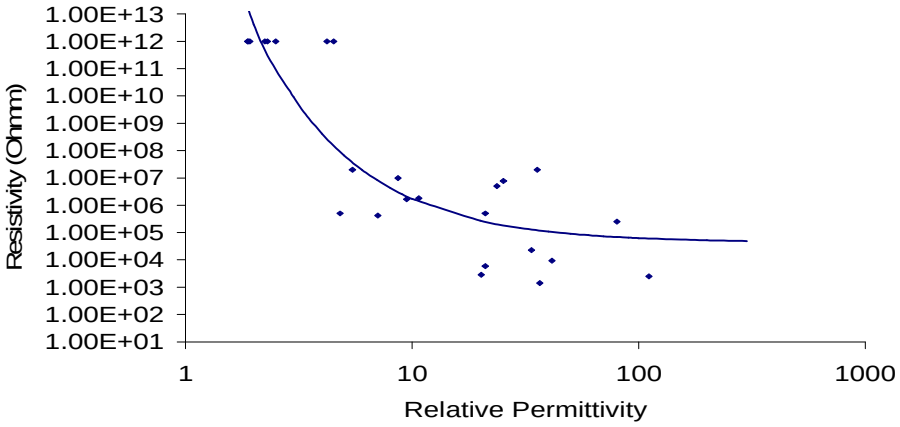

Figure 5. 4: Relative permittivity vs resistivity in dielectric fluid. These results are reported more in detail in Table 5.1

As a preliminary investigation, the properties of a series of liquids have been investigated. Only a few of them have been effectively utilised in the micromanipulation experiments. However, it has been interesting to see how the measurements follow the trend proposed by Sharbaugh (1965), and introduced in section 2.4.4. The results are reported in the graphs and the table 5.1.

Table 5. 1: Results of measuring of permittivity and ohmic conductivity for different dielectric fluids (see appendix D for uncertainty).

Fluid	**Permittivity**	**Conductivity (S/m)**
Acetaldehyde	21.0	2 E-04
Acetone	21.0	2 E-06
Acetonitrile	36.6	7 E-04
Aniline	7.1	2 E-06
Carbon Tetrachloride	2.2	1 E-12
Chloroform	4.8	2 E-06
Ethyl alcohol	25.3	1 E-07
Formamide	111.0	4 E-04
Ethylene Glycol	41.4	1 E-04
Triethylene Glycol	23.7	2 E-07
Heptane	1.9	1 E-12
Texane	1.9	1 E-12
IPA	20.2	4 E-04
Methyl Alcohol	33.6	4 E-05
Nitrobenzene	35.6	5 E-08
Toluene	2.3	1 E-12
Water distilled	80.0	4 E-06
Silicone oil (doped with 2.5% BA)	2.5	1 E-12 (5 E-11)
Methyl salicylate	9.5	6 E-07
Ethyl salicylate	8.7	1 E-07
Ethyl benzoate	5.5	5 E-08
Castor oil (doped with 0.2mM of TBATPB)	4.2	2 E-11 (1 E-10)
FD40	1.9	1 E-12
Methylene Chloride	10.7	6 E-07
Olive oil	3.1	2 E-12
Polychlorinated biphenyl (pyralene, Aroclor)	4.5	1 E-12

The fit shown on the graph is with:

$$-\log\sigma = a/\varepsilon_r + b \text{ where } a=36.731 \text{ and } b=10.678 \qquad (5\text{-}1)$$

Polychlorinated biphenyl is now illegal. Therefore, it was impossible to measure a sample. The value presented has been found in literature (Pardini, 1971).

5.2.2 PROPERTIES OF THE SILICONE OIL

The oil used is a Corning Dow Silicone oil. The measured dynamic viscosity was 47.5±3.3mPa·s, (50cS), and the measured density was 950±95kg/m^3. The oil was treated using a molecular sieve to reduce the water content. The value of relative permittivity was measured using an interdigitated electrode with an HP 4192A Impedance Analyser; the measured value was 2.5. The ohmmic conductivity was measured on a 200±50μm gap parallel plate capacitor; the measured value was $2\pm1.27\times10^{-12}$S/m. The variation of the conductivity with the electric field strength was also tested. The observed conductivity σ_f appeared to follow the Onsager's theory, and could be expressed by the formula given by Atten et al. (1994) (see section 2.4.4). The measured values of the constants were: $\sigma_f(0) = 2\times10^{-12}$ S/m, A = 0.0005, $E_c = 2.23\times10^5$ V/m. The value of $\sigma_f(0)$ is in agreement with the values measured by Atten et al. (1994) and Wu and Conrad (1996; 1997). The values of A and E_c are materially lower.

Ionic mobility is another important characteristic of a dielectric fluid. An extensive study of the mobility in silicone oil has been conducted by Tsuchida and Ueda (1980). They made some controlled doping of the silicon oil measuring the mobility of each added ionic species. He established that the mobility in silicone oil has an average value of 5×10^{-9} m^2/Vs, but that in general the mobility is higher for negative ionic species.

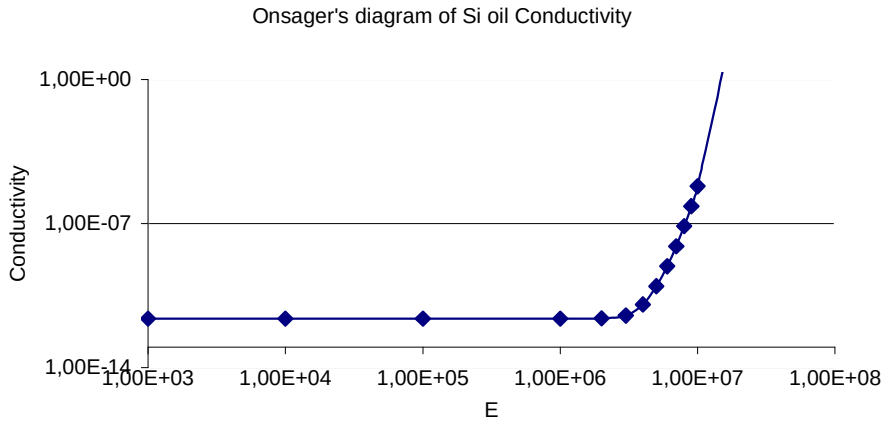

Figure 5. 5: Ideal Onsager behaviour for the conductivity of a silicone oil respect to the electric field.

5.3 PZT FIBRES

The PZT fibres involved in the present research project are made by extrusion and supplied by Ceranova Corp. (US) (see pictures 5.6).

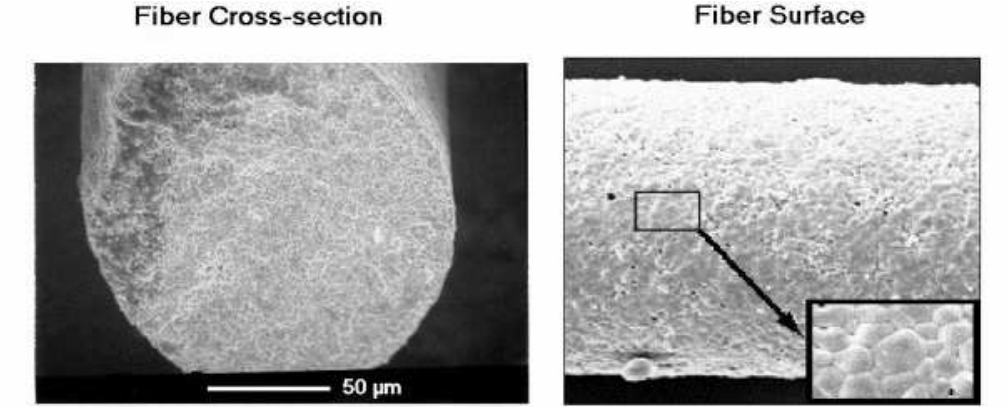

Figure 5. 6: SEM pictures of a PZT 5A fibre supplied by Ceranova Corp (US).

Their diameter was 140±5 µm. To try to reduce any effect due to water absorbed on the surface caused by the environmental moisture, an effect difficult to control, the fibres, before being used, underwent a "standard procedure": they were washed in acetone, dried, and stored in Silicone oil for more than 10 days. An interesting series of

experiments about the effect of the moisture on the dielectric properties of material in form of particulate can be found in (Tombs and Jones, 1993).

The fibre density was extrapolated from the ratio between mass and volume, and was 7750±850kg/m^3. The volume has been calculated from the measurement of radius and length and the weight has been measured using a scale Ohaus Adventurer Pro. The precision of the scale was $\pm 10^{-4}$g (Ohaus Corp., US). The measured value of density is practically equal to the theoretical one for the bulk material. Consequently we can assume that, considering the tolerance of the measure, the densification of the fibres is bigger than, or at least equal to 90%.

5.3.1 MEASURING OF THE PERMITTIVITY

To measure the dielectric properties of the fibres, different ways have been tried. A brief summary is listed below:

1) We measured the capacitance of a device made connecting in parallel a few pieces of fibre connected by adding silver paint at the extremities. Unfortunately the measurement is very imprecise because of the error in determining of the effective length of the fibre.

2) The impedance of a capacitor built by fixing a fibre between two parallel plate electrodes was measured. Then, using the FEM a calibration chart was traced in order to extrapolate the value of permittivity (figure 5.7 and 5.8).
   One of the principal critical points of this method was the difficulty in establishing a good contact between the fibres and the electrodes. It is essential to have a good measure but this was compromising the repeatability of the measure. To improve the contact, a soft electrode in aluminium was used, applying a pressure force of 1.81 kg (4 lbs).

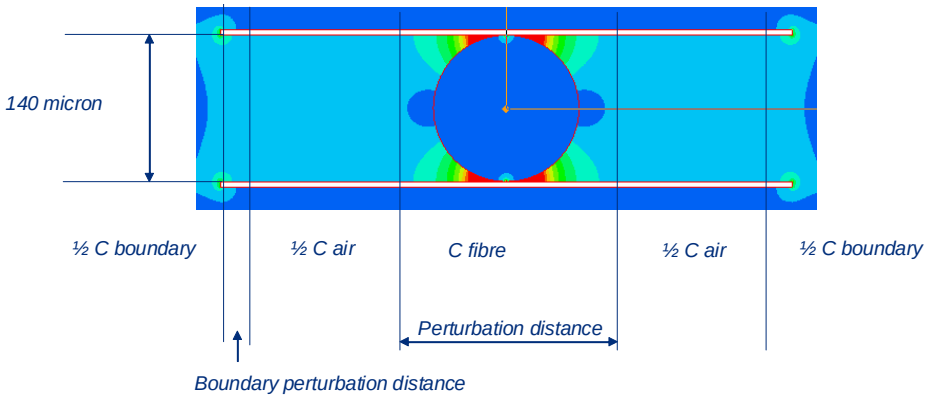

Figure 5. 7. FEM simulation of the electrostatic field capacitor achieved fixing a PZT fibre between two parallel plate electrodes.

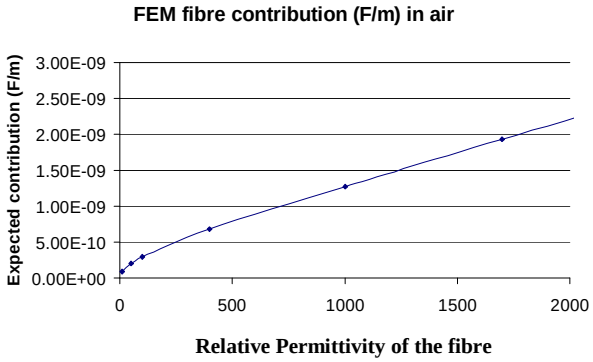

Figure 5. 8. Calibration chart used to extrapolate the value of permittivity, measuring the capacitance of a sample achieved fixing a PZT fibre between two parallel plate electrodes.

3) The same strategy has been used with an interdigitated sensor. The advantage of this sensor is that, compared with the parallel plate capacitor, the precision is not limited by the exact knowledge of the gap. An FEM model of the interdigitated sensor was created to obtain a calibration chart. Unfortunately the measured permittivity was too small. The mismatch was attributed to a poor contact between the electrode and the fibre. However, some useful information concerning the behaviour of the fibre coatings and the polarisation in different fluids was extrapolated using this setup (see appendix C).

4) The value of permittivity was extrapolated using the hysteresis curves (polarisation P in function of applied electric field E) supplied by Ceranova Corp (US). No information about the precision of these curves has been received.

Measuring $\Delta P/ \Delta E$ at low voltages, in a region in which there is no residual polarisation, it is possible to calculate the permittivity (with an accuracy estimated at ±20%) as:

$$\varepsilon_{rp} = (\Delta P/ \Delta E)\, \varepsilon_0 + 1 \qquad (5\text{-}2)$$

being ε_0 the permittivity of the free space.

The permittivity of the PZT 5A fibres extrapolated from the Ceranova polarisation chart was 1800±20%. Instead the value calculated using the parallel plate capacitor was around 1200. This could show the presence of organic residual substances from the extrusion process on the surface of the fibres. In fact this difference was also observed measuring the permittivity of a normal supplied fibre and on a fibre etched by DRIE to remove any presence of organics using an interdigitated electrode (see appendix C).

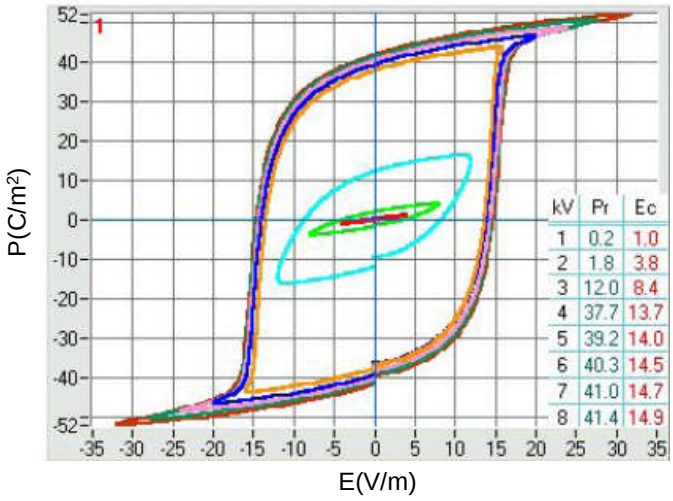

Figure 5. 9: Hysteresis cycle for PZT5A Ceranova fibres (Ceranova Corp., US)

5.3.2 MEASURE OF THE CONDUCTIVITY

The conductivity of the PZT fibre has been identified as a key factor influencing the EFS process. For that reason, a lot of effort was made to measure directly this property instead of considering the value of the bulk material.

A direct measure of fibre conductivity was possible by deposing two electrodes directly on the side of the fibre. In this way it was possible to maximise the resistant section and to minimise the length. This resulted in the fibre having sufficient conductivity for it to be measurable.

The two electrodes were deposited by Dr. Chris Shaw in the Laboratories of Cranfield University, using the process described below:

1. To fix the fibre to the supporting plate using some photoresist
2. To evaporate the chrome on the fibre to reach a coating on the above surface
3. To gently grind the side of the fibre opposite to the supporting plane to create a discontinuity in the conducting layer
4. To wash the photoresist with acetone

Then, the electrodes on the fibre were measured using the optical microscope and a FEM model was made. This model allowed the value of conductivity from the values of conductance directly measured in the chart V-I, using the Keithley electrometer, to be derived. The uncertainty of the current measurement was 1% (Keithley, US). The measures were repeated on two different samples and show a good reliability.

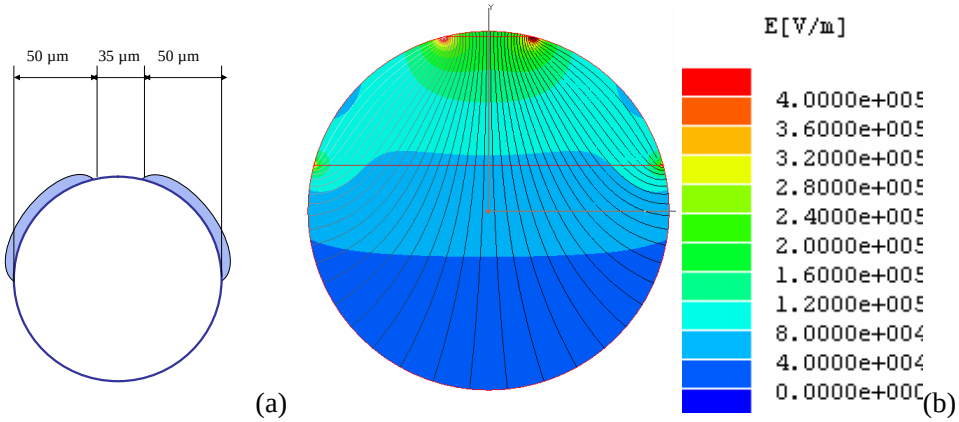

Figure 5. 10: SAMPLE 1. Geometry of the sample (a) and FEM of the electric field in the experimental conditions (b).

Table 5. 2: SAMPLE 1. Results of the V-I measurement (see appendix D for uncertainty)

V(V)	I (pA)	G(pS)
5	15	3.0
10	32	3.2
15	49	3.3

The average is 3.16±0.034 pS. The FEM result for the fibre conductivity is 0.35±0.22nS/m

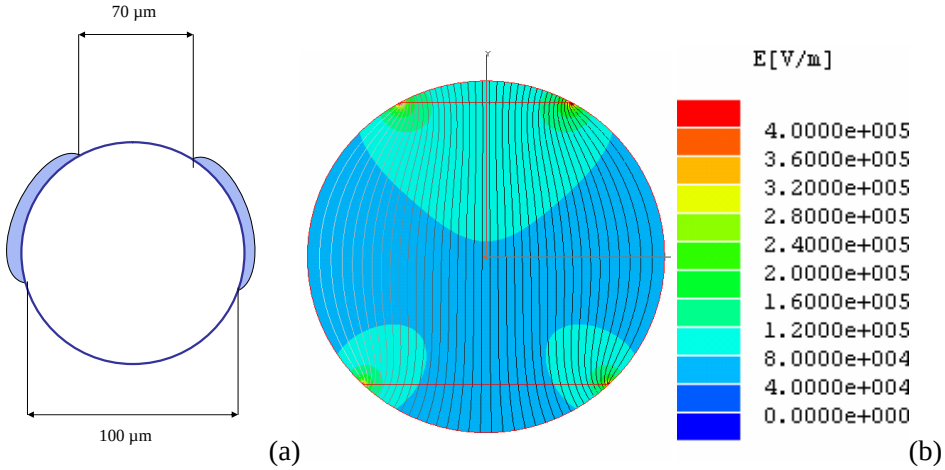

Figure 5. 11: SAMPLE 2. Geometry of the sample (a) and FEM of the electric field in the experimental conditions (b).

Table 5. 3: SAMPLE 2. Results of the V-I measurement (see appendix D for uncertainty)

	Dry		Wet	
V(V)	I (pA)	G(pS)	I (pA)	G(pS)
5	7	1.40	11	2.20
10	15	1.50	21	2.10
15	23	1.53	30	2.00
20	Unreliable			

The average measure is 1.48pS if dry and 2.10pS if wet. The FEM result for the conductivity of the dry fibre is 0.137 nS/m and 0.194 nS/m for the wet fibre.

Wu and Conrad (1996), working on glass spheres of 250µm diameter, pointed out that the conductivity of this kind of particulate was only due to surface conductivity phenomena deriving from a surface film of water. Considering that this film is 22,2nm thick and considering that the conductivity of water equal to 0.18 mS/m, they approximated the conductivity of the particle with a value of 10^{-8} S/m, which is in agreement with experimental evidence. Unfortunately, under the same conditions, the conductance should be equal to 1.028 nS, which is a value much higher than what was

measured in the course of this thesis. In conclusion: the conductivity of these fibres is not given by a continuous water film. It could be a bulk conductivity, or a discontinuous conductivity surface path, or both.

Considering that PZT5A is a ferroelectric material, it exhibits pyroelectricity. If the material is exposed to a temperature gradient, it generates a pyroelectric current I_p:

$$I_p = A\ p\ dT/dt \qquad (5\text{-}3)$$

where A is the cross section and p is the coefficient describing how the polarisation changes, changing the temperature: $p = (dP/d\theta)_T$.
In our case $A \approx 1.4\times10^{-6}$ and $p=2\times10^{-4}$. Consequently, establishing a temperature gradient of 2.7°C/min, it is possible to originate a pyroelectric current of 13pA, of the order of dimension of the current measured. It is consequently fundamental to the reliability of the measure to operate in conditions of thermal equilibrium on the sample.
To give an example, by simply switching off the lamp of the microscope used to verify the positioning of the measuring electrodes, on the dry sample, the current drops to 2.7pA and 7.3pA respectively when 10V and 15V are applied. This is a demonstration of the influence of the pyroelectric effect, explained above, on the measured current. In this case there is a cooling effect, and the pyroelectric current therefore is negative.

5.3.3 TRIBOCHARGE MEASURING

The humidity in the laboratory where the experiments were carried out was between 18 and 26%. These environmental conditions could allow condensation of a water deposit on the particle; unfortunately such an occurrence was not significant enough to render it antistatic. This means that some tribocharges are expected on the fibres.
To support the interpretation of some results presented in chapter 7, we measured the tribocharges on PZT fibres and on some copper rods, for the purpose of comparison.
These measures were carried out using a Faraday pail (see Cross (1987) for details) coupled with the Kethley Electrometer 6517A. The uncertainty of the charge measuring is 0.4% (Keithley, US). The Faraday pail was set up to take the measure in Silicone oil, to be sure that any possible effect derived from the presence of the dielectric liquid was

taken into account. The tribocharge was measured for Cu and PZT rods on a PTFE plate, which lay on a stainless steel grounded plate. The charge of PZT was also measured when the fibre was in contact with a grounded stainless steel plate. Table 5.4 reports the averaged value on a series of groups of 9 fibres each, all 30mm long.
All values are compared with the Gaussian limit, Moore (1973) of charge for a fibre of 140μm of diameter. This limit is related to the maximum charge acquirable by a particle before it spontaneously discharges in air by corona injection.

Table 5. 4: Measured and calculated value of tribocharge for different kind of fibres, with calculation of the Gaussian limit, the electric field in the gap and the adhesion force (see appendix D for uncertainty).

	Gaussian Limit	PZT on steel	PZT on PTFE	Cu on PTFE	Cu on Steel (FEM)	Cr-PZT on Steel (FEM)
Q (pC)	9000	5	37	66	-5.76	-4.35
Qs (μC/m^2)	682	0.38	2.8	5.1	-0.318	-0.329
Q/L (nC/m)	300	0.16	1.2	2.2	-0.192	-0.145

An attempt at measuring the tribocharge on PZT was also made at microscopic level using the AFM. These measures gave some promising preliminary results (see appendix B), but unfortunately, further investigation is necessary before reliable evaluations can be obtained.

5.3.4 ANALYSIS OF THE CHARGE ACQUIRED BY A PZT FIBRE BEAM FROM THE SPACE CHARGE IN THE FLUID

To analyse the dynamic charging phenomenon of a PZT fibre immersed in silicone oil and exposed to an electric field, the deflection of a fibre beam, 20±1mm long, was monitored by applying a DC field with magnitude 1.25MV/m.

Let us consider a reference system like the one in figure 5.12. The linear charge density (Q/L) can be related to the Coulomb force distribution (F_C/L) by:

$$Q/L = (F_C/L)/E \qquad (5\text{-}4)$$

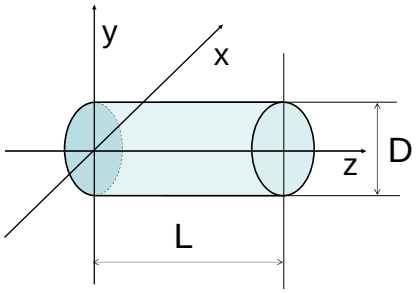

Figure 5. 12: Coordinate system for the computation of the fibre deflection

It is a well known result (Sacco, 1994) that $\Delta y(L)$, the deformation at the extremity of a cantilever beam, can be evaluated as:

$$\Delta y(L) = (F/L)L^4/8Y_xI_y + \chi_z(F/L)L^2/2G_yA \quad (5\text{-}5)$$

$$G = [m/2(m+1)]Y \quad (5\text{-}6)$$

$$\chi_z = A/I_z \int_s [S_z^2(s)/b(s)]ds \quad (5\text{-}7)$$

$$S_z = \int_A ydA = y_G A = \phi^3/12 \text{ (circular section)} \quad (5\text{-}8)$$

Where:

E: electric field

Y_x: Young modulus

G: torsion modulus

m: Poisson's ratio = dy/dx =dz/dy

χ_z: shear modulus

I_i: axial moment of inertia, and in our specific case:

$$I_z = \int_A y^2 dA = \pi \phi^4/64 \text{ for a circular section} \quad (5\text{-}9)$$

$$I_y = \int_A z^2 dA \quad (5\text{-}10)$$

Working with PZT:

$$m=0.35 \text{ (PZT SA4 Navy typeII) (Morgan Electro Ceramics, US)} \quad (5\text{-}11)$$

$$Y_x=66 \text{ GPa} \quad (5\text{-}12)$$

Where the value of the Young's modulus Y_x has been verified exposing the fibre to a well known DEP force.

We observed that, when exposed to a positive voltage, the fibre deflected negatively (downward), showing, as expected, a positive charge (see tribocharge measurement, in table 5.4). The deflection was: 79±10μm (i.e. F/L=7.5±3.5mN/m and Q/L = 6±2.82nC/m).
After 30s, the bias was suddenly inversed. The fibre instantaneously started to deflect positively. The measured deflection was: 56±10μm (F/L=5.3±2.6mN/m, Q/L=4.24±2nC/m). However, unexpectedly, continuing the application of the negative field, a progressive decrease of the deflection value, caused by a continuous negative charging of the particle was observed. 30s after the voltage inversion, the value of deflection became 140±10μm (i.e. F/L=12.1±6mN/m and Q/L = 10.6±5nC/m).
The linear charge indicated in brackets was calculated from the displacement Δy using:

$$Q/L = \Delta y/\{E_0 L^2[\chi_z/(2G_y A) + L^2/(8\, Y_x I_y)]\} \qquad (5\text{-}13)$$

where A is the resistant section area, χ is the shear factor, I is the moment of inertia, G the torsional stiffness, and Y the Young's modulus.

This experiment reveals the presence of a space charge in the liquid bulk and of a charging dynamic like the one theoretically described in section 3.3.2.4 and 3.3.2.5. It confirms the presence of a pre-existing positive tribocharge on the fibre, of the same order of dimension as the one measured using the electrometer. Even if this method is not precise for the computation of the rod charge, it gives an important result.

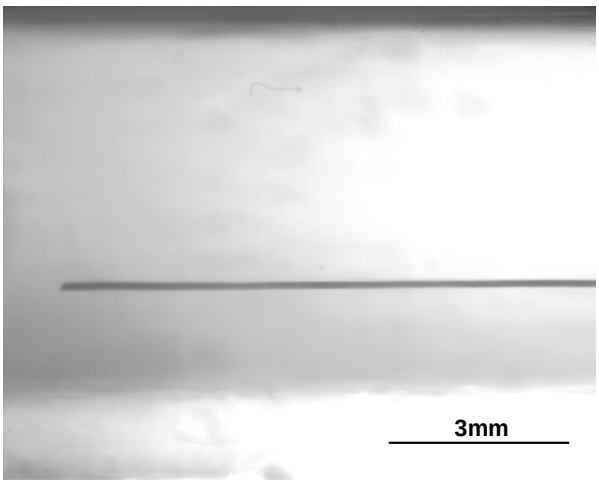

Figure 5. 13: PZT fibre beam, as positioned in the experimental setup

The flow of positive charge carriers is smaller than that generated by negative carriers. The consequence of that is that a rod exposed to an electric field acquires a net negative charge after a certain time, whatever its pre-existing charge.
This difference in current density could be due to a bigger mobility of the negative species in respect to the positive ones.

5.4 OTHER MATERIALS EMPLOYED IN THE PRESENT RESEARCH WORK

In the course of this study, other kinds of particles have been considered. A list of these materials and their main properties is exposed below:

- **Cu fibres**: these fibres have a density of 8230 kg/m^3, a diameter of 192μm and a length varying between 1 and 3mm (see picture 5.13).
- **Cr coated PZT fibres**: some standard PZT5A fibres have been coated with a continuous layer of Cr by evaporation; this operation was done in two steps, respectively on both sides of the fibres using an BOC Edwards 306 evaporator (see picture 5.13).

- **PZT5H 30 μm**: to test the influence of the fibre dimension on the EFS phenomenon some thinner PZT5H (another type of ceramic with properties very similar to the PZT5A) fibres made with sol-gel (Kamiya et al., 1990) were also tried.
- **PZT5A 260 μm**: still in the attempt to test the influence of the fibre dimension on the EFS phenomenon, some PZT5A Ceranova fibres with a double diameter were also tested.
- **Carbon fibres**: a test of the EFS technique was also carried out on some carbon fibres; the fibres come out from a chopped Z-pin carbon wire of polygonal section with a width larger than 400 μm; carbon fibres have normally an ε=12-15, an σ=5-20S/m and a density of 1800 kg/m^3 (Amato and Montanaro, 2000).

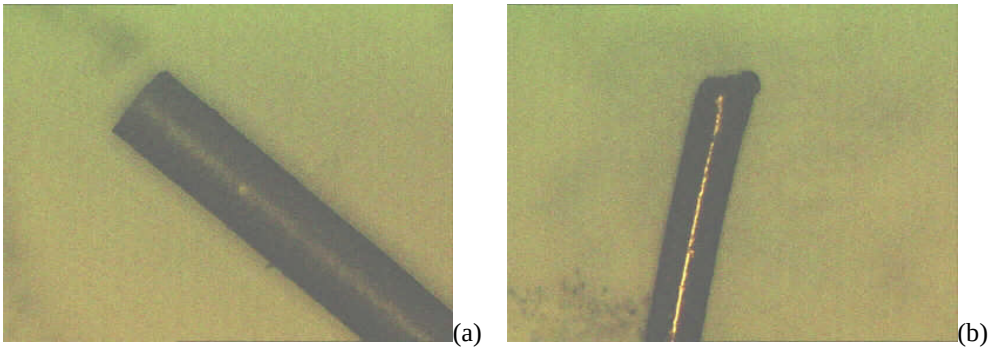

(a) (b)

Figure 5. 14: Particles tip details. (a) PZT rod (b) copper rod

Chapter 5: MATERIAL CHARACTERISATION AND PRELIMINARY INVESTIGATIONS

Chapter 6

CONDUCTION AND ELECTROHYDRODYNAMICS OF AN HOMOGENEOUS DIELECTRIC FLUID IN A NEEDLE-PLANE ELECTRODES CONFIGURATION

In this chapter the behaviour of the fluid exposed to a highly non-uniform electric field is studied. Considering that in these conditions fluid instability can be generated, an analysis via particle imaging velocimetry (PIV) has been proposed.

6.1 HEURISTIC PRESENTATION OF THE PHENOMENA IN AIR

6.1.1 NEEDLE PERTURBATIONS AND ELECTRIC WIND

Experiments were carried out applying a certain electric potential to a 120μm diameter needle, where the distance between the tip and the bottom electrode was 16mm. In this configuration, under certain conditions of electric field, a lot of perturbations are generated on the needle.

The perturbations are always present for frequencies lower than 1 kHz. Above this frequency the needle becomes motionless. The phenomenon is observable only with a negative voltage. Moreover the amplitude of the oscillations increases when the applied voltage increases and when the tip-plane distance decreases.

This oscillatory motion of the needle also happens when the needle is partially immersed in oil.

Though some air motion visualisation would be necessary to assess it, it can be supposed that this motion is due to an electric wind resulting from a corona charge injection through the needle. This injection could arise both from the tip and from the lateral face of the needle. This air motion becoming turbulent and the air could transfer a certain momentum to the flexible thin needle. This hypothesis can also be validated by the fact that the amplitude of the needle oscillation increases and so decreases the dimension of the vessel containing the needle (see picture 6.1).

The phenomenon of the corona induced oscillation of a wire shaped object has already been studied in cylindrical geometry by Farzaneh and Teisseyre (1988). It has also been proposed as a mechanism with which new micro-actuators could be designed (Kawamoto et al., 2005; 2006).

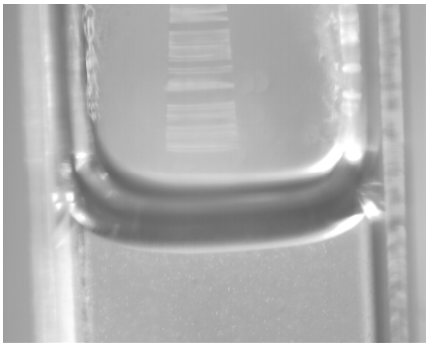

Figure 6. 1: An example of very big perturbation in a 10mm cuvet on silicone oil at 100Hz

6.2.1 THERMAL CAMERA CHARACTERISATION

The corona injection is normally followed by a local Joule heating in correspondence with the needle-tip. Even if the current flowing through the tip is relatively weak, the fact that it flows through a relatively small area, generates a local current density that can reach 250-2500 C/m^3. This is a huge value but it is localised in a very small area. Considering that air is a bad heat conductor compared to metal, in these circumstances the needle tip would heat up. However, in the case of corona injection, the heating up is practically negligible in the conditions of the experiments conducted for this thesis. This is an important consideration as it validates the assumption to neglect any effect linked to electrothermal motion. Unfortunately, due to the fact that silicone oil is not transparent to infrared, this observation cannot be made when the current is injected through the tip in a dielectric fluid. Nevertheless, as the current is of the same order of magnitude in air and in oil, it can be assumed that the hypothesis is still accurate.

As a matter of comparison, the increase of temperature in condition of air breakdown has also been tested. In this case, as expected, the heating up is considerably more intense and can be detected with the infrared camera (see picture 6.2).

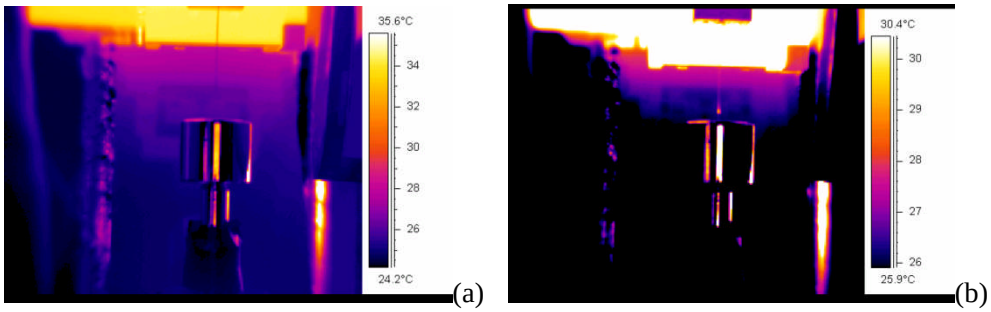

Figure 6.2: Distribution of the temperature in condition of corona injection (a) or air breakdown (b). As it is possible to see, the thermal camera did not revealed great temperature changes on the needle tip when corona injection occurred. However, a temperature change is visible in condition of air-breakdown.

6.2CONDUCTION MEASUREMENT IN LIQUID

6.1.2 CONDUCTION IN THE NEEDLE-PLANE CONFIGURATION

The current flowing from a needle-like upper electrode to a bottom flat electrode, 6mm distant from each other, has been measured using a Keithley electrometer. The I-V charts (see figure 6.3) are shown to be well interpolated by the equation proposed by Atten et al. (1996):

$$(I)^{1/2}=A(h)(V-V_{th}) \qquad (6\text{-}1)$$

where V_{th}=4kV, i.e. $E_{th}\approx$1.5MV/cm, for both the positive and the negative cases.

When the voltage overcomes V_{th} the current becomes very unstable, and the values are oscillating continuously, with a behaviour very similar to corona in air. Therefore, the values reported here are the averages taken over a time of 1 minute.

In this formulation the slope of the curve after V_{th} is directly related to the hydrodynamic mobility. The orange trace has been obtained considering a k_H 1.25×10^{-7} m/Vs. We can see that the value of the mobility is very close to the predicted one when the applied field is negative. For a positive field the mobility is longer. Given its physical meaning, k_H should not be related to the nature of the carriers. Thereby, it should be independent from the bias of the electric field. This implies that the result needs further investigation. However, it seems plausible that the injection in the positive case is not very strong, that the energy transfer would become less efficient and would therefore differ from the observations of Atten et al (1997).

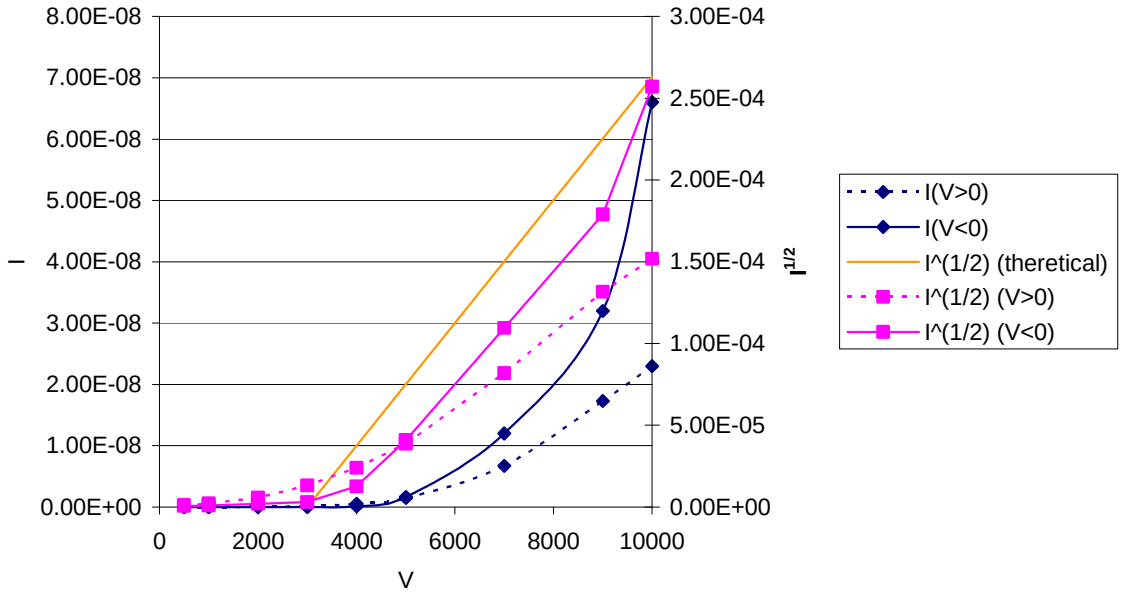

Figure 6. 3: Experimental measurement of V-I characteristic of the needle plane system, and comparison with the theoretical value calculated by using (6-1)

6.2.2 CONDUCTION IN THE INSULATOR COATED NEEDLE-PLANE CONFIGURATION

The current flowing from a insulator coated needle-like upper electrode to a bottom flat electrode, 6mm distant from each other, was measured using a Keithley 6517A electrometer. The current measured in this case is comparable to the case without coating when $V<V_{th}$. Nevertheless, no instability is visible and the conductivity shows a quasi ohmmic behaviour. The conductivity slightly increases with the voltage, this may be due to some electric field enhanced effects.

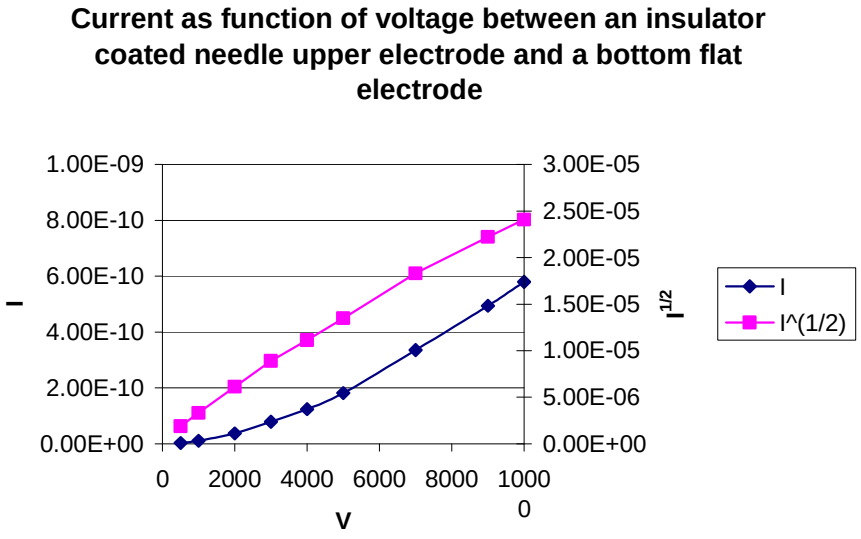

Figure 6. 4: Experimental measuring of V-I characteristic of the needle plane system, when the needle is insulator coated with an insulator

6.3 PIV CHARACTERISATION AND QUANTITATIVE ANALYSIS OF EHD PLUMES

6.1.3 THE PIV TECHNIQUE AND THE EXPERIMENTAL SETUP

To investigate the EHD flow phenomena in dielectric liquids, it is necessary to visualise the fluid motion. Dark field photographic techniques, such as the Schlieren photography, can be useful to map the fluid trajectory, but are less able to produce a quantitative measurement of the fluid speed in a certain point (see picture 6.5). Instead, laser Doppler velocimetry can be employed to measure the flow speed in a certain area (Albrecht, 2003).

Another interesting method is the PIV (Particle Imagery Velocimetry) (Fukumoto and Ohyama, 2003; Ryo-ichiro and Kiyoji, 1997; Sekino et al., 1998). In this technique, a certain amount of seeds are dispersed in the fluid. A relatively thin part of the fluid is cleared using a laser sheet. In this way, the fluid motion can be observed indirectly from

the seeds' motion. Particularly in EHD visualisation it is important for the seeds to be neutral and to have a dielectric constant as similar as possible to the fluid's dielectric constant. In this way any action of the electric field on the seeds is minimised.

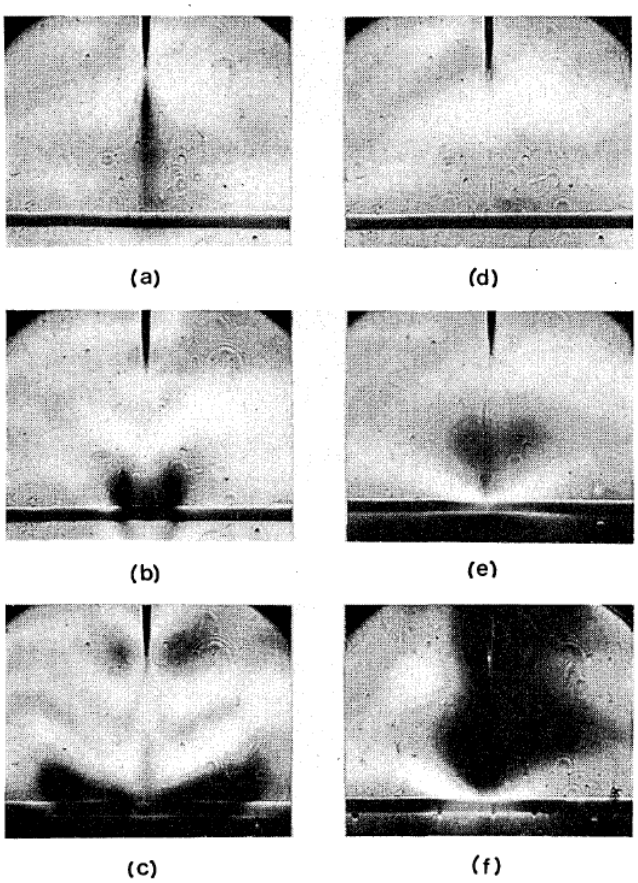

Figure 6. 5: Schlieren photographs of silicone oil after application of 7kV to the blade (Sueda and Kao, 1980)

The vector field of the speed is computed by taking a sequence of two digital images of the flow with a delay τ. The images contain the information of the position of the fluid at a given time. The images are then divided in a matrix of small areas. To obtain a good final result it is necessary to find the frame rate and the dimension of the cells so as to have at least 5 seeds in each cell and to have the same number of seeds in the first and in the second frame. The algorithms of PIV are based on an analysis of the maximum correlation between the two images.

The setup supplied for the experiments was a courtesy of TSI system and included:

- A TSI Nd:YAG double pulse laser (50 mJ/pulse) complete with a light sheet optics
- A POWERVIEW™ Plus CCD camera with frame-straddling
- An INSIGHT™ 3G-2DTR Software Package for data acquisition, analysis and display
- A LASERPULSE™ 610034 Synchronizer

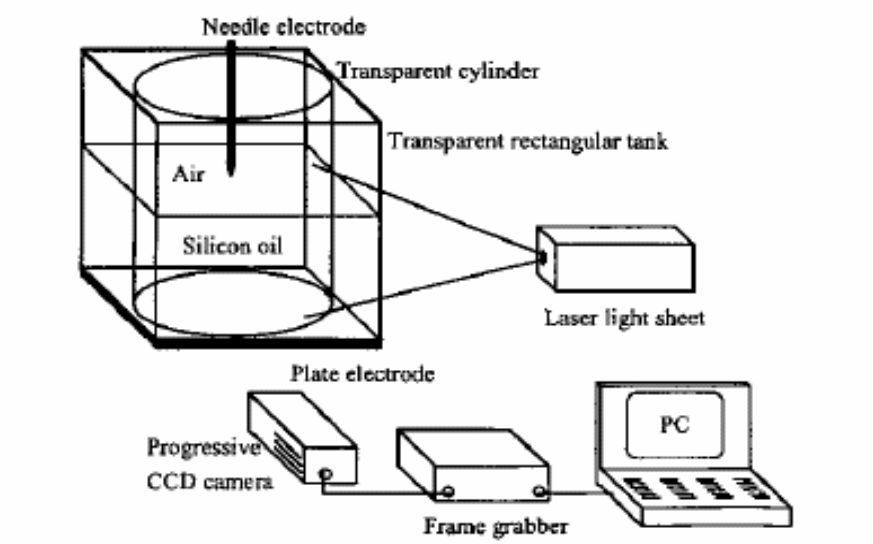

Figure 6. 6: Schematics of the experimental setup for EHD liquid flow velocity distribution measurement by particle image velocimetry

An uncertainty of 5% is a reasonable value for the present PIV setup (Hyde, 2005).

6.2.3 DC EXPERIMENTS

When applying a V=10kV on an 8.5mm gap, as a consequence of an injection of charge through the needle, an instability arises with generation of an EHD plume (see section 2.5.3.2). The speed has been estimated by PIV being 0.15-0.2 m/s near the needle tip

and decreasing to 0.12-0.14m/s in proximity of the bottom electrode. This value is in line with what can be found in the literature (Ohyama and Kaneko, 1996; 1997; 1998).
The vectorial field of the speed and a plot of the vorticity are reported in figure 6.7. The speed seems to be higher near the needle tip. This could be explained by the fact that this region concentrates the maximum field and charge. However, a considerable increase of the speed has also been detected in the centre of the plume. This result is important because it confirms the conclusion of Perez et al. (1995). Nevertheless, the theoretical model proposed by Perez et al. (1995) does not address an increase of speed near the tip.

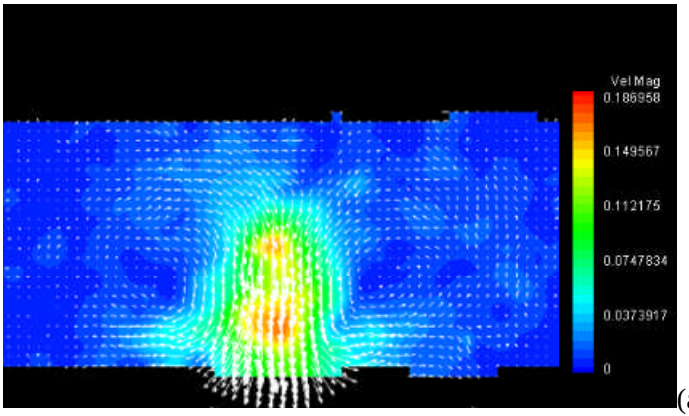

(a)

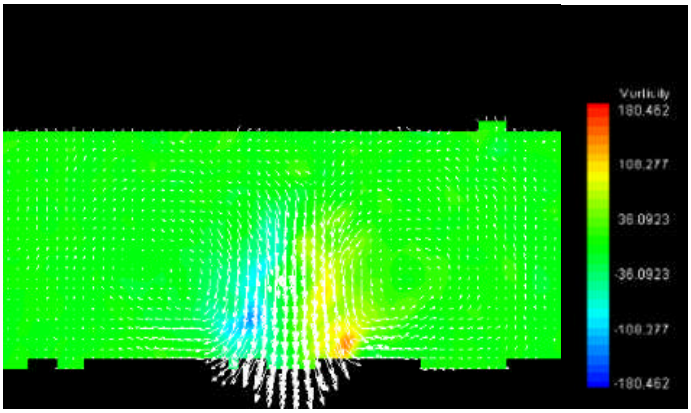

(b)

Figure 6. 7: Vectorial plot of the speed distribution in a silicone oil. A DC voltage of 10kV has been applied an needle-like electrode 8.5mm far from a flat bottom electrode.
The PIV plot report a colour map relative to the magnitude(a) and the vorticity(b)

No great difference in the speed distribution was noticed when applying a positive or a negative electric field, and in both cases the speed is in the same range of dimension as

expected given a k_H of 1.25×10^{-7} m/Vs. An explanation for the difference in current value cannot be drawn from this observation. To explain it is necessary to assume that the threshold of instability depends only on the electric field and that the plume speed is related only to the fluid characteristics. Nevertheless, the injection strength could vary in the positive and negative case, and the plume, although it has the same speed, it does not have the same charge density. Further investigations are necessary to confirm this type of behaviour.

6.3.3 AC EXPERIMENTS

As viewed in the theory exposed in section 2.5.3.2, the unipolar charges injected need a certain diffusion time, and when applying an alternate field they can diffuse up to a maximum travel distance L_{ion}, equal to:

$$L_{ion} \approx kE/2f \qquad (6\text{-}2)$$

L_{ion} has the tendency to become negligible for high frequency. In figure 6.8 L_{ion} for different voltages is reported considering the ionic and the hydrodynamic mobility.

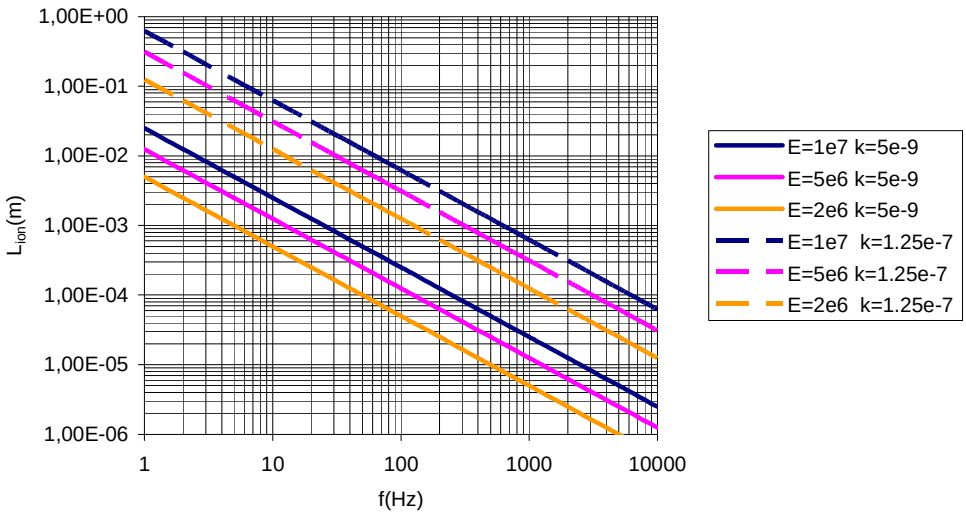

Figure 6. 8: Averaged distance travelled from an injected ion in a system without instability ($k=5\times10^{-9}$) or with instability ($k=1.25\times10^{-7}$).

Moreover, the instability is not instantaneous and needs a certain time to occur, normally around 0.5s. Consequently, no instability can exist above a certain frequency.

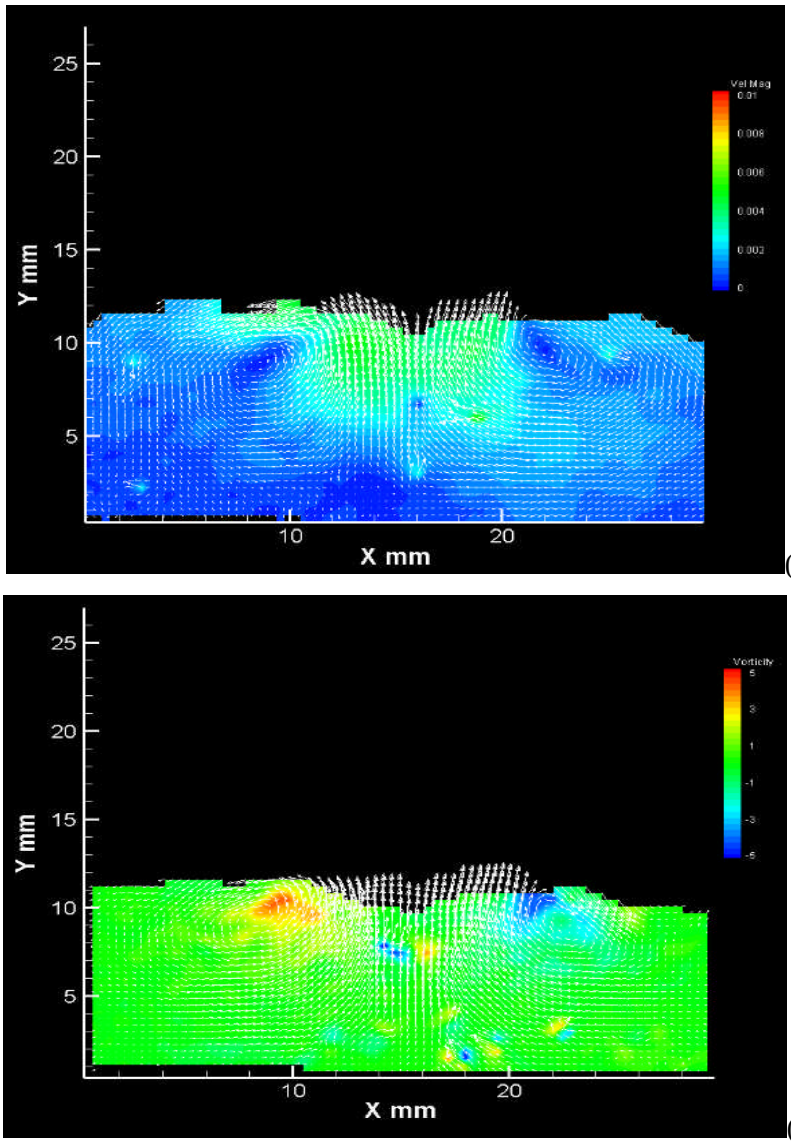

Figure 6. 9: Vectorial plot of the speed distribution in a silicone oil. A 1kHz signal of 7kV has been applied an needle-like electrode 8.5mm far from a flat bottom electrode.
The PIV plot report a colour map relative to the magnitude(a) and the vorticity(b)

Figure 6.9 shows a PIV analysis operated applying a field at 1kHz and 7kV. As expected, no EHD plumes exists. Nevertheless, a new EHD instability is observed. The fluid moves tangentially to the surface between oil and air going away from the needle.

The maximum speed is 6mm/s, and the maximum is located area closer to the intersection between the needle surface and the surface separation between air and oil. One of the points of minimum speed is located near the needle tip. This instability is not instantaneous and takes 12s to happen.

6.4 FLUID MOTION VISUALISATION AND QUALITATIVE ANALYSIS IN DIFFERENT ELECTRODES CONFIGURATIONS

Table 6. 1: Summary of the different kind of EHD instabilities observed with different kind of electrode configurations. The speed uncertainty has been evaluated as equal to 6.8% (see appendix D).

- 120 N: indicate a configuration with a 120μm diameter upper needle and a bottom flat electrode
- 750 N: indicate a configuration with a 750μm diameter upper needle and a bottom flat electrode
- 120 CN: indicate a configuration with an insulator coated upper needle and a bottom flat electrode
- 120 CNCB: indicate a configuration with a 120μm diameter upper needle and a PTFE coated bottom flat electrode
- SPH: 120 N: indicate a configuration with an 8mm diameter spherical upper needle and a bottom flat electrode

Elettrode configuration	**Motion after switch on**			**Motion after switch off**		
	Motion type	**Speed (mm/s)**	**Incubation time (s)**	**Motion type**	**Speed (mm/s)**	**Incubation time (s)**
120 N 10kV DC	A	100	0	B	1.2	660ms
120 N -10kV DC	A	110	0	B	2.6	660ms
120 N 10kV 1Hz	A	105	0	No		
120 N 10kV 10Hz	C	2.1	0	B	1.0	660ms
120 N 10kV 50Hz	C	5.0	0	No		
120 N 10kV 500Hz	C	4.0	0	No		
120 N 7kV 500Hz	C	3.2	7	No		
120 N 7kV 1kHz	C	3.1	12	No		
750 N 10kV DC	B	4.2	0	No		
750 N -10kV DC	B	4.1	0	No		
750 N 10kV 1Hz	B	4.2	0	No		
750 N 10kV 10Hz	No		0	No		
750 N 10kV 50Hz	No		0	No		
750 N 10kV 500Hz	C	0.8	0	No		
750 N 7kV 1kHz	C	0.3	15	No		
120 CN 10kV DC	B	5.6	0	No		
120 CN -10kV DC	B	5.3	0	No		
120 CN 10kV 10Hz	No		0	No		
120 CN 10kV 50Hz	No					
120 CNCB 10kV DC	B	5.6	0	No		
120 CNCB -10kV DC	B	5.5	0	No		
SPH 10kV DC	B	4.9	0	No		

Apart from the quantitative analysis carried out by PIV, a series of qualitative evaluations has been made on a series of other electrode configurations and voltage conditions.

The EHD observations has been carried out using the Redlake camera described in section 4.2, and the movies have been recorded at frame rates between 60 and 500 fps. Depending from the necessity, a post-processing, carried out by an operator who analysed the seeds motion on each single frame of the movies, allowed the extrapolation of the flow speed in some opportune selected areas. Most importantly these analyses made it possible to map the flow patterns.

The distance between the above and the bottom electrodes was fixed to 5mm. The electrodes were immersed in silicone oil, and the distance between the free surface of the oil and the bottom electrode was 10mm. Table 6.1 summarises the results of the observations.

All cases shown in table 6.1 can be placed in three main pattern categories.

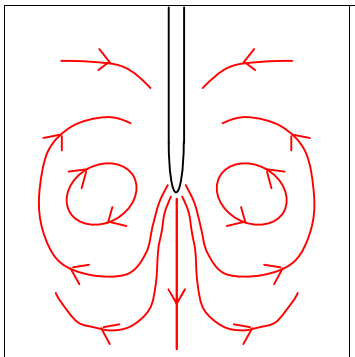	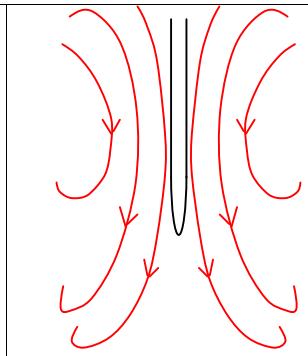	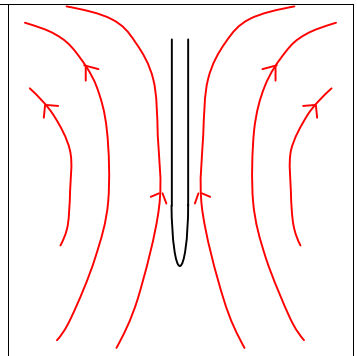
Motion pattern type A Jet flow from the needle tip It occurs in case of injection of charge through the needle-tip	Motion pattern type B Bulk motion up It occurs in case of injection of homo-charge on the air-liquid boundary	Motion pattern type C Bulk motion down It occurs in case of injection of hetero-charge on the air-liquid boundary

Figure 6. 10: Summary of the different patterns characterising the different EHD instabilities

Pattern A is characteristic of systems in which there is a plume instability due to charge injection. This type of pattern was always encountered when a DC field was applied across a 120μm diameter needle upper electrode and a bottom flat electrode. We observed the same motion behaviour in section 6.2.3 presenting the PIV vector plots. The speed of the fluid near the needle tip was in the order of 0.1 m/s, as already measured by PIV.

Pattern B describes a very different type of motion. In this case the motion was due to a tangential motion of the oil free surface towards the needle. This kind of motion has been observed for any system, except when a 120μm diameter needle was exposed to a DC voltage. The speed was considerably lower than in pattern A, oscillating between 4 and 5mm/s. The speed was measured at the point closer to the needle surface and 8mm far from the bottom electrode.

Pattern C describes a motion following a trajectory very close to pattern B, but in the opposite direction. This kind of motion happens normally at frequency above 50Hz in the systems presenting the behaviour in DC described by pattern A. The speed was between 2 and 5mm/s and was measured in the same point as in pattern B. However, a pattern C motion was also observed in the case of a 750μm diameter needle opposed to a bottom flat electrode. But in this case, the maximum speed was considerably smaller, between 0.3 and 0.8 mm/s.

The behaviour at 1Hz is normally as observed in DC, but with the instability showing a 2Hz oscillating behaviour.

No motion exists at a frequency of 10-50Hz in the electrode configuration characterised by the type B motion in DC. On the contrary, as mentioned above, in systems characterised by pattern A, if exposed to a DC field, for frequencies of 10-50Hz, there is a motion as in pattern C.

Another interesting aspect of the EHD motion following pattern A (i.e. a 120μm diameter needle upper electrode in front of a bottom flat electrode) is that after the field was switched off, and after a short time of latency (660ms), the fluid start to move again. This motion follows the B pattern at a speed between 1 and 2 mm/s for almost 7.5s.

6.5 DISCUSSION OF THE RESULTS

As shown above when a system consisting of an upper probe-like electrode immersed in a dielectric fluid located opposite to a bottom flat electrode is exposed to an electric field, some EHD motion can occur. These instabilities are normally of three kinds (see figure 6.10).

The A type instability normally occurs when the upper electrode is a very sharp needle. This instability is due to a charge injection through the tip. The maximum speed is normally around 0.15 m/s, a result aligned also with PIV results already published. Another important observation is that the speed along the plume is not constant. The speed is maximal close to the tip and has the tendency to increase again in the centre of the stroke. This result confirms the conclusion of Perez et al. (1995) tested in a 2D system.

Types B and C are patterns that could be described assuming that a surface charge exists at the boundary between air and liquid. Figure 6.11 shows the results of a couple of FEM simulations carried out with FEMLAB. The pictures illustrate the electric field flow lines in the case of a 120μm and a 750μm diameter needle upper electrode, in our experimental conditions. Considering this electric field distribution, when a surface charge at the interface generates a fluid motion, the sign of the charge has to be opposite to the one of the needle voltage in pattern B, and equal to the needle voltage in pattern C.

In B pattern, the accumulation of charge can result only from ohmmic conductivity phenomena. The charges move from the bulk following the field line and then reach the interface. Next, due to a blocking effect imposed by the interface, the surface charge on the boundary rise. This hypothesis would explain why type B motion happens always in DC when no injection exists.

The presence of a homocharge, that can justify C type instability, can be explained by a corona injection from the lateral wall of the needle onto the oil surface. This type of instability is only observed when working with the thinner needle. However, considering that the alternate voltage applied has a zero average value, the sole

hypothesis of a corona injection is not enough to explain a net steady motion. Such a motion can be explained assuming a mismatch in positive and negative corona in air.

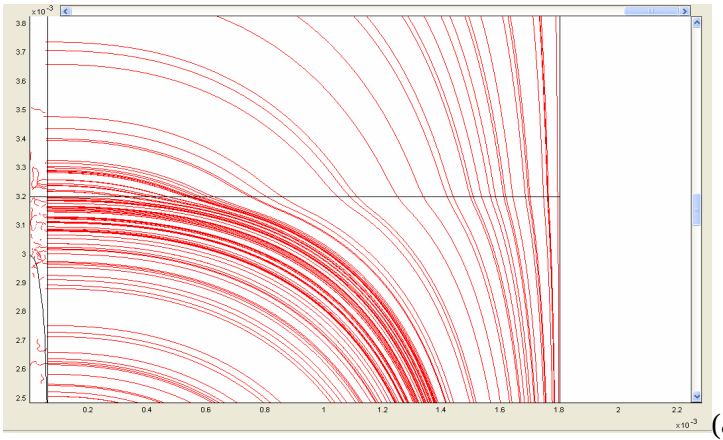
(a)

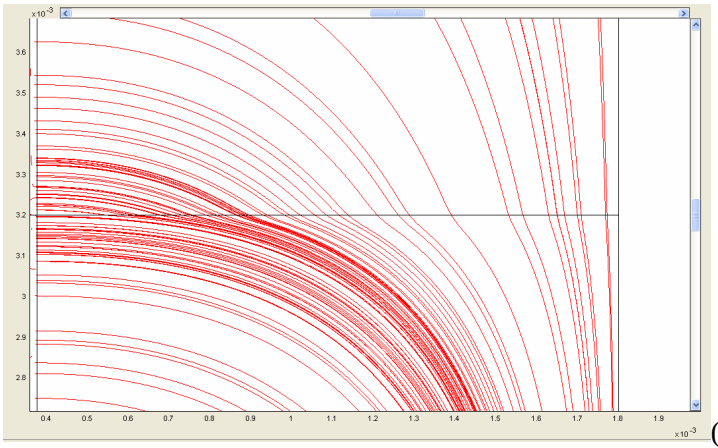
(b)

Figure 6. 11: FEM simulation of the electric field flow lines across the air-liquid interface in the case of a needle with a diameter of 750mm (a) or 120mm (b).

This assumption has already received several experimental confirmations in other systems (Ohyama and Cheng., 2000). Moreover, this hypothesis could explain having an incubation time for the lowest field. The existence of a motion would be the result of the breaking of the symmetry between the positive and the negative parts of the voltage period.

Also the B type motion observed some time after the switch off could be due to a surface charge. Unfortunately, considering that the motion happens when both electrodes are earthed and no field is applied, the motion is probably only due to some image interaction and to the reciprocal repulsion of the charges resting on the oil surface. It is difficult to say a priori what the sign of the charge could be. However, taking into consideration the comments on motion type C above, it is reasonable to assume that the surface charge is generated by a corona injection and that it is then a homocharge.

Chapter 7

ELECTROHYDRODYNAMICS OF A SINGLE MICRO-FIBRE EXPOSED TO A UNIFORM AND DIVERGENT ELECTRIC FIELD

The objective of this chapter is to study and compare the motion and charging mechanisms of different kinds of particles exposed to an electric field, in different configurations of electrodes and electric field topologies.

In classical approaches to this subject, all the interest was focused only on conductive particles, because they can be charged by induction (Felici, 1966). A lot less interest has been paid to insulating particles. In the present study focuses on ferroelectric particles (see section 2.3.4), which can be described as dielectric material with a very high dielectric constant.

When a cylindrical insulating particle lies on a grounded electrode, exposed to an electric field, the particle generates a field enhancement in the contact zone, directly dependent on the ratio $\varepsilon_p/\varepsilon_l$. Consequently, if the particle is ferroelectrical, it is possible to reach, in the contact zone, an electric field value higher than the dielectric strength of the dielectric liquid. This can generate a current, the particle can become charged, and consequently, the particle can move.

The rod-like particles considered in this chapter are copper, PZT (see section 5.3 and 5.4) and some PZT fibres coated with a thin film of chrome to test the effect of a metal coating on an insulator fibre.

The charging phenomena have been evaluated in an injection free uniform electric field system. In this configuration an evaluation of the lift-off electric field for the three kinds of particles has been measured and compared with the theory. The study was completed by an analysis of the charge, carried by the particles, calculated from the motion characteristics. Only for a metallic particle, a relationship between such charge and the electric field has been also evaluated. Finally, the behaviour of the particles exposed to an AC voltage has also been considered.

The same kind of analysis was also carried out in the needle-plane electrode configuration characterised by an injection of charge through the tip.

The last part of the study has been spent analysing how the particle dynamics changes when one, or both, of the electrodes are coated with a layer of insulator.

7.1. FINITE ELEMENT SIMULATION

7.1.1. METALLIC PARTICLES

A series of FEM simulations has been computed to evaluate the force acting on a cylindrical particle exposed to an electric field.

All the FEM models were designed for both, a PZT and a copper particle, in silicone oil. The particle was a sphere or a horizontal cylinder with a radius r=70μm in a field of 1.666MV/m.

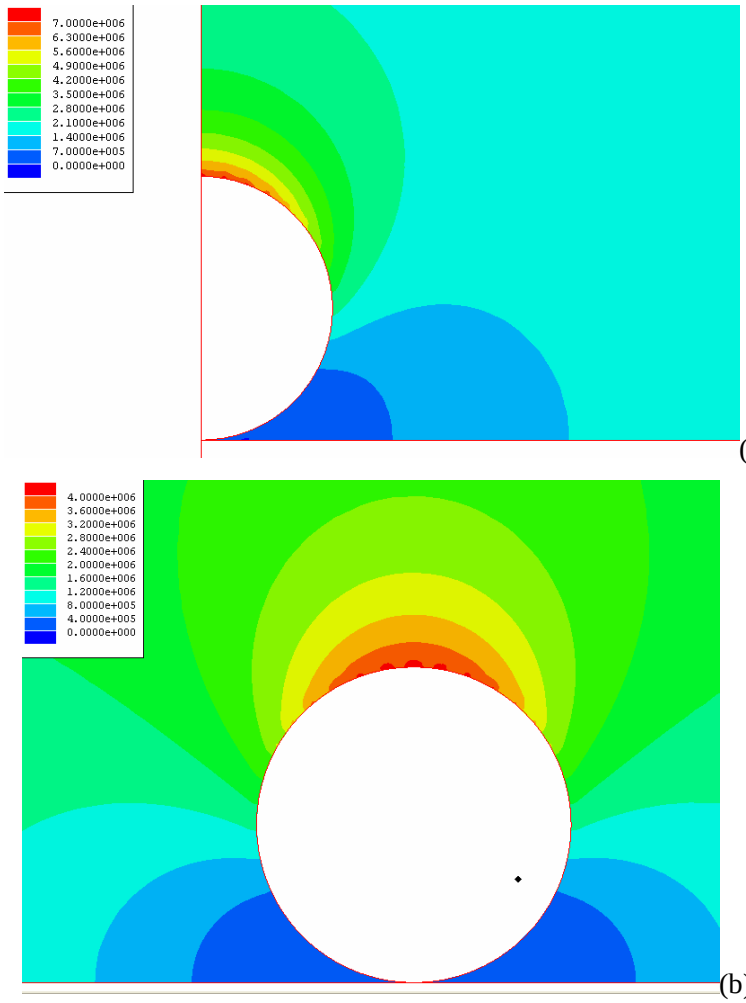

Figure 7. 1 Maxwell FEM analysis of the electric field distribution around a conductive sphere (a), or an horizontal conductive cylinder (b), in silicone oil, if exposed to E=1.666MV/m (d=0.5 μm).

Two simulations relative to a sphere and a cylinder isopotential with the grounded substrate on which it is at rest in are shown in figure 7.1. The FEM (theoretical) value of the lifting force for the sphere is 5.16 (5.17) μN, while the force per unit of length for the cylinder is 19.56(19.32) mN/m. There is a good agreement between the simulation and the theory. As expected, in this configuration, no electric field enhancement exists in the contact zone.

As already presented in section 3.3.4.2.2, due to the image charge, the boundary problem of a sphere at a certain distance d from a grounded plane is equivalent to the problem of two spheres at a distance 2d from each other.
Therefore, the reliability of the FEM simulation in the computation of the electric field, has been verified solving the problem of a conductive sphere 0.5μm away from the plane, assuming zero charge on the sphere. The results have been compared with the value calculated by the Arp and Mason (1977) formula (section 3.3.4.2.2). The plot of the electric field in the gap (in figure 7.2) shows a good agreement with the value of 113MV/m, calculated by Arp and Mason (1977). This simulation provided evidence of one of the weakest points of the conductivity models presented by Atten at al. (1994), and Wu and Conrad (1996). In these models, the electric field in the gap is estimated using the formula:

$$E_{gap} = V/d = E_0 (r + d)/ d \qquad (7\text{-}1)$$

Where d is the distance between the particle and the plane electrode. This formula arises from the hypothesis that the field lines of the electric field are vertical and parallel. Potentially fruitful further work would be to design a conductivity model using (3-36), the Arp and Mason formula, to compute the electric field in the gap.

7.1.2. PZT PARTICLES

In this section, an FEM model for a spherical and a cylindrical PZT particle is presented. The model shows, that the case of a PZT sphere, characterised by $\varepsilon_p/\varepsilon_l \approx 1000$, is well approximated by the limit case of an insulated zero charged conducting

sphere, with $\sigma_p/\sigma_l \rightarrow \infty$. The electric fields, have practically the same distribution (shown in figure 7.3 and 7.4), and the adhesion in the case of PZT, it is equal to 20.09 μN, a value just slightly lower than the at $\sigma_p/\sigma_l \rightarrow \infty$. It is interesting to highlight that this value is in a range between the value calculated by Tao et al. (1995) and that calculated by Jones (1995), both are shown in table 3.2. Moreover, this value is considerably higher than 1.04μN and 5.16 μN, respectively the electrostatic adhesion and the lift force in the case of a conducting sphere isopotential with the substrate (Felici (1966)'s model).

For the cylindrical geometry, according to the model, the adhesion force is 81.80 mN/m.

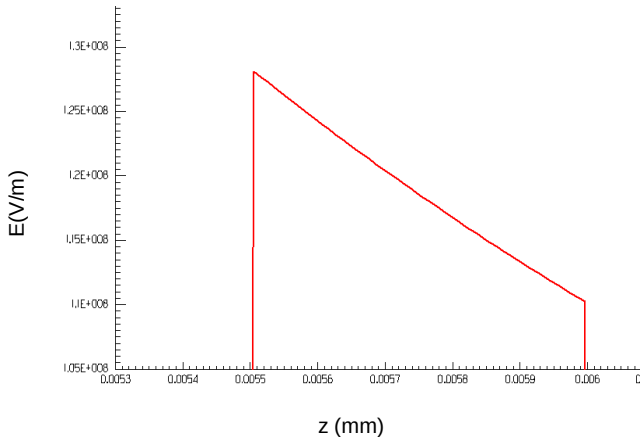

Figure 7. 2 Maxwell FEM analysis of the electric field distribution in the gap separating a metallic sphere from a grounded plane, in silicone oil, if exposed to E=1.666MV/m (d=0.5μm), in the case of sphere insulated from the substrate, with no residual charge. This plot shows a good agreement with the value of 113MV/m, calculated by Arp and Mason (1977)

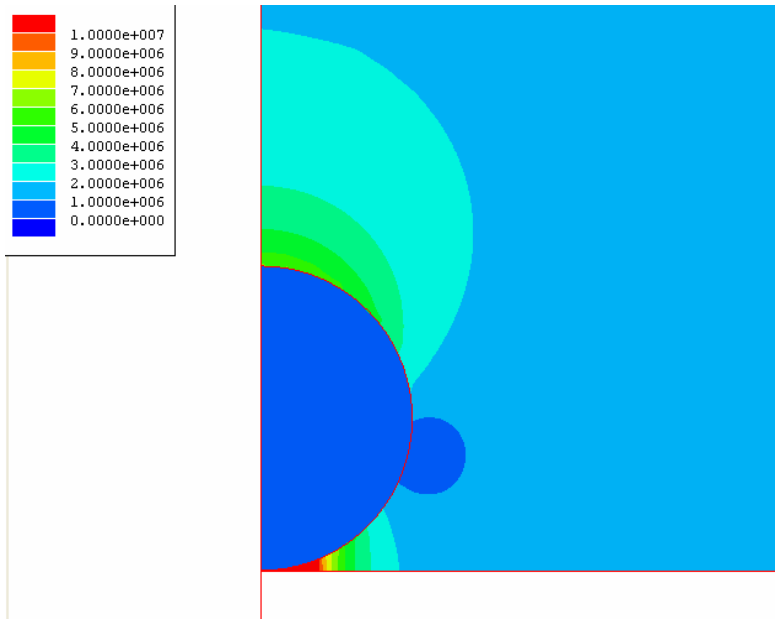

Figure 7. 3 Maxwell FEM analysis of the electric field distribution around a PZT sphere, in silicone oil, if exposed to E=1.666MV/m (d=0.5 μm).

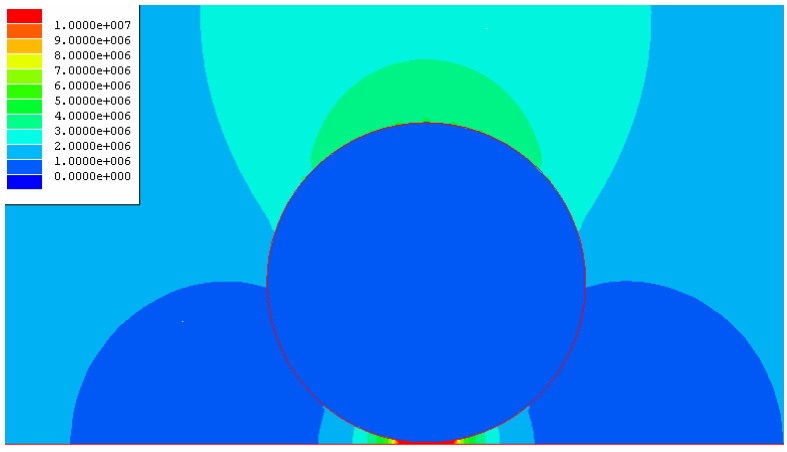

Figure 7. 4 Maxwell FEM analysis of the electric field distribution around a PZT cylinder, in silicone oil, if exposed to E=1.666MV/m (d=0.5 μm).

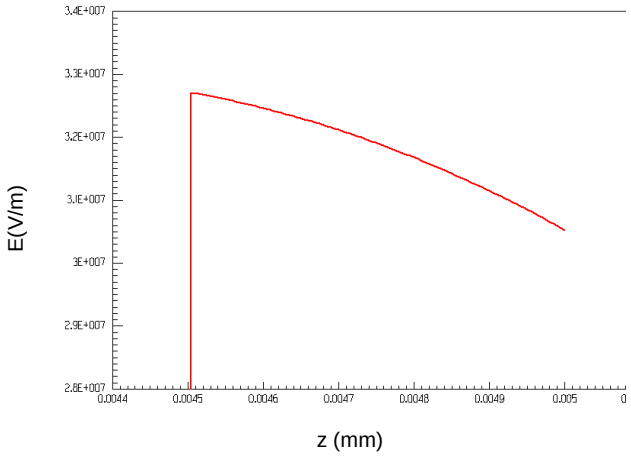

Figure 7. 5: Maxwell FEM analysis of the electric field distribution in the gap separating a PZT cylinder from a grounded plane, in silicone oil, if exposed to E=1.666MV/m (d=0.5 μm).

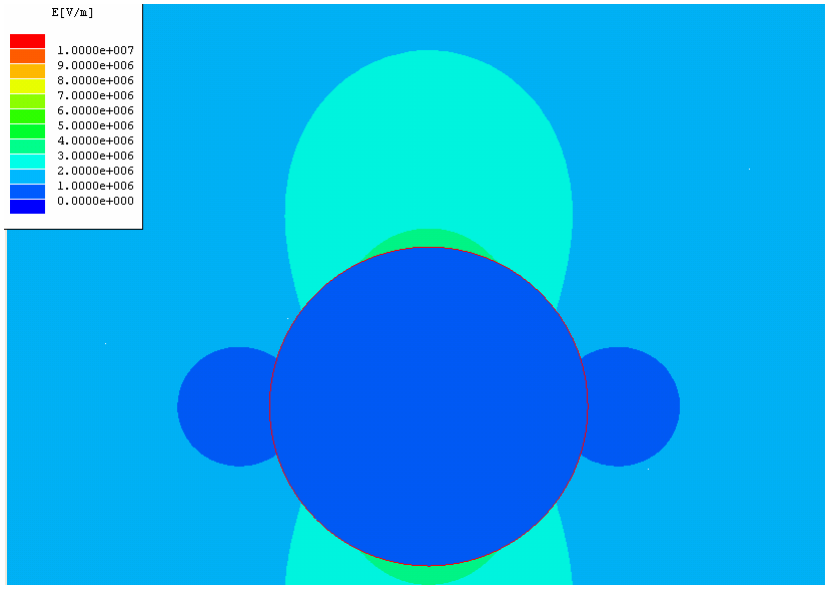

Figure 7. 6: Maxwell FEM analysis of the electric field distribution around a PZT cylinder, in silicone oil, if exposed to E=1.666MV/m (d=0.5 μm). The bottom electrode is PTFE coated.

Another FEM computation of the electrostatic adhesion on a PZT cylinder exposed to an electric field was carried out supposing the bottom electrode coated with a 0.5mm thick layer of PTFE. As expected, given the dielectric constant of the PTFE and that of the silicone oil is so closed, the adhesion is negligible. However, the value of 68 μN/m,

resulting from the simulation, is a very important one because it can give an indication of the precision of the simulation.

7.2. ANALYSIS OF THE MOTION OF A FREE FALLING PARTICLE IN A DIELECTRIC FLUID

To check the reliability of the formula (3-18) (see section 3.3.3.1) in calculating the drag force, a series of measures of the free falling time were taken. The results are reported in table 7.1. The table shows the limiting speed for falling fibres of different length, when they are falling either horizontally or vertically. The last column shows the ratio between the particle weight and the theoretical drag force. Supposing that speed is the limiting factor while weight and drag force have the same magnitude, it is possible to conclude that the weight/drag ratio indicates the ratio between the real and the calculated viscous force.

The same trend regarding the ratio can be seen for the metal particles as well as for the PZT particles. In the case of a longer particle which falls horizontally, where the extremity effects are negligible, the force predicted by the formula is slightly lower than the experimental one. In the case of a vertical the underestimation is considerably greater.

In the case of shorter rods, in the vertical case, the error is still the same. Nevertheless, it is in the horizontal case that the error reaches a maximum.

Regarding the experimental data in Table 7.1, all the computations relative to the viscous resistance of short rods have been carried out multiplying the theoretical value by a factor of 1.4.

Table 7. 1: Summary of experiment of free falling on different fibres (see appendix D for uncertainty)

Fibre length(mm)	Position	Speed(m/s)	Weight/Drag
PZT			
10	Vertical	0,01	1,35
10	Horizontal	0,0056	1,06
1,85	Vertical	0,00625	**1,35**
1,85	Horizontal	0,00378	1,57
Cu			
15	Vertical	0,024	1,43
15	Horizontal	0,014	1,08
2,2	Vertical	0,0139	**1,43**
2,2	Horizontal	0,0096	1,58

7.3. FLAT ELECTRODE

7.3.1. RESPONSE TO A VOLTAGE PROGRESSIVELY INCREASING AND DETERMINATION OF THE LIFT-OFF ELECTRIC FIELD

The lift-off electric field E_m of each kind of particle has been measured on batches of 5 fibres. The collected data are reported in the chart in figure 7.7, and the averaged results are reported on the Table 7.2. This table indicates:

- Q_F that is the theoretical charge that the particle should acquire at E_{th} (Q_F is equal to $2\pi\varepsilon_l r E_{th}$)
- Q_{mF}, that is the theoretical charge at E_m (Q_{mF} is equal to $2\pi\varepsilon_l r E_m$)
- Q_w that is the minimum value of the particle charge that allows the particle to exceed the weight and the adhesion forces at E_m; this value is extrapolated from the equilibrium between weight, adhesion force, and Coulomb force (Q_w is equal to $mg/[0.715\ E_m]$)

In the case of lift-off experiments, if no additional adhesion forces exists Q_w.expresses the effective value of the charge acquired by a particle exposed to the electric field $E_{m.}$

Given the dispersion of the results, the lift-off field $E_{m,}$ expressed by the ratio with respect to the theoretical value $E_{th,}$ is not sensitive to the fibre length. By contrast an influence of the sign of the field was observed.

If the applied electric field was positive, the averaged lift-off electric field on copper fibres was practically the same as that predicted by Felici (1966). Instead, on coated and uncoated PZT fibres, the lift-off was almost one and a half times higher than the theoretical one.
When the electric field was negative the lift-off is significantly lower than the predicted one for both the conductive particles. Surprisingly, in the case of insulating PZT particles applying an electric field, which progressively decreased up to -1.666MV/m, no motion was observed. However, when an instantaneous positive field of 1.666MV/m

was applied at the end of the slope, the fibres moved instantly. This could be due to an accumulation of negative charge on the PZT fibres when exposed to a negative voltage.

A lift-off electric field higher (lower) than the theoretical one could be associated with two main factors:

1) A lower (higher) than expected charge acquired by the particle
2) An additional adhesion (detachment) force

If 1) were the right explanation, Q_w, corresponds to the effective charge acquired by the particle, and Q_w/Q_{mF} would express the ratio between the real charge acquired and the calculated one when the particle lift-off. While, if 2) is the hypothesis, the additional electrostatic adhesion can expressed as:

$$F_{adh}= 0.715 (Q_{mF} E_w - Q_F E_{th}) \quad (7\text{-}2)$$

Concerning the hypothesis of an additional adhesion force, the difference in behaviour due to the voltage sign would be a hypothesis to attribute to the tribocharge. If this were true, the linear density of tribocharge would be 1.6 nC/m for the copper and 1.9 nC/m for the chromium.

Looking at the band theory, we can see that the work function of the chromium is 4.6eV, that of the copper is 4.65eV, and that of stainless steel is 4.4eV. The contact potential difference would then become 0.2-0.25 V, and the fibres should therefore be negatively charged. If this were correct, the adhesion would be stronger in the negative case, and not, as experimentally observed, in the positive one. However, it has been shown, that if an oxide film or other impurities exist on an electrode surface, the work function would be considerably increased. As a consequence a tribocharge opposite to the one expected can arise on the fibre. Harper (1967) showed that the work function of an oxidised metal is around 5.5eV, which is not very dependent on the metal nature.

Table 7. 2 Summary of the data relative to the lift-off field

	E_{th} (kV/m)	Q_F/L (nC/m)	E_m/E_{th}	Q_w/Q_F	Q_{mF}/Q_F	Q_w/Q_{mF}	F_{adh}/L (mN/m)
Tobazeon							
Steel V>0	784	23.95	1.02	0.98	1.02	0.96	0.27
Present study							
Cu V>0	486	6.49	1.09	0.91	1.09	0.83	0.22
Cu V<0	486	6.49	0.87	1.13	0.88	1.28	-0.23
Cr PZT V>0	373	3.34	1.48	0.67	1.49	0.44	0.64
Cr PZT V<0	373	3.34	1.12	0.88	1.13	0.77	0.12
PZT V>0	373	3.34	1.42	0.69	1.44	0.47	0.56
PZT V<0	373	3.34	No motion applying a field up to 1.666 MV/m				

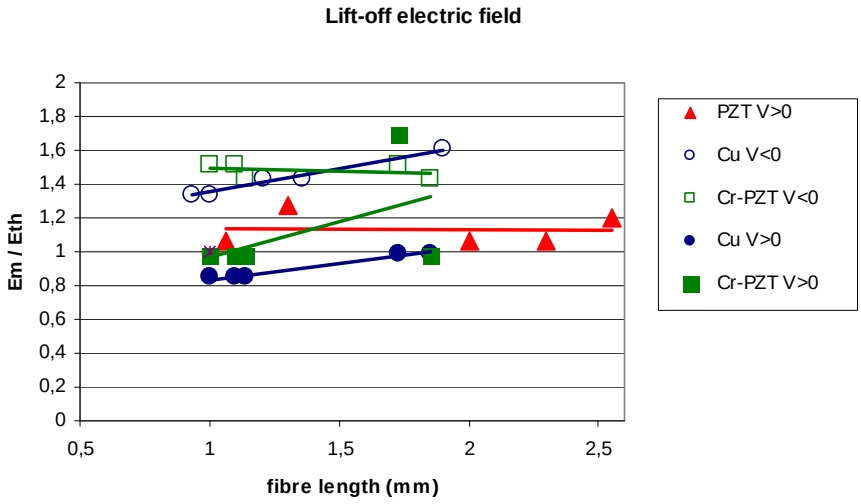

Figure 7. 7: Lift-off electric field as a function of the length of different kind of fibres.

Table 5.4 in chapter 5 shows a charge computation resulting from an FEMLAB finite element modelling of a case in which the contact potential is theoretical.

Considering that the charge increases linearly with the contact potential difference, a linear density of tribocharge of 1.6 nC/m for the copper, and 1.9 nC/m for the chrome, would need a contact potential difference of 1.66V and 3.28V respectively. These values are too big, especially considering an oxidisation of the stainless steel electrode.

Moreover, the charge value measured on PTFE is not very different in the case of a conducting material or in the case of the PZT. Therefore, although the tribocharging on PTFE is different from that on steel, it is difficult to believe that the charge value would make so little difference to PTFE and a so large a difference to steel. As a consequence one can conclude that the influence of the tribocharge is not a determining factor in the lift-off mechanism. The difference in behaviour between the negative and positive cases has to be attributed to the charging phenomena.

In concluding about the lift-of phenomenon, it is important to remark that the fibre motion, once the lift-off voltage is reached, is not always instantaneous. The "dwell" time can take up to few seconds to occur. This delay could be attributed to a high contact resistance.

7.3.2. RESPONSE TO A STEP VOLTAGE, ANALYSIS OF THE MOTION AND CHARGE COMPUTATION

7.3.2.1. Charge dependence on the electric field

An extensive study of the motion of a conductive cylindrical particle in an electric field has been achieved by Tobazeon. He considered the problem only in the case of electric field smaller than 1 MV/m. For this reason, an investigation into the motion of a conducting particle for an electric field higher than 1MV/m has been conducted. A comparison between the results of that investigation and the Tobazeon data has been presented.

Tobazeon (1996) used Marcol oil, an oil with relative permittivity of 2.2, very close to that of the silicone oil, but with a viscosity 4 times smaller. Consequently the speed he measured was high enough to be in the intermediate regime. As pointed out by Tobazeon, for that reason C_D could not been calculated using the Stokes formula, because its validity is restricted to the viscous regime. Unfortunately, due to insufficient experimental data, in the intermediate regime, it is difficult to have a reliable expression for C_D. It is therefore necessary to make some assumptions. Tobazeon:

$$C_D=K/Re^{1/3} \qquad (7\text{-}3)$$

with K=10 for a cylinder moving parallel to its axis. This assumption works relatively well when 50<Re<1000. In the, 5<Re<31, range in which Tobazeon's results are situated the approximation may be less accurate.

The graph in figure 7.8 compares the drag force computed in three different ways, i.e. using the expression for viscous, intermediate and inertial regime.

The force in the viscous regime has been calculated using (3-18) corrected by an experimental factor of 1.4 (see section 7.2), the force in the intermediate regime has been calculated using (7-3), and the force in the inertial regime has been calculated using (3-14), and imposing $C_D=1$, as suggested by Tobazeon (1996). The values of the forces have been all normalised respect to the value of the drag force calculated with (3-18).

As it is possible to see, considering (3-18) accurate at Re<1, to consider a variation based on (7-3) when Re>1 would impose a discontinuity difficult to justify in the physical point of view. A smooth transition from (3-18) to (7-3) when 1<Re<15 is consequently suitable. Considering that, in this study the charge gas been computed using still (3-18) for Re<15, and (7-3) only for bigger Re.

In the study carried out for this thesis the charge acquired by a copper rod 1.3mm long, 192μm in diameter, in silicone oil, has been computed from the terminal velocity measured on the recorded movies. The motion conditions were always in a viscous regime, and the charge was calculated for a field between 1 and 1.666 MV/m, according to the considerations set out in section 7.2.

After Felici (1966), the surface charge would be expressed as $Q_S=bE$ where, considering the two extreme cases of horizontal and vertical particle the value of b results:

$$\varepsilon_l \le b \le [\ln(2L/r)-1]^{-1}\ \varepsilon_l\ \ (L/2r) \qquad (7\text{-}4)$$

All the results, including Tobazeon's, are summarised in Table 7.3. The quantities with suffix *i* are referred to the first lift off, the ones with suffix *u* and *d* are relative to the values of a fibre going up or down respectively, and the quantities with suffixes *h* and *v* refer to the fibres in horizontal or in vertical position respectively.

The value Q_{Fv}/Q_{Fh} expresses the ratio between the theoretical charge that a cylinder would acquire when it is in vertical and horizontal position. This value depends on the aspect ratio of the fibre; in our case Q_{Fv}/Q_{Fh} is always around 3.

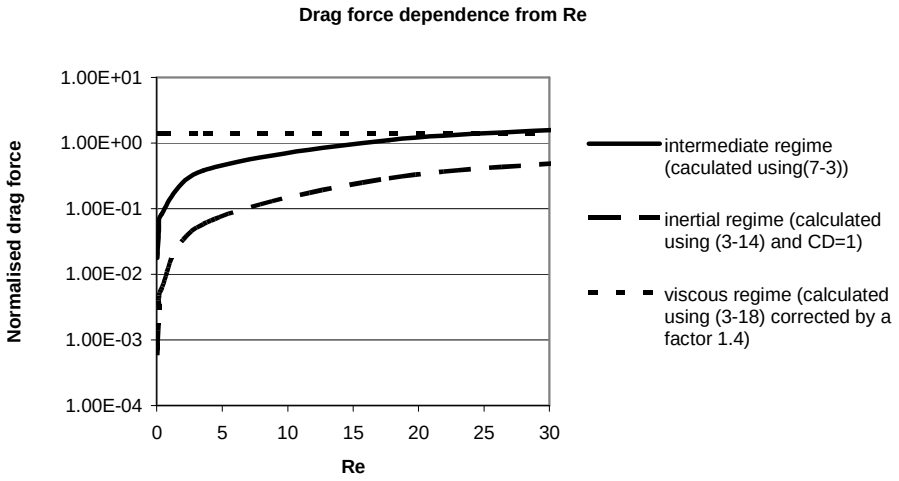

Figure 7. 8: Comparison between the values of drag force, calculated using the formula relative to different regimes. The values are normalised with respect to the drag force calculated using (3-18)

All the measured values of charge have been normalised in respect to Q_{Fh}, and these normalised values decreased from 1.7 to 0.95 when the electric field increased from 0.4 up to 1.66 MV/m. This means that the magnitude of the charge acquired by a particle is always lower than the one predicted for a vertically positioned conductor. For the smallest value of the electric field the value reached 60% (E=500kV/m), but for the samples we measured in silicone oil it was normally around 30-40%.

Another observation of interest is connected to the first lift-off. The particle starts to rotate from the horizontal to the vertical position. The particle remains in contact with the bottom electrode until it takes off. After the take-off the particle should stop gaining charge. Given that when the particle takes-off it is not yet vertical (it is normally at an angle of 45 º with respect to the bottom electrode), the expected charge should be lower the theoretical vertical one. Conversely, we can observe that the charge acquired after the first lift-off have almost the same value as the charge evaluated during the following up and down oscillations.

Table 7. 3: Charge computation summary (see appendix D for uncertainty). These tables show how the relative charge acquired by the rods progressively decreases if the electric field increases. This trend can be identified by comparison between the averaged charges extrapolated from Tobazeon's data (1996) (only values indicated in bold) and the averaged charges listed in (c), relative to the present study. The averaged values in (c) have been calculated using: $\langle Q/Q_{Fh} \rangle = (Q_u+Q_d)/2\ Q_{Fh}$)

(a)

Tobazeon						
E (MV/m)	$\langle u_i \rangle$ (m/s)	$(Q/L)_{Fh}$ (nC/m)	Q_w/Q_{Fh}	Q_{Fv}/Q_{Fh}	$\langle Q/Q_{Fh} \rangle$	
					Viscous	Intermediate
0.4	0.2 (Re=7.1)	12.2	3.83	3.53	**1.68**	0.75
0.5	0.4 (Re=14.1)	15.2	2.47	3.53	2.14	**1.53**
0.6	0.5 (Re=17.7)	18.3	1.71	3.53	1.87	**1.54**
0.7	0.6 (Re=21.3)	21.4	1.24	3.53	1.64	**1.53**
0.8	0.7 (Re=24.8)	24.5	0.95	3.53	1.46	**1.51**
0.9	0.8 (Re=28.4)	27.6	0.75	3.53	1.32	**1.49**

(b)

Present work									
E (MV/m)	u_i (m/s)	u_u (m/s)	u_d (m/s)	$(Q/L)_{Fh}$ (nC/m)	Q_w/Q_{Fh}	Q_{Fv}/Q_{Fh}	Q_i/Q_{Fh}	Q_u/Q_{Fh}	Q_d/Q_{Fh}
1.00	0.066	0.063	0.085	13.3	0.24	2.95	1.17	1.12	1.12
1.15	0.099	0.092	0.109	15.6	0.19	2.95	1.20	1.09	1.09
1.33	0.133	0.120	0.134	17.8	0.13	2.95	1.23	1.05	1.05
1.50	0.150	0.138	0.161	20.0	0.11	2.95	1.09	0.98	1.00
1.66	-	0.156	0.188	22.2	0.09	2.95	-	0.91	0.96

(c)

Present work (averaged values)	
E (MV/m)	$\langle Q/Q_{Fh} \rangle$
1.00	1.12
1.15	1.09
1.33	1.05
1.50	0.99
1.66	0.94

It is remarkable that on the first lift-off in silicone oil, when E=1.666 kV/mm, the particle was unable to reach the upper electrode. For that no value has been reported for Q_i in table 7.3.

The chart in figure 7.9 shows the dependence of the speed on the electric field. In the case of the more viscous fluid the curve shows the existence only of a single regime. More complicated is the case of a low viscosity fluid. Clearly two regimes are visible, one at Re<15, represented only by an experimental point, and another, intermediary.

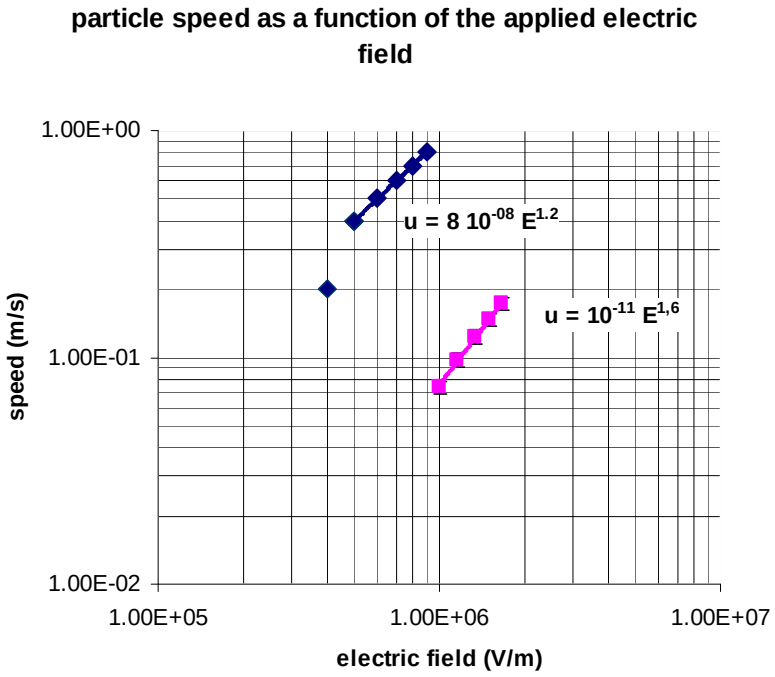

Figure 7. 9: Particle speed as a function of the electric field and the best fitting. The diamonds report the Tobazeon (1966) results, and the squares reports the results in silicone oil.

Returning to the surface charge, and the related previous explanation, the dependence of the surface charge on the electric field should fit a bE expression where:

- $2.21\times10^{-11}<b<7.81\times10^{-11}$ C/Vm in the case of the silicone oil
- $1.94\times10^{-11}<b<6.87\times10^{-11}$ C/Vm in the case of the Marcol oil used by Tobazeon (1996).

As shown in the graph in Figure7.10, this dependence suggests a $b=3\times10^{-11}$ C/Vm, as expected from the results in table 7.3. Two important considerations derive from this analysis:

1) The linear fit is the same in the two sets of experiments.
2) The linear fit is accurate for Tobazeon's experiments, conducted at lower field, but not for the experiments conducted in silicone oil at higher field. The different behaviour could be due to:
    - the difference in oils
    - the different ratio gap/particle length (0.15 of the Silicone oil case compared with 0.21 of the Tobazeon case)
    - the different rod tip shape
    - the different magnitude of the electric field range (this is considered to be the main reason)

A polynomial squared fit:

$$Q_S = -aE^2 + bE \qquad (7\text{-}5)$$

fits well in the silicone oil case. This suggests that another mechanism dependent on the field square (e.g. a charge subtraction or an additional resistance should be added when the field increases) should be added to the linear dependence on the electric field given by the charging phenomena. Space charge injection through the rod, phenomenon already observed in air Asano et al. (2000b; 2002), could be an explanation of the quadratic dependence, and moreover to the singular behaviour of the initial motion of the copper rod at E=1.666MV/m expressed in table 7.3.

Supposing a charge injection through the rod tip, a rough overestimated calculation of *a* could be done by treating the system vertical rod-plane as a pin-plane system. Coelhot and Debeau (1971), making some crude assumption in the current density profile and considering as zero the electric field on the tip, in the hypothesis of space limited current (SCLC), suggested a formula to calculate the relation relating the current and the voltage:

$$I = 4\varepsilon k(V^2/s) \qquad (7\text{-}6)$$

where k represents the mobility, and s the distance between the extremity of the rod closest to the opposite electrode, and the electrode.

Assuming a linear uniform motion and a terminal velocity of the particle, h = u t.

To achieve the integration it is necessary to find an accurate expression for V.
V can be expressed as: $V=g\,(Q, h)\,V_0$, with $g<1$.
A metallic particle moving in a parallel plate capacitor, which is not in contact with one of the electrodes and which is uncharged, assumes a potential changing during the particle displacement. This potential is equal to the one that would exist on the iso-potential line crossing the middle of the particle if the particle was not there. Neglecting the contribution due to the charge acquired by the particle, which contributes for only a few hundreds of volt in the potential difference, it is possible to have a rough approximation of the integral supposing a linear law like:

$$g = 1 - s/h – L/2h \qquad (7\text{-}7)$$

The expression becomes:

$$dQ_S/dt = 4\varepsilon k(V^2/s) \qquad (7\text{-}8)$$

$$dQ_S/ds = 4\varepsilon k(V^2/u\,s) \qquad (7\text{-}9)$$

$$dQ_S = (4\varepsilon k/us)[(w - s/h)V_0]^2\,ds \quad \text{where } w = 1 - L/2h \qquad (7\text{-}10)$$

$$Q_S=4\varepsilon k(V_0^2/u)\{w^2\ln[s_{min}/(h-L)] – 2w/h\,[s_{min} - (h-L)] + 1/2h^2\,[s_{min}^2 - (h-L)^2]\} \qquad (7\text{-}11)$$

$$Q_S=4\varepsilon k(E_0^2\,h^2/u)\{w^2\ln[s_{min}/(h-L)]–2w/h\,[s_{min} - (h-L)]+1/2h^2\,[s_{min}^2 - (h-L)^2]\} \qquad (7\text{-}12)$$

Considering $\varepsilon = 2.5\varepsilon_0$, $k=5\times10^{-9}m^2/Vs$, $h=6mm$, $u=0.1m/s$, $s_{min}=1\mu m$, $L=1.3mm$ the expression becomes:

$$Q_S = -5.4\times10^{-22}\,E_0^2 \qquad (7\text{-}13)$$

considerably lower than the value measured experimentally. This could mean that effects other than the injection are mainly responsible for the negative squared term of equation (7-5), ultimately perhaps either a charge decrease on the particle, or an EHD instability around the edges of the particle creating an additional resistance.

The enhancement field factor on the tip of an uncharged (charged) conducting rod, with rounded edges and with axis parallel to the applied electric field, has been calculated to

be around 12 (30) when the distance between the rod and the electrode where it discharges is bigger than 5 times its radius Tobazeon (1996). This means that by applying a field of 1.666MV/m the field on the rod extremity can reach 20 (50) MV/m.

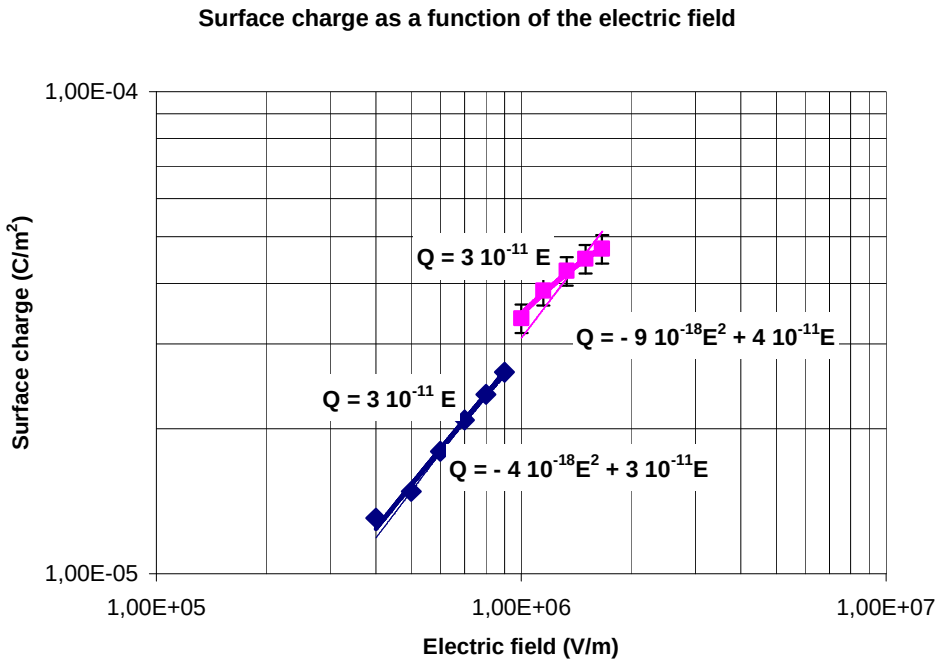

Figure 7. 10: Surface charge computation as function of the electric field, and interpolation. The diamonds report the Tobazeon (1996) results, and the squares reports the results in silicone oil (see appendix D for uncertainty).

A FEMLAB simulation of the electric field distribution around an uncharged cylindrical rod has been carried out using different rod edge geometries:

- rounded edge
- sharp edge
- squared cut edge

The simulation confirms the literature values for the rounded edges (Tobazeon, 1996). In the case of a square cut cylinder, at the face centre, the enhancement factor is 7; in the sharp edge case this factor is 36. Considering that in the Onsager's theory, for a field bigger than $10E_c$, the fluid starts to increase the conductivity, and practically becomes a

conductor if $E>100E_c$, it is possible to assume a field-enhanced dissociation on the rod tip. This could be another method by which charge subtraction plays a role in the lack of linearity of the particles' charging phenomena, and could also be useful to explain why the charge acquired by a vertically positioned rod is so low compared with the one predicted by theory.

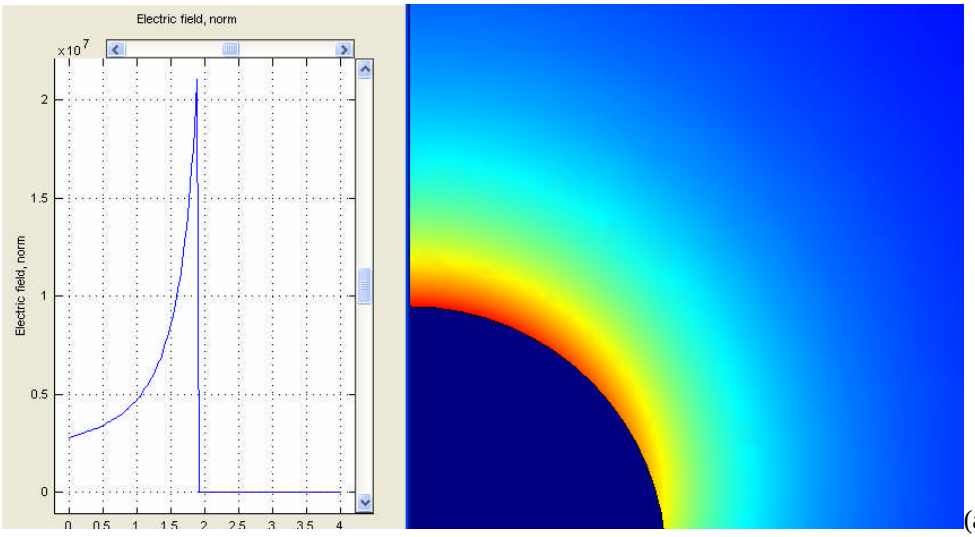

(a)

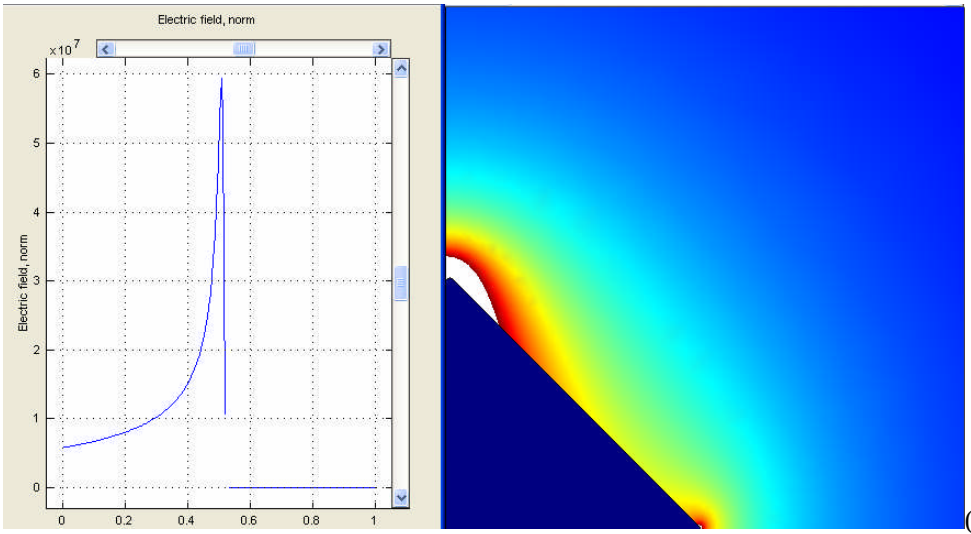

(b)

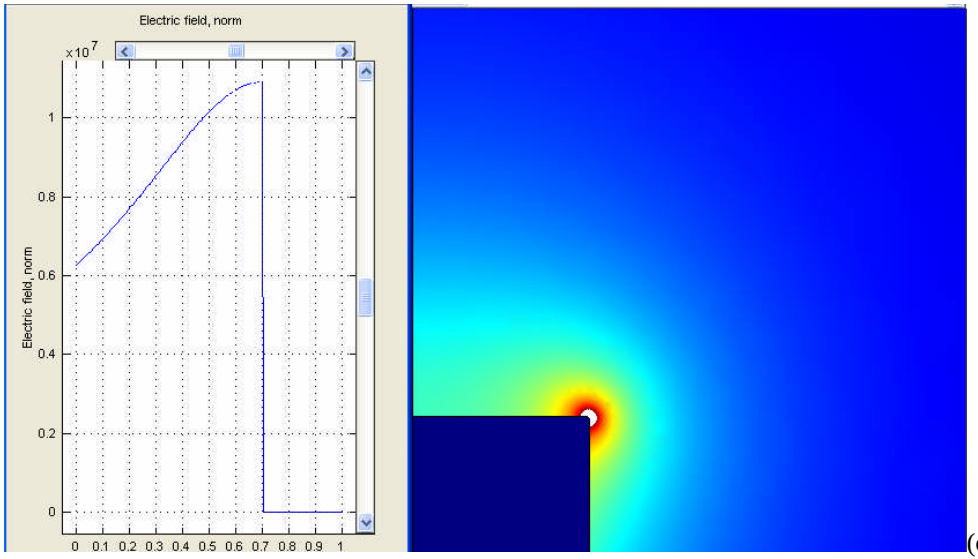

(c)

Figure 7. 11: Electric field distribution on the tip of a conductive particle exposed to an electric field of 1.666MV/m in silicone oil: (a) rounded edge (b) acuminated edge (c) squared cut edge.

7.3.2.2. Charge dependence on the material

This section is dedicated to the relationship between the charging mechanisms and the material of the fibres. The charge values were extrapolated from a series of observations of the particle's motion under a suddenly applied electric field of 1.666MV/m.

The experimental results show that the charge density acquired by a particle is always between the half of the whole and the whole of the charge acquired by a horizontal rod-like particle calculated by Felici. This charge is normally bigger for the first motion than for the following motions, in which the particle moves across the gap remaining vertical. This difference is emphasised in the case of a PZT particle. As already pointed out in section 7.3.2.1, the charge is always very low compared with the one that the particle would be expected to acquire according to the Felici (1966) model for a cylindrical particle in vertical position.

Despite the very different nature of the charging mechanism, the charge acquired by an insulating PZT rod is comparable with the one acquired by conductive Cr-coated PZT fibres, and by a copper rod.

Given the dispersion of the results no relation has been shown between particle charge and its length.

Since the charging is normally not instantaneous, and that the charge is lower than the theoretical one, Asano et al., (1997a; 2000a) considered the hypothesis that the particle detached from the lower electrode before the charge exchange was completed. Assuming a continuous charging phenomenon, if this hypothesis is correct, the particle should always lift-off once it reaches a charge Q_m. For that reason, for the purpose of comparison, in the graphic in figure7.12, the values of Q_m/Q_F have also been reported. These values show that the measured charge is always considerably bigger than Q_m. As a consequence, the charging mechanism should be different. At a quantity of charge equal to:

$$Q_{peak} = Q_{final} - Q_m \qquad (7\text{-}14)$$

should be transferred instantaneously in a burst of current. However it is peculiar that such a charge transfer would be not instantaneous, but would take a certain incubation time. To try to give an explanation, the following scenarios can be proposed:

1) The ion transfer rate in the gap increases with time. This is due to the fact that the counter-ions, in the non-equilibrium layer (see section 2.4.4.3) create an electrical double layer, which enhances the electric field, therefore favouring the injection.
2) The particle charging is operated by some cluster impurities that get charged on the bottom electrode and then stuck on the particle transferring the charge. The incubation time would then be the charging time of those particles to get charged.
3) The particle charge depends on an hazardous event related to the nature and an eventual modification of the contact zone. For example if, as a consequence of the high field, an electropolymerised waxy deposit is formed in the gap, the occasional event could be the micro-breakdown inside that deposit.

Further closed examinations would need to monitor the charge transfer during the incubation time.

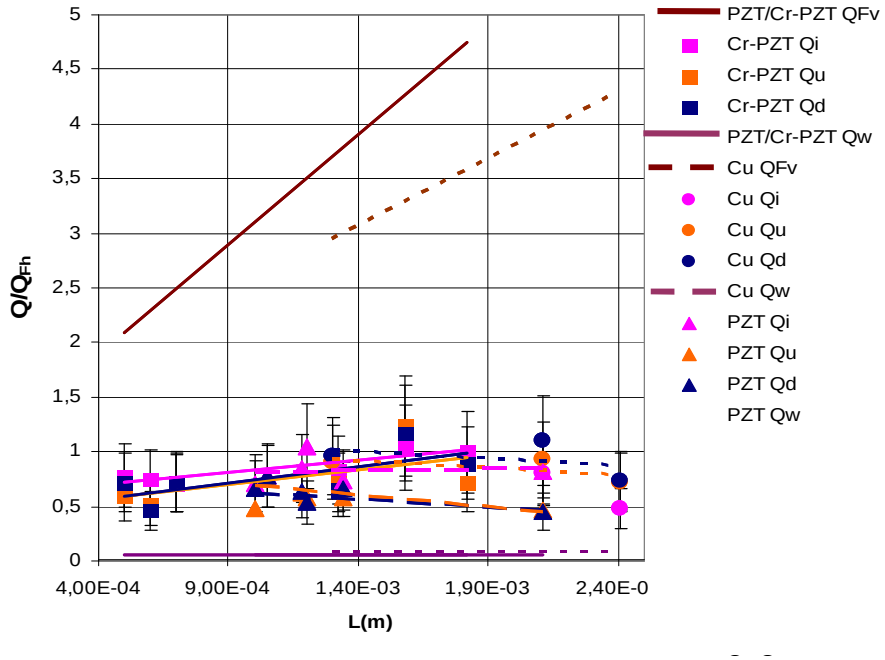

Figure 7. 12: Summary of the charge acquired by different kind of particles when exposed to a field of 1.666MV/m (see appendix D for uncertainty)

7.3.2.3. Description of the characteristics of the motion

In this section some general findings, pertaining to the motion of the different kinds of rods, when a DC step of 1.666MV/m was applied, are reported.

In general, copper rods did not move instantaneously. They took up to 80ms before starting to move and around 90ms to get the vertical position. These times were not shown to be sensitive to the fibre length.

In contrast to what was reported in (Asano et al., 1997a; 2000a), concerning spherical conductive particles in silicone oil, no “dwell” time was observed in this case. Once the electric field was applied, the fibres rotated to the vertical position, and then started a continuous up and down oscillating motion. The motion stopped only when the voltage

was switched off. At that point the particle stopped moving, and returned to rest in a horizontal position on the bottom electrode.
It is difficult to describe precisely the mechanism of discharge of the particle reaching the opposite electrode. The most respected theory is that when the particle is very close to the electrode surface the electric field, enhanced by the presence of the fibre, causes a breakdown of the small gap. This regulates a very short burst of current, also confirmed by the creation of some very small bubbles in the contact zone, and by the generation, on the electrode surface of many small craters.

Although they are also conductive, the Cr coated PZT particles behaved differently from the copper ones. They took up to 125ms to start to move, even though they took a time comparable to the copper particles to rotate. After the lift-off, the rods started to oscillate, but, in contrast to the copper particles, they had a certain “dwell” time of between 5ms and 50ms. This “dwell” time had the tendency to increase with time up to a point when, in some cases, the rod stopped moving and remained in contact with an electrode without discharging. When this happened after the field was switched off, the particle took up to 3mins to discharge. For that reason the behaviour of the Cr coated PZT particles can be considered as the intermediate stage between the copper fibres and the PZT fibres.

The PZT particles behaviour was not symmetrical with respect to the sign of the electric field, i.e. they did not react in the same way to positive or negative step voltage. The particles moved with more difficulty (i.e. they took a longer time to react) if they were exposed to a negative step voltage than if they were exposed to a positive one. Moreover, a particle always moved if exposed to a positive voltage, but in 30% of cases, the particle did not move in a negative field. In these particular no motion cases, the particle instead moved instantly if the field was suddenly inverted, probably because it acquired a positive charge.
When the PZT particles moved, they started to move after between 300ms and 30s. After the lift-off the particle started an oscillatory movement like that of the conducting particles described above. This movement was characterised by a “dwell” time progressively increasing, from 40ms to few hundred milliseconds, while the motion

proceeded. The oscillatory movement stopped after a time which ranged between a few seconds and up to 30 seconds. When the particle stopped moving, it remained in a vertical position in contact with the electrode. At this point, inverting the field caused the particle to start the oscillatory motion. When the particle started to move again, the motion had the same characteristics as before, with a progressively increasing "dwell" time, until the particle stopped. If, at this point the field was switched off, the particle took up to 3min to discharge, always remaining in vertical position.

7.3.3. RESPONSE TO AN AC VOLTAGE.

7.3.3.1. The behaviour of particles exposed to an AC field in a gas: a brief review

Farral and Hudda (1980) proposed a model which described the motion of conductive rods in vacuum. They calculated all the forces modelling the particle with an array of opportunely spaced point charges. In this way they computed the tilting and the translation of different kinds of metallic rods exposed to a uniform electric field. Farral and Hudda verified experimentally this model in DC obtaining a good agreement between the theoretical and the experimental results. Then they applied the same calculation to a sinusoidal signal with frequency 50Hz and a peak of 2.3 MV/m (24.5mm gap), on a copper particle, 260μm in diameter, and 2mm long. Following their calculations the particle should have taken off after 5ms. Then, after 25ms, the particle should have reached an equilibrium height (10mm), starting a series of minor oscillations. The model showed an intense tilting activity of the particle.
This kind of behaviour is not comparable with the one observed in the systems where the particle moves in a viscous fluid. In this case the particle takes a longer time to align vertically with the electric field, and from then on the particle's movement remains vertical without any significant tilt. Unfortunately no equivalent models exist to describe the behaviour of particles with respect to the drag force.

Prakash et al. (1997) extensively studied the effect of particle contaminant on the breakdown mechanisms in gas insulated high voltage devices as GIS (Gas Insulated

Switchgear) and GITL (Gas Insulated Transmission Lines). They investigated the benefit generated by coating the electrodes with an insulator.

A. K. Chakrabarti et al. (1989) analysed the behaviour of conducting and insulating particles. They showed that insulating particles do not affect the breakdown sensitivity of these devices. A model of the motion of the particles in a gas insulating device created. This model computed the radial motion from the equilibrium force, and the axial motion operating a Montecarlo simulation. M. M. Morcos (2000) et al. considered the motion of a particle in a gas insulated device exposed to a 60Hz field. In this analysis Morcos, considered different restitution coefficients, and concluded with a good understanding of a pseudo-resonance behaviour occurring at opportune values of electric field magnitude and frequency.

7.3.3.2. The behaviour of particles exposed to an AC field in a fluid: a heuristic approach

The motion of a particle exposed to an electric field can be broken down into two consecutive phases:

a) The particle rotation

After the voltage is switched on, the particle, in contact with the bottom electrode, becomes charged by induction. The charge polarity changes according to that of the applied signal. The particle becomes polarised, and starts a rotation trying to align its polarisation vector to the external electric field vector. It is important to consider that, during this phase, the particle charge changes, because it depends on the angle between the particle and the bottom electrode (see section 3.3.2.3). At a certain angle (normally around 45°), when enough charge has been acquired, the particle lifts-off. After the lift-off, the flight phase starts.

b) The particle flight

Discounting any charging or discharging phenomena through the fluid, it is possible to assume that the particle charge should not vary after the lift-off, and the value of Q depends only on the time t_0 of detachment.

To find a model for the rotation phase of the motion is a very difficult task, and the results are not very reliable. However, it is possible to attempt a rough model for the flying phase. This model, even if it is not going to give a precise description of the motion, can be useful to give an indication of the value of the maximum height and the flying time.

7.3.3.2.1. A model for the particle flight phase

Assuming that:

- before leaving the electrode the particle is vertically positioned
- the charge Q, at time t_0, has the same value that would have in DC at $V(t_0)$,
- we can ignore the image charge as it influences the dynamic of the motion only for distances of the order of the particle radius
- the inertia mass m_i is equal to the particle mass m

the dynamic of the flying phase of the particle can be described by:

$$(d^2z/dt^2)\, m_i + (dz/dt)\, \kappa + QE_{max} \sin\omega t + mg = 0 \qquad (7\text{-}15)$$

and the solution of the ordinary differential equation becomes:

$$dz/dt = u(t) = -g\,\tau\ -\zeta\,[(1/\tau)\sin\omega t - \omega\cos\omega t] + \ c_1\, e^{-t/\tau} \qquad (7\text{-}16)$$

where $\tau = m/\kappa$, $\kappa = (2\pi\eta L)/[\ln(L/2r)+0.193]$, $\zeta = QE_{max} / (m\,[1/\tau^2 + \omega^2])$

In general the motion is not instantaneous, but happens at a certain time, t_0. The particle has an initial speed depending on the rebound and any possible interfacial phenomena on the electrode.

The equation is then solved when $u = u_0$ when $t = t_0$

$$c_1 = e^{t0\,/\tau}\,\{u_0 + g\,\tau + \zeta\,[(1/\tau)\sin\omega t_0 - \omega\cos\omega t_0]\} \qquad (7\text{-}17)$$

The second integration gives the following expression:

$$z(t) = -\,g\,\tau\,t + \zeta\,[\sin\omega t + \cos\omega t/(\omega\tau)] - c_1\,\tau\,e^{-t/\tau} + c_2 \qquad (7\text{-}18)$$

which, when $z = 0$ and $t = t_0$ becomes:

$$c_2 = g\,\tau\,t_0 - \zeta\,[\sin\omega t_0 + \cos\omega t_0/(\omega\tau)] + c_1\,\tau\,e^{-t0/\tau} \qquad (7\text{-}19)$$

It can be seen that in order to properly describe the particle motion, it is necessary to evaluate the initial conditions.

Unfortunately, as stated above, to model the rotation phase of the motion and establish the exact moment in which the particle takes-off as well as its charge, is a very difficult task. Nevertheless although a precise description of the whole motion is impossible, the maximum height and the flying time range can be deduced by analysing the model at a particular instant, e.g. t_0=1-3-5-8 ms, corresponding to signal phase angle ϑ = 18°-54°-90°-144°.

To improve the understanding of the solution of the differential equation, the description of the two extreme cases of motion in vacuum and over-damped motion has been treated.

Motion in vacuum

When the particle is moving in the vacuum, or in a very low viscosity system, the drag force is negligible, and the expression reduces to:

$$(d^2z/dt^2)\,m_i + QE_{max}\sin\omega t + mg = 0 \qquad (7\text{-}20)$$

and the solution is:

$$dz/dt = (QE_{max}/m\omega)\cos\omega t - gt + c_1 \qquad (7\text{-}21)$$

$$c_1 = u_0 - (QE_{max}/m\omega)\cos\omega t_0 + gt_0 \qquad (7\text{-}22)$$

$$z(t) = (QE_{max}/m\omega^2)\sin\omega t - (1/2)\,g\,t^2 + c_1 t + c_2 \qquad (7\text{-}23)$$

$$c_2 = -(QE_{max}/m\omega^2)\sin\omega t_0 + (1/2)\,g\,t_0^2 - c_1 t_0 \qquad (7\text{-}24)$$

when $z(t_0) = 0$ and $u(t_0) = u_0$. The graphics in figure7.13 show the results of (7-19) for a 1.3mm copper particle with a 192μm diameter, exposed to a field with maximum value 1.666MV/m, at 50Hz. The blue curves represent the solution of (7-19) for t_0=0 at different Q, and the red ones represent the solution of (7-19) for different t_0, with the

relative $Q(t_0)$ calculated as indicated by the DC experiments . The role played by the inertia is remarkable. The particle, in fact does not return to the point of departure at the end of the cycle.

As shown in figure7.13, the particle flying time is between 1.5 and 5 cycles depending on t_0. The particle has an oscillatory movement with pseudo period almost 50Hz. These results are very similar to the ones shown by Farrel and Hudda (1980).

The maximum height and the flying time depend mainly on the value of Q (and consequently on t_0), and they can vary by one order of dimension between 1.6mm and 16mm. Considering these results it is expected that a particle exposed to an AC field will start jumping. The jumps should have a height and a duration between the two limit values resulting from the calculations.

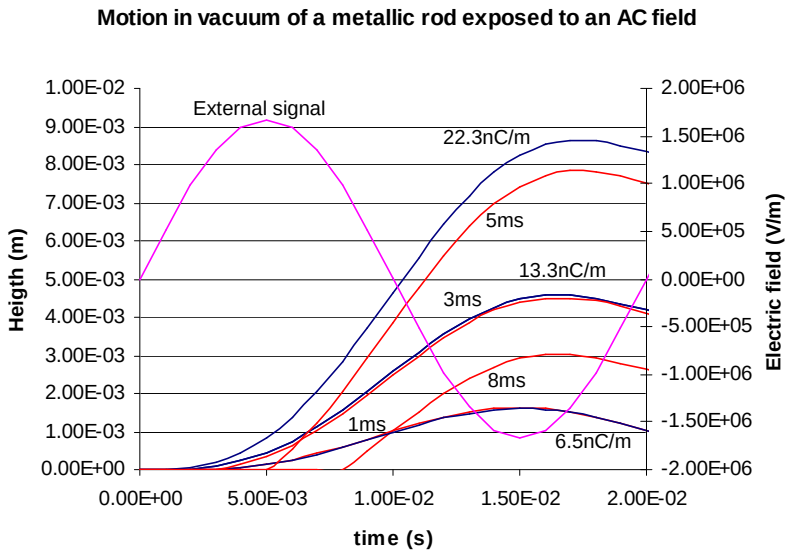

(a)

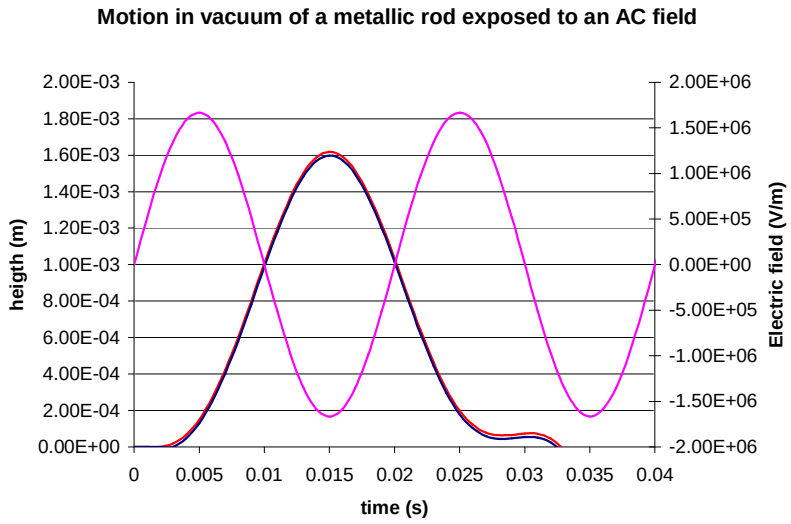

(b)

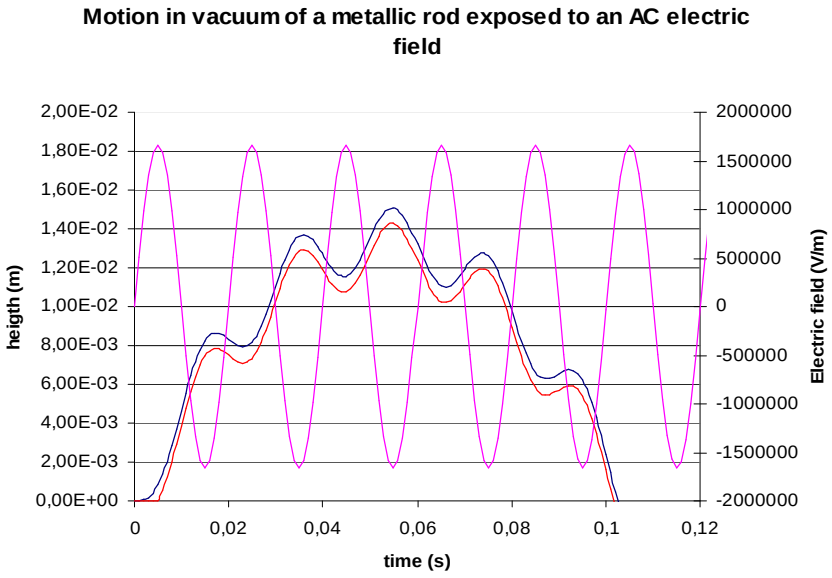

(c)

Figure 7. 13 Models of motion of a metallic rod exposed to an AC voltage calculated in vacuum. (a) at different t_0 (red) and different Q (blue) only the first period, (b) t_0=1ms (red) and Q=6.5nC/m (blue) extending time range, (c) t_0=5ms (red) and Q=6.5nC/m (blue) extending time range.

Motion in a high viscous fluid: over-damped solution

The over-damped case is different from that of the vacuum. The particle nearly always moves at the terminal velocity, and the inertia could be not taken into consideration. The expression (7-14) simplifies to:

$$(dz/dt)\,\kappa + QE_{max}\sin\omega t + mg = 0 \qquad (7\text{-}25)$$

and the solution becomes:

$$dz/dt = -(QE_{max}\tau / m)\sin\omega t - g\,\tau \qquad (7\text{-}26)$$

$$z(t) = (QE_{max}\tau / m\omega)\cos\omega t - \tau\, g\, t + c_1 \qquad (7\text{-}27)$$

$$c_1 = (QE_{max}\tau / m\omega)\cos\omega t_0 - \tau\, g\, t_0 \qquad (7\text{-}28)$$

It could be easily verified that, for rods moving in silicone oil, the over-damped solution approximates to the general solution.

In the over-damped case as in the vacuum case, Q influences the maximum height, and its value can be between a few hundredths of a micron and 0.7mm (see figure 7.14). Nevertheless, different to the vacuum case, in the over-damped case the flying time is never bigger than 1 cycle. The maximum height and flight time are reached when the particle takes-off at the beginning of the half-cycle. Conversely the minimum is achieved when the take-off happens at the end of the half cycle, when the field is approaching the polarity inversion.

From this model it would expected that a conducting particle exposed to an alternating field jumps, with a jump height of 0.7mm down to a few hundredths of a micron, and has a flying time of between a few milliseconds, for the shorter jumps, and 175ms. It is important to observe that for values of Q up to the theoretical one calculated by Felici for a vertical cylinder, the particle flight time is never longer than a period of the applied signal.

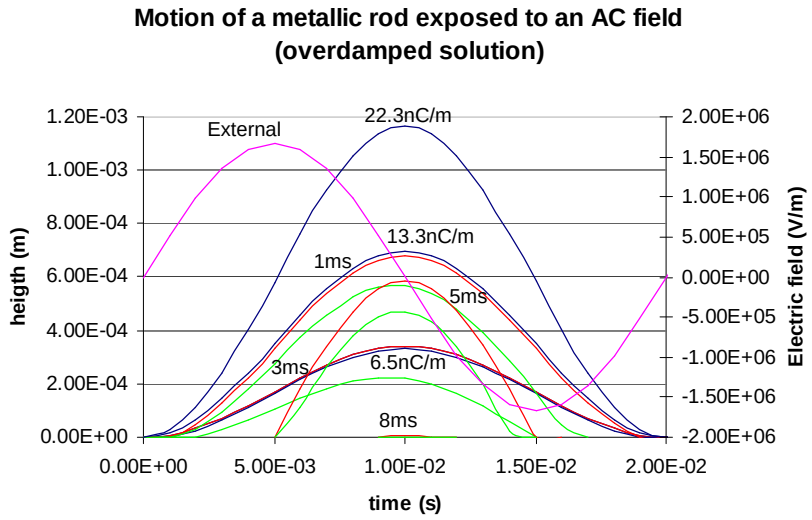

Figure 7. 14: Models of motion of a metallic rod exposed to an AC voltage calculated in silicone, with over-damped solution. The trajectories have been calculated for different Q(blue), and for different t_0 with or without considering the particle weight (green or red respectively.

The complete solution: dependence on the initial speed

At last, considering the formula (7-14), it would be interesting to analyse the influence of the initial speed on the AC motion. The graphics in figure 7.15 shows the results for an initial speed from 0 to 1m/s supposing the particle take-off after 1 or 5ms. The maximum height increases if the initial speed increases, but the point of inversion of the motion is always around 11ms. It is confirmed that the maximum height increases if Q increases. For a speed higher than 0.5m/s if t_0 = 1ms and for a speed of 1m/s if t_0 = 5ms, the formula predicts that the particle does not follow a simple up and down path, but it begins to climb again before touching the bottom electrode, with an oscillatory motion of progressively decreasing maximum height. The pseudo period of this motion is almost 50Hz, the same as the external voltage.

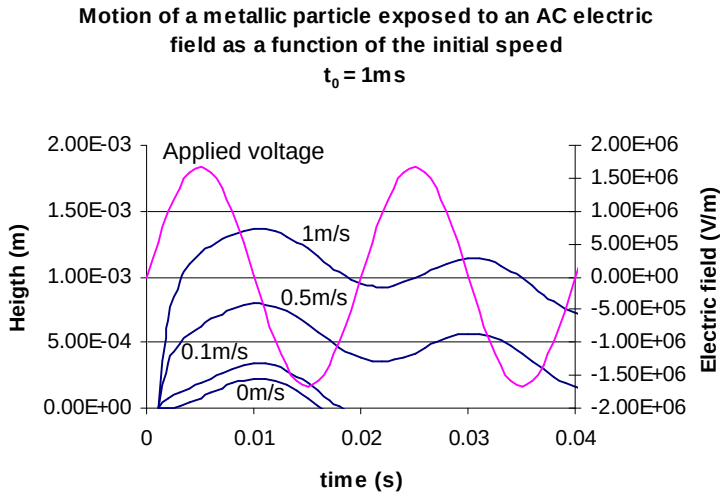

(a)

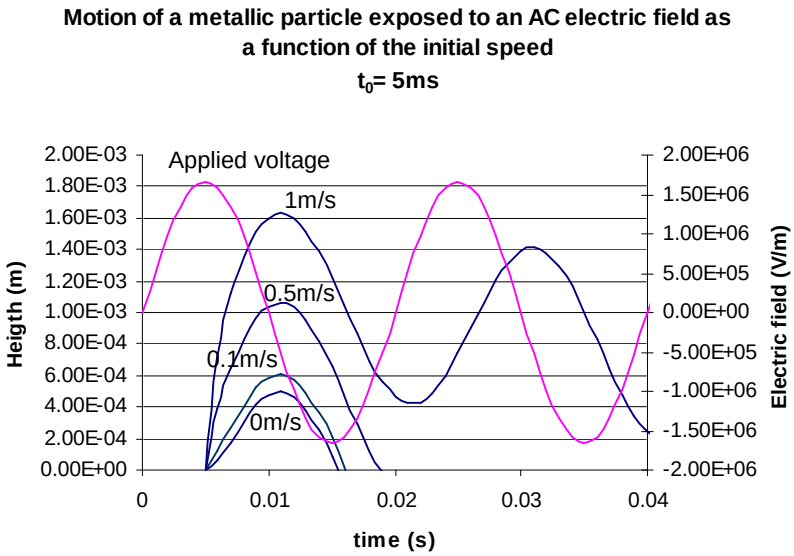

(b)

Figure 7. 15: Models of motion of a metallic rod exposed to an AC voltage, calculated using the general solution as function of the initial speed. u_0 = 0 - 0.1 - 0.5 – 1m/s. (a) t_0 = 1ms, (b) t_0 = 5ms.

7.3.3.3. Experimental results

Table 7.4 summarises the principal results of a series of experiments achieved applying a 1.666 MV/m field at different frequencies.

At 50Hz copper particles are able to become vertical in a few hundreds milliseconds. Once oriented, they can start an alternative motion with a flying time of between 2ms and 16ms. The stroke height can vary between 0.7 and 1.9mm. Normally, a bigger stroke is associated with a bigger flying time, and vice versa. Shorter and longer strokes are alternated with regularity. The results show that the oscillating behaviour is not related to the particle length. It is interesting to see that for a frequency 10 times bigger, the positioning time is very similar, but the oscillation becomes irregular, and the stroke reduces to almost zero.

Cr coated PZT fibres are considerably less reactive. If exposed to a 50Hz signal, they are unable to move. If exposed to a 10Hz signal they take more than 10 times longer than the copper fibres to reach the vertical position. Then they start to oscillate with a flying time of 100ms and with a stroke comparable to the one of Cu rods.

A test on an insulating PZT fibre showed a surprising result. The fibre shows almost the same behaviour of Cu rods in term of positioning time, stroke and motion frequency. The big difference was that PZT fibre motion was not as regular as for Cu rods. “Dwell” periods of a few hundreds of milliseconds long separate the continuity of the particle oscillation, and any oscillation stops after 5s.

Table 7. 4: Summary of the AC motion experimental results

Particle type	Length (mm)	Signal frequency(Hz)	Positioning Time(ms)	Min-max stroke (mm)	Min-max flight time (ms)
Cu	1.3	50	205	0.08-1.9	2-16
Cu	2.3	50	330	0.08-2.3	2-16
Cu	1.3	500	185	0.08	5-15
Cr-PZT	1.0	10	3975	1.0-5.0	100
Cr-PZT	1.0	50	No orientation	-	-
PZT	1.9	50	285	1.0-2.6	14-28 with breaks of 60-200ms. After 2s motion stop.

7.3.4. CONSIDERATIONS ABOUT THE RESPONSE IN A PARALLEL PLATE CONFIGURATION

7.3.4.1. Consideration about the DC voltage motion

All the experiments conducted in the parallel plate capacitor configuration can give some useful insights into the charging mechanisms of the different kinds of particles.
Given the mechanisms of electrification already presented in section 3.3.2, when the rods are lying on the bottom electrode affected by an electric field, it is possible to make the following assumptions:

- the conductive particles charge by induction
- the insulating (PZT) particles are charged by the space charges in the fluid.

In metallic fibres, the charge transfer happens through the tiny contact area. However, considering that the lift-off it is not instantaneous, it is reasonable to assume the existence of some contact resistance. This could be due to the reduction of the contact area as a result of the roughness of both, the electrode and the particle surface, or it could be due to some impurities.
To understand the effect due to roughness one can imagine that the current flowing through a very tiny area of contact, among the apexes of the superficial asperities, generates a considerable current density. This phenomenon could have two main effects on the contact resistance:

a) the creation of a local electro-polymerisation of the silicone oil which generates a waxy deposit as observed in some instances of very high electric field

b) the generation of some decomposition products if local micro-breakdown occur.

In the case of insulating fibres it is interesting to focus on the preference of the fibre for moving under a positive voltage as opposed to a negative one.
To interpret the results shown in section 7.3 we could assume that, in the case of a PZT particle, two simultaneous charging mechanisms are in competition.
The first mechanism arises from an ionic current, caused by the space charge in the bulk generating when a field is applied between the two parallel plate electrodes.

Simultaneously, a second charging mechanism arises from the fact that in the space between the fibre and the bottom electrode, a considerable electric field enhancement (see FEM simulations in section 7.1.2) promotes the creation of charge by dissociation or by injection. As pointed out by Boissy et al. (1996), if the area of interest in the enhanced field dissociation is small there comes a point at which there are not enough carriers to sustain the Onsager's behaviour. At that time, either a saturated current regime is generated in the gap or there is an injection of charge from the electrode.
Assuming that the two charging mechanisms are relatively independent of each other, at the end, the final charge on the particle would be the result of the balance between the two carrier streams (see section 3.3.2.5). The phenomenon is schematically illustrated in figure 7.16.

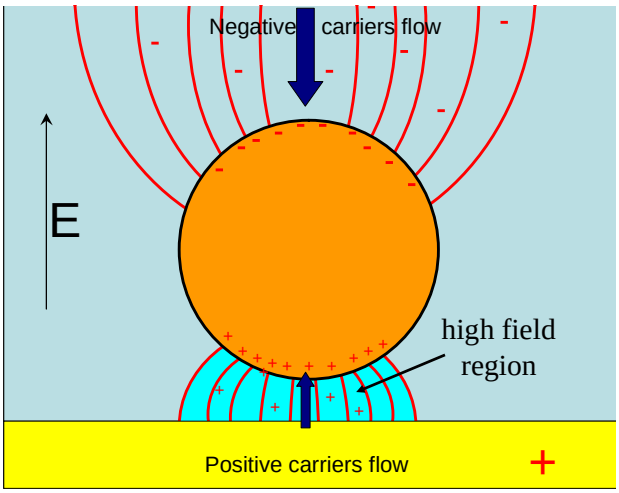

Figure 7. 16: Charging mechanism of a rod lying of a ground bottom electrode and exposed to an electric field. On the bottom the charges coming from the bulk are stacking on the upper part of the particle. On the lower part, the charges generated in the high field region between the particle and the grounded electrode adhere on the lower part of the particle.

The experiment on the fibre beam described in section 5.3.4 showed that the PZT fibre has a remarkable preference for becoming negatively charged. This could be due to a major affinity of the PZT for the negative charge (perhaps due to its positive tribocharge) or to an unbalanced ionic stream where:

$$J+ < J- \qquad (7\text{-}29)$$

The fact that the fibre mostly moved in a, suddenly applied, electric field of 1.666 MV/m but never moved in a progressively increasing negative field, unless the voltage

was suddenly inverted (section 7.3.1and 7.3.2), suggests that the two opposite mechanisms of charge do not have the same time constant. Probably the charging from the bulk is slower than from the gap.
In conclusion, by combining together the unbalanced current and the different charge kinematics, it would be possible to explain the observed behaviour. When the voltage is positive, the particle charges negatively and always moves. When the voltage is negative, but it is applied slowly, the particle charges positively from the bottom and also negatively from the top. However, given enough time, the negative charge becomes bigger. On the contrary, when the voltage is suddenly applied, the particle charges faster positively from the bottom than negatively from the top, and it can move.

The same kind of conclusion could be drawn regarding the charge exchange mechanisms between the fibres and the electrodes, regarding the subsequent up and down motion, after they have reached the vertical position. The peculiarity of this behaviour is that the conductive fibres have an oscillatory motion, without interruption, and without “dwell” time, while the motion of the PZT fibres have a “dwell” time which progressively increases with time, and the oscillatory motion interrupts after a few cycles. Also the metal coated PZT fibres have the same behaviour as the uncoated PZT. This is probably due to the fact that the charge exchange mechanism is mostly controlled by the fibre corners, and that the corners are not coated with the metal (the metal was only sputtered on the lateral cylindrical surface).

The observations of insulating fibres can be explained by considering the charge exchange phenomena presented above. In contrast to what happens in conductors, the charge in insulators does not have a great degree of freedom. As a result of that it is possible to suppose that the charge transferred by the electrode lies in an area close to the fibre tip. This means that when the fibre moves across the electrode gap, maintaining a vertical position, it acquires a charge from both the electrodes alternately. The charge accumulated on the two extremities then has the opposite sign, and consequently the fibre becomes a dipole.
Each time the fibre approaches an electrode, exploiting the field enhancement in the progressively reducing gap, it acquires a charge on the tip closer to the electrode. The problem is that the counter-charge on the other tip is not easy to neutralise. Therefore

when the fibre flies off from the electrode, it has an excess of homocharge on the extremity closer to the electrode, while still having some counter-charge on the other tip. This charge would be preferably located on the base of the fibre, because it is the most difficult place to reach for neutralisation.

When the fibre moves toward the opposite electrode, the residual charge on the fibre base, would reduce the electric field, decreasing the field enhancement, and increasing any charge exchange mechanisms. As a consequence, the "dwell" time increases. This mechanism is repeated for a few cycles, until no charge transfer becomes energetically convenient and the fibre stops moving. It is remarkable that the probability of a fibre stopping on either the upper or lower electrode is exactly the same.

7.3.4.2. Consideration of the AC voltage motion

A comparison of the experimental results showed in section 7.3.3.3 and the theoretical prediction made in section 7.3.3.2, shows a remarkable similarity between the real flight time and the one predicted in the over-damped model. On the other hand, there is no similarity between the theoretical and the real measure of the stroke. This could be due to the effect of an initial speed or to the fact that the acquired charge is bigger than the predicted one. Both hypotheses should be verified, although much doubt still exists in relation to the results in section 7.3.3.3.

In the case of the PZT, the intermittent character of the motion is quite consistent with the one observed in DC. Conversely, the size of the stroke height, is surprisingly high, and the possibility that some other charging mechanisms (e.g. from space charge) are occurring during the motion should be considered.

Though an understanding of the phenomenon still needs further investigation, it is remarkable to see how the AC behaviour extrapolated from the DC measures and characteristics, cannot be used to predict reliably the physical reality.

7.4. NEEDLE-PLANE CONFIGURATION

7.4.1. RESPONSE TO A VOLTAGE PROGRESSIVELY INCREASING AND DETERMINATION OF THE LIFT-OFF ELECTRIC FIELD

As we extensively showed in chapter 6, applying a V=10kV on a 6mm gap, an injection of charge occurs through the needle that generates a fluid jet. A PIV measure of the injection speed has been estimated at 0.15-0.2m/s near the needle tip, decreasing to 0.12-0.14m/s in front of the bottom electrode.

With the objective of understanding how an instability due to an injection of charge can modify the lift-off characteristics, a series of tests was carried out on groups of 3 fibres, exposing the particles to a divergent and progressively increasing electric field.

Copper fibres around 2mm long moved for voltages between 3 and 3.8kV on a 6mm gap; the motion was never instantaneous.
Using the formula (2-28), this voltage should correspond to an electric field between 121 and 154kV/m. This electric field is materially lower than the value of 486kV/m, experimentally validated in the injection free case (see section 7.3.1). This mismatch could be explained with reference to the fact that the electric field on the bottom electrode can be modified by the space charge, arising from the injection phenomenon, accumulated at the flat electrode surface. Tilmatine et al. (2004), considering the corona injection in air, pointed out that the effect of the space charge can be examined using:

$$E = \lambda_{sc} V/h \qquad (7\text{-}30)$$

Where E is the field that exists between two parallel, flat electrodes separated by a distance h multiplied by a constant $1< \lambda_{sc} <1.5$. In the present study, with $\lambda_{sc}=1$, the electric field would be: $500<E<633$ kV/m. This value matches reasonably well with the experiments.

Cr coated PZT fibres, around 2mm long, showed the same threshold value as the copper ones, except that in one case no motion was observed. In that case, the particle moved instantaneously if the bias was inverted.

PZT fibres of length between 1 and 2mm, did not move at all when a progressively increasing voltage from 0 to 10kV was applied. But, if at the end of the progressive increase, suddenly, a negative voltage with magnitude 10kV was applied, the particle moved instantaneously.

7.4.2. RESPONSE TO A STEP VOLTAGE OF 10KV, ANALYSIS OF THE MOTION AND CHARGE COMPUTATION

The 3 different kinds of fibres (length between 1 and 2mm) had all the same behaviour when exposed to a 10kV voltage step in both cases - negative or positive.

After the voltage was switched on, they did not move for a certain incubation time. This time was variable, and varied from half a second up to few seconds for the three kinds of fibres. Although the copper fibres had the predisposition to have a bigger incubation time there was no other discernable correlation between the different fibre types and the incubation time.

Once the incubation time had elapsed the fibres started to rotate. This motion occurred unpredictably either clockwise or anticlockwise. Before becoming perfectly vertical, the particle started to lift, moving toward the needle.

Regarding the initial positioning of the particle (the left corner of the particle on the needle axis): the clockwise orientation was less favourable to motion. In this case the fibre was immediately exposed to the central region of the fluid jet. The fibre started to lift with an average speed between 0.007-0.015m/s, stopped climbing, started to move downward after 15-25ms and having reached a height of 0.175-0.225mm. In the anticlockwise case, the particle adopted a curved trajectory to the needle tip. Because the fibre was not directly in contact with the region of stronger liquid injection, the upward motion was faster, i.e. 0.023-0.030m/s. After, 75-90ms, at a height of 1.7-2.7mm the particle was intercepted by the fluid jet, and the motion was reversed. This was also true for the case in which the particle was unable to reach the needle tip.

In both cases the particle was repulsed by the liquid jet toward the bottom electrode. Once back in contact with the bottom electrode, the fibre charged another time and returned to lift.

The process described above, iterated a few times, established that there was an up and down oscillating motion of the particle.

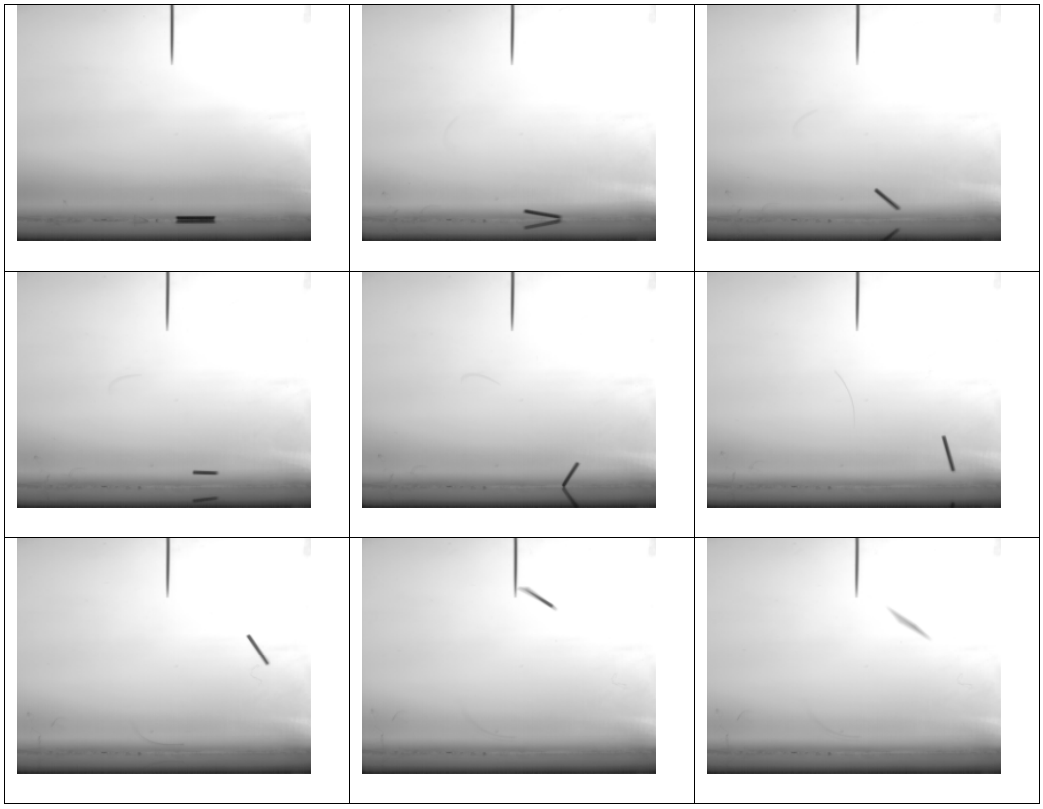

Figure 7. 17: Motion of a Cr coated PZT fibre orienting anticlockwise and then reaching the needle

Considering that, in close proximity to the bottom electrode, the liquid had the tendency to flow away from the needle axis (see chapter 6), the particle, while oscillating, moved away from the injection axis.

When the particle reached a position 2.5-3mm from the jet axis, which was far enough away so that it could not be intercepted by the charged jet anymore, the particle was able to move toward the needle electrode. This motion had an averaged speed of 0.04-0.05 m/s.

When the particle touched the upper electrode, it was repulsed with a violent force at an averaged speed of 0.3-0.45m/s. This value, the average value across the whole gap, is considerably below the instantaneous speed immediately following the needle contact.

The behaviour of PZT fibres, coated and uncoated, was very similar, with the exception of the insulating fibres' case. In that case the contact on the bottom electrode could take up to several ms, instead of being almost instantaneous as it was for the coated fibres.

When the fibre reached the contact with the needle on the cylindrical part on the side, the angle between the fibre and the needle axis was the same for any kind of particle: around 62°.

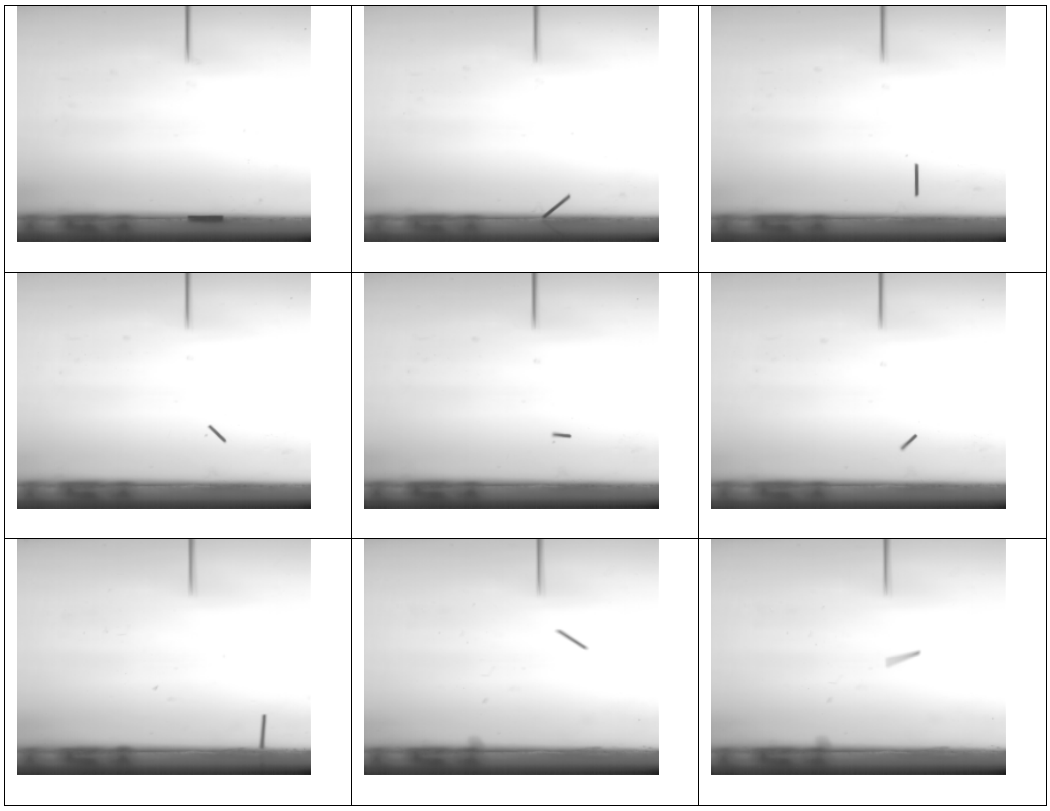

Figure 7. 18 Motion of a Cr coated PZT fibre orienting clockwise and not reaching the needle. The fibre is repulsed down.

A rough approach to the charge calculation can be achieved starting from the consideration that the fibre has an average speed of 0.3-0.45 m/s. Except for the first instant of the motion in which the fibre experience a great acceleration, the motion of the fibre could be assimilated to the one of a fibre with a speed like the average distance, exposed to an electric field of 0.556 MV/m. This field is the averaged field in

a range between 1.2mm far from the tip (the fibre is 1.2±0.01mm long), and the bottom electrode. The charge hence estimated is equal to:

$$Q_m = 106\text{-}160\text{pC equivalent to a linear density of } Q_m/L = 88\text{-}133\ \text{nC/m} \qquad (7\text{-}31)$$

Considering the theory of the charging of the particles by injection, this charge can be compared with the one that the particle should acquire for a field of 8,16 MV/m. This is the average field in a range of 1.2mm from the needle tip. For a similar field the theoretical charge should be:

$$Q_{FV} = 313\ \text{pC} \quad \text{and} \quad Q_{FH} = 88.5\ \text{pC} \qquad (7\text{-}32)$$

Where Q_{FV} and Q_{FH} are the theoretical charge for a field of 8,16 MV/m in case of a particle in vertical or horizontal position respectively.

As we can see Q_m is between 1.5 and 2 times bigger than Q_{FH}. This value seems to be slightly overestimated in respect to the results relative to the injection free case (see section 7.3), even if, considering the uncertainty on the charge value, no conclusion can be presented (see appendix D).

7.4.3. AN APPROXIMATED MODEL

An approximate model describing the behaviour of a particle in an injection dominated electric field, can be derived by adapting a model presented by Dascalescu et al. (1995) to describe the motion of conducting particles, in air, in a corona dominated electric field.

The equation of the motion of a particle in a divergent electric field (neglecting the adhesion forces because they act only when the particle is very close to the electrode boundary), is still similar to (3-12):

$$\mathbf{F_{DEP}} + \mathbf{F_C} \pm \mathbf{F_w} - \mathbf{F_D} = m_i\mathbf{a} \qquad (7\text{-}33)$$

considering that in silicone oil the motion is over-damped (see section 7.3.3.2), the inertia can be neglected and $m_i = m_p$.

F_{DEP} indicates the multipolar contribution to the lift force due to the gradient of the external field. For sufficient electrode separation this force is negligible compared with the columbic forces. This is because the field is almost uniform after a certain distance from the needle tip (see section 2.2.2).

F_D is still equal to κu, but this time $u_r = u_{EHD}-u_p$, where u_{EHD} can be derived from the PIV evaluation.

F_C needs a series of considerations. In contrast to the injection free case in this instance charging from the fluid can occur, following the mechanism proposed by Pauthenier (see section 3.3.2.4). The rate at which the particle charges from the fluid is expressed by the formula:

$$dQ/dt= (Q-Q_{max})^2/(\tau Q_{max}) \tag{7-34}$$

where $\tau=4\varepsilon_l/(qk)$, q is the space charge density, and k the charge mobility. Considering the experiment in a fluid, k would be the hydrodynamic mobility, and can be approximated by:

$$k_H = (\varepsilon_l/\rho_l)^{1/2} \tag{7-35}$$

For a silicone oil $k_H =1.52\times10^{-7}$ m^2/Vs.

To calculate the charge density q some information about the charged plume is necessary. The plume jet, as visualised by PIV, has a certain radius δ, around 0.5mm. However, the most recent theory, suggests that the charge should be concentrated in a narrower region in the jet core of radius R. A good approximation is $a/\delta = 0.2$, and q can be calculated as:

$$q = I/(u_{EHD} \pi r^2) \tag{7-36}$$

where I is the measured current.

Considering the conditions of the research project, V=10kV, and q = 0.46 C/m^3. $\tau = 1.26\times10^{-3}$ is calculated.

The first order differential equation is solved when z(0)=0, u(0)=0, $Q(0)=Q_F =Q_0$. Q_{max} is given by (3-6) as specified by Pauthanier (1932). After integration, Q(t) results:

$$Q = Q_s + \frac{1}{\frac{1}{Q_0 - Q_s} - \frac{t}{Q_s \tau}} \tag{7-37}$$

For the present case, with V=10kV, considering the saturation charge in the case of horizontal particle:

$$Q_s = -2Q_{Fh} = -2Q_0, \text{ when } t = \tau, Q = -0.8Q_0 \text{ and } Q=0 \text{ when } t=0.33\ \tau. \quad (7\text{-}38)$$

Considering that the particle's terminal velocity was measured for V=10kV is 0,15-0,18 m/s, and that the plume speed was measured 0.12-0.14 m/s near the bottom electrode (see chapter 6), a speed of 40±3mm/s would be an estimate of the particle speed directly after the switch on of the field. This speed should decrease until:

$$Q = Q_{stop} = (mg + \kappa u_r)/E. \quad (7\text{-}39)$$

$$t = t_{stop} = Q_s\tau[(Q_0-Q_s)^{-1}-(Q_{stop}-Q_s)^{-1}]<0.33\ \tau \quad (7\text{-}40)$$

Where t_{stop} is the time that the particle needs to stop rising and to reverse its motion direction. When this condition is verified, Q_{stop} represent the value of charge on the particle.

At that point the particle would invert its motion. For a copper particle 1.3mm long and 192μm in diameter, $t_{stop}= 6.04\times10^{-5}$ s.

Considering the results shown in section 7.4.2, this model gives a good estimation of speed. Conversely, the time of inversion of the motion results is considerably underestimated. The principal reason of such a mismatch could be an error in the evaluation of q. In fact, although the estimated q is a decent approximation in the liquid jet centre far from the electrode, this is absolutely not reliable in close proximity to the lower electrode; there, the jet spread on the plane, also creates a toroidal vortex. For an exact calculation it would be necessary to know the exact spatial distribution of the current density. Considering the experimental results, a q equal to one thousands of the value calculated using 7-35 (i.e. ~ $5\times10^{-4}C/m^3$) seems to be a good approximation.

To complete the theoretical analysis, it is necessary to remark that the real Q_0 would be bigger than the one predicted previously. As explained in section 7.4.1, this derives from the space charge modification of the electric field accumulating near the bottom electrode.

7.4.4. CONSIDERATION ABOUT THE RESPONSE IN ANEEDLE-PLANE CONFIGURATION

The motion in the needle-plane configuration is characterised by the presence of an injection of homocharge through the needle tip. This happens when the field passes a certain threshold value that, in this case, has been measured at around 4kV. One of the consequences of this injection is the generation of an instability that contributes to the creation of an additional drag on the fibre. The fibre's behaviour is then in equilibrium between a hetero-charging phenomenon through the bottom electrode and a homo-charging phenomenon from the space charge injected in the fluid, and a liquid stream contributing to an additional resistance to the motion.

If the charging through the bottom electrode can overtake the injected one, the particle can lift-off. At this point, the particle stops charging from the bottom electrode and its charge is progressively neutralised by the injected charge. The coulombian force decreases, and at a certain time the particle stops its upward motion and starts to move downward. This oscillatory motion can continue until, the particle can move outside the injection area. At that point the particle can charge once more through the bottom electrode, and then it can lift-off, reaching the needle tip. When the fibre touches the needle, it instantly receives an opposite charge and it is forcefully repulsed away. This behaviour can generate an oscillating motion across the two electrodes, until the fibre is launched too far to be intercepted. It is remarkable, that, except slight differences, this behaviour is very similar to that of any kind of fibres.

7.5. INSULATOR COATED NEEDLE-PLANE ELECTRODE

To investigate the case of a non-uniform, a series of tests was run using an insulator coated upper electrode, and a bottom flat electrode.
A series of lots of copper and PZT fibres (length between 1 and 2mm) was exposed to a square wave signal, with a duty cycle 50%, zero averaged and with a period of 4 minutes, and applying a voltage V=10kV on the needle.

In the case of copper fibres, no motion existed on the first positive half cycle, and a motion was, only occasionally, observed when the field became negative in the second half cycle. When the field again changed polarity (i.e. for a positive voltage), the fibre started an oscillatory motion up and down. By contrast, when the field became negative the particle remained in contact with the upper electrode unable to discharge.

PZT fibres were considerably less reactive. The behaviour of a group of 20 fibres was analysed several times. Only in one case a motion was observed in the second half (i.e. after two minutes) of the first negative cycle. Nevertheless, to generate a large motion of the particle it was necessary to wait 10 minutes. After such time during a negative half a cycle, 50% of the fibres moved toward the upper electrode. The fibres moved in direction of the upper electrode, with a speed of 0.3-0.5 m/s (averaged across the whole gap), independent of the fibre length.

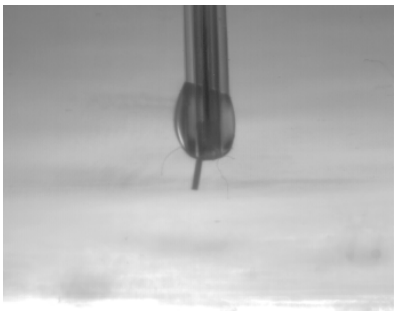

Figure 7. 19: fibre captured by a insulator coated needle upper electrode

In a first approximation, as calculated using the Durand (1966) formula, the electric field in proximity to the bottom electrode can be assumed to be around 0.3 MV/m. In reality this value of the electric field is an underestimate because the dielectric constant of the needle coating is bigger than that of the silicone oil, and consequently, the field inside the liquid is increased. However, it is evident that the lifting field is very close to the theoretical lift-off field, also validated by the experiments (see section 7.3.1). The fact that the fibres prefer to move when exposed to a negative electric field confirms once more the results reported in section 7.3.

7.6. FLAT-PTFE COATED PLANE CONFIGURATION

The current measured in a parallel flat electrode system without any fibre, if one of the two electrodes is coated by a 500±50μm thick PTFE layer, is almost four times smaller than when there is no coating. This is almost the value expected considering the value of the resistance of the PTFE and the silicone oil.

7.6.1. THE TRANSIENT IN A SERIES CAPACITOR

A system of two parallel flat electrodes immersed in silicone oil, where one of the electrodes is coated with an insulator, can be modelled with a series of capacitors.
Applying a step voltage V at t = 0, and switching it off at t = t_0, the relations expressing the voltage in time are:

$$V=V_1+V_2 \tag{7-41}$$

$$V_1= [VR_1/(R_1+R_2)] \{\Im-[(\tau-R_2C_2)/\tau]e^{-t/\tau}\} \tag{7-42}$$

Where:

$$\tau = (R_2\tau_1 + R_1\tau_2) / (R_1 + R_2),$$

$$\tau_i = R_iC_i \ (i=1,2), \tag{7-43}$$

if $t<t_0$ $\Im=1$ and if $t \geq t_0$ $\Im=[(\tau-R_2C_2)/\tau]e^{-(t-t0)/\tau}$

where V_i is the potential drop in the ith capacitor and R_i and C_i are its capacitance and its resistance respectively.
When applying this equation to the case analysed for this thesis, it is possible to observe that, directly after the voltage is switched off, and V=0 across the dielectric cell, a transient occurs, resulting in a negative voltage applied across the oil gap.
The bigger t_0, the bigger is the transient negative voltage peak. If $t_0 > 5\tau$ (i.e. the switch on transient is finished), V can reach 56% of the applied step voltage (see figure 7.21).

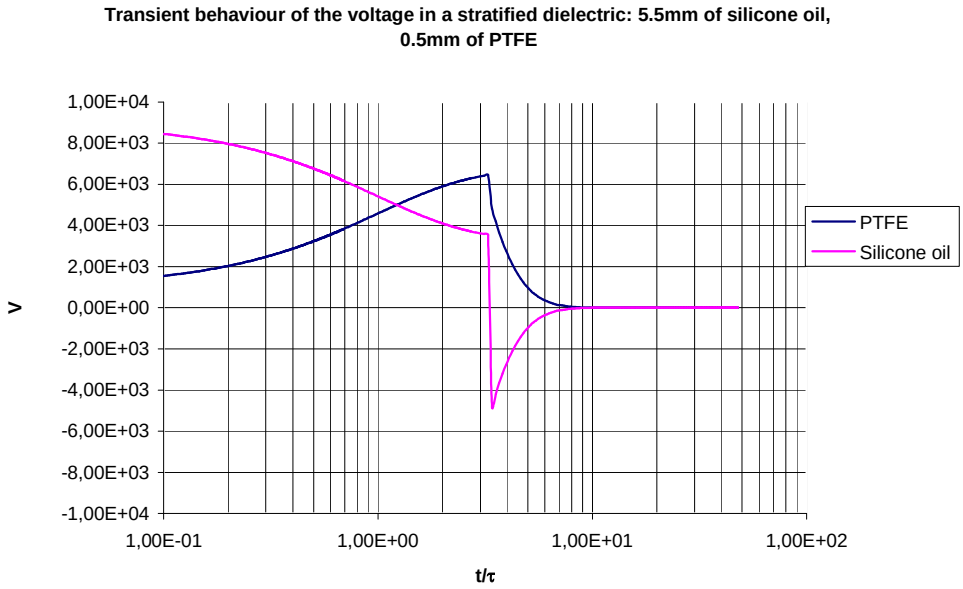

Figure 7. 20: Voltage transient behaviour in a stratified dielectric, with silicone oil and PZT. The time axis is expressed respect to the time constant τ of the capacitor.

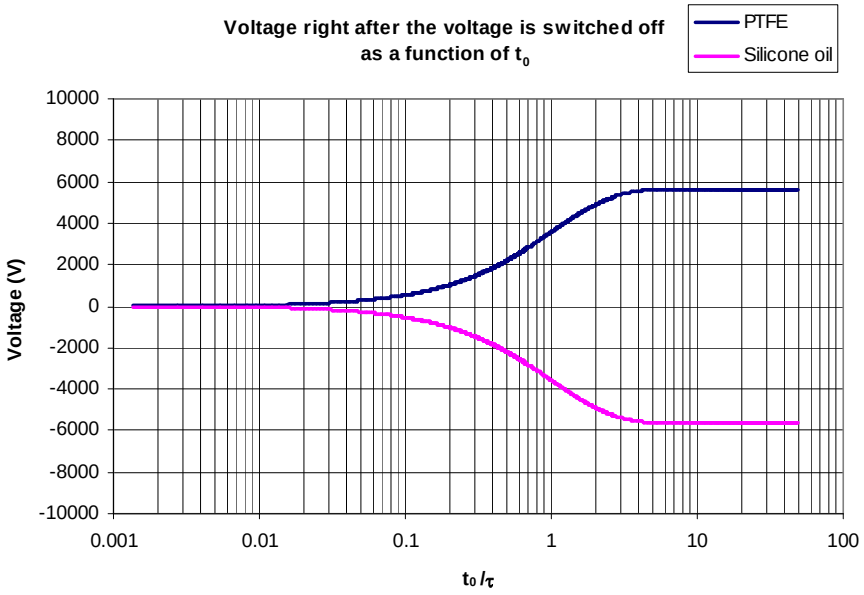

Figure 7. 21: Voltage immediately after the voltage switched off, in a stratified dielectric, with silicone oil and PTFE as a function of $t_{0.}$

7.6.2. RESPONSE TO A VOLTAGE PROGRESSIVELY INCREASING AND DETERMINATION OF THE LIFT-OFF ELECTRIC FIELD

5 fibres of copper and PZT fibres were exposed to a slowly increasing electric field between two parallel flat electrodes immersed in silicone oil, where one of the electrodes is coated with PTFE. The lift-off electric field was measured. The experiment was repeated several times.

In the case of copper fibres only, when a positive voltage was applied, 1 fibre oriented at E=0.77MV/m, and was able to move once up and down when E=1.23MV/m. This particle began to move again when E=1.666MV/m, and did not stop moving, but instead started a continuous oscillating motion.

On the application of a negative voltage, 2 fibres oriented when the field reached 1.333MV/m. At a field slightly higher, one of them was able to start to oscillate up and down.

Given the explanation in section 7.6.1, a greater attention was paid to the switch off transient.

A series of experiments was conducted by applying a series of voltage steps 100s in magnitude, increasing progressively. It has been observed that when the electric field was lower than 1.35MV/m, no motion of particles existed after the switch off. Nevertheless, when the voltage overtook this value, after the voltage switch off, all the particles have a collective lift-off motion.

This behaviour can be explained in terms of tribocharge accumulated on the fibres in contact with PTFE. Let us consider that:

- on a PTFE substrate the image attraction is almost equal to zero
- the voltage across the silicon oil gap right after the switch off has the value calculated using (7-41)

In this case the fibres should carry a charge at least of Q/L=3.97 nC/m to display the behaviour described above. This value is very close to the tribocharge directly measured (see section 5.3.3) using the Faraday pail (Cross, 1987). Then we can assume that the motion of the fibres in a system where the bottom electrode is coated with a thick film of PTFE is sensitive to the tribocharge.

In the case of PZT dielectric particles, exposed to a positive bias, 4 particles out of 5 moved. The first two particles for E=0.333 and 0.533MV/m, and the others for E=1.466MV/m. Always, before moving, the particles oriented for fields 50kV/m lower than the one at which they lifted-off. It is interesting to observe that the particles did not stay vertical after the voltage was removed as happened in the case without coating.
Similarly to what happens to copper fibres for field magnitudes bigger than 1.433MV/m, the PZT fibres had a collective motion toward the upper electrode right after the voltage was switched off. This means that the particles acquired a linear charge around 1.46 nC/m. Also in this case this value is very close to the directly measured tribocharge (see section 5.3.3).

7.6.3. RESPONSE TO A STEP VOLTAGE, ANALYSIS OF THE MOTION AND CHARGE COMPUTATION

The response of different kinds of fibres, to a step voltage of 1.666MV/m, applied between two parallel, flat electrodes immersed in silicone oil, where one of the electrodes is coated with PTFE was tested. The tests were carried out, several times, on groups of 13 fibres with lengths between 0.5 and 2mm.
The experiments confirmed what was expected given the observation in section 7.6.1 and 7.6.2.

When a positive voltage was applied to copper, no motion was observed except for a fibre after a minute and another after 2.5 minutes. On the contrary consistent motion was verified directly after the voltage switched off. Applying a negative voltage, the fibres moved instantly, all together, towards the top electrode. This behaviour can be attributed to the tribocharge on the fibres. The electric field switch off was followed by a collective motion of the particles.

The behaviour of PZT fibres was investigated. The phenomenon was very similar to that in the case of copper fibres. When a positive voltage was applied, only a single fibre moved up and down. After a minute some others raised up in a vertical position,

but without lifting. A collective motion of fibres was then observed when the field was switched off. On the application of a negative voltage the fibres moved instantaneously, and they were able to make few up and down oscillating movements. Also in this case, the electric field switch off was followed by a collective particle movement.

7.6.4. CONSIDERATIONS ABOUT THE RESPONSE IN A PLANE-PTFE COATED PLANE CONFIGURATION

As expected, the main effect of the insulator coating was to greatly increase the lift-off field. This confirmed what was already pointed out by Srivastava and Van Heeswijk (1985) who analysed extensively the effect of a coating on the breakdown resistance of a gap filled with pressurised insulating gas and polluted with conducting rods. This behaviour could be attributed to a residual leakage of current through the insulator.

Another interesting effect is related to the response to the switch off transient.
As it can be calculated, in the instance of a parallel plate capacitor filled with silicone oil, and the bottom electrode of the capacitor is coated with PTFE, right after the voltage is switched off, a transient will occur. The field in the silicone oil, before decaying to zero has a polarity inversion. Moreover, since a particle, in contact with PTFE, has the tendency to acquire a big positive tribocharge, a fibre that normally does not move when the field is applied does start to move when the voltage is switched off. The effect is not observed when a negative field is applied, because in that case the fibre moves, driven by its tribocharge, immediately when the voltage is switched on.

7.7. NEEDLE-PTFE COATED PLANE CONFIGURATION

A series of experiments has been conducted in a system having a needle-like upper electrode facing a PTFE coated bottom electrode. A step voltage of 10kV was applied across a gap of 6mm. The behaviour of different kinds of fibres with a length between 1 and 2mm was investigated.

The current without any fibres was measured at around 4±0.04nA (i.e. one fifth of the current measured without any PTFE coating).
In the cases of both a copper and PZT particle, and for a voltage of both positive and negative polarity, the particles started to rotate right after the field switched on. Unfortunately, the turbulence generated in front of the bottom electrode by the plume instability pushed the fibres far from the needle axis. Once the particle was 2.5-3mm away from the needle axis, the particle remained for a certain "dwell" time in a vertical position. After this latency time, that was in the order of 5-20s for a copper fibre, and 1 minute for the PZT fibre, the particle moved towards the upper needle. Although a movement of a copper fibre always occurs, for the PZT fibre that was not always the case.

This experiment showed that the injection was still active although the bottom electrode was coated with PTFE. Moreover, it was clear that the bigger adhesion between fibre and bottom electrode occurs when the fibre is directly in contact with the metal.

7.8. INSULATOR COATED NEEDLE- PTFE COATED PLANE CONFIGURATION

A series of experiments equivalent to those conducted in section 7.5 was carried out. However in this case a bottom electrode coated with PTFE, on a group of 10 fibres (length between 1 and 2mm) was also considered. The experiment was, again repeated several times.

The current without any fibres was around 130pA, smaller than a quarter of the current without PTFE coating.

In this configuration a movement was observed on the first negative half period, both on copper particle (4 on 10) and on PZT fibres (3 on 10). Then the particles discharged after the field changed polarity, and nothing else was observed after that. Also in this case, the results confirmed the behaviour already observed in the previous experiments.

7.9. DISCUSSION OF THE RESULTS

The present chapter analysed the electrohydrodynamics of some fibres immersed in silicone oil and exposed to an electric field. As matter of comparison different kind of fibres have been analysed:

- Copper
- Cr coated PZT
- Uncoated PZT

The behaviour of these different kinds of particles has been analysed under different electrode configurations:

- the case of a parallel plate capacitor geometry has been treated to study the charging phenomenon of the fibre through the bottom electrode, and a value of the charge has been extrapolated from films recording the particle motion
- the case of a needle-like upper electrode and bottom flat electrode has been analysed to verify the influence of a space charge injected from the needle tip on the fibre motion
- the effect of a insulator coated needle-like of a 0.5mm thick PTFE coating on the bottom electrode associated to the previous three kind of upper electrodes has also been investigated

The experiments showed that in the case of a metallic fibre the charge transfer was mainly electronic, through the contact area, even if evidences of a certain contact resistance have been noticed. Different hypotheses have been proposed (see section 7.3.4.1).

In the case of insulating fibres, it is interesting to focus the attention on the preference of the fibre to move under a positive voltage in respect to a negative one. The results exposed in section 7.3 suggest that two simultaneous charging phenomena are in competition in the case of a PZT particle:

1) When a field is applied between the two parallel plate electrodes, a ionic current is generated, due to the presence of ionic impurity in the bulk.
2) In the space between the fibre and the bottom electrode, the electric field enhancement induced by the presence of the fibre favour the creation of a charge, either by dissociation, or by injection through the micro-asperities on the electrode fluid interface, or both.

Assuming that the two charging mechanisms are relatively independent from each other, the final charge on the particle would be the result of the balance between the two carrier streams. Experimental evidences (see section 7.3) suggest that the two opposite mechanisms of charge do not have the same time constant. The charging from the bulk is slower. Moreover, an experiment shown in section 5.3.4 demonstrated that the PZT fibres in silicone oil have a remarkable preference to get charged negatively.
The same considerations could be made to explain the charge exchange mechanisms between the fibres and the electrodes for the following motion up and down after they rose into vertical position.

The charge acquired by the particle was always below the one predicted by theory for a vertical conducting particle. Moreover the charge does not increase following a linear proportional dependence from the electric field, but the ratio Q/E decreases when the electric field increases. This mean that, for higher values of electric field, the particle can lose some charge due to space charge generation. This consideration has also been supported by some measurements and conclusion derived from the observation of the motion of particles exposed to low frequency (few tenths of Hz) electric fields.
The charge, for the maximum value of electric field that has been tested (1.666MV/m), was only equal to the value predicted by Felici (1966) for an horizontal conducting particle, which means up to 3 times smaller than the value calculated for a vertical particle. However, despite the difference in the charging mechanisms, the amount of charge acquired by a PZT insulating particle was almost equal to the one acquired by a metal particle. A rough evaluation demonstrated that also in the case of motion of particles in a highly divergent electric field, the charge acquired by the particle was

predictable in a reasonable order of dimension using the model describing the charge of particle in uniform electric field.

Particular attention has been dedicated to the behaviour of a fibre exposed to the highly divergent electric field existing between a needle-like upper electrode and a bottom flat electrode. The system was characterised by a strong jet instability due to a charge injection through the needle tip. Such an instability prevents the fibre to easily reach the upper electrode. However, after a series of oscillations the particle reached the tip. Once the contact had been established the fibre was forcefully repelled. This repulsion was due to an excess of homo-charge transferred from the needle to the tip. In fact coating the needle with an insulator so as to avoid any charge transfer helped the particle to be successfully captured on the upper electrode.
Also in this case, no great difference has been noted between the behaviour of the metallic or the insulating particle.

Another interesting effect was observed analysing the motion of a fibre in a uniform electric field when the fibre was resting on a PTFE-coated bottom electrode.
Once the particles were exposed to an electric field, they moved with difficulty. This was due to the fact that the insulating coating compromised the charging mechanisms. Nevertheless, right after the field was switched-off, a transient lift-off occurred. This was due to the fact that, after the switch-off, the field in the silicone oil inversed its polarity, before decaying to zero. Considering that a particle in contact with a PTFE surface has the tendency to acquire a big positive tribocharge, a fibre that normally does not move when the field is applied starts to move when the voltage is switched off only because of its tribocharge. For this reason, the effect was not observed when a negative field was applied.

Chapter 8

CAPTURE OF SINGLE MICRO-RODS

This chapter shall describe the behaviour of different kinds of fibres exposed to a divergent electric field in AC. Also in this case the discussion of the results is reported at the end of the same chapter.

8.1. HEURISTIC DESCRIPTION OF THE PHENOMENON

The equilibrium of the forces acting on an elongated particle resting on a flat electrode, and exposed to the divergent electric field generated by a sharp probe upper electrode is summarised in the picture 8.1.

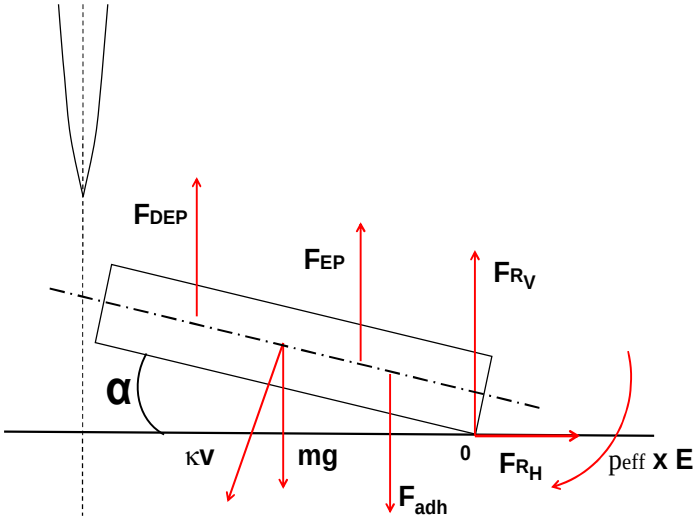

Figure 8. 1: Equilibrium of force and momentum acting on single fibre exposed to a divergent electric field generated between a needle-like upper electrode and a plane bottom electrode.

The equilibrium can be described in terms of forces and momentum. The equilibrium equations are written below:

equilibrium of the forces:

$$\mathbf{F_R} + \mathbf{F_{DEP}} + \mathbf{F_{EP}} - m\mathbf{g} - \kappa\mathbf{v} - \mathbf{F_{adh}} = m\mathbf{a} \qquad (8\text{-}1)$$

equilibrium of the momentum respect to the pivoting point O:

$$\mathbf{F_{DEP}} \times \mathbf{d_{DEP}} + \mathbf{F_{EP}} \times \mathbf{d_{EP}} - \mathbf{F_{adh}} \times \mathbf{d_{adh}} - \kappa'\boldsymbol{\omega} - m\mathbf{g} \times \mathbf{d_G} + \mathbf{p_{eff}} \times \mathbf{E} = m\boldsymbol{\theta} \qquad (8\text{-}2)$$

Where:

$\mathbf{F_R}$: the reaction of the supporting plane

m**g**: the weight force

$\mathbf{F_{DEP}}$: the dielectrophoretic force

$\mathbf{F_{EP}}$: the electrophoretic force

$\mathbf{F_{adh}}$: the adhesion forces, mainly due to electrostatic adhesion due to the image charge

$\kappa\mathbf{v}$: the linear viscous force

-m**a**: the inertia force

$\mathbf{d_{DEP}}$: the distance between the application point of DEP and the fibre pivoting point O

$\mathbf{d_G}$: the distance between the centre of gravity and the fibre pivoting point O

$\kappa'\boldsymbol{\omega}$: the viscous torque

$\mathbf{p_{eff}} \times \mathbf{E}$: the orientation torque

$-m\boldsymbol{\theta}$: the inertia torque

8.2. FINITE ELEMENT ANALYSIS

A series of finite element simulations was carried out to understand the behaviour of a fibre exposed to a highly divergent electric field. In particular the dependence of electrostatic adhesion on the angle between the fibre and the substrate was analysed. The force acting on a particle exposed to a divergent electric field was considered, as was the electric field. In addition the force acting on a vertical fibre when it is close to the needle tip was investigated to simulate what happens once the particle has been picked-up,

8.2.1. THE ELECTROSTATIC ADHESION AS A FUNCTION OF THE ANGLE BETWEEN THE ROD AND THE SUBSTRATE

The simulation was run with Maxwell 3D considering a PZT particle 140μm in diameter, 1.2mm long, exposed to a field of 1.666MV/m, in silicone oil resting on a supported grounded plane with a distance from the plane of 0.5μm.

The reliability of the FEM solver was tested calculating the torque and the force acting on the upper cited fibre, free standing in the dielectric medium at an angle of 45° with respect to the horizontal plane. The FEM calculated torque, was 20.3 nN·m; the analytically calculated value was 15.09 nN·m (see section 3.3.3.3). The difference can be attributed to the fact that the analytical formula treats the fibre as an ellipsoid, and the FEM gives results for a perfectly cylindrical particle. The agreement between the two values can be considered sufficient, for some phenomenological evaluations to be made.

The force computed by FEM was smaller than 0.1 μN in any direction. This value can then be considered to be the sensitivity of the numerical method.

Another important check of the FEM solver was the calculation of the force acting on a fibre with the characteristics cited above, positioned horizontally using Maxwell with both the 2D and the 3D solver. The value of the force calculated with the 3D solver was 45% bigger than the value calculated by the 2D solver. This could be due to the influence of the boundary effect on the total force.

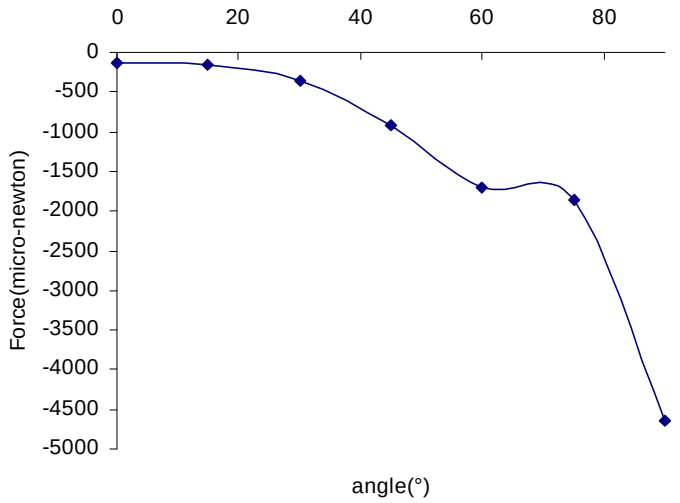

Figure 8. 2: Adhesion force acting on PZT rod with a diameter of 140μm when exposed to an electric field of 1.666MV/m, when positioned at different angles respect to the horizontal

Once the reliability of the 3D solver was verified the values of the net force acting on a particle lying on a metallic bottom electrode when positioned with a certain angle with respect to the horizontal was calculated (see chart in figure 8.2).

The electrostatic force applied to the dielectric rod was always negative, which demonstrated that no particle lift can be possible in this configuration. The electric field enhances the adhesion between the particle and the bottom electrode. When the angle increased up to 60° the module of the force increased monotonically. Between 60° and 75° the value remained almost constant and then started to increase again, reaching its maximum at 90°.
Although a progressive increase in the force in accordance with increase in the angle was expected, the inflection between 60° and 75° was not. In light of this, it would be necessary to investigate more in detail the computation of the force for these particular angle values before drawing any firm conclusions.

The net momentum respect to the point O (see figure 8.1), was also computed. The results are reported in figure 8.3.
The net momentum $\mathbf{T_{tot}}$ is the sum of the orientation torque and of the momentum due to the adhesion force. However, without knowing the application point of the adhesion force, it is impossible, from the value of $\mathbf{T_{tot}}$, to establish the value of the orientation torque. Consequently the following torque values, also plotted in figure 8.3, have been considered:

- $\mathbf{(T_{orient})_{th}}$: the value of the orientation torque calculated with the formula explained in section3.3.3.3 for a particle in a dielectric fluid far from any space discontinuity
- $\mathbf{T_{adh}}$: the value of the torque due to the net electrostatic force as it would be if the force was applied in the centre of gravity of the particle ($\mathbf{T_{adh}=F_{adh}\times d_G}$)
- $\mathbf{T_{orient}}$: the value that the orientation torque should assume if the torque was $\mathbf{T_{adh}}$ ($\mathbf{T_{orient} = T_{tot} - T_{adh}}$)

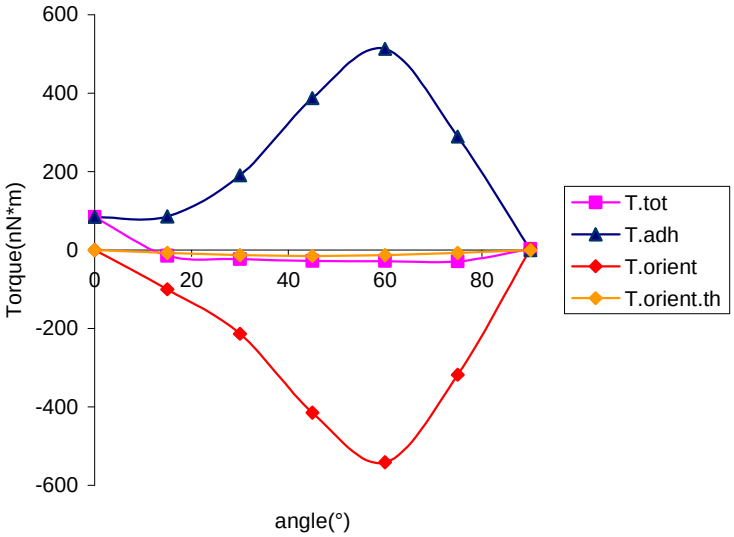

Figure 8. 3: Torque acting on PZT rod with a diameter of 140μm when exposed to an electric field of 1.666MV/m, when positioned at different angles respect to the horizontal

From an analysis of the results it can be seen that $\mathbf{T_{adh}}$ was always positive ($\mathbf{F_{adh}}$ is always negative), and that $\mathbf{T_{tot}}$ was always negative. As a consequence it can be concluded that $\mathbf{T_{orient}}$ overcomes $\mathbf{T_{adh}}$, and that any rotation of the particle should be attributed to the orientation torque. However, a value of $\mathbf{T_{orient}}$ like the one extrapolated assuming $\mathbf{F_{adh}}$ applied in the centre of gravity of the particle, it is not very consistent, because it would have an inexplicably large value given $\mathbf{(T_{orient})_{th}}$. Consequently, the most appropriate conclusion is that, except when $\alpha=0$, the point of application of $\mathbf{F_{adh}}$, is not near the centre of gravity, but is very close to the point O. Therefore the momentum becomes smaller than the orientation torque, and the orientation torque becomes the principal determining factor of the electrostatically induced rotation of the particle.

To understand the importance of such a result it is necessary to recall that when the particle is resting on a plane, the action of an orientation torque generates a lifting force due to the reaction of the support. This means that if the orientation torque is big enough, even if the particle is exposed to a net adhesion force, it could still rise up and position itself vertically, obviously without leaving the plane.

In the chart below the value of $\mathbf{F_{adh}}$, and the force induced by the orientation torque $\mathbf{F_{orient}}$ are reported. It can be seen that, $\mathbf{F_{orient}}$ was always smaller than $\mathbf{F_{adh}}$. As a result it can be concluded that no motion of the particle is theoretically possible in the configuration analysed to this point.

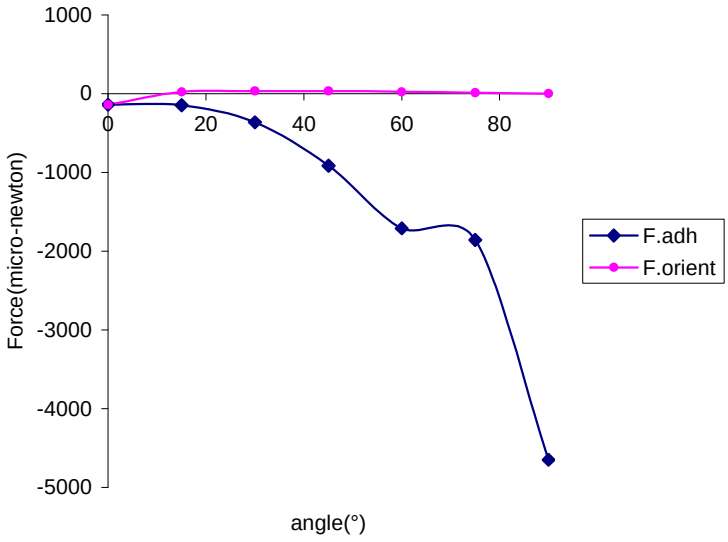

Figure 8. 4: Comparison between the adhesion force and the lifting force issued from the orientation torque

The particle adhesion is mainly due to image adhesion. By reducing the multiple image interaction, a net lift force on the particle can be achieved. A simulation conducted with a fibre lying horizontally on a PTFE coated plane, showed a net upward electrostatic force F=1.02 μN, and a torque of T = -0.614 nN·m. where:

- Weight force: 0.14309 μN
- Weight torque: 85.8539 pN·m

It is possible to conclude that by reducing the image force, e.g. by coating the supporting electrode with a dielectric substrate, the particle can lift-off.

A further series of simulations was completed under the same conditions described above except that on this occasion a perfectly conducting particle was used.

As expected, in this case the particle became charged by induction and the Coulomb force was big enough to overcome all the effects of the adhesion and the weight force. The lift force was shown to increase uniformly when the angle with respect to the plane increased.

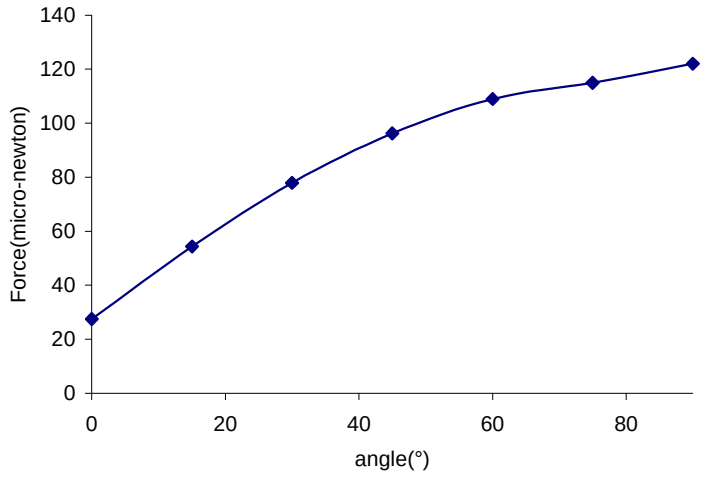

Figure 8. 5: Lift-force acting on metallic rod with a diameter of 140µm when exposed to an electric field of 1.666MV/m, when positioned at different angles with respect to the horizontal

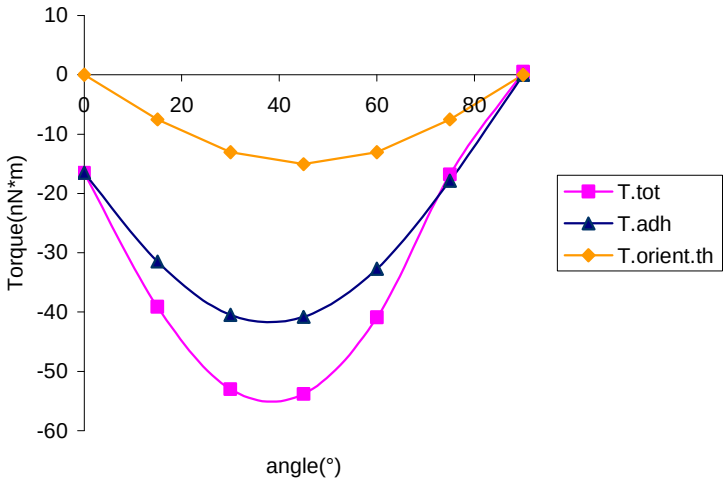

Figure 8. 6: Torque acting on metallic rod with a diameter of 140µm when exposed to an electric field of 1.666MV/m, when positioned at different angles with respect to the horizontal

The torque $\mathbf{T_{tot}}$ was also computed. It reached a maximum at 45°. However, due to the fact that the particle had a charge, and the distribution was not known, establishing any correspondence between $\mathbf{T_{tot}}$ and $\mathbf{(T_{orient})_{th}}$, is a complex task. Therefore, in contrast to the case of the PZT particle, it is very difficult to give any indication relative to the point of application of the electrostatic force.

8.2.2. THE FORCE ACTING ON A FIBRE IN A DIVERGENT ELECTRIC FIELD

In the pictures 8.7 (a) and (b), a qualitative view of the electric field distribution for the geometry analysed in the present study is reported. These pictures evidence the field localisation near the needle-tip, from where the dielectrophoretic effect arises. Moreover, it is possible to appreciate how the shape of the electric field changes according to whether the fibre is supported either by a metallic electrode, or by an electrode coated with an insulator layer. In the first case the isopotential lines are more concentrated near the tip, because the fields on the plane have to be zero. In this case the electrostatic adhesion is at a maximum, and virtually no motion of the fibre is possible. In the second case, even though the gradient of the field near the tip is smaller, the electrostatic adhesion is almost zero, and an electrokinetic effect on the particle is allowed.

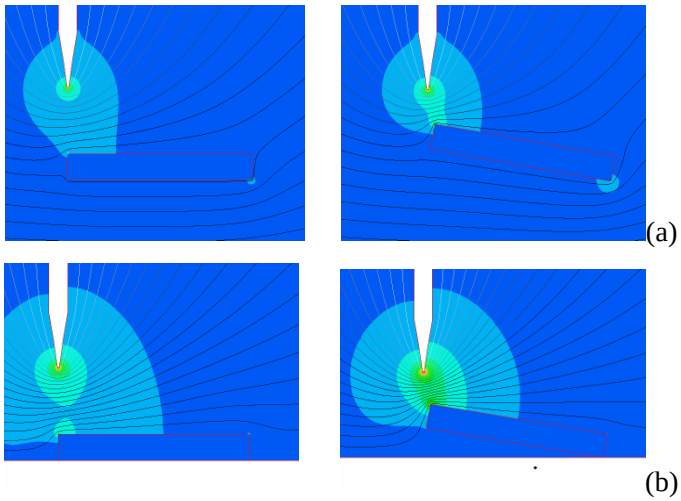

Figure 8. 7: Electric field distribution around a PZT fibre exposed to a divergent electric field, with and without insulating coating on the bottom flat electrode ((a) and (b) respectively)

Some 3D simulations of the force exerted on both a PZT and a conducting fibre, 1.2mm long, 140μm in diameter and immersed in silicone oil, have been carried out where the fibre was exposed to a divergent electric field. The field was applied between a needle and a plane. The needle was 120μm in diameter, and had a tip radius of 6.5μm. The voltage applied to the needle was 10kV.

Table 8. 1: Summary of the 3D simulations carried out to measure the force acting on a fibre exposed to the divergent electric field generated between a needle (diameter=120μm, tip radius=6.5μm) and bottom flat electrode.

	h (mm)	F_x(μN)	F_z(μN)	T(nN·m)
PZT fibres Grounded bottom electrode				
	0.25	-128	-2640	1786
	0.50	-23	-1368	888
PTFE coated bottom electrode (coating thickness 0,5mm)				
	0.25	-42	177	-256
	0.50	-5	30	-58
	1.00	-1	6	-15
Conducting fibres Grounded bottom electrode				
	0.5	-29	290	-230

The results are summarised in table 8.1, where the force and the torque for different distances “d” between the needle tip and the supporting plane are reported.

The force is always an adhesion when a PZT fibre rests on a grounded plane. Conversely, the force is always a lifting force in the case of conducting particles and also in the case of a PZT fibre on a PTFE coated flat electrode. However, the lifting force is 10 times bigger in the case of a conducting particle.

In the case of PZT particles, the module of the adhesion force in the case of metallic uncoated flat electrode is at least one order of magnitude higher than the lifting force in the case of a coated electrode.

The force acting parallel to the z axis is always at least one order of magnitude stronger than the one acting on the x axis. Even though the number of simulations carried out is too small to establish a trend, it is important to remark that the magnitude of the adhesion force in the case of a PZT fibre resting on a ground plane appears to be

inversely proportional to the tip-plane distance. However, in the case of a PZT fibre lying on a PTFE coated plane, the dependence of the lift force seems to be inversely proportional to the square of the distance.

8.2.3. THE INTERACTION BETWEEN THE NEEDLE AND THE ROD

In the previous sections particular attention was accorded to the electrostatic interactions between the fibre and the plane since they are fundamental to the understanding of any fibre capture process. It should be noted that once a lift-off result is possible, the interaction between the tip and the fibre is a factor worthy of particular attention.

As already shown in chapter 2, the electric field near the needle tip, in the case of a needle with a tip radius of 6.5μm, can easily overcome the breakdown resistance of the dielectric fluid, and such a high level of electric field can trigger a charge injection into the fluid. The possibility of such an injection is intensified when a PZT fibre is placed in close proximity to the needle tip. In fact, since the permittivity of the PZT is higher than the permittivity of the surrounding fluid, the field results increased closer to the needle tip. This phenomenon it is evidenced in the simulation in figure 8.8.
In table 8.2 the FEM computation of the force acting on a PZT fibre, and the electric field in the gap, in different conditions of distance tip-fibre, and for different fibre dimensions are reported. A distance tip-plane of 1mm and a voltage on the needle of 10kV was considered.

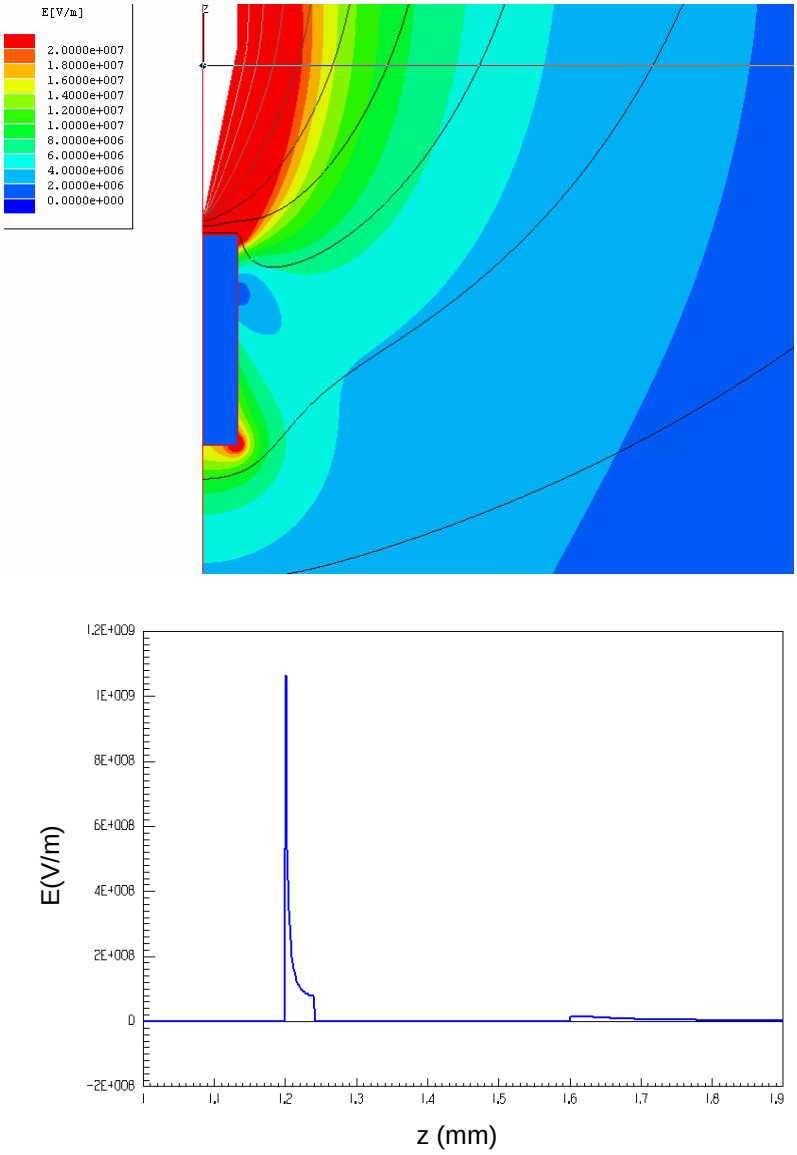

Figure 8. 8: FEM simulation of the electric field in the gap between needle (diameter=120μm, tip radius=6.5μm) and a PZT fibre ((diameter=140μm) when a fibre is captured.

The data in table 8.2, as expected, show a decrease in the force with respect to distance and that such a dependence was more important if the distance was smaller. Concerning the fibre length, it can be seen that at the same distance, the force decreased if the length increased, assuming a negative value when the fibre length reached the tip-plane

distance of 1mm. This is because with an increase in fibre length, the influence of the adhesion to the bottom electrode also increases.

The electric field in the gap depends on the tip-fibre distance. It followed almost the same trend as the force. However, in contrast to the case of the force, the maximum field was not too sensitive to the fibre length. The most important observation is that the maximum field always exceeded 1 MV/mm, reaching a value considerably higher than the breakdown field of the dielectric liquid, and the threshold field for the injection instabilities.
Given this finding, it is reasonable to assume that the conditions for perfect insulation of the fluid are not physically possible in the gap since a current would be generated decreasing the field in the gap.

To make a finite element model to analyse the case of a current controlled electric field in the gap is a complex task. However, in order to generate a useful approximation of what happens in these particular conditions, a series of models were created. These models assumed that either the upper face of the fibre or both the upper and the lateral faces, were isopotential with the needle. This simulated the condition in which the fluid inside the gap was short circuited. This condition occurs in nature when the field is very close to the breakdown value, and an important field enhanced dissociation occurs in the gap.

As expected, when the fibre was isopotential with the needle, the fibre acquired a homo-charge and was repulsed by the needle (the force was negative). Such a force was not very sensitive to the needle-tip distance, and moreover, it was almost the same whether only the upper face or both faces were considered isopotential.
It is likely that even if a current should exist in the gap, the real situation is not as severe as the isopotential model predicts and instead it would be between the ideal zero conductivity case and the isopotential case. It is interesting to note that, even if a net charge exists on the tip, and the force is negative, this behaviour is still compatible with a fibre capture in AC. In fact, if the liquid viscosity and the signal frequency are high enough, the continuous charge transfer, accompanied by the sign inversion of the signal,

can be compatible with a rod capture. Nevertheless, in this case, the nature of the pick-up would not be purely “dielectrophoretic”, but also partially “electrophoretic”. This is due to a Coulomb force acting on the charge transferred by induction to the fibre.

Table 8. 2: Summary of the FEM computation of the attractive force between needle (diameter=120μm, tip radius=6.5μm) and a PZT fibre ((diameter=140μm) when a fibre is captured. Different hypotheses are considered for the field distribution in the gap.

	L(mm)	d(μm)	F(mN)	E_{max}(MV/mm)
Perfectly insulating fluid				
	0.36	5	10.9	5.55
	0.36	20	1.02	1.27
	0.36	40	0.533	1.06
	0.72	40	0.338	1.18
	1	40	-5.75	1.12
Upper face of the fibre isopotential with the needle				
	0.72	5	-1.70	-
Upper and lateral face of the fibre isopotential with the needle				
	0.72	5	-1.72	-
	0.72	20	-1.53	-
	0.72	40	-1.53	-

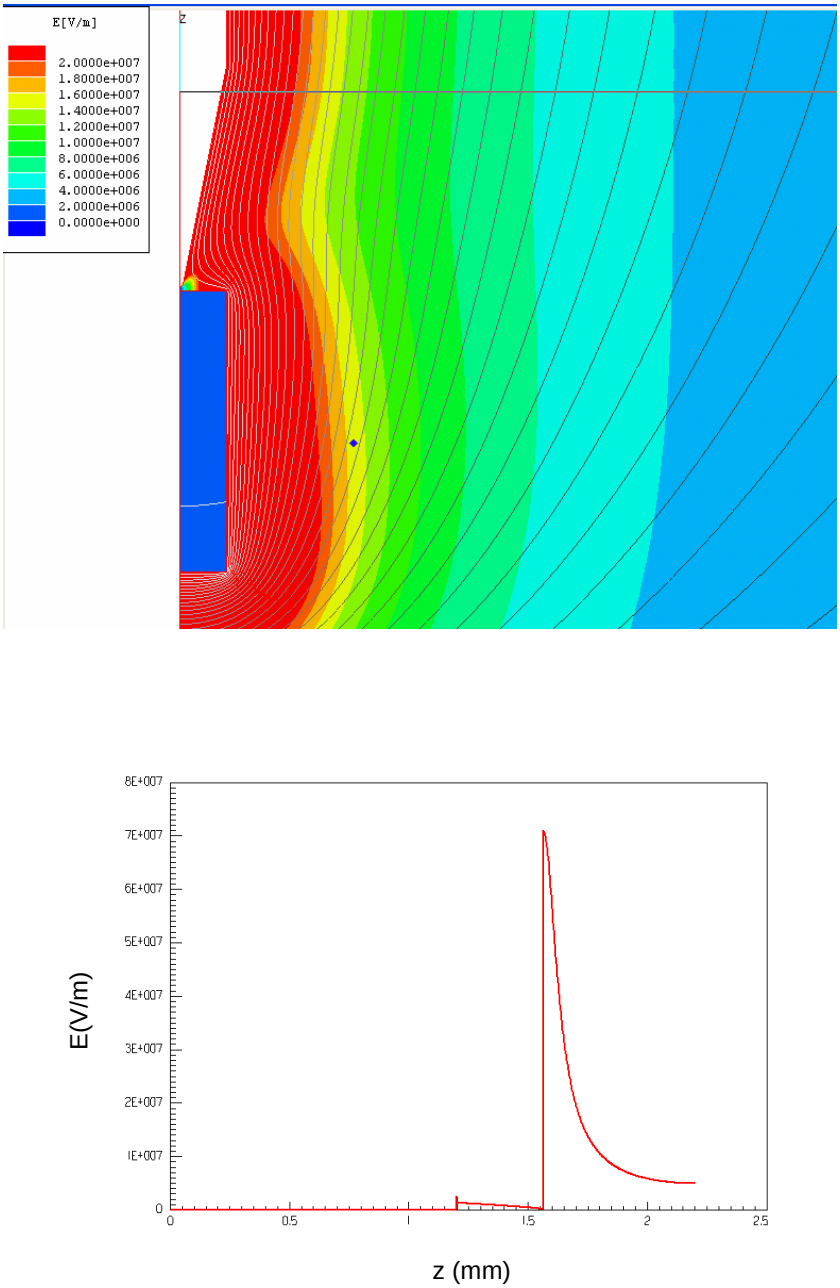

Figure 8. 9: FEM simulation of the electric field in the gap between needle (diameter=120µm, tip radius=6.5µm) and a PZT fibre ((diameter=140µm) when a fibre is captured. The hypothesis is that the upper face of the fibre is isopotential with the needle

8.3. THE EXPERIMENTAL RESULTS

The behaviour of a PZT fibre, 140μm in diameter, 1.2mm long, exposed to the divergent electric field generated between a needle of 120μm diameter and of 6.5μm tip radius has been tested. The needle was excited with a voltage of 1kHz of frequency and a magnitude between 2 and 7kV.
Starting from a needle-plane distance of 6mm, the distance was reduced until either breakdown occurred or the needle was in contact with the fibre. As predicted by the FEM simulations no motion of the fibre was observed for any voltage at any distance.

With the objective of allowing the lift-off, while avoiding the electrostatic adhesion, a series of experiments, coating the bottom flat electrode with a 0.5mm thick PTFE film, was carried out. The influence of the applied voltage (frequency and the magnitude), of the fibre material, the dielectric fluid was considered. Importantly the influence in the capture phenomenon of a coating on the needle-like electrode was also considered.
Each experiment was conducted by applying the voltage when the needle-plane distance was equal to 6mm. That distance was progressively reduced by moving the needle toward the plane at a speed of 0.2mm/s. The needle motion was stopped when the fibre started to lift-off. To describe the fibre pick-up behaviour, particular attention was paid to this inception height as well as to a series of qualitative evaluations.

8.3.1. THE FIBRE CAPTURE AS A FUNCTION OF THE VOLTAGE FREQUENCY

The dependence of the pick-up behaviour on the voltage frequency was tested by applying a signal of 3kV at a frequency varying from DC up to 1kHz. All the observations are summarised in the table 8.3.
The phenomenon in DC was characterised by an injection due to an instability in the fluid that avoided any possible contact between fibre and needle.

Table 8. 3: Summary of a series of experiment showing the dependence of the capturing behaviour of a PZT fibre from the voltage frequency. The voltage was 3kV.

Frequency (Hz)	Inception height (μm)	Capture (YES/NO) Behaviour	After switch off behaviour
DC	0	NO Injection through the needle	-
50	120	NO Fibre oscillation between needle and bottom flat electrode with generation of bubbles	-
100	260	NO Fibre oscillation between needle and bottom flat electrode with generation of bubbles	-
500	90	YES Fibre oscillation near the tip with a 52μm amplitude and generation of bubbles	The fibre remains attached to the needle
1000	200	YES Fibre oscillation near the tip with a 25-30μm amplitude and generation of bubbles	The fibre drops

The phenomenology was different for the AC case. The inception height for the fibre motion was always around 100-200μm. This characteristic height did not appear to be related to the frequency.

For frequencies up to 100Hz, although the lift-off of the particle is achieved, still no capture of the particle was possible. In that case the particle oscillates continuously between the tip and the bottom electrode. Once the inception was reached, by moving up the needle electrode, the fibre was no longer attracted when the distance tip-plane exceeds the 0.6-0.8mm.

This behaviour can be explained with reference to the fact that, as already confirmed in DC in chapter7, some charge transfer always happens from the tip to the rod. Therefore, when the frequency was low enough to allow an up and down motion in one voltage

period, an oscillatory motion was able to occur. The value of maximum distance, 0.6-0.8mm, is in agreement with the results presented in chapter 7.

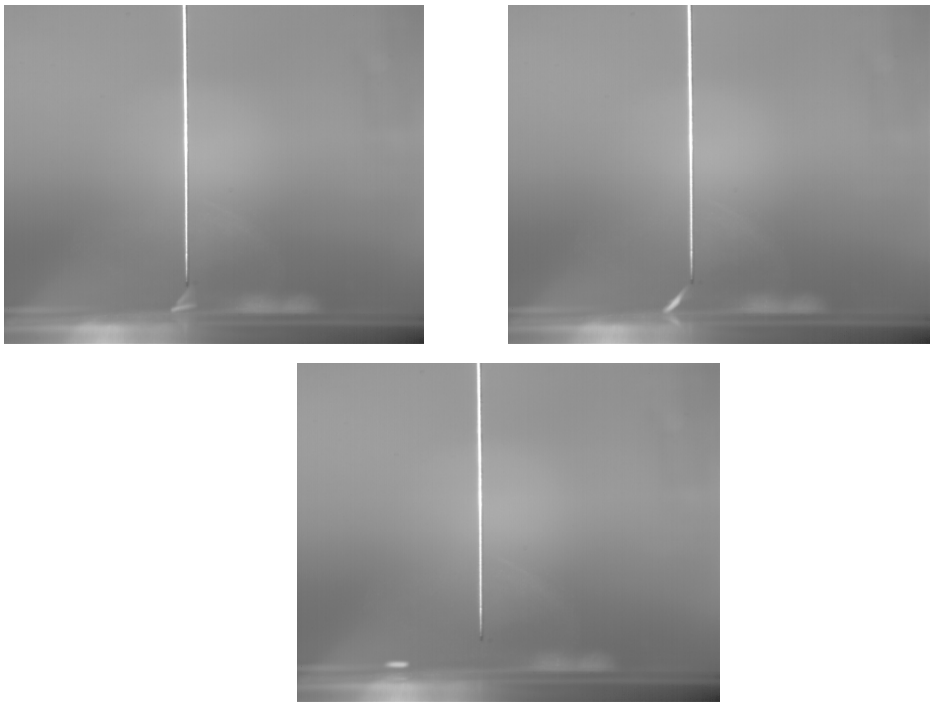

Figure 8. 10: Different steps of an impossible pickup of a PZT fibre (140µm of diameter) exposed to a signal at 3kV-50Hz.

When the frequency was equal to 500Hz it was possible to capture the fibre. The fibre remained in proximity to the needle tip, even after it was moved up to 6mm away from the bottom electrode. Nevertheless the rod was not perfectly in contact, but oscillated within a distance of 25-50µm from the tip. After the voltage was switched off, the captured fibre remained in contact with the needle.

In every experiment, a fluid decomposition inducing a formation of tiny bubbles was observed.

8.3.2. THE PICK UP AS A FUNCTION OF THE VOLTAGE MAGNITUDE

In this section the importance of the effect of the voltage magnitude on the electrostatic capture of fibres is explained.

Table 8. 4: Summary of a series of experiment showing the dependence of the capturing behaviour of a PZT fibre from the voltage magnitude

Magnitude (kV)	Inception height (μm)	Capture (YES/NO) Behaviour	After switch off behaviour
1	20	YES The fibre stays in contact with the tip	The fibre drops
3	200	YES Fibre oscillation near the tip with a 25μm amplitude and generation of bubbles	The fibre drops
5	250	YES Fibre oscillation near the tip with a 50-96μm amplitude and big generation of bubbles	The fibre remains attached to the needle
7	350	NO Fibre oscillation near the tip with generation of bubbles until when h=833μm and the fibre is repelled far away	The fibre remains attached to the needle

All the tests have been conducted by applying a signal at a fixed frequency of 1kHz and with a magnitude varying from 1 up to 7kV. Considering the results in section8.3.1, 1kHz is the optimal frequency at which to carry out the capture of the fibre.
All the observations have been summarised in the table 8.4.

In contrast to what was observed in section8.3.1, from the data in table 8.4 the inception length depends directly on the magnitude of the voltage. Therefore we can see that also the electrostatic lift force increases with the voltage magnitude. Such a dependence is not proportional, but the increase in the inception height with respect to the voltage magnitude occurs at a higher rate at low voltage than at higher voltages.

The optimum of the pick-up performance was at the minimum magnitude tested. At 1kV, the fibre was captured, and remained in contact with the needle.

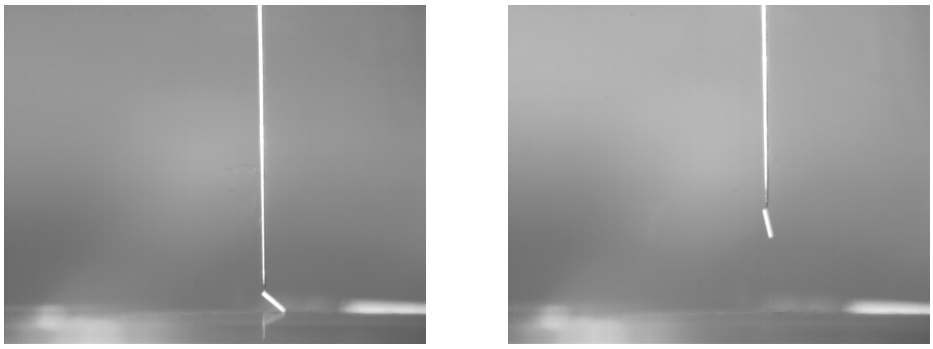

Figure 8. 11: Different steps of a capture of a PZT fibre (140μm diameter) operated at 1kV-1kHz (Capria and Wilson, 2006a)

When the voltage was increased to 3kV, some phenomena associated with fluid decomposition occurred. The fibre was still captured, but some instabilities were visible near the tip. These instabilities generated an oscillatory motion on the fibre with an amplitude of 25-30μm.

When the voltage increased, the fluid instabilities became stronger and the amplitude of the pseudo-oscillation increased.

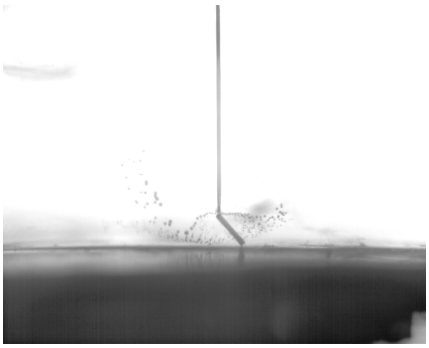

Figure 8. 12: Bubbles generation during a capture of a PZT fibre (140μm of diameter) operated at 3kV-1kHz

Figure 8. 13: Bubbles generation and EHD motion during a capture of a PZT fibre (140µm of diameter) operated at 5kV-1kHz

When the voltage reached 7kV, the instabilities became so strong that no pick-up was possible. The fibre motion became too important, and above a certain distance tip-plane, no capture of the fibre was possible.

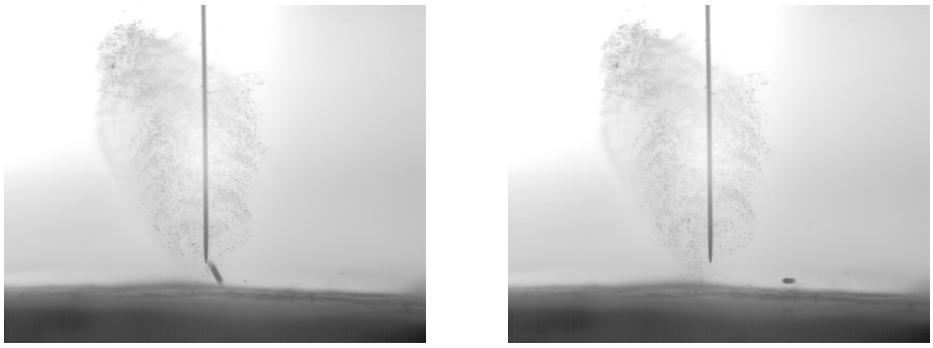

Figure 8. 14: Impossible capture of a PZT fibre (140µm of diameter) operated at 7kV-1kHz

Observing the motion of the bubbles issued from the fluid degradation, it is reasonable to assume that, when the voltage overcame the 5kV, also EHD instability was generated. This is supported by the observation that for a voltage below 5kV, the bubbles generated were released randomly from the tip area into the fluid and without a great acceleration. Once released, the bubbles then moved slowly upwards, owe to their buoyancy. Differently from voltages above 5kV, the bubbles moved faster from the needle-tip gap, in the upward direction. As visible in figure 8.14 the flow evolved tangentially to the needle lateral face of the needle.

After the voltage was switched off, for a voltage up to 3kV the fibre dropped down. For a higher voltage, the fibre had the tendency to remain attached to the needle tip. This

was probably due to the fact that the fluid decomposition generated a waxy deposit responsible for the adhesion. It is reasonable to suppose that such a waxy deposit would be stronger at a bigger voltage. This would explain why this post-switch-off adhesion occurred only for higher voltages.

8.3.3. THE PICK UP USING AN INSULATOR COATED NEEDLE

To understand in more depth the charge transfer phenomena through the needle tip, two experiments were carried out using an insulator coated needle (see chapter4 for constitutive details). The experiments were carried out by applying a voltage at a frequency of 1kHz and with a magnitude of 3 and 7kV.
In both cases, a pick-up of the fibre was possible, without any fluid decomposition phenomena, and in both cases the fibre was released after the field was switched off.

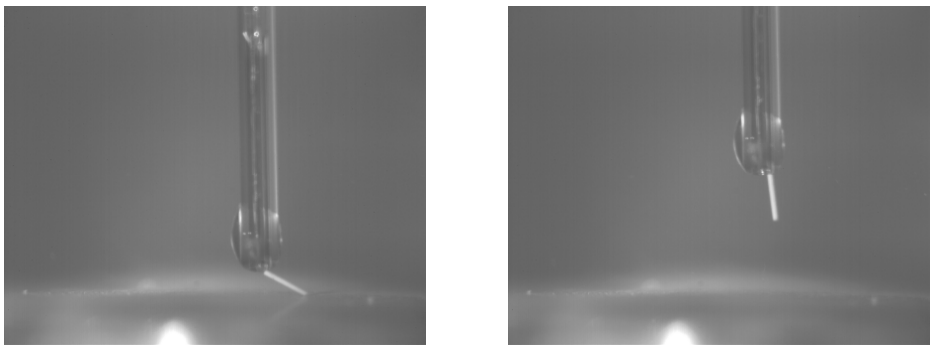

Figure 8. 15: Capture of a PZT fibre (140μm of diameter) operated at 3kV-1kHz using an insulating coated needle-like upper electrode.

8.3.4. THE PICK UP VARYING THE SURROUNDING FLUID AND THE FIBRE MATERIAL

In this section we report some observations we implemented to test the micromanipulation dynamics using a conducting fluid or a conducting fibre. The voltage applied on the needle was always at 1kHz and 1kV which appeared to be the best configuration to accomplish a micromanipulation.

An initial experiment tried to capture a PZT fibre when immersed in isopropyl alcohol (IPA). With the permittivity of such a fluid being more than ten times bigger than that of the silicone oil, this case was considered particularly interesting to maximise the dielectrophoretic force. Unfortunately, right after the voltage switch off, when the distance tip-plane was still 6mm, a fluid instability generated a convective motion that repelled the fibre far from the needle axis and no pick-up was possible.

In another experiment we tried to capture a conducting carbon fibre with a diameter of 130μm, immersed in silicone oil. The inception height was 150μm (bigger than in the PZT case) and a capture of the fibre was possible.
In contrast with the PZT case bubble generation was observed. The bubbles were not accelerated after their generation and their average size was bigger than that generated above the 3kV in the PZT case.
The fibre did not detach from the tip after the field was switched off.

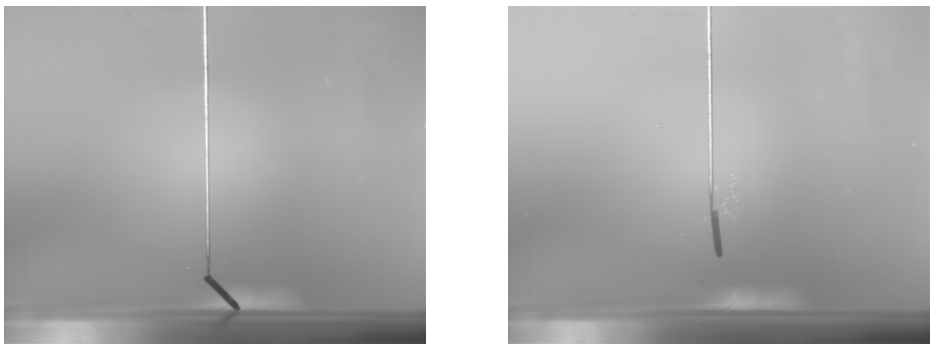

Figure 8. 16: Capture of a carbon fibre operated at 1kV-1kHz

This second experiment is particularly important because it shows the possibility of micro-manipulating also conducting fibres. However, the fact that for a voltage of 1kV, bubble generation was observed only in the case of conducting fibres, and with a bigger averaged bubbles size and moreover the fact that the fibre was unable to detach after the voltage was switched off, it is a suggestion that in the conducting case the electric field in the needle-fibre gap is bigger than in the PZT case. Consequently, a micro-breakdown in the gap could be induced with generation of a waxy deposit, bonding the fibre to the needle tip even at lower voltage.

8.4. DISCUSSION OF THE RESULTS

In this chapter the equilibrium of a PZT rod 140μm in diameter and 1.2mm long was analysed. The rod was immersed in a dielectric oil and exposed to a divergent electric field generated between an upper needle-like electrode (6.5μm tip radius) and a bottom flat electrode. The magnitude of the applied voltage was between 1 and 7kV and the frequency varied from DC up to 1kHz of frequency was. Considering the difficulty of analytically solving the boundary problem, a series of FEM simulations was carried out with the objective of estimating the electrostatic force.

In the ideal case of a neutral (with no net charges on it) insulating rod, the electrostatic force can be directed upward or downward, depending to the field geometry. In this particular case, the FEM predicted and the experiments confirmed that when the particle was in rest on a metallic electrode the electrostatic force was directed downward. To have a particle lift-off, it was necessary to coat the bottom electrode with a 0.5mm thick PTFE coating. Therefore, a series of experiments was carried out in this configuration.

Studying the dependence of the phenomenon on the frequency of the applied voltage, we observed that no rod capture was possible for frequencies below or equal to 100Hz. The charge transferred from the needle to the fibre, generated an oscillatory motion compromising any pick-up phenomena. Nevertheless, when the frequency overcame the 500Hz the rod capture was efficient.
Considering the voltage magnitude, the best result in terms of fibre micro-manipulation was achieved with the lowest voltage tried: 1kV. In this case, the fibre was in contact with the needle and no side effects were noticed. For voltages between 3 and 5kV, the capture was still possible, but decomposition of the liquid near the needle tip was visible. This phenomenon generated some bubbles. At the same time, a pseudo-oscillatory motion of the rod in proximity to the tip was observed. The amplitude of such oscillations was between 30 and 50μm, increasing with the voltage magnitude. At 7kV it was important to achieve any stable contacts between fibre and needle, due to the instability induced by the fluid decomposition.

When analysing these results it is important to specify that, in the case of 1kV, we cannot exclude any oscillation of the fibre. We can only say that, considering the resolution of the optical system, the particle, during the experiment, never travelled at a distance longer than 5-15μm from the electrode.

After the voltage was switched off, in the case in which a fibre was captured, the fibre dropped down or remained attached to the needle in the cases of lower or higher voltage respectively. This behaviour was related to the generation of a waxy deposit in the gap. The waxy deposit can be more precisely described as an electro-polymerised residual of the fluid degradation. This would also explain why, such an adhesion to the needle was observed when a strong voltage was applied. Further details about this phenomenon are detailed in chapter 9.

A possible interpretation for the resulted listed above can be the following one.
Given the results of the FEM simulation in section 8.2, at a voltage range between 1 and 10kV, the electric field in the gap separating the fibre and the needle, varies between 100 and 1000 MV/m. These values always overcome the breakdown voltage. Therefore a failure of the dielectric, is suitable in the gap and a conduction path in the gap can be established. The fibre can then acquire a net charge, with consequent reduction of the field; the field in the gap would be reduced. Such a charge transfer could be caused by injection, electric field enhanced dissociation or micro-breakdown.

If this description of the phenomenon is correct the particle should oscillate, with a frequency depending on the applied voltage (frequency and magnitude), on the fluid viscosity, on the particle and fluid density, and on the charge acquired by the particle. This would be due to the fact that the particle, would get a homo-charge from the needle, and would be forcefully repelled. But, inverting the field sign (as in the AC case), the particle would be newly attracted, and maybe a new injection of homo-charge could occur. Perpetuating this phenomenon for several cycles, an oscillatory motion could be produced.
Considering the process described above, even if the particle were captured, such a capture would be not only “dielectrophoretic”, but there would be also an

"electrophoretic" contribution. This kind of mechanism has been already proposed by Chen et al. (1991) (see chapter3.4.2) to explain the interactions responsible for the electrorheological effect involving purely conducting powders.

An overview of the experimental results, reveals a mechanism like the one proposed above really occurs for any case in which a fluid degradation existed, i.e. for a voltage of 3kV or higher. The forming of bubbles was a confirmation that a micro-breakdown existed in the gap and that it was a consequence of a too intense electric field. The particle then became a vector of charge, and the expected oscillating motion of the fibre was partially observed.

More of uncertainty is addressed to the case at 1kHz and 1kV, where no fluid degradation is observed. In this case it would be tempting to say that no dielectric failure exists in the gap, and that the fibre capture was only due to polarisation forces. However, in the context of the FEM simulations this hypothesis is not coherent because of the high value of the electric field.

The most reasonable conclusion would appear to be that, if no micro-breakdown exists it is only because the charge transfer to the fibre happens as a result of other mechanisms, reducing the electrical stress in the gap before the breakdown could happen. In other words, for lower voltages (1kV), the phenomenon is not different from what happens at higher voltages. The only difference is that the homo-charge on the fibre is acquired before the dielectric fluid failure. Consequently, it can be interesting to estimate the value of charge that the particle should acquire to relax any oscillatory motion at 1kV and to compare it with the data already acquired in chapter7.

A calculation of the oscillation amplitude is reported in figure 8.17. In this chart we explain the amplitude of the oscillations of the particle in respect to the frequency for different values of both linear density of charge and electric field.

After the charge transfer occurs, 2 MV/m is a reasonable value for the field in the gap. This is the electric field when the conductivity of the fluid is controlled by the field enhanced dissociation (see figure 5.5). In this condition, a fibre can be considered relaxed (i.e. its oscillation amplitude is smaller than 15μm) at 1kHz, if it has a charge of 7nC. This value fits perfectly with the value of charge transferred from a needle to a

PZT particle estimated in chapter 7. In this case, when applying a DC voltage of 10kV, after contact with the needle, the fibre acquires a charge of ~100nC. This means that for a value of the voltage equal to the RMS of 1kV, the charge transferred on the particle must be 7.071nC. This value fits well with the value of 7nC extrapolated from figure 8.17.

However, it is worth to consider that the dynamic of charge transfer between the needle and the fibre is a complicated task. An accurate definition would need a deeper knowledge of the charge transfer kinetics, and of the properties of the dielectric fluid and the fibre, that are exposed, in the needle-fibre gap, to a very intense electric stress. Therefore, although the conclusions stated above are without any doubt very interesting, other experimental validations are probably needed before claiming such a good fit between the experimental results and the models.

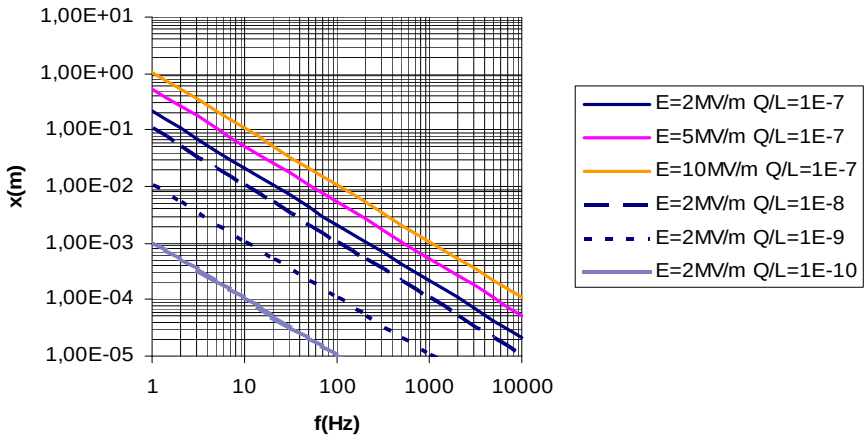

Figure 8. 17: Amplitude of the oscillation of a fibre captured in proximity of a needle upper electrode.

The last important conclusion of this chapter is that a capture of a fibre using a needle-plane system, was possible also with conducting fibres (carbon fibre). Nevertheless, this kind of material may enhance the fluid dissociation in the gap because, due to its high conductivity, it generates a bigger field in the gap.

Chapter 9

ELECTRIC FIELD STRUCTURING OF A GROUP OF MICRO-RODS

This chapter it is the longest, the most complex and the most important of the chapters of the experimental results. This chapter considers the behaviour of a group of fibres when exposed to a divergent electric field. The dependence of the phenomenon on the characteristics of the electric field, and on the dielectric liquid, and the particle characteristics have been considered. Moreover an evaluation of the influence of the drag speed on the structuring process has been made. Once more, the discussion of the most important result has been proposed at the end of the chapter.

9.1. DIFFERENT APPROACHES TO THE ANALYSIS OF THE PROBLEMATIC OF A GROUP OF FIBRES

There are at least two approaches to analysis of the behaviour of a group of fibres exposed to an electric field:

a) to consider the group of fibres as a whole, continuous fluid characterised by constitutive equations on which the mechanics of the continuous media can be applied
b) to consider each fibre as a single rigid body, on which the equilibrium of the force and the momentum can be applied

The first approach is particularly interesting if the dimension of the solid filler is small compared to the dimension of the system, and if the system can be considered “as a whole”. In this approach, our system of particles can be considered as a dispersion.
When no electric field is applied to the system, the dispersion behaves like a Newtonian fluid (see section 3.4.1). When an electric field is applied, the dispersion reacts to a shear applied normally to the field as a Bingham fluid (see section 3.4.1). In this second case, it is more difficult to understand what happens when the shear is parallel to the electric field.
In any case, a physical description of the system can be obtained by solving the boundary problem using the equations of the continuous mechanics presented in chapter2, describing the equilibrium of an elementary volume of the fluid.

This approach is used in the model of electrorheological fluid and has been utilised by Trau et al. (1995) in their "electric-field-induced pattern formation in colloidal dispersions".

The second approach becomes reliable when the dimensions of the filler are too big and when the hypothesis of continuity fails (see section 2.1.1).
In this configuration, to achieve a quantitative and precise description of the system, the problem should be solved considering the equilibrium of any single particle immerged in the fluid as a rigid body. That approach is obviously resource efficient when a relatively low number of bodies are involved.
When the system is constituted of a relatively high number of bodies, a qualitative approach, aiming at a more general description of the behaviour of the group, would be interesting. This could be achieved in at least two ways:

1) To write a code able to generate a random distribution of bodies in the system and to solve the total boundary problem.
2) To understand the mechanics of the group of particles analysing the behaviour of a single body in particular boundary conditions, taking into account the effect of the neighbouring particles.

Method 1) has been adopted for example by Klingenberg et al. (1989), then by other researchers (e.g. Kadaksham et al., 2004; 2006), for a time-solved simulation of an electrorheological fluid to understand the kinetics of the formation of the pearl-chain structures.
The solvers involved in these multi-body simulation approaches are not based on normal finite element computations. Normally these solvers first need to introduce the expression of the force in respect to some simple macroscopic characteristics of the system (distance between the particles, applied electric field, conductivity and permittivity of the fluid and the particles, etc.). Considering the asymmetries which characterise our system (cylindrical particles generate 3 supplementary degrees of freedom respect to the spherical particles), and the limit conditions dictated by the use of a highly divergent electric field (involving phenomena of electric field enhanced

conductivity and injection), the numerical approach becomes too complicated and not relevant to the objectives of the present study, which is more oriented towards the experimental approach.

All attempts to understand the phenomenon using the numerical model have been carried out using method 2). Some FEM simulations have been completed to understand how a single particle or a group of particles in given arrangements behave. Reasoning on the basis of the results, an attempt was made to understand the behaviour of the whole system.

9.2. HEURISTICAL DESCRIPTION OF THE PHENOMENON

The dynamic behaviour of a group of fibres exposed to a non-uniform electric field, generated by two electrodes which are relatively large in comparison with the fibre dimensions will now be explained.

The batch of fibres can be treated as a continuous fluid, behaving like an electrorheological fluid. In this case, if a non-uniform field is applied, the field generates a force on an elementary volume. Having chosen the elementary domains following the field lines, this force can be divided into two components:

a) A cohesion force connecting two consecutive elements (related to the interparticle force), applied parallel to the field lines

b) A dielectrophoretic body force due to the field non-uniformity

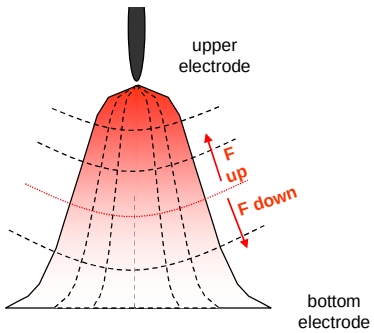

Figure 9. 1: Schematic representation of an electrostatic deformation of a continuous body exposed to a non-uniform electric field. An increase of the colour intensity means an increase of the cohesion force.

As showed by Misono et al. (2004) and confirmed by our experimental observations described later in the present chapter, all contributions to the cohesion acting perpendicular to the field lines are negligible comparing with the ones acting parallel..

In this configuration, when an electric field is applied, a behaviour like the one summarised in figure 9.2 is suitable. The upper electrode is close to the surface of the bunch of fibres and when the cohesion forces inside the dispersion are overcome by the body forces, the bunch can deform, and below a certain inception height the bunch of fibres can become in contact with the upper electrode.
As it moves up the upper electrode the fibre bunch deforms and a structuring, between the two electrodes is energetically favourable.

The force balance on each single isopotential surface can be written as the balance between:

- F_{up}: cohesion force between the element lying on the isopotential surface
- F_{down}: the sum of the weight of the elements below the surface and the adhesion contributes related to electrostatic adhesion with the bottom electrode

If there is a closed path between the upper and the bottom electrode in which each elementary volume respects the condition:

$$F_{up}>F_{down}$$

the group of fibres starts to extend, moving upward, creating a columnar finger type structure. When increasing the height of the upper electrode, the field decreases, and the average diameter column also decreases until there is a section of the column in which:

$$F_{up}<F_{down}$$

If this happens in a section in the middle of the column, some of the fibres drop down, and some remain attached to the upper electrode. Otherwise, if this happens near the upper electrode surface (the point supporting the biggest stress), no capture of the fibre would be possible.

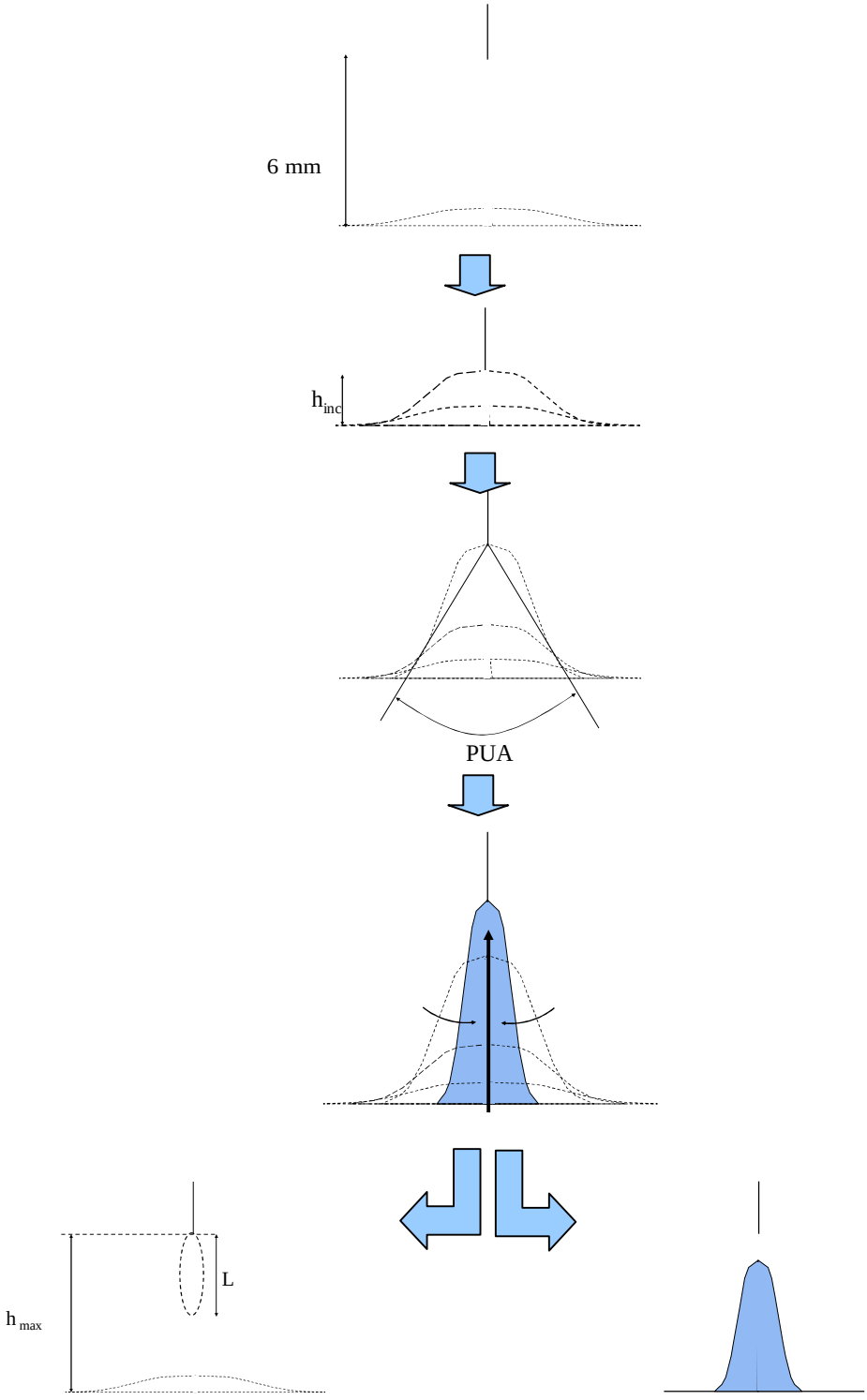

Figure 9. 2: Heuristic description of the structuring of a continuous fluid exposed to a non-uniform electric field.

Obviously, after the column breakdown, if some fibres are still in contact with the upper electrode, there are more possibilities to carry this matter to a higher level. After the chain breakdown, the total weight acting on the upper electrode surface decreases, and because the adhesion disappears too, there is no more connection with the bottom electrode.

Based on this reasoning, it is a logical conclusion that sharper the probe is, the higher the gradient in proximity to the upper electrode, and consequently the higher the probability that some fibres would be captured.

Even if the model presented above is very useful for making some general considerations, when the dimension of the needle decreases too much (as is the case in the present study) the hypothesis of continuity would not be respected. To understand the dynamic needle tip-fibre it would be necessary to treat the problem specifically. Moreover, when the tip of the needle becomes really sharp, a series of other phenomena related to the behaviour of the dielectric liquid exposed to high fields arises, as already presented in the preceding chapters.

Moving from the hypothesis of continuity to the particular behaviour of a fibre as a rigid body, it is important to remark that when a group of fibres lies on a grounded electrode, and is exposed to a non-uniform electric field generated by a probe-plane system of electrodes, each single fibre in the batch is still exposed to all the interactions presented in section 8.1 in the case of an isolated particle. Moreover, in the case of a bunch, two more effects have to be considered:

- an interparticle force, due to the mutual polarisation of the particles, is generated between the fibres in contact inside the bunch
- the neighbouring fibres create a modification of the electric field; this means that the electrostatic forces acting on a fibre inside a cluster are not the same as for an isolated one

Also in this case, due to the orientation torque, the particles orientate with their major axis parallel to the electric field lines. Nevertheless, this would be certain only for the

fibres far from the bottom electrode. For the ones close to it, the rotation could be compromised by the electrostatic adhesion.

9.3. FINITE ELEMENT ANALYSIS

A series of FEM simulations relative to some critical configurations has been carried out to try to understand in more depth the interactions between fibres in a batch.
Particular attention has been given to the following aspects:

- how the electrostatic adhesion on a particle in a bunch is influenced by the surrounding fibres
- the interparticle force in different configurations
- the electric field between the fibres constituting the bunch

It is important to focus the attention on the fact that no FEM results exist in the literature concerning purely 3D problems inherent to cylindrical dielectric particles.

9.3.1. MUTUAL ATTRACTION BETWEEN HORIZONTALLY POSITIONED RODS IN DIFFERENT CONFIGURATIONS

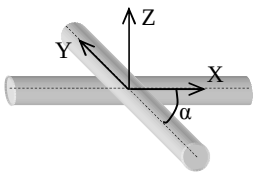

Figure 9. 3: Geometrical configuration considered in the FEM simulations to calculate the mutual attraction between horizontally positioned rods in different configurations

Consider a group of cylindrical rods randomly arranged on a surface. A certain number of fibres is distributed horizontally on the substrate, with different angles in the xy plane. Superposed onto that layer of fibres, another layer of fibres is in contact with the one leaning on the plane, at least at one point. The upper ones are in contact with the ones below, while the angle between their axes can vary.

Once the field is applied, an interparticle force is developed between neighbouring fibres, directly related to the structuring dynamics. It would then be interesting to see how the particles' interaction would depend on the angle between the fibres.

With this objective, a series of simulations was carried out to calculate the interparticle force between two PZT rods, 140µm diameter, disposed parallel to the plane xy, with an angle their major axis varying from 0 to 90°, separated by a gap of 1µm, and exposed to an electric field of 1.666MV/m (see figure 9.3). Two cases have been considered:

- the two fibres are assumed to be far from any space discontinuity
- one of the two fibres is supported by a grounded flat electrode

The magnitude of the adhesion force exerted on the upper fibre is reported in the chart in figure 9.4.

As we can see, the force is at its maximum when the two rods are parallel aligned. When increasing the angle from 15° to 90°, the force decreases, but not drastically. This result was expected. Moreover, the adhesion force more than doubles when the bottom fibre lies on a grounded electrode. Again, this result is logical when considering the action of the adhesion forces.

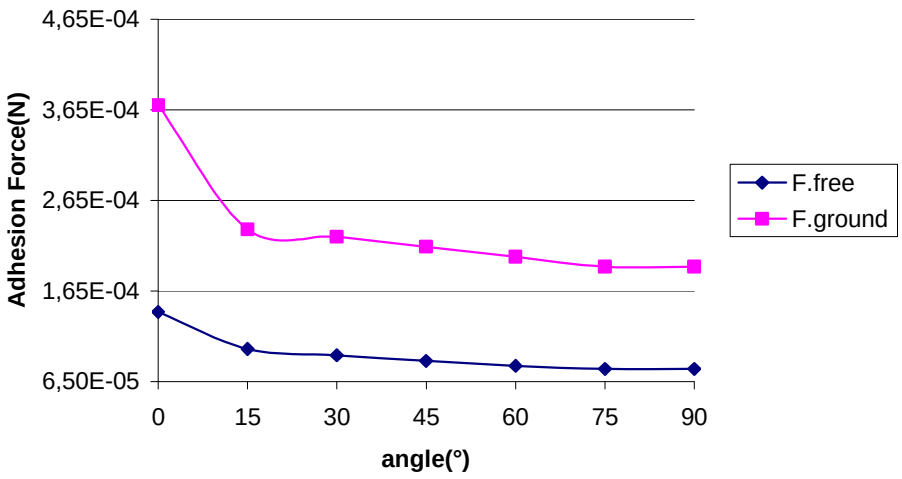

Figure 9. 4: Adhesion force between two PZT fibres (140µm of diameter) disposed as in figure 9.3 calculated by FEM (E=1.666V/m)

Another set of simulations has been done in the same conditions as described above, but increasing the number of supporting fibres to 2 and then to 3.

As expected, when increasing the number of supporting rods from 1 to 2, the force almost doubled. When adding another bottom particle, in the case of a supporting grounded plane, the force still increased, but at a lower rate. On the contrary, in the case of isolate fibres, the force started to decrease. This last behaviour is quite difficult to understand.

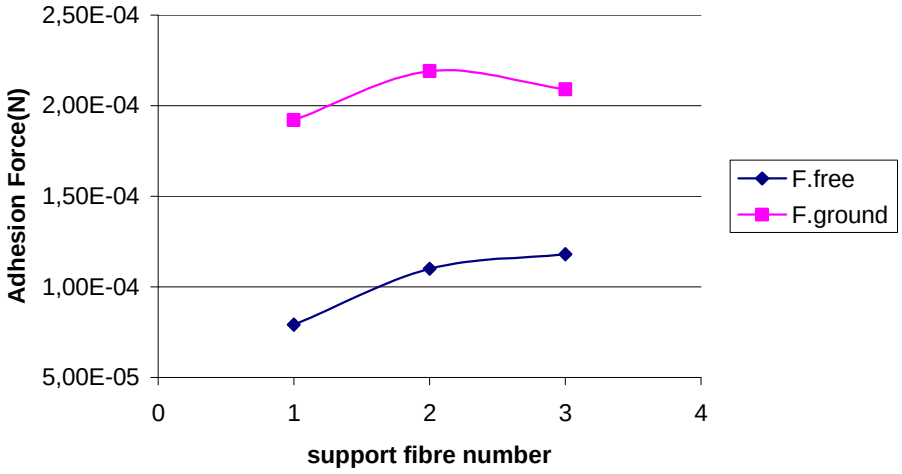

Figure 9. 5: FEM computation of the adhesion force acting on a PZT fibre (140µm of diameter) when it is lying on a certain amount of other fibres all equally spaced (E=1.666V/m)

A general conclusion seems to be that when two fibres are superposed and disposed parallel to the xy plane, with a certain angle with respect to their major axis, the maximum of adhesion force is reached when the fibres are in contact and their major axes are aligned parallel. Therefore the upper limit for the interparticle force is reached when an entire group of fibres is positioned perfectly horizontal and parallel to the bottom electrode. In any case, in a group of fibres distributed in a stochastic way, the interparticle force would always be smaller.

9.3.2. MUTUAL ATTRACTION BETWEEN VERTICALLY POSITIONED RODS IN DIFFERENT CONFIGURATIONS

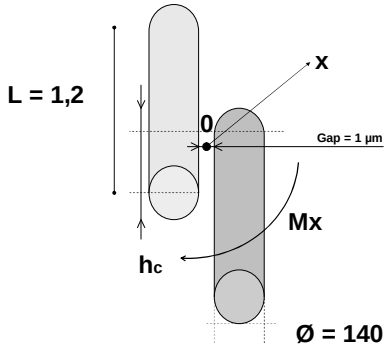

Figure 9. 6: Geometrical configuration employed in the FEM simulations to calculate the mutual attraction between vertically positioned rods in different configurations

When the upper electrode is moved up, the fibres form a columnar structure. In this structure, the particles are commonly arranged with a major axis parallel to the field lines, and they are in contact on the lateral side, and superposed for a certain distance h_c (see figure 9.6).

In this section the results of a simulation carried out to understand how the electric field in the gap and the interparticle force depend on h_c, and also the field distribution in the gap, are presented. All the simulations have been carried out with Maxwell 3D, using fibres with 140µm in diameter, 1.2mm long, separated by a gap of 1µm and exposed to a field of 1.666MV/m. The fibres have been considered as to be far apart and isolated from any space discontinuity.

The values of the field in the gap are shown in the chart in figure 9.7. With E_{gap} indicating the averaged value, while $(E_{gap})_{max}$, indicates the maximum value, close to the fibre edge (see figure 9.7).

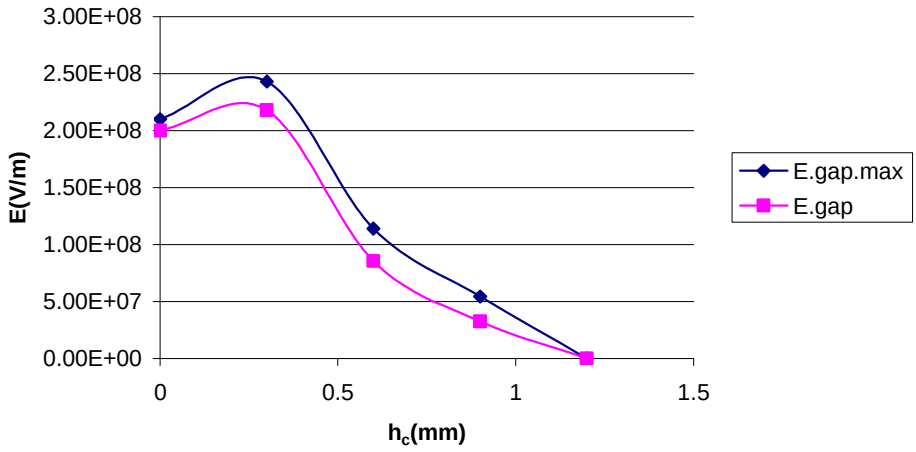

Figure 9. 7: Adhesion force between two PZT fibres (140μm of diameter) disposed as in figure 9.6 calculated by FEM (E=1.666V/m)

As illustrated by the results in figure 9.7, the electric field is 61.4 kV/m when the fibres are perfectly aligned (h_c=1.2mm). Then, the field has the tendency to increase when h_c decreases. The average and the maximum field follow the same trend, and both are always bigger than 54.3 MV/m. For this value of the electric field, it is possible that a charge transfer occurs in the gap, reducing the dielectrophoretic force.

In figure 9.8 we report some of the results to show the electric field distribution in the gap.

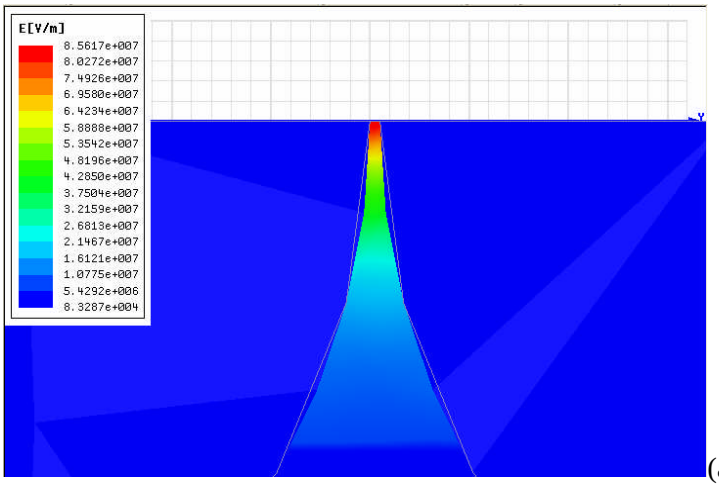

(a)

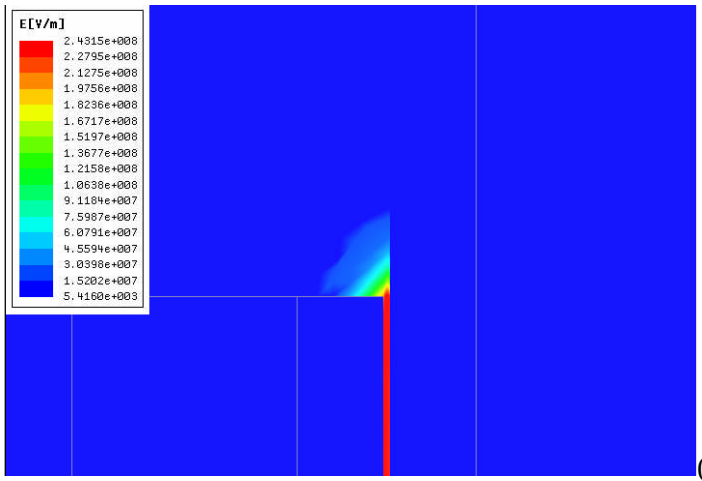

(b)

Figure 9. 8: Electric field distribution in the gap between two PZT fibres (140μm of diameter) positioned as in figure 9.6 (h_c=3mm; E=1.666V/m).

Figure 9.9 shows another picture of the electric field distribution when the particles are in contact end-to-end.

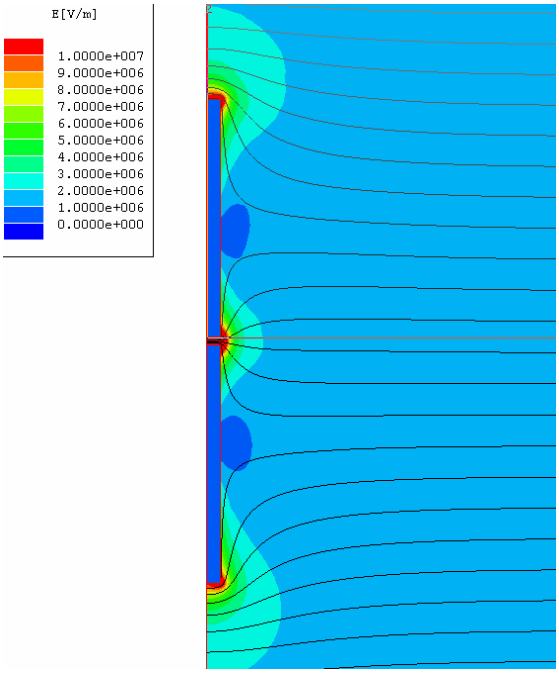

Figure 9. 9: Electric field distribution in the gap between two PZT fibres (140μm of diameter) perfectly aligned (E=1.666V/m).

After some consideration of the electric field, how the force relates to h_c can be considered. The computation of F_y and F_z, and moreover the values of the force magnitude and of the angle between the force and the vertical axis were reported.

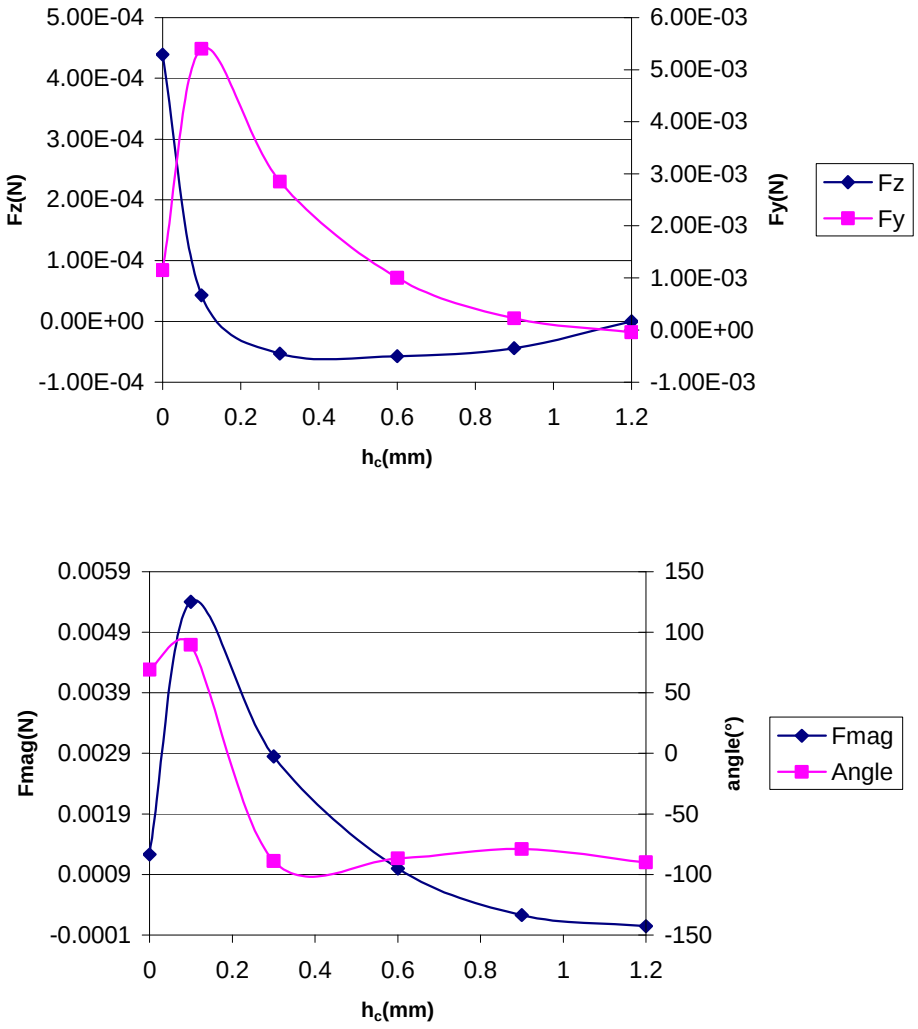

Figure 9. 10: Adhesion force between two PZT fibres (140µm of diameter) disposed as in fig. 9.6 calculated by FEM (E=1.666V/m)

It is clear from the analysis of the results that F_y is always acting to push the two particles against each other. Such a force normally decreases when h increases. Also F_z has a maximum for h_c =0 and then decreases. Unfortunately its direction becomes downward when $h_c \approx 0.2$mm.

To conclude, the force would be an adhesion force preventing the particle from falling down only if h would be, in this case, 1/6 of the particle length. Moreover, for h below that value the force is still increasing.

The value with h_c=0, is not very meaningful, because in this situation a configuration like the one proposed in figure 9.9 is more suited.

In this case, the force is always directed upward, and depends on the interparticle distance. The force has been computed with a 2D solver, considered more reliable for this particular case (see tab. 9.1):

Table 9. 1: Adhesion force between two PZT fibres (140μm of diameter) disposed as in figure 9.9 calculated by FEM (E=1.666V/m)

Interparticle distance(μm)	F(mN)	E_{gap} (MV/m)
1	5.36	197
40	0.232	35.5

The differences between the values evaluated with a 2D and a 3D simulation are close within the 10% of the 2D value.
The force and the field, are in this case very sensitive to the interparticle distance. Also in this case the value of E_{gap}, is high enough to suppose a failure of the dielectric liquid.
It is remarkable as the force calculated with a distance of 1μm it is very close to the value of F_{mag} for h_c=0.1mm.

A simulation especially designed to test the dependence between force and fibre dimension has been run. It confirmed that the force has a quadratic dependence on the fibre dimensions. Considering that the fibre weight depends on the cube of the dimension, in proportion, the bigger the particle, the weaker the mismatch between weight and electrostatic force.

9.3.3. GLOBAL CONSIDERATIONS ABOUT THE MUTUAL ATTRACTION BETWEEN RODS IN A CLUSTER

To understand how the fibre arrangement influences the interaction in a cluster, a series of simple 2D simulations was carried out, solving the boundary problem for different

arrangement of horizontal and parallel 140μm diameter PZT fibres. The interparticle distance was 1μm and the fibre and the applied field was 1.666MV/m.

Considering that the parallel position is the one that maximises the interparticle forces (see section 9.3.1), it could be assumed that the results presented in this scenario represent the upper limit of the inter-particle adhesion force.

The particles were arranged in vertical chains with a number of particles from 2 to 4, or in more compact arrangement, following a squared or hexagonal symmetry (see figure 9.11). The force was computed on the most central fibre in contact with the bottom electrode (noted with 12) and on the one opposite it (noted with 34).

To calculate the force, each particle has been sectioned in two half parts 1 and 2 (or 3 and 4), where the smaller number refers to the lower section. The force 12 (or 34) has been calculated as the sum of the force acting on the two half sections.

All these values have been compared with the value for a single fibre resting on a grounded plane.

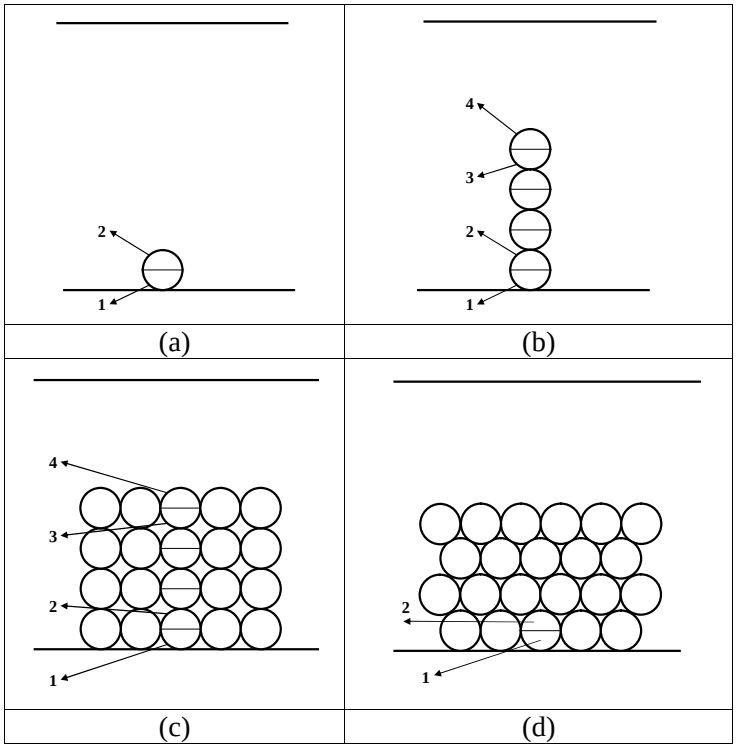

Figure 9. 11: Geometrical configuration employed in the FEM simulations to calculate the mutual attraction between horizontally positioned rods parallels to the plane electrode

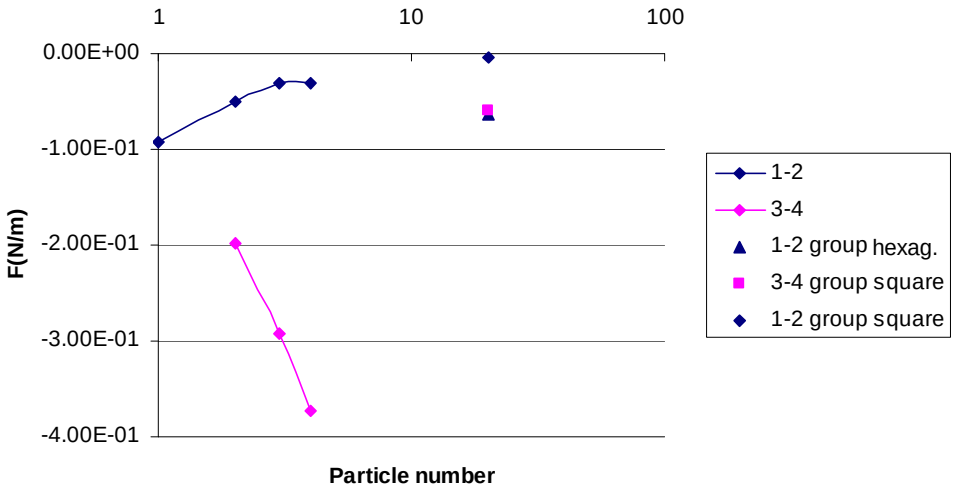

Figure 9. 12: Adhesion force on a PZT fibres (140μm of diameter) disposed as in figure 9.11 calculated by FEM (E=1.666V/m)

The chart in figure 9.12 shows that on a chain of particles, the module of the electrostatic adhesion exerted on the rod in contact with the bottom electrode (12) decreases to less than the half of the single particle value, increasing the number of particles up to 4. The situation is even more interesting in the case of a group of fibres. When the particles are arranged in squared symmetry, the electrostatic adhesion on the bottom electrode (12) decreases to a value of 4.40mN/m, which is two orders of dimension smaller than the single fibre value, and it is still negative. If the arrangement is hexagonal the adhesion force (12) can reach value -63.7 mN/m.

After these results it can be concluded that the adhesion on a fibre in contact with a grounded electrode is reduced when surrounded by other similar particles. This is a reasonable assumption, because the surrounding particles would partially screen the particle from the electric field, and they would attract the particle resting on the support competing with the image charges, to establish the final value of the electrostatic adhesion. Therefore the adhesion results notably reduced, even if the force would be still negative.

The adhesion force acting on the particles positioned far from the bottom electrode (34) has the tendency to increase, considerably increasing the number of particles. Moreover, this type of force (34) is always bigger than the electrostatic adhesion (12), in the case

of both, the chain and the group of fibres arrangement. Moreover, the adhesion on an external particle (34) in a chain increases, increasing the number of particles.

9.3.4. GLOBAL CONSIDERATION ABOUT THE FIELD IN A GROUP OF FIBRES

The image in figure 9.13 shows a qualitative picture of the electric field in a chain like structure of fibres as normally formed in reality.

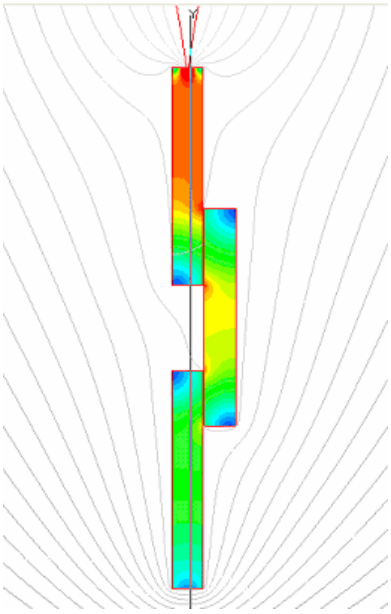

Figure 9. 13: Qualitative representation of the field distribution inside a chain of PZT fibres immersed in silicone oil

It is noticeable that the major field gradient is reached close to the needle tip. Displacing downward from the needle-tip there is a rapid decrease of the field, and the gradient decreases. The field flows through the continuous path formed by the fibres, from one fibre to another through the line of contact. The field is concentrated near the fibre edges, and the fibres are almost iso-potential. The maximum portion of voltage then drops preferentially in the surrounding media. This overview confirms and summarises the observations already made.

The situation could be summarised by saying that the highest gradient is concentrated near the needle tip, and it is almost all experienced by the first one or two fibres. All the fibres below experienced a quasi-constant field, despite the decrease of the field (and consequently of the interparticle force) for the fibres far from the tip.

Another specific particularly interesting configuration to consider is the one where all particles are perfectly aligned.

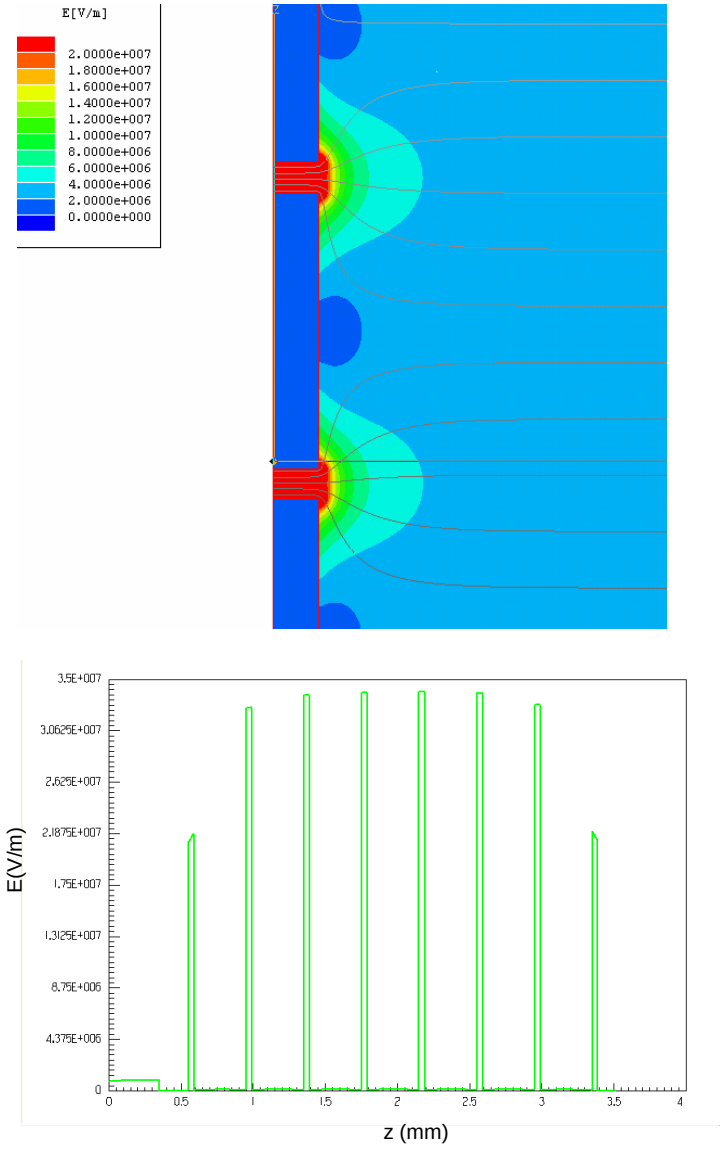

Figure 9. 14: Electric field in the gap between two PZT (140mm of diameter) fibres perfectly aligned (E=1.666V/m)

When the electric field is applied between two parallel plate capacitors and when a chain of perfectly aligned particles is bridging the gap, the field distribution in figure 9.14 is achieved. The model is made using PZT rods with a diameter of 140μm, 1.2mm long, exposed to a field of 1.666MV/m. The voltage drops almost entirely in the gap separating the particles. The field in the gap varies between 20 and 35 MV/m and is bigger between the particles in the middle of the chains than close to the electrodes. The same kind of behaviour has been confirmed by different research groups (see section 3.4.2).

Executing the same kind of simulations, with the same sort of particles, in a needle-plane system and applying on the needle a field of 10kV, a surprising result can be observed. The voltage drops entirely in the gap separating the needle from the first fibre. All the other fibres in the chain remain isopotential, no field exists between them and, consequently, no interparticle force.

However, it must be remembered that the model presented above is purely theoretical and that it would not be able to exist in nature. The reason is that the electric stress in the gap is too high and there would surely be a passage of current between needle and fibre.

In figure 9.16, another simulation in the same conditions as described above is shown. The only difference being that: in this simulation the upper fibre was considered as isopotential with the needle. In this circumstance, the field distribution is close to the expected one. The voltage drops mainly into the gap between the fibres and decreases moving far from the needle tip.

Regarding the transfer of charge through the needle tip and the hypothesis of having an isopotential fibre near the tip, the matter has been widely discussed in chapter8 and will be addressed again in the conclusion of the present chapter. So far, the most important conclusion is that this hypothesis is the only one coherent with the FEM.

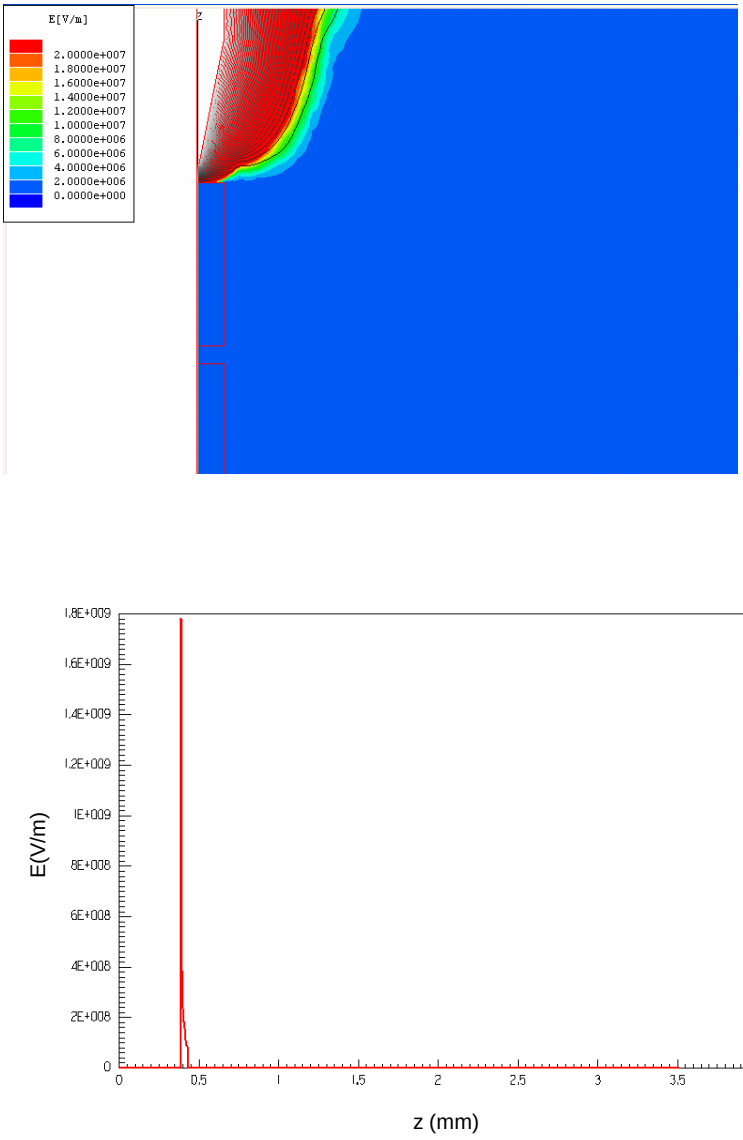

Figure 9. 15: Electric field in the gap between the PZT fibre (140mm of diameter) when the fibre is in proximity to a needle-like electrode (E=1.666V/m)

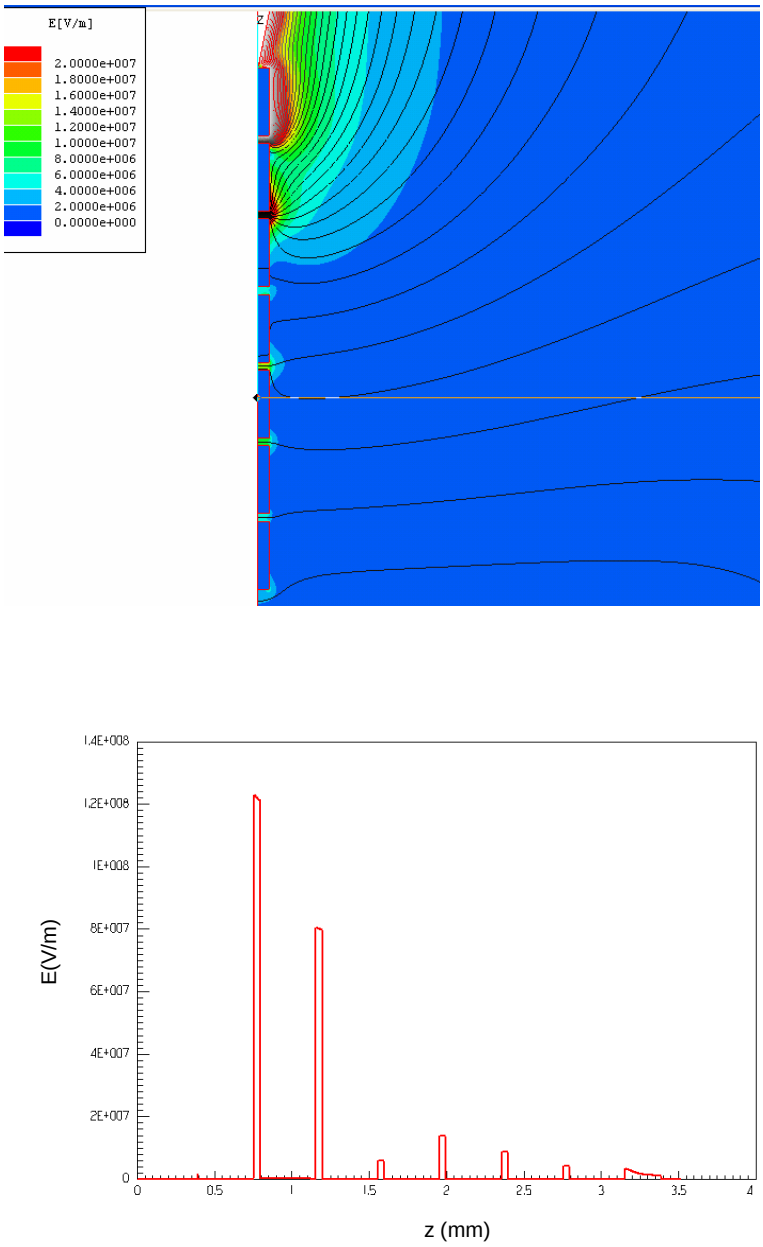

Figure 9. 16: This FEM simulation respects the same geometry that the one in figure 9.14, but in this case the fibres are exposed to a non-uniform electric field, generated between a needle electrode (diameter=120mm; tip radius=6.5mm) ad a flat electrode (V=10kV)

9.3.5. METHODOLOGY AND IDENTIFICATION OF THE PROCESS INDICATORS

In the next section the main experimental results are presented. These results aim to try and explain the structuring process, and in general the behaviour of a group of fibres, immersed in a dielectric fluid, when exposed to an electric field. Different electrode geometries have been tried, in different: electric field conditions, drag speed, and with different materials (fluid and fibres).

In line with the objectives of this work, two different protocol procedures were used; these were alternated following the demand: a non-contact protocol and a contact protocol.

In the contact protocol, the upper electrode was moved in contact, and then the field was switched on. At this point the electrode was moved at a drag speed of 2mm/s. In the not in contact procedures, the voltage was already applied when the tip was 6mm from the bottom electrode. Then the needle was brought near the bottom electrode at a speed of 0.2mm/s, until at least one fibre was in contact with the needle. At that point the motion was inverted and the upper electrode moved up at a speed of 2mm/s.

To describe the phenomenon, a series of macroscopic process indicators was identified and related to some microscopic characteristics. These indicators are listed below.

V. threshold

This is the minimum value of voltage at which there is a capture of at list a fibre. This is useful to understand the dependence of the needle-fibre interaction on the frequency.

Max length

The maximum length of the column able to be captured could be a good way to measure the force exerted by the needle on the bunch. Unfortunately it showed to be not repeatable.

Max h

Maximum height at which at least one fibre can be carried. This gives an idea about the force exerted by the needle on the group of fibres.

Inception height

It is the distance tip - group of fibres at which at least a fibre can reach the contact with the needle. This can still be related to the body force exerted by the needle on the system of particles.

Pick-up angle (PUA)

It is the most important indicator, as it directly relates to the interparticle force in the bunch, or to phrase it differently, it relates to the cohesion force inside the boundary.

It is used when the upper electrode is a needle. As can be shown in this case the deformed columnar structure of fibres assume a cone shape, with the vertex near the tip. The measure of the cone angle when the distance needle-plane equals to 3mm, is the PUA (see figure 9.17).

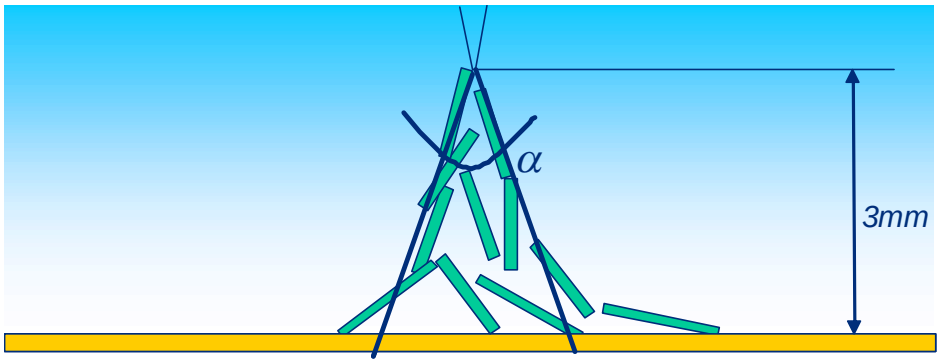

Figure 9. 17: Pick-up angle definition

The direct relation between PUA and interparticle force is clear for at least two reasons:

1. *Microscopic reason*

   If inside the columnar structure achieved during the structuring process the particles are arranged as considered in section 9.3.2 (see figure 9.18), then it

follows that a smaller interparticle force would mean a smaller h. Considering the sum of all these microscopic local contributions, a smaller h would translate into a smaller PUA.

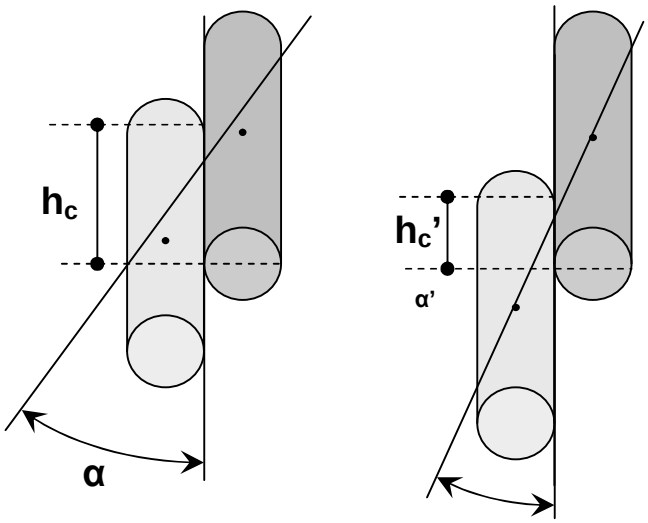

Figure 9. 18: Relation between the PUA and the disposition of the fibres

2. *Macroscopic explanation based on the mechanics of continuum*

A further interpretation can be given by the mechanics of the continuum.

Let's consider an electrorheological dispersion and deform it using a divergent electric field. The upper electrode acts as dielectrophoretic tweezers. Due to the internal cohesion of the material a cone shape deformation is generated. However, under the action of the weight acting on the lateral bonding (see figure 9.19), the cone angle decreases. Therefore, the cone angle depends on the weight and on the cohesion. Considering that the weight does not change in experiments with the same material, the cone angle, i.e. PUA, depends only on the internal cohesion of the system, which can be related to the interparticle force.

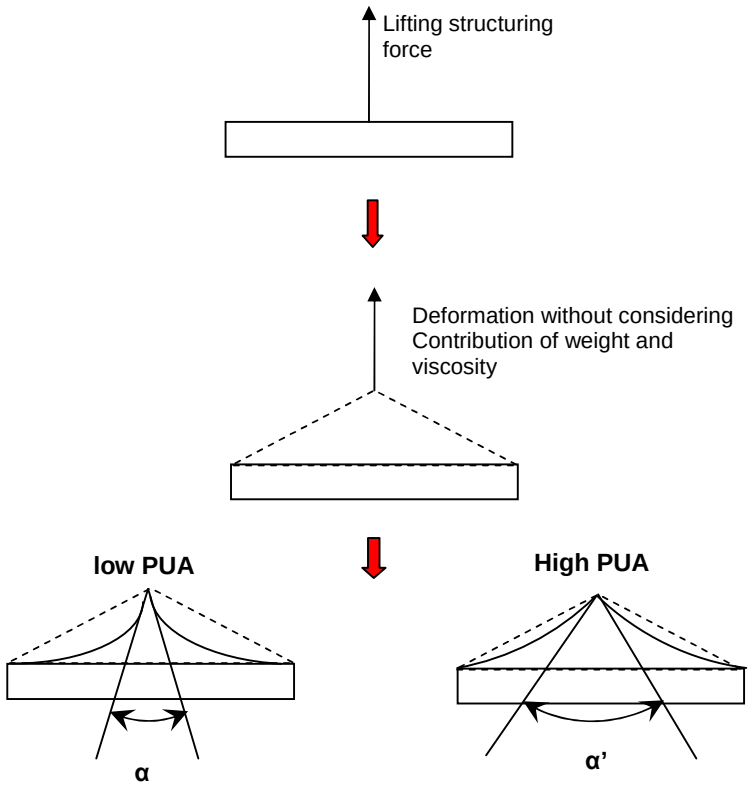

Figure 9. 19: Schematic representation of the direct correspondence between PUA and the cohesion force inside a generic continuous body.

9.4. THE EXPERIMENTAL RESULTS

9.4.1. THE BEHAVIOUR IN THE NEEDLE – PLANE CONFIGURATION

The structuring induced on a group of fibres by a needle-like upper electrode, acting in the non contact mode, has been considered in this chapter. The main influences investigated are the frequency and the voltage magnitude.

9.4.1.1. The behaviour as a function of the voltage frequency

The needle was a stainless steel needle with a diameter 120μm and a tip radius 6.5μm.
A series of experiments has been carried out on a bunch of PZT fibres, 140mm in diameter. To test the action of the frequency on the phenomenon, a frequency varying from DC to 4kV in conditions of relatively low field 2kV, and high field 7kV was considered.
The main results are summarised in the table 9.2.

Table 9. 2: Summary of a series of experiment showing the dependence of the structuring of a bunch of PZT fibres from the voltage frequency. The (*) means that a "pearl-chain structuring is achieved.

V (kV)	Freq. (Hz)	Inception height (mm)	Pick-up angle(°)	Structuring possible (YES/NO)	Bubble generation (YES/NO)	Fibre released after switch off (YES/NO)
2	DC	-	-	NO	NO	-
	10	1.10	0 (*)	YES	NO	YES
	50	0.75	0 (*)	YES	YES	YES
	100	1.00	15	YES	YES	YES
	500	1.00	30	YES	NO	YES
	1000	0.75	40	YES	NO	YES
	3000	0.70	38	YES	YES	NO
	4000	0.80	44	YES	YES	NO
7	DC	6.00	-	NO	NO	-
	50	2.20	-	NO	YES	-
	500	2.00	-	NO	YES	-
	1000	1.50	-	NO	YES	-

As shown in table 9.2, it is not possible to capture a fibre by applying a DC signal. For a 2kV voltage, once the inception length is reached, the fibres orienting and moving toward the electrode and then being forcefully repulsed can be seen. This phenomenon derives from the charge transfer mechanisms already analysed in chapter 7. When the voltage is equal to 7kV, it is enough to apply the field at the initial height (6mm), and a collective motion of fibres toward the upper electrode can be seen. Evidently, there is a charge transfer from the bottom electrode that allows a lift-off of the particles toward the upper electrode. During their up and down motion the fibres follow the field lines of the electric field, although, no fibre lift-off has been observed from the central area. This is probably due to the charge injection influence.

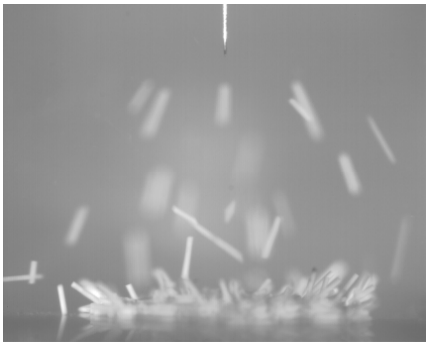

Figure 9. 20: A bunch of PZT fibres (140μm of diameter) exposed to a signal 7kV@DC. An intense electrophoretic response is visible and pick up is impossible.

When the frequency increases, with a voltage of 2kV, it is always possible for structuring to occur.

Between 10 and 100Hz the experiments show an astonishing behaviour for a frequency. The fibres near the tip are characterised by a certain oscillatory behaviour that moves the particles in proximity to the needle tip in a range of around 100μm. Moreover, moving up the needle electrode, a certain instability can be seen in the columnar structure. This culminates in the generation of a perfectly aligned structure like the one visible in figure 9.21. Nevertheless, the interparticle force seems to increase with the frequency. In fact, at 10Hz, no transport of fibres is possible above 1.8mm. This distance increases when increasing the height. Moreover, it can be seen that at 100Hz, differently to what happens at 50Hz, a certain pickup angle is visible and only after

further moving up the needle does the aligned structure appear. Also the instabilities seem to decrease in intensity with the frequency.

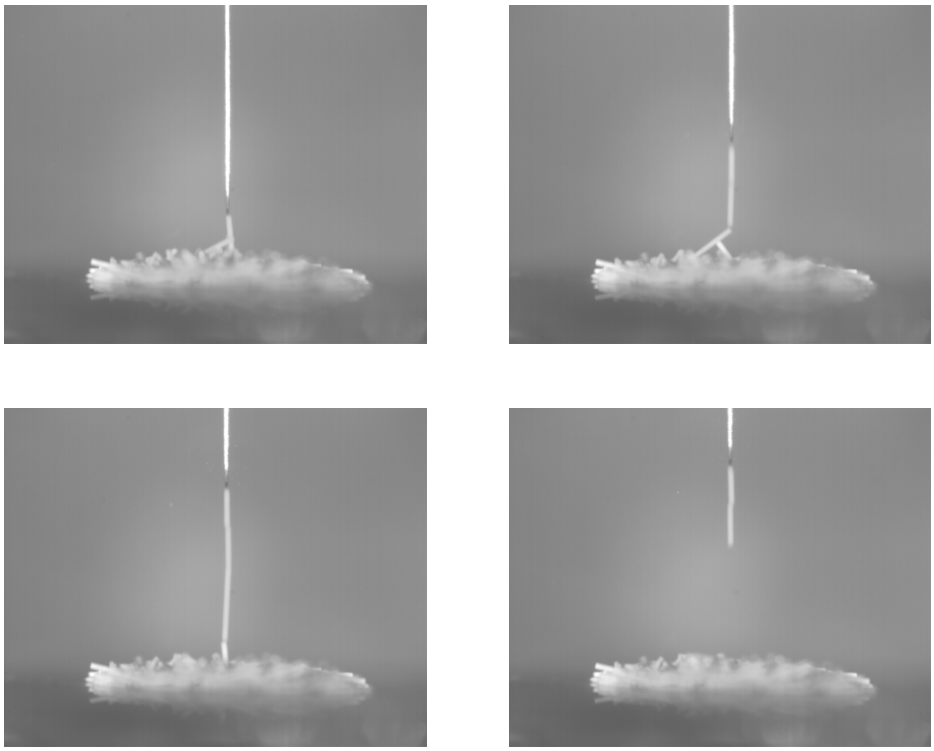

Figure 9. 21: Different steps of a "pearl-chain " structuring of a PZT fibre (140μm of diameter) exposed to a signal 2kV@50Hz.

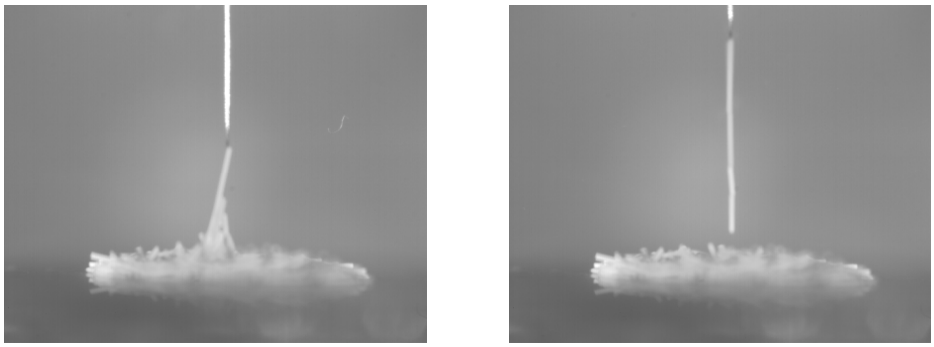

Figure 9. 22: "Pearl-chain " structuring of a bunch PZT fibre (140μm of diameter) exposed to a signal 2kV@100Hz.

For a frequency higher than 500Hz, the formation of a cone shaped structure can be seen. The PUA increases between 500Hz and 1kHz, and seems to stabilise around an average value of 42° for frequencies higher than 1kHz.

The formation of a small amount of bubbles (10μm of diameter) issued from a fluid degradation has been observed at very low (10-50Hz) and very high frequency (3-4kHz); the interpretation of this behaviour is still controversial. Moreover for the frequency range of between 3 and 4kHz an adhesion of the particles to the tip after the voltage was switched off was also observed.

As already observed in the case of a single fibre in chapter 8, the inception height does not seem to be dependent on the frequency, rather it is directly related to the applied voltage.

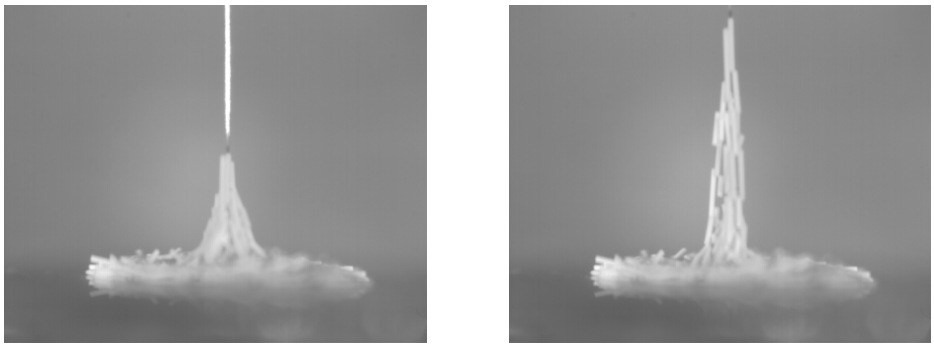

Figure 9. 23: "Cone-like "structuring of a bunch of PZT fibres (140μm of diameter) exposed to a signal 2kV@500Hz.

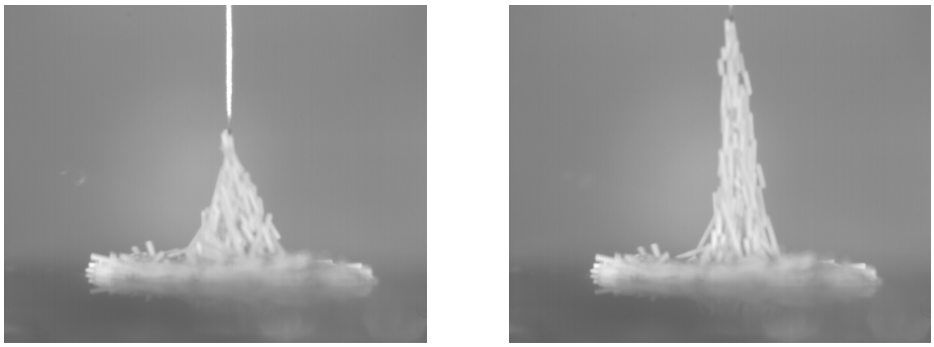

Figure 9. 24: "Cone-like "structuring of a bunch of PZT fibres (140μm of diameter) exposed to a signal 2kV@1kHz


(a)

(b)
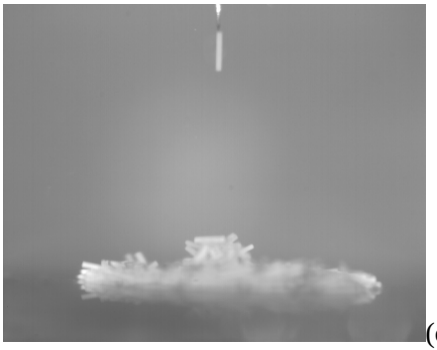
(c)

Figure 9. 25: "Cone-like "structuring of a bunch of PZT fibres (140μm diameter) exposed to a signal 2kV@3kHz. (a) Behaviour during the application of the voltage. (c) Behaviour after the voltage is switched off.

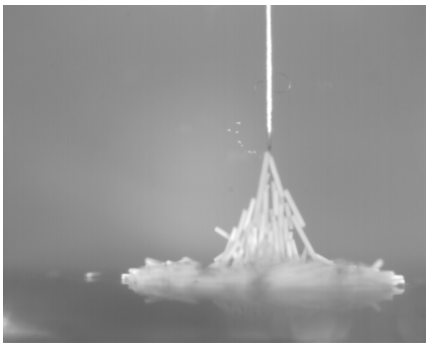

Figure 9. 26: "Cone-like "structuring of a bunch of PZT fibres (140μm of diameter) exposed to a signal 2kV@4kHz

The experiment run at higher voltage (V=7kV) showed a more dramatic picture. An intense generation of bubbles exists at practically every frequency and no pickup is possible.

At 50Hz there is a continuous motion of the fibres oscillating between the upper and the lower electrode. Consequently, no fibre can be captured by the needle. This is a further

demonstration that at this frequency a mechanism of charge transfer between the needle and the fibre is active.

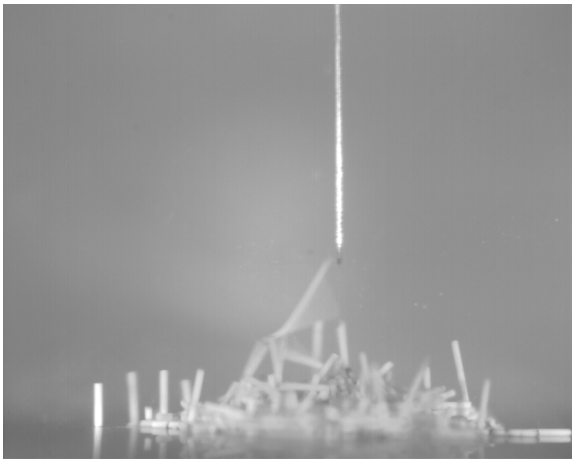

Figure 9. 27: A bunch of PZT fibres (140μm of diameter) exposed to a signal 7kV@50Hz. Due to the intense electrophoretic effect a pick up is impossible.

At 500Hz, even if the fibre suffers an intense instability in proximity to the tip (150μm wide), a certain structuring is visible. Unfortunately, when h>4.8mm, no fibres can be dragged by the needle anymore. After a considerable electric field fluid decomposition, a black deposit of materials appears on the fibre edges.

The situation is even worse at 1kHz. In this case no chain-like structure is normally established. However, in some special cases, i.e. when the first fibre which moves toward the needle is very long (see figure 9.30), a “pearl-chain structuring” like the one observed at low frequency and low voltage is observable.

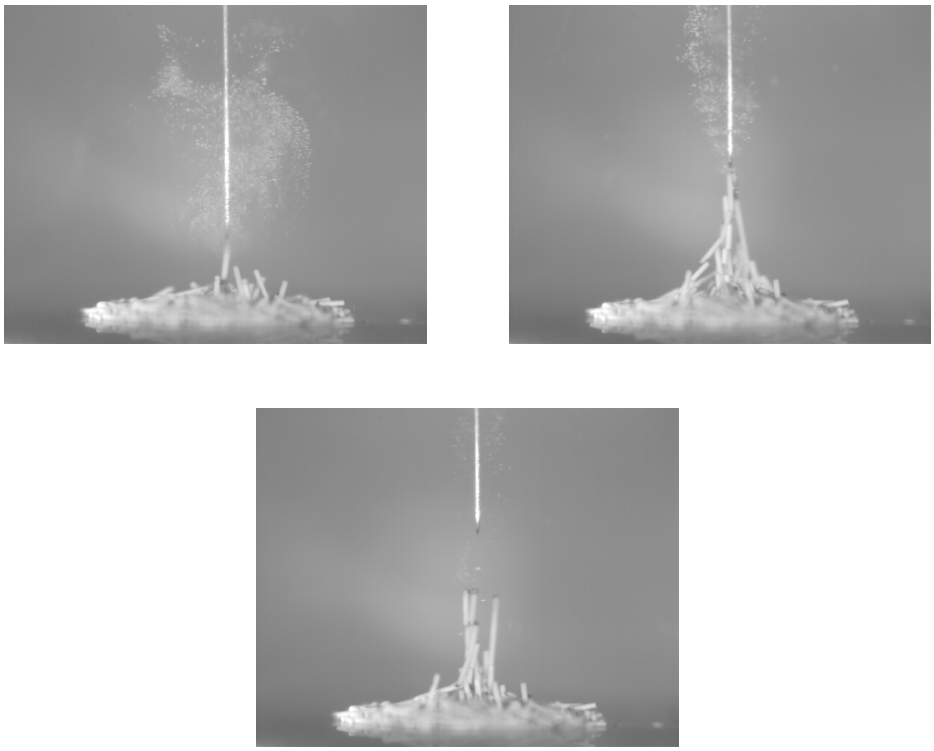

Figure 9. 28: A bunch of PZT fibres (140µm of diameter) exposed to a signal 7kV@500Hz.

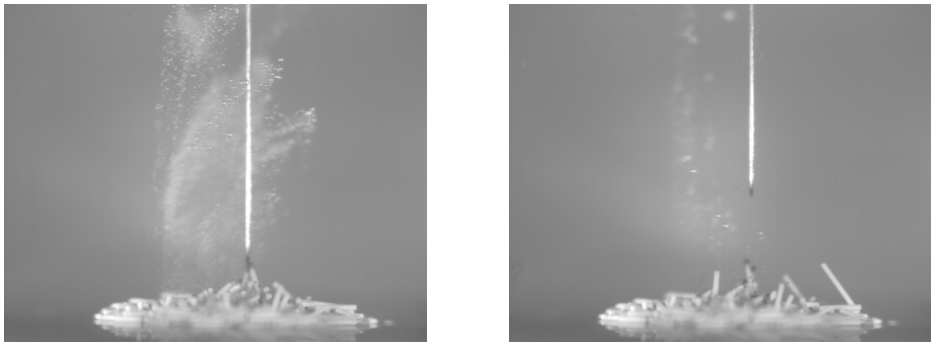

Figure 9. 29: A bunch of PZT fibres (140µm of diameter) exposed to a signal 7kV@1kHz.


(a)
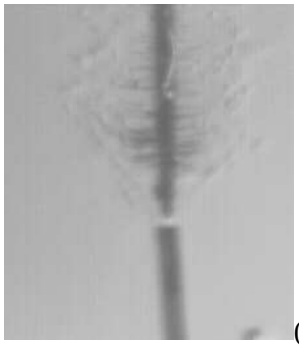
(b)

Figure 9. 30: (a) A rare case of "pearl-chain" structuring of a bunch of PZT fibres (140μm of diameter) exposed to a signal 7kV@1kHz. (b) The detail of the needle tip reveals some products of decomposition consequent to the intense activity of micro-breakdown inside the gap.

A further consequence of the dielectric failure near the electrode is the generation of a sort of "hairy deposit" of dust near the needle tip.

9.4.1.2. The behaviour as a function of the voltage magnitude

The needle was a stainless steel needle with a diameter 120μm and a tip radius 6.5μm.
The influence of the voltage magnitude on the behaviour of a bunch of PZT fibres, 140mm in diameter, has been tested in a series of experiments. The test was carried out at a fixed frequency of 1kHz at a voltage between 0.3 and 7kV.
The frequency of 1kHz was the highest at which the generator was able to supply 7kV, and it has been chosen to limit as much as possible any electrophoretic contribution. Moreover, the lower limit of 0.3kV, was the threshold value of the voltage. Below 0.3kV, no particle capture was possible.
The principal results are summarised in the table 9.3.

The experiments show that the pickup is always possible for a voltage up to 4kV. Moreover, when the voltage increases, the PUA and the inception height increase too. An intense generation of bubbles is observable when the voltage exceeds 3kV. This observation finds an important correspondence in the behaviour after the voltage is switched off. In fact, it is only when no fluid decomposition occurs that the fibre is

released. When the voltage is higher than 3kV, after the switch off the fibre remains in contact with the needle tip.

Table 9. 3: Summary of a series of experiment showing the dependence of the structuring of a bunch of PZT fibre from the voltage magnitude. The (*) means that a "pearl-chain structuring is achieved, and the (**), means that to achieve the structuring, it was necessary to be in contact.

V (kV)	Inception height (mm)	Pick-up angle(°)	Structuring possible (YES/NO)	Bubble generation (YES/NO)	Fibre released after switch off (YES/NO)
0.3	0 (**)	0 (*)	YES	NO	-
0.5	0 (**)	20	YES	NO	-
1	0.70	20	YES	NO	YES
2	0.75	44	YES	NO	YES
3	0.80	47	YES	YES	NO
4	1.10	60	YES	YES	NO
5	1.00	-	NO	YES	-
7	1.50	-	NO	YES	-

For lowest voltage values 0.3kV and 0.5kV, it is not possible to carry the captured fibres higher than 3.6 and 8mm respectively.

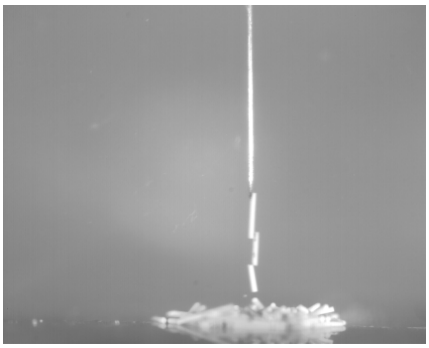

Figure 9. 31: Structuring of a bunch of PZT fibres (140μm of diameter) exposed to a signal 0.3kV@1kHz. This voltage is the threshold one. For voltages smaller than this one, no fibre capture is possible

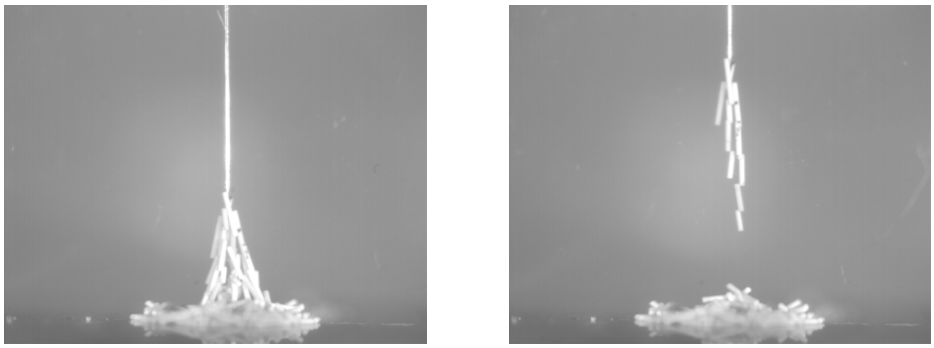

Figure 9. 32: Structuring of a bunch of PZT fibres (140µm of diameter) exposed to a signal 0.5kV@1kHz.

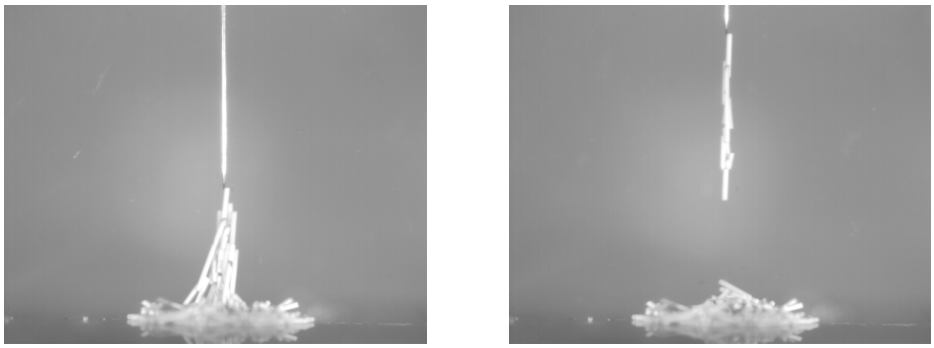

Figure 9. 33: Structuring of a bunch of PZT fibres (140µm of diameter) exposed to a signal 1kV@1kHz.

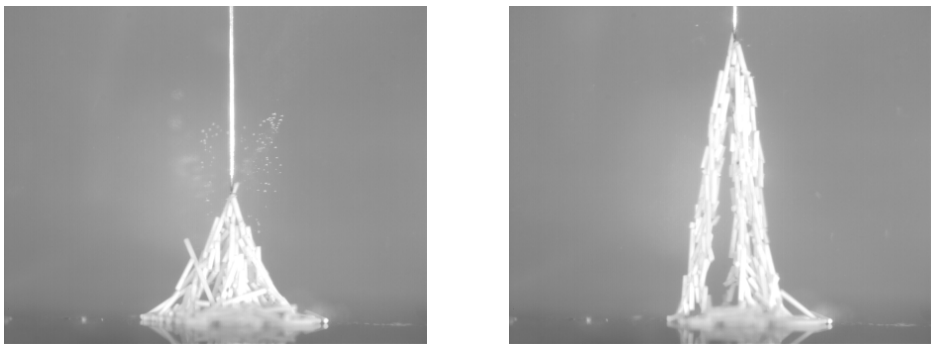

Figure 9. 34: Structuring of a bunch of PZT fibres (140µm of diameter) exposed to a signal 3kV@1kHz.

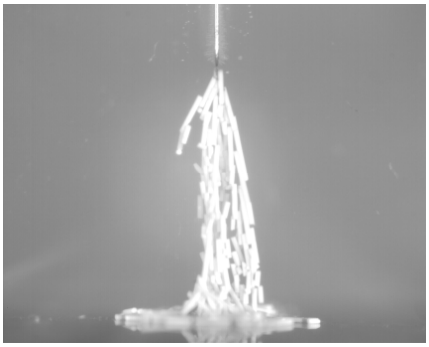

Figure 9. 35: Structuring of a bunch of PZT fibres (140µm of diameter) exposed to a signal 4kV@1kHz.

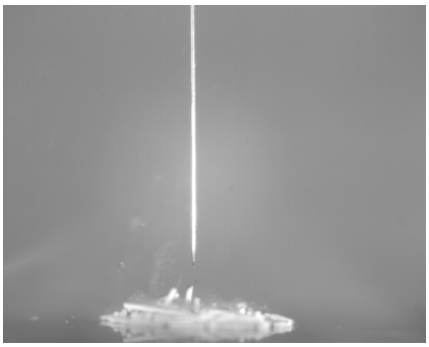

Figure 9. 36: Structuring of a bunch of PZT fibres (140µm of diameter) exposed to a signal 5kV@1kHz.

9.4.1.3. Influence of a bias superimposed to a voltage

In this section, what happened when a fibre group was exposed to a voltage of 1kV, at 1kHz, on which a 1kV DC bias had been superimposed. The fibres and the needle were the same as used in previous sub-section 9.4.1. This experiment is particularly interesting because it could give more evidence of eventual electrophoretic effects playing a role in the structuring phenomena.

Since the considerations expressed in section 3.3.3.2, DEP resulting from a zero averaged AC signal is dependent on V_{RMS}^2. Considering that in our case a DC bias (V_{DC}) was also superimposed on the AC zero averaged signal (V_{AC}), the DEP contribution to the interparticle force would be directly proportional to:

$$[V_{DC}+(V_{AC})_{RMS}]^2 = 2.9 \text{ kV}$$

Consequently, if no electrophoretic effect exists, an intermediary behaviour between the one observed at a zero-averaged signal at 2kV-1kHz (V_{RMS}^2 = 2.0 kV) and at 3kV-1kHz (V_{RMS}^2 = 4.8 kV) would be expected. As can be seen in the picture 9.37 this was not the case. The structuring in presence of a bias was considerably less important. The amount of displaced fibres was lower and the results looked more like those ascertained at lower frequency (50Hz) than at 1kHz.

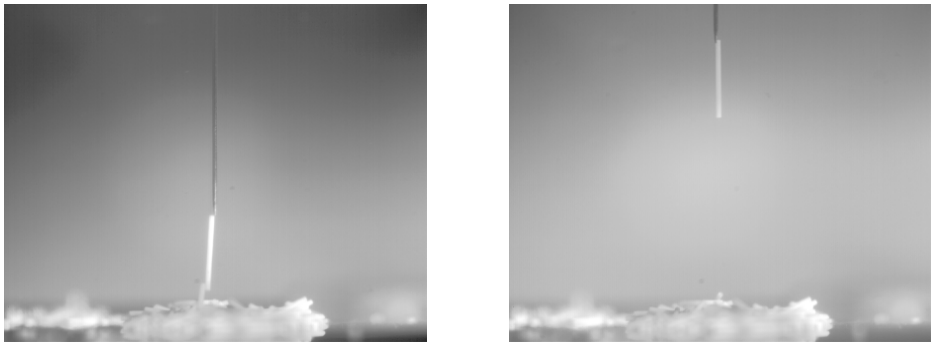

Figure 9. 37: Structuring of a bunch of PZT fibres (140µm of diameter) exposed to a signal 1kV@1kHz at which a 1kV DC bias has been superimposed

This observation could allow for the following conclusions:

1. The phenomenon is not purely dielectrophoretic, but also some charge transfer mechanisms in the gap between particles and between needle and fibre can play a role

2. The similarity between the phenomenon at lower frequency, and that observed in the superimposed bias case, considerably build on the idea that the particular alignment observed at low frequency is also due to some charge transfer phenomenon.

9.4.1.4. Influence of the immersion depth

Before concluding the section 9.4.1 it would be interesting to place some attention on a final aspect of the phenomenon. When instead of having a single fibre in contact with the needle, there are a lot of fibres; there is also a change in the distribution of the electric field near the tip (see figure 9.38). More precisely, the group of fibres would create a screening effect, so that once the field near the tip was reduced, it would, in turn, reduce the instabilities and the charge transfer as well.

Figure 9. 38: Different possible configuration for a fibre-needle interaction

This effect has been shown by an experiment at 2kV, 1kHz in “contact mode”.
The needle was a stainless steel needle with a diameter 120µm and a tip radius 6.5µm.
By increasing the contact between the needle and the bunch of fibres (because the field was switched on when the needle was well penetrated inside the fibre bunch) it was possible to increase the number of fibres involved in the chain like structure.

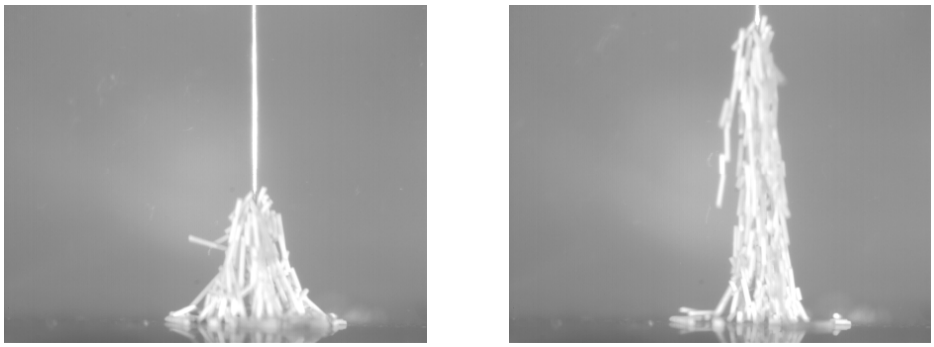

Figure 9. 39: Structuring of a bunch of PZT fibres (140µm of diameter) exposed to a signal 2kV@1kHz, using the "contact mode" protocol of application of the electric field.

9.4.1.5. Influence of the tip radius of the needle

The needle was a stainless steel needle with a diameter of 750µm and a tip radius 25µm.

All tests were run applying a voltage of 2kV at 1kHz.

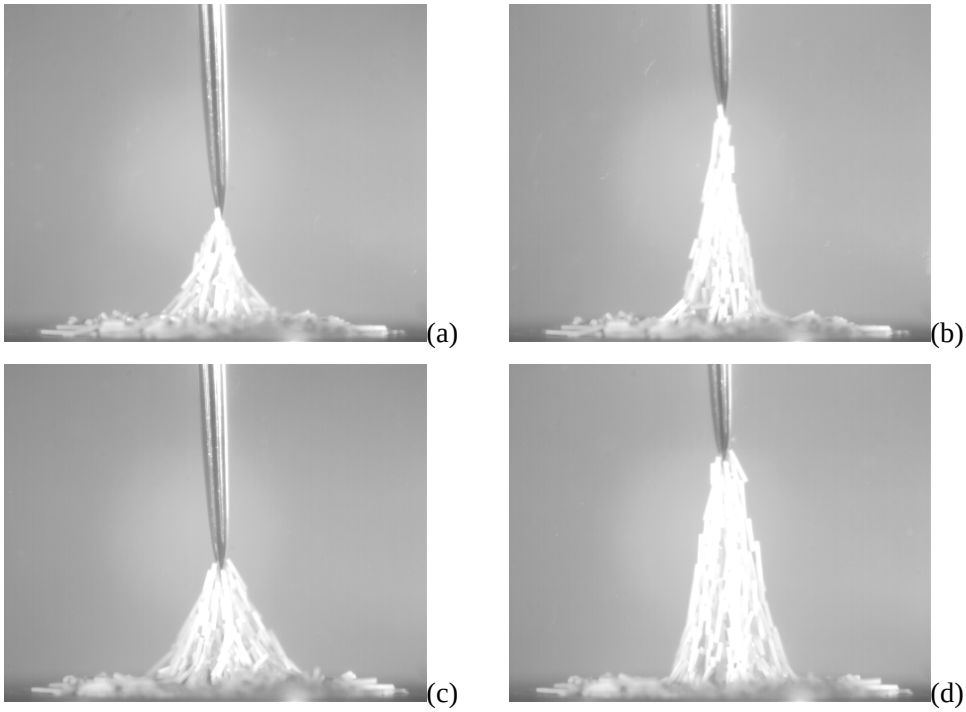

Figure 9. 40: Structuring of a bunch of PZT fibres (140µm of diameter) using a needle like upper electrode with a diameter of 0.75mm and a tip radius of 25µm. The voltage is 5kV@1kHz. Te pictures represent the phenomenon in "non-contact mode" ((a),(b)), and "contact mode" ((c),(d))

The fibre was captured at h = 0.7mm with a PUA of 50°. The value of the inception value was close to the one observed using a thinner needle, while, the PUA was bigger. Moving the electrode upward, generated a columnar structure. The amount of displaced fibres, as observed already in section 9.4.1.3 was bigger when the voltage was applied when they were already in contact.
As expected, the resolution power of the capturing process is notably reduced by the fact that the tip radius is bigger. In this case it is impossible to block a single fibre on the needle tip as done with a thinner needle.
The fibres were always completely released after the switch off.

9.4.2. THE BEHAVIOUR USING DIFFERENT INJECTION FREE ELECTRODE CONFIGURATION

To improve the understanding of the phenomenon and in particular of the influence of the charge injection through the needle, a series of experiments in different electrode configurations characterised by the absence of charge injection was setup. The bottom electrode was always a metallic conducting plate. The upper electrode was, according to the different experiments:

- another flat electrode: to test what happens in condition of uniform field
- a sphere with a diameter of 8mm: to test what happens in a non-uniform field
- a needle coated with an insulator: to test what happens in a non-uniform field with an upper electrode unable to exchange any charge with the fibre

9.4.2.1. Flat-flat

In this section the results related to the behaviour of a group of PZT particles, 140μm diameter, exposed to a uniform electric field are shown. The fibres were exposed to an electric field of different frequency and magnitude. Every structuring was carried out using the “contact” protocol, even if the “no contact” protocol was used to establish the inception height.

To quantify the "structuring performance", considering that the PUA does not have anymore meaning in this configuration, a further "structuring factor" was introduced. This factor is calculated by elaborating a picture of the structuring process.

Only the portion of the picture representing the 6mm of the gap between the two flat electrodes is taken. Then, using Adobe Photoshop (Adobe, US), a picture in black and white was made up, and after adjusting with the threshold value, an image was created in which in white there was only the shape of the fibres well focused in the picture. Once this last step was completed a picture like the one in figure 9.41 was achieved. At that point, an analysis of the picture revealed the "structuring factor" as the percentage of white in the elaborated picture.


(a)

(b)

Figure 9. 41: Definition of the structuring factor for the experiments in parallel plate capacitor configuration.

The results of the experiments are reported in tab.9.4.

Table 9. 4: Summary of a series of experiment showing the behaviour of a bunch of PZT fibres when exposed to the field of two parallel plates.

V (kV)	Freq. (Hz)	Inception height (mm)	Structuring factor	Structuring possible (YES/NO)	Bubble generation (YES/NO)	Fibre released after switch off (YES/NO)
2	DC	5	10%	YES	NO	YES
	50	2.5	25%	YES	NO	YES
	1000	2.35	40%	YES	NO	YES
7	DC	6	12%	YES	NO	YES
	1000	3	41%	YES	NO	NO

When considering the phenomenon in DC, it can first be pointed out that the phenomenon was not significantly dependent on the voltage polarity.

In DC, the inception height was a lot bigger than in the AC case since there was also an electrophoretic response from the system. A lot of fibres used to oscillate between the two electrodes. In this up and down motion, when the fibres were in proximity to other fibres, they used to join because they were exposed to an interparticle force due to reciprocal polarisation. Due to the high mobility of the fibre, the phenomenon evolved quickly to a situation in which some fibres were in columns and some others going up and down. The column seemed weaker than in the AC case, and sometimes they break to reform in some columnar structures with a bigger diameter. Differently from the AC case the columns were not conical, but they were cylindrical narrower in the middle.
When the applied field wais 2kV, except for some isolated fibres which stayed still in contact with the upper electrode, the fibres dropped down instantaneously, after the voltage was switched off. When the applied field was 7kV, the fibres needed 20s before to completely discharge and being released. A part from that, the structuring phenomenon it is not so different at 2 or 7kV.

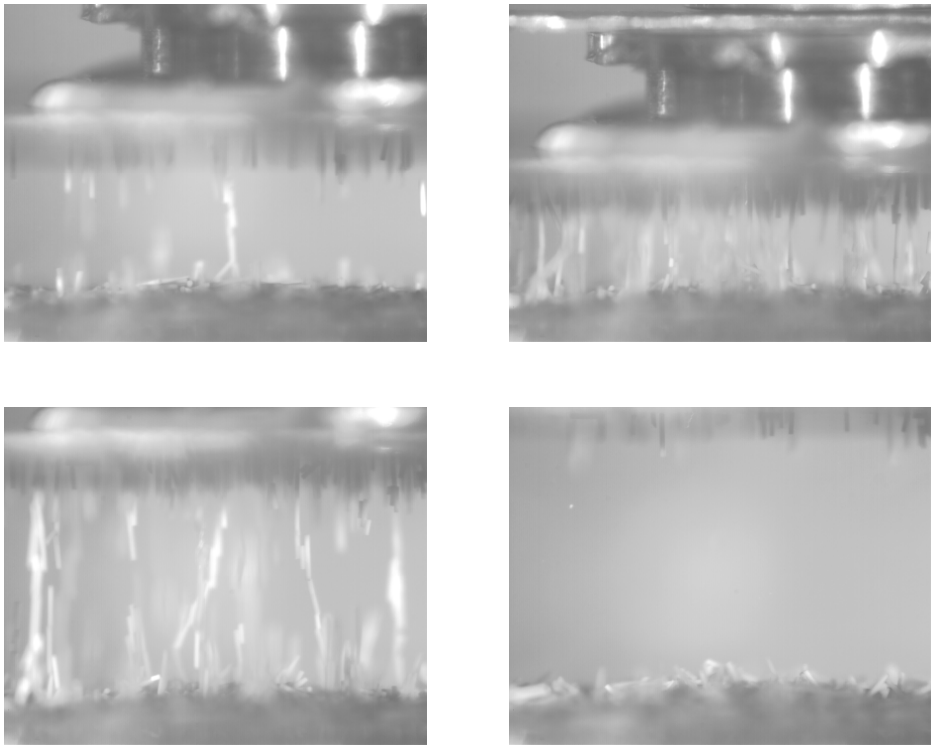

Figure 9. 42: Structuring of a bunch of PZT fibres (140μm of diameter) in a parallel plate configuration exposed to a signal 2kV@DC

Applying an AC field, the structuring showed some differences. The main difference was that no oscillatory motion of isolated fibres was observed. Therefore, this means that any electrophoretic effects were relaxed. The columnar structures were considerably stronger in AC than in DC, and the structuring factor increased with the increasing frequency of the field. When the voltage was increased it was not visible a so important increase in the structuring factor.

When the applied field was 2kV, after it was switched off the columns were released in a time up to 20s. It was interesting to observe how after the switch off the columns detached from the upper electrode without disaggregating.
When the applied field was 7kV a phenomenon of electropolarisation between the fibres in the chain structure was probably witnessed. In fact, after the switch off a lot of structures were not released for at least 30min.

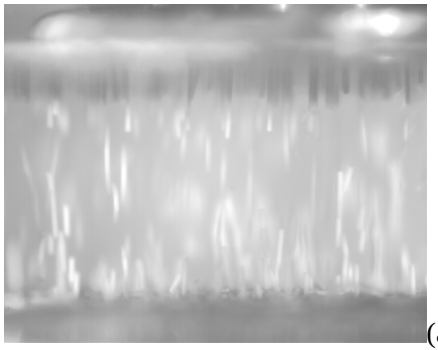
(a)

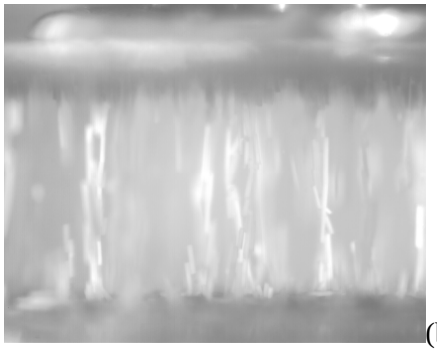
(b)

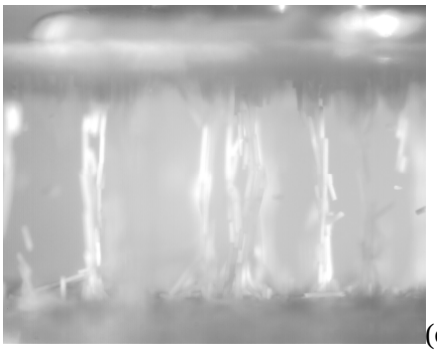
(c)1s

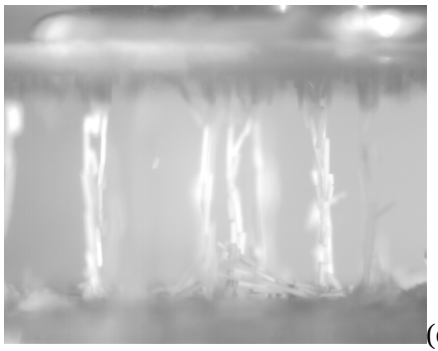
(d)5s

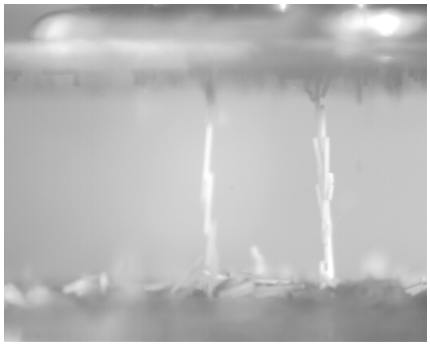
(e)15s

Figure 9. 43: Structuring of a bunch of PZT fibres (140µm of diameter) in a parallel plate configuration exposed to a signal 7kV@DC. (a)(b) Phenomenon during the application of the voltage. (c)(d)(e) Phenomenon after the switch off

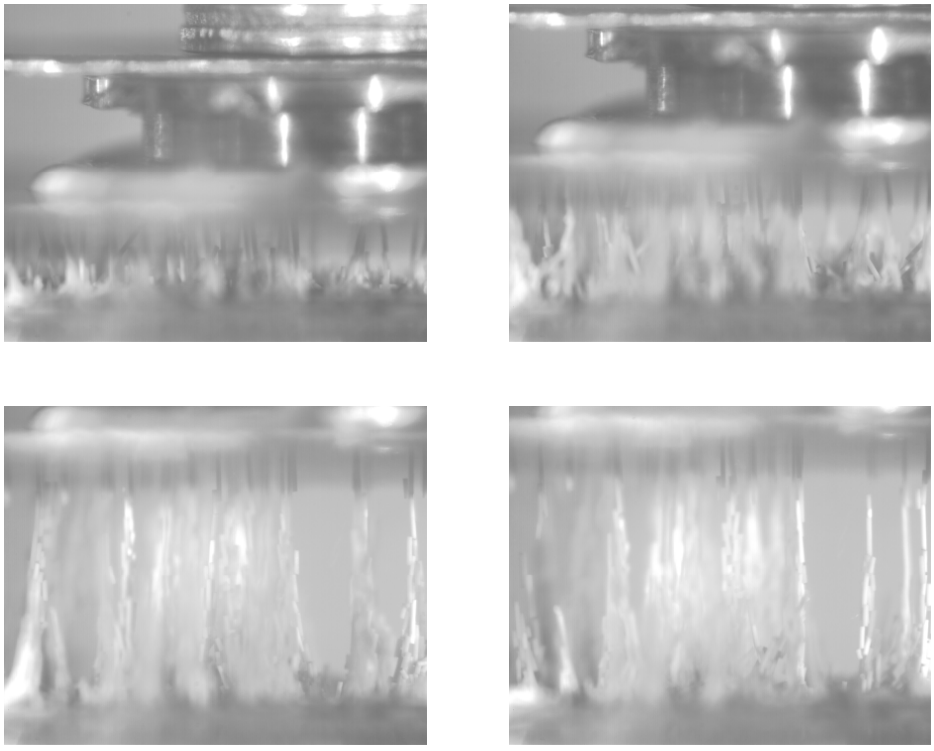

Figure 9. 44: : Structuring of a bunch of PZT fibres (140µm of diameter) in a parallel plate configuration exposed to a signal 2kV@50Hz

Figure 9. 45: Structuring of a bunch of PZT fibres (140µm of diameter) in a parallel plate configuration exposed to a signal 2kV@1kHz

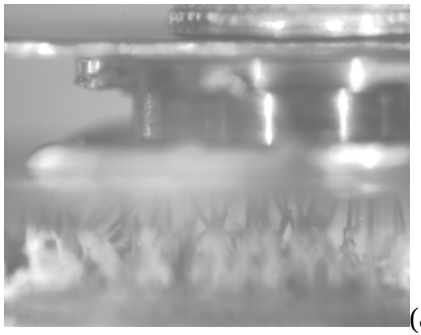
(a)

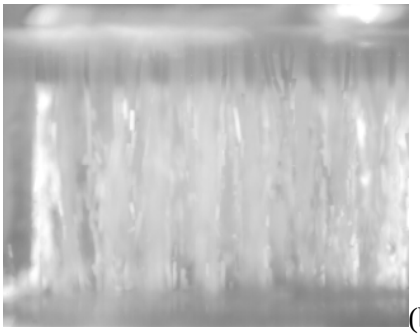
(b)

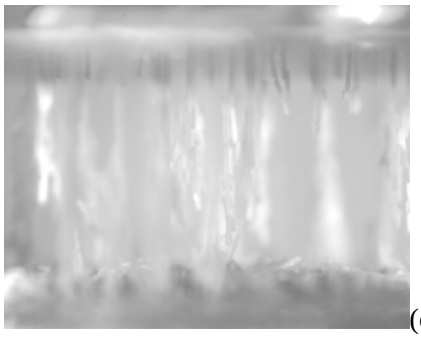
(c) 0min

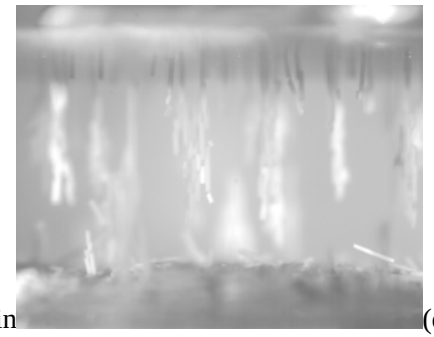
(d)5min

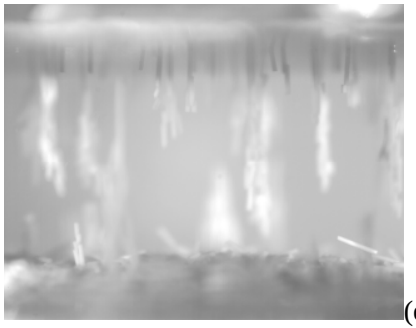
(e)15min
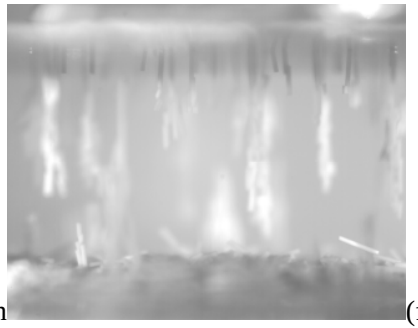
(f)30min
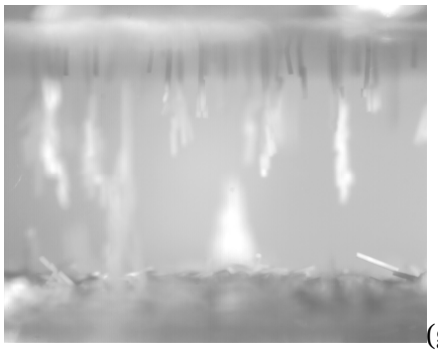
(g)60min

Figure 9. 46: Structuring of a bunch of PZT fibres (140μm of diameter) in a parallel plate configuration exposed to a signal 7kV@1kHz. (a)(b) Phenomenon during the application of the voltage. (c)(d)(e)(f)(g) Phenomenon after the switch off

9.4.2.2. Sphere-plane

In this section the results relating to the behaviour of a group of PZT particles, 140μm diameter, exposed to the electric field of a sphere with a diameter of 8mm, are presented. The bunch of fibres was exposed to an electric field of different frequency and magnitude. As in the case of the parallel flat electrode treated in section 9.4.2.1, every structuring was carried out using the “contact” protocol, and the “no contact” protocol was used to establish the inception height.

The performance factor was calculated in the same way as for the parallel plate case.

The table 9.5 summarises all the principal results.

Table 9. 5: Summary of a series of experiment showing the behaviour of a bunch of PZT fibres when exposed to the field generated between a sphere-like electrode (8mm of diameter) and a bottom flat electrode.

V (kV)	Freq. (Hz)	Inception height (mm)	Structuring factor	Structuring possible (YES/NO)	Bubble generation (YES/NO)	Fibre released after switch off (YES/NO)
2	DC	2.75	3%	YES	NO	YES
	50	2.25	10%	YES	NO	YES
	1000	1.6	20%	YES	NO	YES
7	DC	6	1%	YES	NO	YES
	50	4	5%	YES	NO	YES
	1000	3	21%	YES	NO	NO

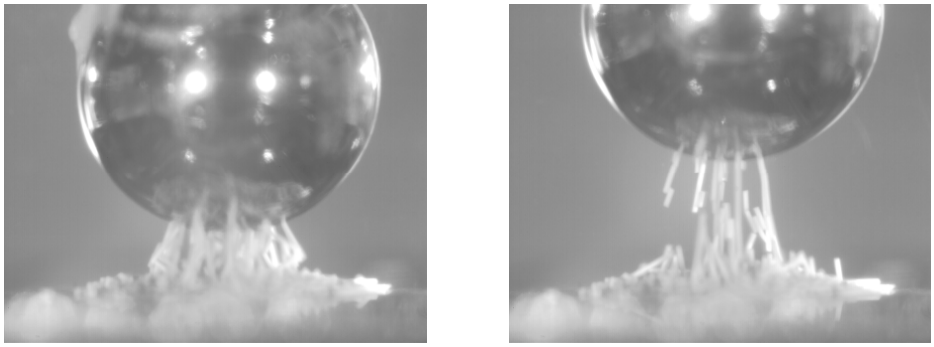

Figure 9. 47: Structuring of a bunch of PZT fibres (140µm of diameter) in a sphere-plate configuration exposed to a signal 2kV@DC

The phenomenon was very similar to what was observed in the parallel plate case. As in the parallel plate case the behaviour in DC was conditioned by the electrophoretic effect, and the structuring performances increased for higher frequencies.

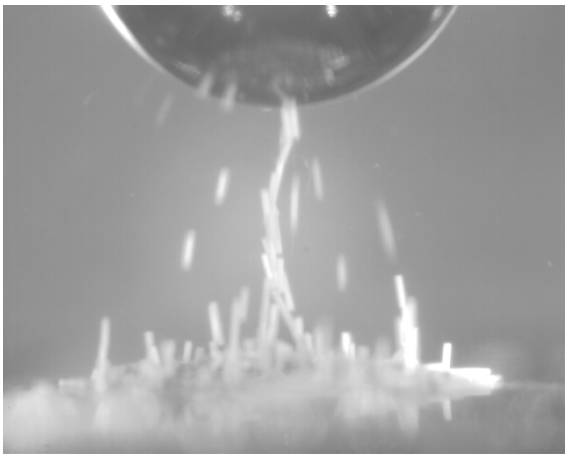

Figure 9. 48: Structuring of a bunch of PZT fibres (140µm of diameter) in a sphere-plate configuration exposed to a signal 7kV@DC

At 2kV and 50Hz, a structuring effect was observed, but no residual structuring was visible when the height overcame h=5.5mm. It is however remarkable as the structuring factor, at 50Hz was bigger for the 2kV case than for the 7kV.

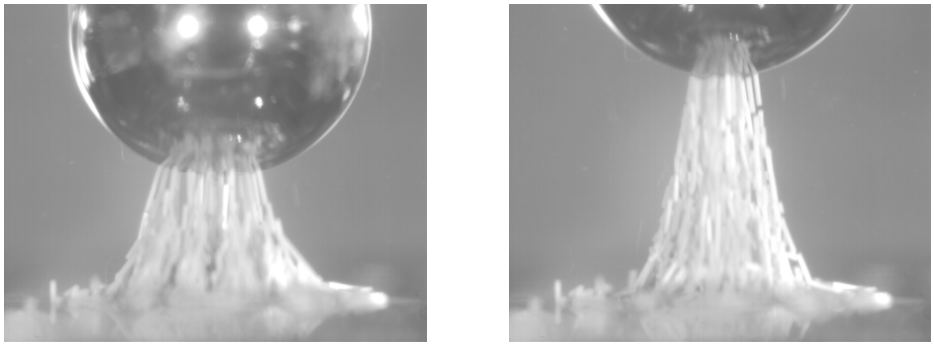

Figure 9. 49: Structuring of a bunch of PZT fibres (140µm of diameter) in a sphere-plate configuration exposed to a signal 2kV@50Hz

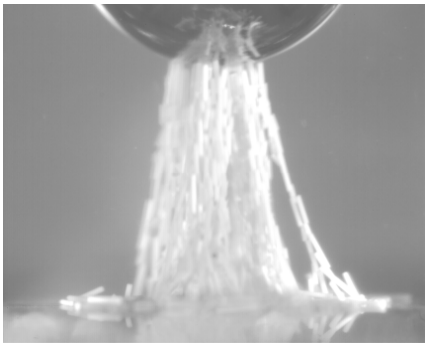

Figure 9. 50: Structuring of a bunch of PZT fibres (140µm of diameter) in a sphere-plate configuration exposed to a signal 2kV@1kHz

After the electric field switch off the fibres were always released, except in the case of V=7kV at 1kHz. In this case a probable electro-polymerisation occurred.

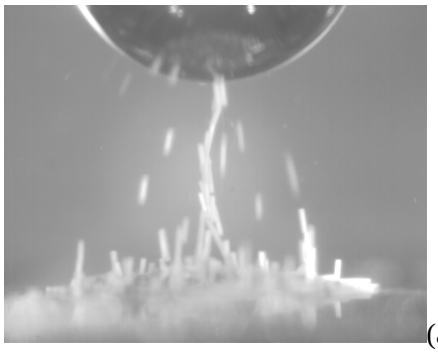

(a) 7kV – DC

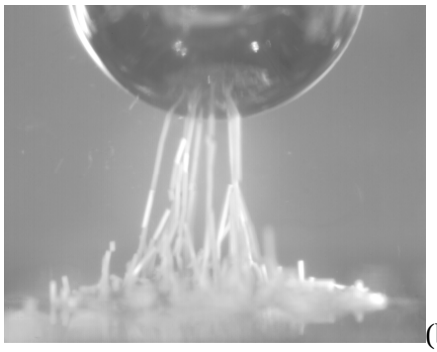

(b) 7kV – 50Hz

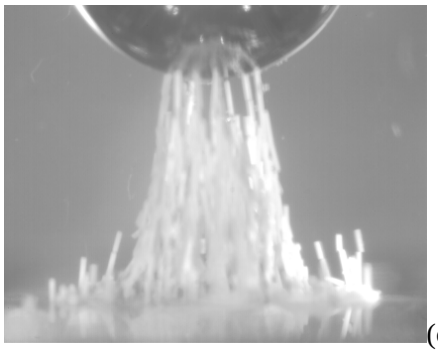

(c)

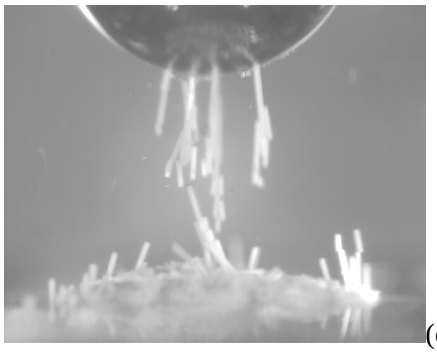

(d)

Figure 9. 51: Structuring of a bunch of PZT fibres (140µm of diameter) in a sphere-plate configuration exposed to a signal (a)7kV@DC; (b)7kV@50Hz; (c)7kV@1kHz; (d)7kV@1kHz 20s after the switch off

9.4.2.3. Insulator coated needle - plane

All the results in the particular case of the electric field applied between an insulator coated needle–like upper electrode and a bottom flat electrode are listed in the table 9.6.

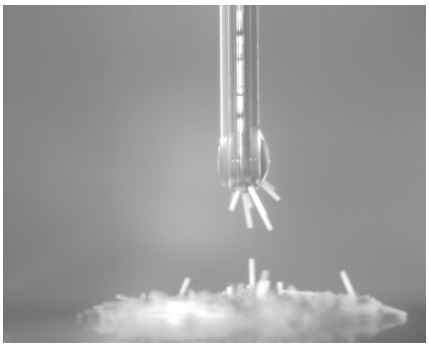

Figure 9. 52: Impossible structuring of a bunch of PZT fibres (140μm of diameter) exposed to the field generated between a insulating coated needle and a plate (2kV@DC)

In this case, the maximum height after which the structuring was not possible anymore was used, as an indicator of performance.

As we can see from the results and pictures in figure 9.52, it was not possible to make any structuring in DC at 2kV. Conversely a thin column raised when applying DC at 7kV. However, such a column was not stable and changes continuously. The action of the electrophoresis was also visible in this case. The fact that the fibre cannot discharge on the upper electrode determines a certain stochastic capture of fibres on such electrode.
It is important to notice that the behaviour in DC was not sensitive to the polarity.

In DC, at 2kV it was possible to have a chain-like structure at 50Hz, but such a structure was not longer than 3.25mm. When the frequency increased the achievable length decreased.

Table 9. 6: Summary of a series of experiment showing the behaviour of a bunch of PZT fibres when exposed to the field generated between an insulating coated needle-like electrode (8mm of diameter) and a bottom flat electrode. The (**) means that to achieve the structuring, it was necessary to be in contact.

V (kV)	Freq. (Hz)	Inception height (mm)	Maximum height	Structuring possible (YES/NO)	Bubble generation (YES/NO)	Fibre released after switch off (YES/NO)
2	DC	1.8	-	NO	NO	-
	50	0(**)	3.25	YES	NO	YES
	1000	0(**)	-	NO	NO	-
7	DC	6	-	YES/NO	NO	-
	50	4	8	YES	NO	YES
	1000	3	5	YES	NO	-

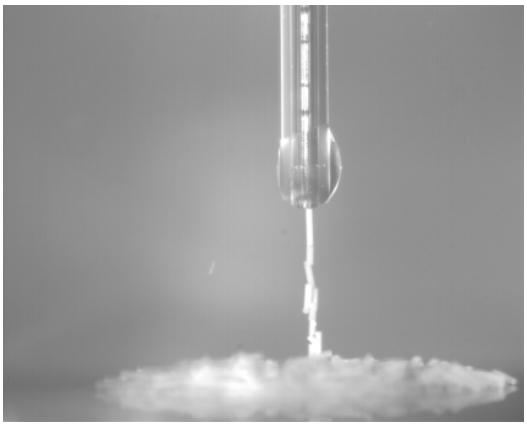

Figure 9. 53: Structuring of a bunch of PZT fibres (140μm of diameter) exposed to the field generated between a insulating coated needle and a plate (2kV@50Hz)

For a voltage of 7kV, the structuring performance seemed to grow up. The structures formed were stronger than the one at 2kV, and the maximum height bigger.
The experiments shown as, at 1kHz, the amount of fibres transported by the electrode was bigger than in the 50Hz case. This was probably due to the fact that there were more fibres and then a bigger weight.

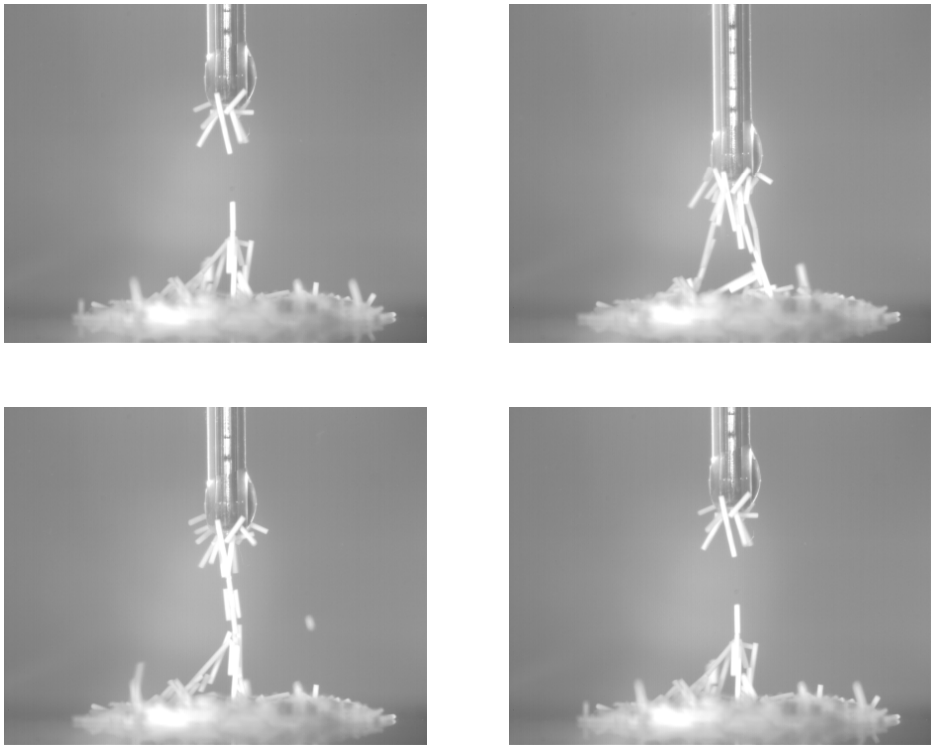

Figure 9. 54: Impossible structuring of a bunch of PZT fibres (140μm of diameter) exposed to the field generated between a insulating coated needle and a plate (7kV@DC)

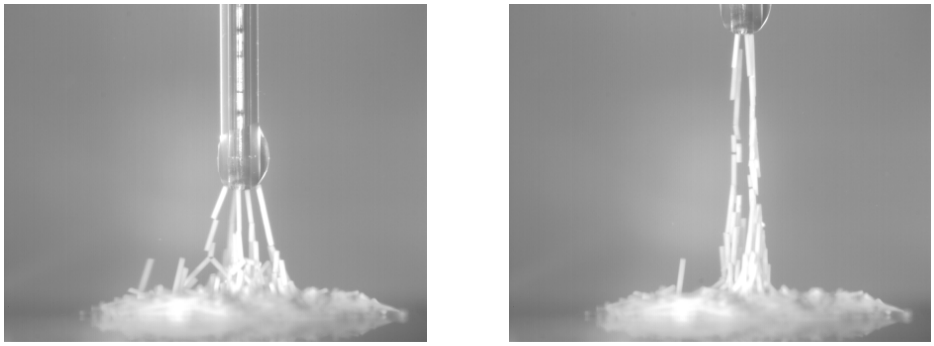

Figure 9. 55: Structuring of a bunch of PZT fibres (140μm of diameter) exposed to the field generated between a insulating coated needle and a plate (2kV@50Hz)

An important aspect revealed by these experiments it is that when the upper electrode is coated by an insulator, the force connecting the last fibre to the upper electrode is lower. This, since the image force relating the fibre to the upper electrode is considerably lower. As a consequence the structuring phenomenon became more difficult.

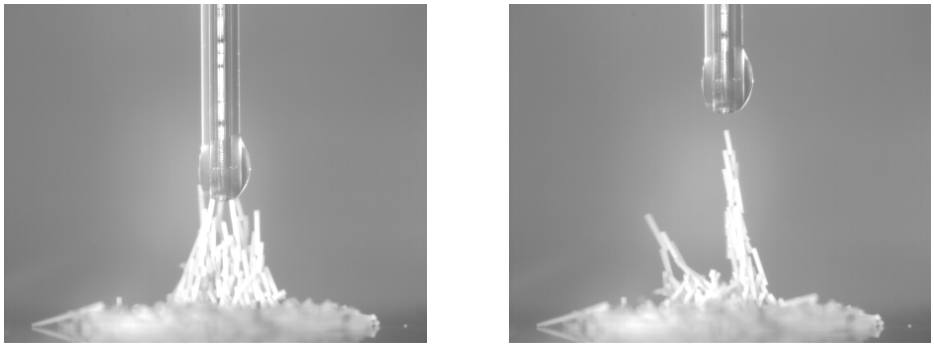

Figure 9. 56: Structuring of a bunch of PZT fibres (140μm of diameter) exposed to the field generated between a insulating coated needle and a plate (2kV@1kHz)

9.4.3. THE BEHAVIOUR VARYING THE SURROUNDING LIQUID CHARACTERISTIC

9.4.3.1. The influence of the viscosity: behaviour in 100cS silicon oil

In the picture 9.57 the results of an experiment conducted at 2kV and 1kHz in the same condition as the experiment described in section 9.4.1.1 are illustrated. In this case a silicone oil with a viscosity double that used in 9.4.1.1 was used.

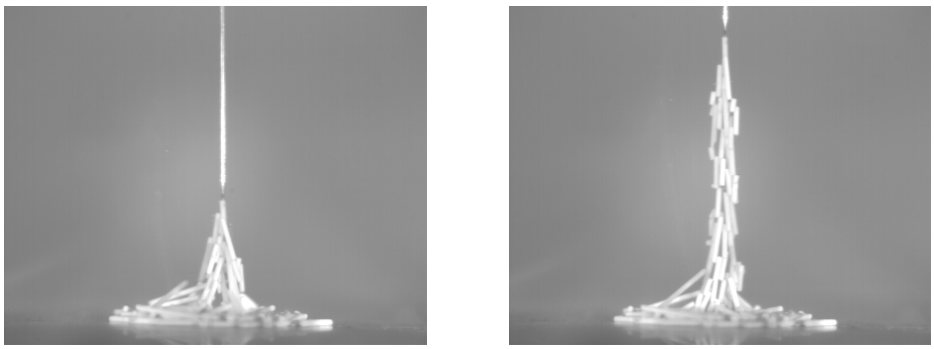

Figure 9. 57: Structuring of a bunch of PZT fibres (140μm of diameter) in a needle-plane configuration (2kV@1kHz). The structuring is operated in a silicone oil with a viscosity the double of the usual one.

As we can see the viscosity acts as a limiting factor for the structuring phenomenon, since the PUA is equal to 34° instead of 40°.

9.4.3.2. Analysis of the influence of the dielectric constant

In this section the results of some experiments, conducted in the same condition as the experiment described in section 9.4.1.1, but using a Castor oil (ε_r=4.2) and an olive oil (ε_r=3.1), to check the influence of the dielectric constant on the system, are illustrated. All experiments have been carried out at 2kV and in DC, 50Hz and at 1kHz.

As it was the case with silicone oil, also with castor oil no fibre was capturable on the tip when the experiments were executed in DC. Moreover, the same interesting alignment observable at 50Hz in silicone oil was also observable using castor oil.
At 1kHz the structuring became conical, as in the most usual case, but PUA was only 30º (in the silicone oil case PUA was 40 º!).

A PUA equal to 30º characterised also the structuring in olive oil.

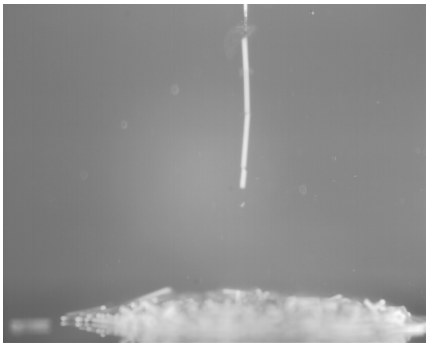

Figure 9. 58: Structuring of a bunch of PZT fibres (140μm of diameter) in a needle-plane configuration (2kV@50Hz). The structuring is operated in castor oil.

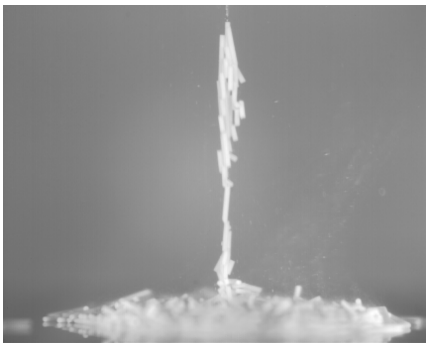

Figure 9. 59: Structuring of a bunch of PZT fibres (140μm of diameter) in a needle plane configuration (2kV@1kHz). The structuring is operated in castor oil.

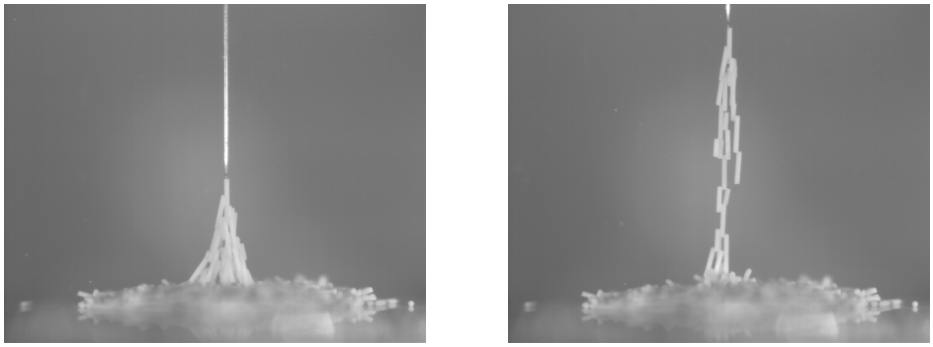

Figure 9. 60: Structuring of a bunch of PZT fibres (140µm of diameter) in a needle-plane configuration (2kV@1kHz). The structuring is operated in olive oil.

9.4.3.3. Analysis of the influence of the conductivity

This section is dedicated to the analysis of the influence of the oil conductivity on the electric field structuring. All experiments were conducted in the same conditions as the experiment described in section 9.4.1.1, but using:

- castor oil doped with 0.2mM of TBATBP (tetrabutyl-ammonium tetraphenylborate), an organic salt ($\sigma=1.2\times10^{-10}$),
- silicone oil doped with 2.5% of butylalcohol ($\sigma=5\times10^{-11}$)
- isopropylalcohol ($\sigma=3{,}50\times10^{-4}$).

All experiments were carried out at 2kV and in DC, 50Hz and at 1kHz.

In the case of doped Castor oil, the noticed behaviour was equivalent to that of pure Castor oil. Also in the case of the doped silicone oil what happened was not so different from the case of the undoped oil. However, in case of doped silicone oil, no structuring was visible at 50Hz, and at 1kHz a structuring was possible, but only with a PUA of 31º.

For the experiment conducted in IPA, the process was characterised by a huge instability in DC and at 50Hz. This instability prevented any kind of structuring. At 1kHz, fibres capture was observed, but it was very unstable. Above 2.75mm no more

pickup was possible. The phenomenon in IPA at 1kHz it is very similar to the one in silicone oil at 50Hz and 7kV.

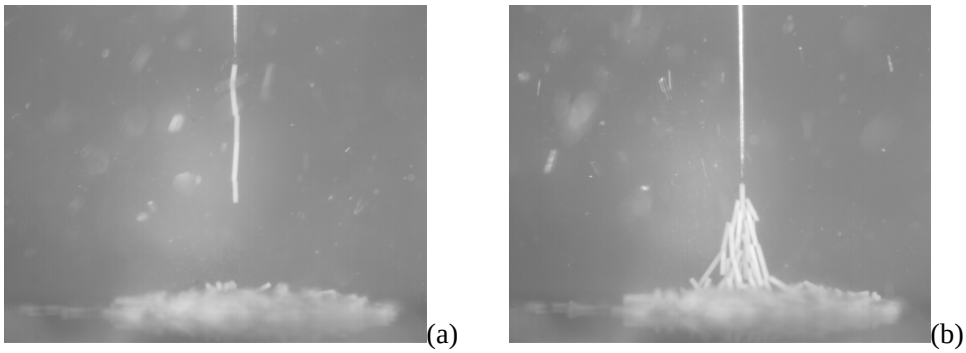

Figure 9. 61: Structuring of a bunch of PZT fibres (140μm of diameter) in a needle-plane configuration The structuring is operated in doped castor oil. The experimental conditions: (a) 2kV@50Hz; (b) 2kV@1kHz

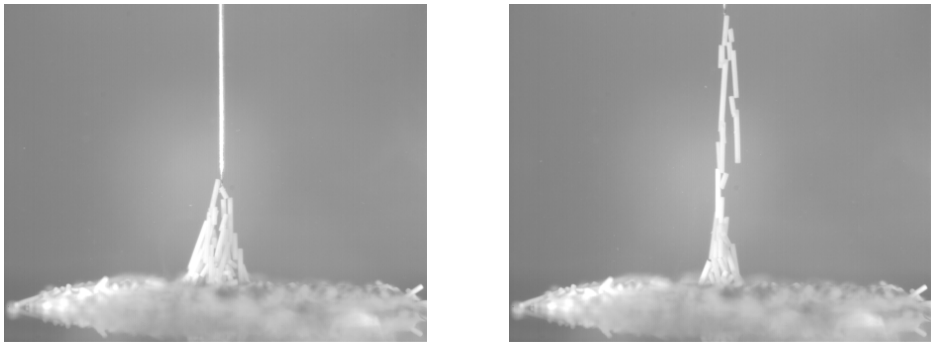

Figure 9. 62: : Structuring of a bunch of PZT fibres (140μm of diameter) in a needle-plane configuration The structuring is operated in silicone oil doped with the 2.5%vol. of Butyl Alcohol.

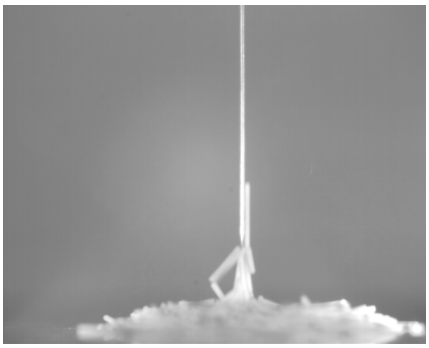

Figure 9. 63: Impossible structuring of a bunch of PZT fibres (140μm of diameter) in a needle-plane configuration The structuring is operated in IsopropylAlcohol (2kV@1kHz)

9.4.3.4. Analysis of the phenomenon in air

In this subsection, an experiment conducted in the same conditions as the other experiments in 9.4.3, but in air, is presented. This experiment was carried out to justify the initial choice to operate the micromanipulation in a dielectric fluid.

The observations show that applying a voltage of 2kV at 1kHz it was impossible to obtain any structuring. Increasing the frequency to 10kHz (the magnitude was decreased to 1kV, due to amplifier limitations), a behaviour very similar to the one observed at 7kV and 50Hz was observed. The formation of some sort of unstable structuring occurred. It was very unstable and accompanied by an intense oscillatory motion of isolated fibres.

This result demonstrates that also the breakdown resistance and the charge mobility inside the fluid can play a role. Given that the field of inception for corona in air is around 3kV/mm (one order of dimension lower than a liquid), probably the activity of injection through the tip is more important in the case of air. Moreover, in air, also the mobility of the charge is around a thousand times bigger than in a liquid. This means that any injection phenomena would take a lot longer before relaxing. These two considerations could justify why, the same kind of effects observed in a liquid were also observed in air, but the effects happen in air for a lower voltage and a higher frequency.

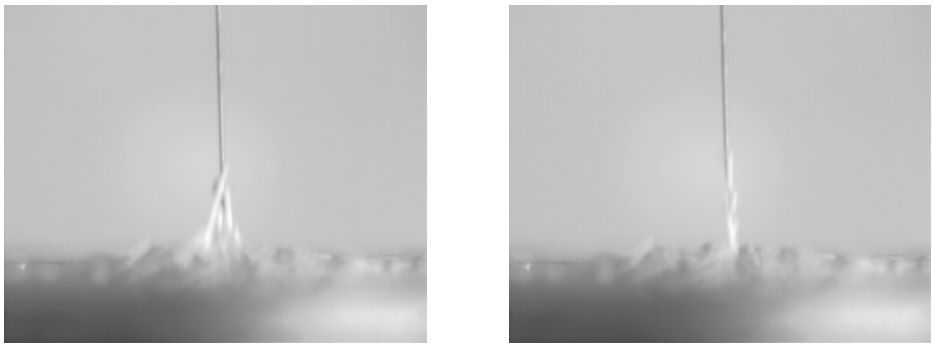

Figure 9. 64: Structuring of a bunch of PZT fibres (140μm of diameter) in a needle-plane configuration, The structuring is operated in air. The experimental conditions: (a) 1kV@10kHz; (b) 2kV@1kHz

9.4.4. THE BEHAVIOUR VARYING THE PZT FIBRE CHARACTERISTIC

9.4.4.1. Analysis of the influence of the conductivity

A particularly important question which needs to be addressed before a complete picture of the structuring process can be obtained is the one of its sensitivity to the fibres' conductivity. To improve the understanding of this particular aspect, a series of experiments was carried out by exposing a batch of PZT fibres, 140μm in diameter (length between 1 and 2mm), to the electric field generated between a plane and a needle-like electrode with a diameter of 120μm and a tip radius of 6.5μm. But, in this case, the fibres were first drenched in water. Immediately after the dip, the fibres were left in contact with some absorbent paper to remove the excess water. The wet filler obtained in this way was used a few minutes later.

The dip process, supplied to a sample of wet fibres coated with a film of water, was assumed to be able to increase the conductivity by a few orders of dimension, and at least up to 10^{-8}S/m. However, no analysis was undertaken to try to characterise the water film structure, or the percentage of water adsorbed on the fibres.

The applied voltage was 2kV in magnitude, and both a DC signal and an AC signal (frequency of 50Hz and 1kHz) was tested.

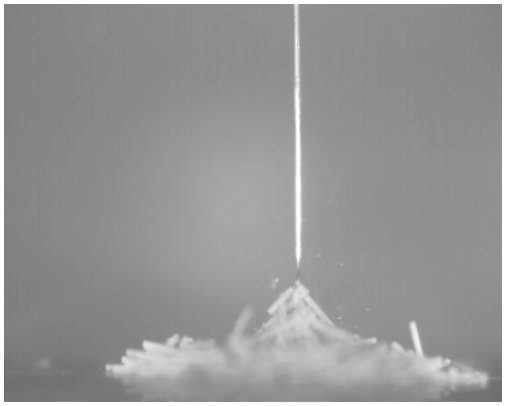

Figure 9. 65: Impossible structuring of a bunch of wet PZT fibres (140μm of diameter) in a needle-plane configuration (2kV@DC)

In DC a behaviour like the one referred for low frequencies at 7kV on the dried fibres was observed. The fibres were continuously attracted and then repulsed and therefore no pick-up was possible. The behaviour was almost identical for positive and negative bias. In the AC cases, the structuring was still not very coherent, however a small chain of particles was established and one or two fibres was captured.

The phenomenon was not very different at 50Hz or 1kHz. When the needle entered into contact there was a generation of gas from the contact point, but also from the inside of the bunch. This gas generation was more intense after the contact established, and the bubbles moved slowly. Then a fibre came into contact with the tip. This contact was persistent even after the field was switched off. The only difference between the phenomenon at 50Hz and at 1kHz is that the averaged bubble diameter was 160μm and 20 μm respectively.

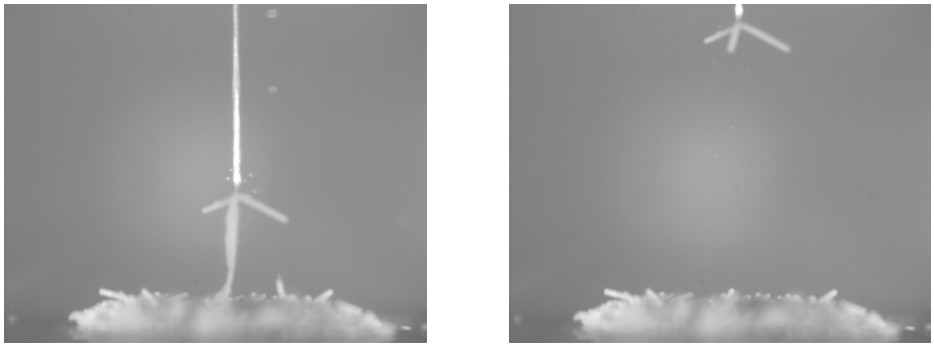

Figure 9. 66: Structuring of a bunch of wet PZT fibres (140μm of diameter) in a needle-plane configuration (2kV@50Hz)

Figure 9. 67: Structuring of a bunch of wet PZT fibres (140μm of diameter) in a needle-plane configuration (2kV@1kHz)

9.4.4.2. Analysis of the influence of the fibres dimension

In this chapter the importance of the particle dimensions in the electric field structuring was further investigated. More exactly, a group of fibres was exposed to the field created between a needle-like upper electrode and a parallel plane bottom electrode. The applied voltage was at 1kHz and 2kV, and the different materials tested were:

- A sample of powder issued from the dry crushing of some PZT5A fibres; the main grain size was between 1 and 5μm, normally with an aspect ratio of between 1:1 and 5:1
- Some PZT 5H fibres 30μm of diameter, around 1mm long, produced using the sol gel processing
- Some PZT 5A fibres 260 μm in diameter, 1-2mm long, produced by extrusion and always supplied by Ceranova Corp.

In the case of the powder, the observations were very similar to the case with bigger fibres. If the field was applied, and the needle was in contact with the powder batch, moving upward the needle, a conical shaped structuring was produced. Continuing to raise the needle, the continuity of the structure was gradually compromised, until only a certain amount of fibres, forming a chain-like structure separate from the bunch remained in contact with the needle.

Figure 9. 68: Structuring of PZT powder in silicone oil. The voltage applied is 2kV@1kHz

There are two principal differences between the powder case and the fibres' case. The first one is the dimension of the structuring. The structuring phenomenon happened on a considerably smaller scale; the PUA was almost the same but the mass of particles involved was considerably lower. This could be due to the fact that the interparticle force varies proportionally to the volume square of the particle, and the weight of the particle is proportional to the volume cubed.

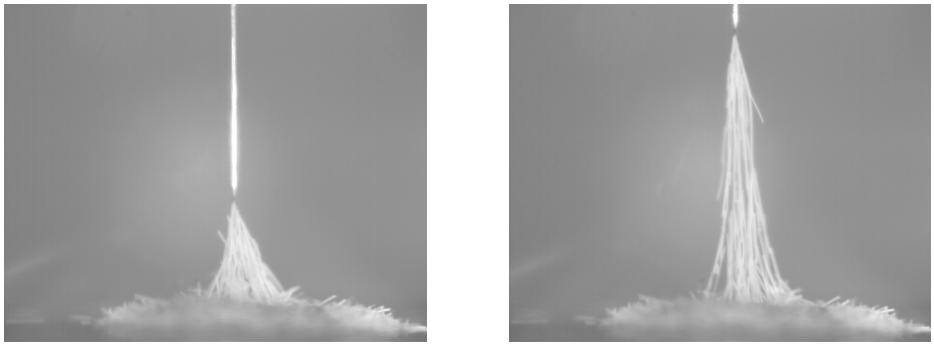

Figure 9. 69: Structuring of a bunch of PZT fibres (30μm of diameter) in a needle-plane configuration (2kV@1kHz)

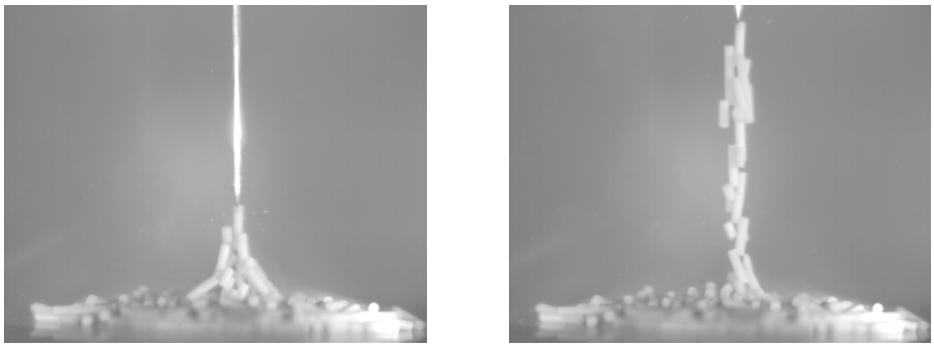

Figure 9. 70: Structuring of a bunch of wet PZT fibres (260μm of diameter) in a needle-plane configuration (2kV@1kHz)

The second and even most important difference during the structuring of a powder were that a lot of instabilities were observed. These instabilities caused the structure to change shape continuously, and it was possible to see how, in particular near the tip, the grains of powder presented a lot of oscillations. This result is important because it can add a further proof to the theory that charge transfer between the tip and the particles exists also at 1kHz. The fact that no particle vibrations were observed in the case of

bigger fibres is due only to the bigger fibres' inertia. If the particle volume decreases by a few orders of dimension, the relaxation frequency would be higher and then, some instabilities can be visualised also at 2kV and 1kHz.

9.4.5. THE STRUCTURING BEHAVIOUR USING CONDUCTING MATERIALS

With the objective of extending the structuring process to capture fibrous materials other than piezoelectrics, it was decided to carry out a series of investigations using conducting materials. The materials we tested were: carbon fibres and copper rods.
To be able to use the results for comparative purposes, a needle-plane electrode configuration was used. The needle diameter was 120μm, and the tip radius 6.5μm.

9.4.5.1. Carbon fibres

A series of experiments using carbon fibres (the characteristics of the fibres are described in section 5.4) was carried out in different conditions of voltage magnitude and frequency. The results are reported in the table 9.7.

Table 9. 7: Summary of a series of experiment showing the behaviour of a bunch of carbon fibres when exposed to the field generated between a needle-like electrode (120μm of diameter) and a bottom flat electrode. The (**), means that to achieve the structuring, it was necessary to be in contact.

V (kV)	Freq. (Hz)	Inception height (mm)	Capture or structuring possible (YES/NO)	Bubble generation (YES/NO)	Sparks generation (YES/NO)	Fibre released after switch off (YES/NO)
0.1	1000	0(**)	YES	YES	NO	NO
0.3	1000	0(**)	YES	YES	NO	NO
2	DC	4	YES	YES	NO	NO
	50	2.5	YES	YES	NO	NO
	1000	1.5	YES	YES	NO	NO
7	DC	6	YES/NO	YES	YES	-
	1000	6	NO	YES	YES	-

In each experiment conducted from the threshold voltage of 0.1kV to the maximum voltage of 7kV, bubble generation was observed. In most cases the diameters of the bubbles were between 100 and 600μm, considerably bigger compared with the cases analysed in the previous sections. The bubbles did not move fast, but, on the contrary, after their generation they had the tendency to stick to the carbon fibre for several seconds. Only as a result of the application of a 7kV some sparks were observed. As it is possible to see from table 9.7, a structuring was always possible, except when some sparks were generated. In particular, applying 7kV@DC, it was possible to see how the fibre moved constantly and some structures were continuously generated and destroyed by the sparks.

Figure 9. 71: Structuring of a bunch of carbon fibres in a needle-plane configuration (2kV@DC)

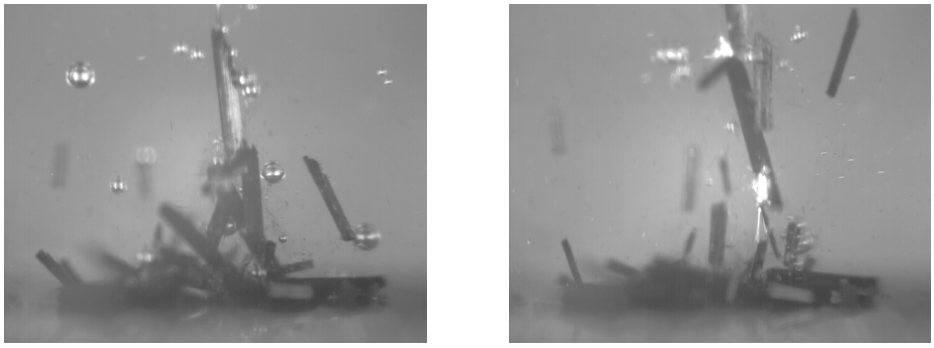

Figure 9. 72: Structuring of a bunch of carbon fibres in a needle-plane configuration (7kV@DC)

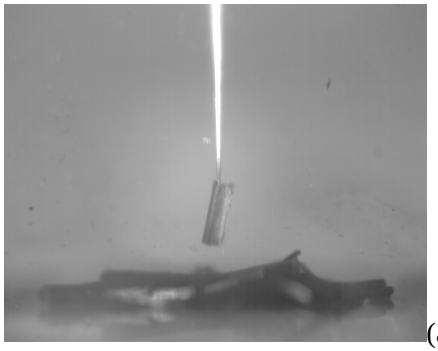
(a)
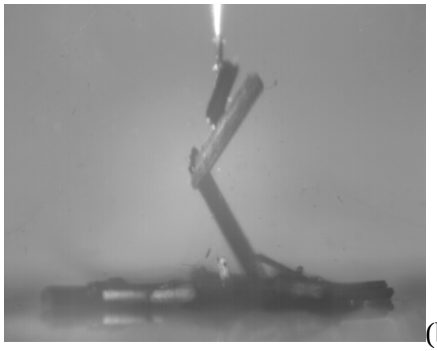
(b)

Figure 9. 73: Structuring of a bunch of carbon fibres in a needle-plane configuration. The experimental conditions: (a) 0.1kV@1kHz; (b) 0.3kV@1kHz

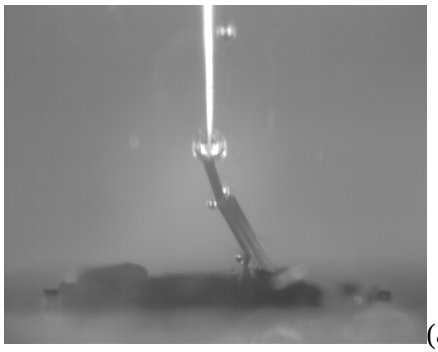
(a)

(b)

Figure 9. 74: Structuring of a bunch of carbon fibres in a needle-plane configuration (2kV@1kHz). (a) uncoated bottom electrode (b) PTFE coated bottom electrode

The fibres captured during the application of the field were never released after the field was switched off. This derived from the intense electro-polymerisation activity occurring in this case.

It is very important to consider that, with carbon fibres, structuring was possible also in DC. However, it is difficult to establish exactly the right nature of the adhesion forces. They could be caused by a strong electro-polymerisation that was counterbalancing the bad effects of the injection.

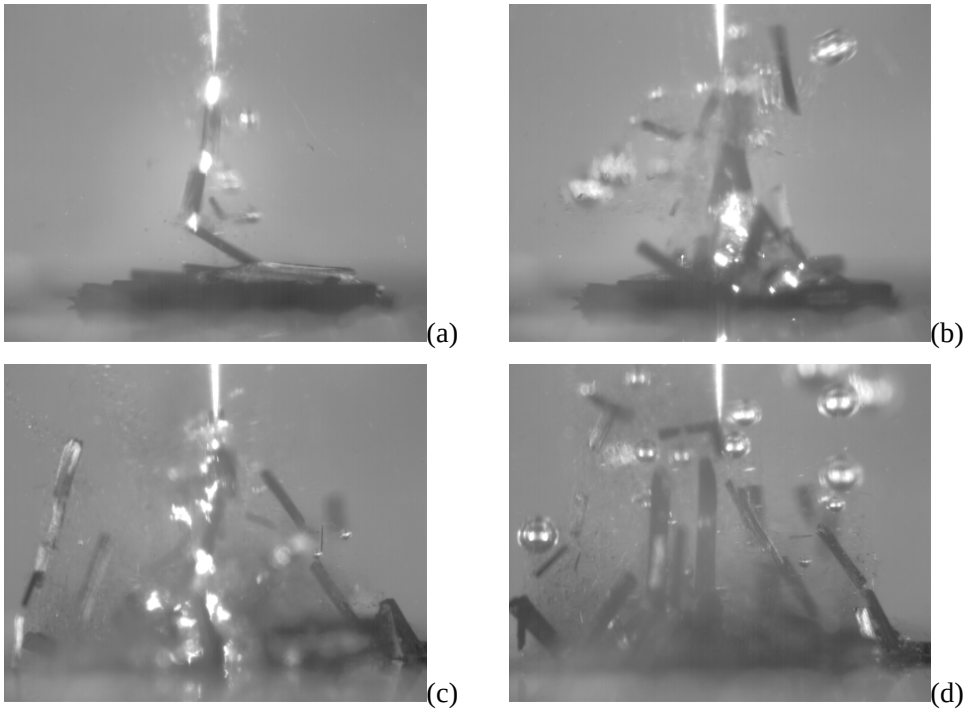

Figure 9. 75: Impossible structuring of a bunch of carbon fibres in a needle-plane configuration 7kV@1kHz). (a)(b)(c)Spark generation during the field application (d) Right after the field is switched off

A final observation can be made concerning the structure of the chain generated with carbon fibres. As seen in the pictures in section 9.4.5.1, the structures generated with carbon fibres did not give any cone shaped structuring. They tended to give some structures like the ones generated in PZT at low frequency. Nevertheless, operating the structuring using a PTFE coated bottom electrode to avoid any conducting phenomena, a conical shaped structuring can be achieved. Moreover, the diameter of the generated bubbles reduced.

9.4.5.2. Copper fibres

This section reports the results of an experiment in which a group of copper rods resting on a PTFE coated bottom electrode was exposed to a voltage of 2kV applied at 1kHz using a needle like the one employed in the previous experiment.

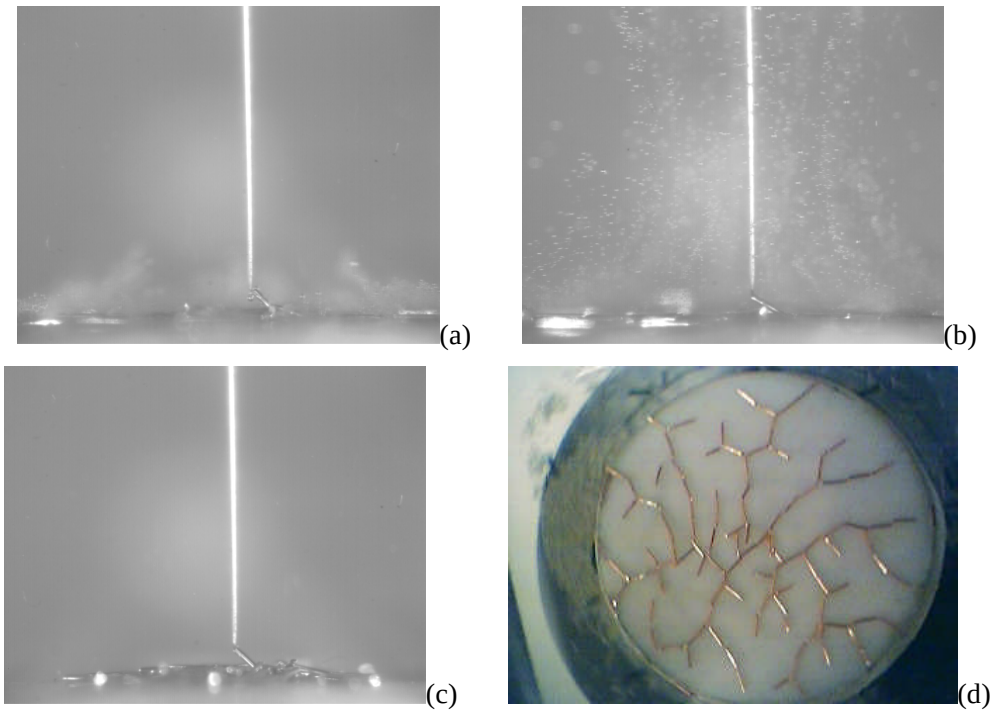

Figure 9. 76: Behaviour of a bunch of copper rods in a needle-coated plane configuration. (2kV@1kHz). (a) Establishing of the contact (b) Bubble generation (c) Equilibrium, no more bubble generation (d) The copper rods formed an interesting fractal structure.

When the needle is at h=1mm, a metallic fibre moved toward the tip establishing the contact. Instantaneously a massive bubble generation occurred. Then, few milliseconds afterwards, an expansion of the fibre bunch was observed, like if there was a repulsion between the fibres. The final structure that formed on the bottom electrode was an interesting fractal-like structure visible in figure 9.76(d).

9.4.6. ANALYSIS OF THE INFLUENCE OF THE DRAG SPEED

To show the importance of the drag speed on the process, a couple of experiments at a voltage of 2kV at 1kHz , in the same conditions as those described in section 9.4.1 were set up. Nevertheless, two different drag speeds were used.

The experiment shows that, as expected, considering all the forces acting on the system, the drag speed is one of the active factors in the study. If the speed increased from 2mm/s to 20mm/s, the PUA decreased from 40° to 30°. However, it means that it is possible to mobilise the fibres at a considerable speed, without loosing too much in structuring performance.

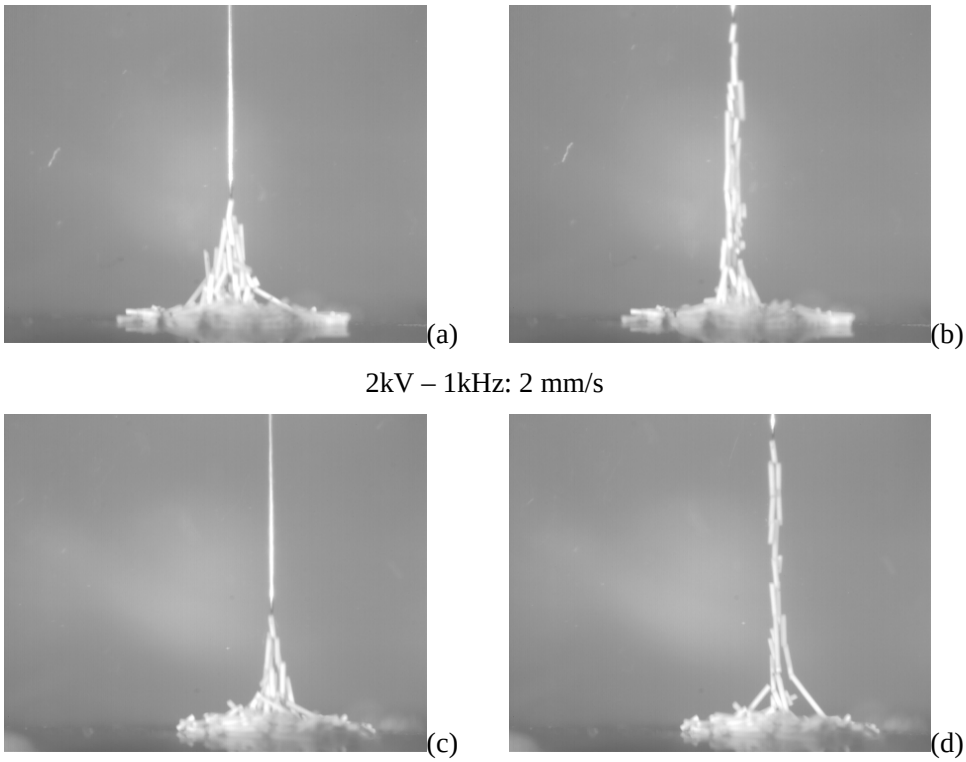

Figure 9. 77: Structuring of a bunch of PZT fibres (140µm of diameter) in a needle-plane configuration (2kV@1kHz). (a)(b) Drag speed=2mm/s (c)(d)Drag speed=20mm/s

9.4.7. ANALYSIS OF THE BEHAVIOUR OF THE FIBRES CROSSING THE INTERFACE AIR – OIL

To design an experimental setup for a use of the process in industrial application to be designed, it is important to understand the characteristics of the fibre-needle contact, when the needle is passing the boundary between the air and liquid.

An experiment, shown in figure 9.78, was setup applying a voltage of 2kV and 1kHz to a needle with a diameter of 120μm. In these experiments it was shown that after a group of fibres is captured by the needle, and it is carried through the air-liquid boundary, the fibres still get the contact. Only occasionally, during the crossing, the fibre in the lowest position detaches from the group dropping down into the liquid.

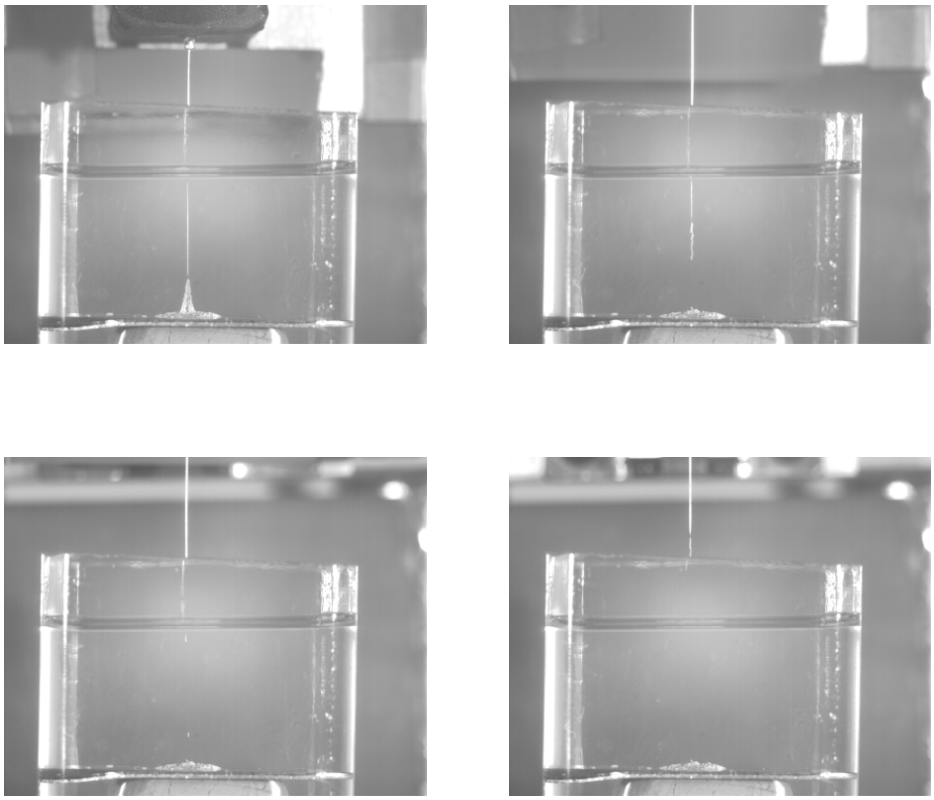

Figure 9. 78: Structuring of a bunch of PZT fibres (140μm of diameter) in a needle-plane configuration (2kV@1kHz). These pictures show how by crossing the air-oil interface the capturing performance is not modified

9.5. DISCUSSION OF THE RESULTS

The principal objective of this chapter was to investigate the structuring which occurred when a group of fibres was exposed to the divergent field between a sharp needle-like upper electrode and a bottom flat electrode. The physical mechanisms and the principal factors influencing the process have been investigated. Moreover, the best operational conditions in which to achieve the desired micromanipulation were identified.

The phenomenon has been analysed with respect to the voltage magnitude and frequency, in different fluids and for different fibre materials. The upper electrode was an acupuncture needle with a diameter of 120μm and a tip radius of 6.5μm. To deepen the needle-fibre contact in the structuring, a series of experiments using different electrode configurations was carried out.

Considering the high number of factors influencing the phenomenology of the electric field structuring, two experimental protocols were established. This enabled the general trends to be extrapolated and the crucial variables identified.
The main experimental protocol was called the “no contact mode”. It was executed by applying the voltage when the distance between the two electrodes was 6mm. After that the upper electrode moved down, until at least one fibre was attracted and made contact with it. The motion was stopped and this distance was noted as the inception height (h_{inc}). After that the electrode moved up at a constant speed of 2mm/s. The motion of the upper needle stopped for a height greater than 6mm and the voltage was switched off. The second experimental protocol, used only in some particular cases, was called “in contact”. It was identical to the first one except that the upper electrode was first moved into contact with the fibre bunch, and then the voltage was applied.

A set of macroscopic indicators was defined to describe quantitatively the phenomenology. These indicators are directly related to some important physical factors. These indicators are:

- inception height (h_{inc}): this is the height at which the first fibres enter into contact with the needle. This indicator it is directly in contact with the electromotive body-force exerted by the needle on the batch of fibres. Looking at equation (2-89), assimilating the fibre group to a continuous ER fluid, this force can be considered as the net force that the electric field exerts on the fluid-air interface.

- pickup angle (PUA): this is the vertex angle of the cone shape assumed by the bunch of fibres when they are pulled up by the upper electrode at a conventional height of 3mm. There is a direct correlation between this factor and with the interparticle force inside the bunch of fibres.

- the maximum height (h_{max}): this indicator expresses the maximum height at which it is possible to carry a fibre. This indicator correlates with the force exerted by the needle on the captured fibre.

A general description of how the process can evolve is given in the flow chart in figure 9.79.

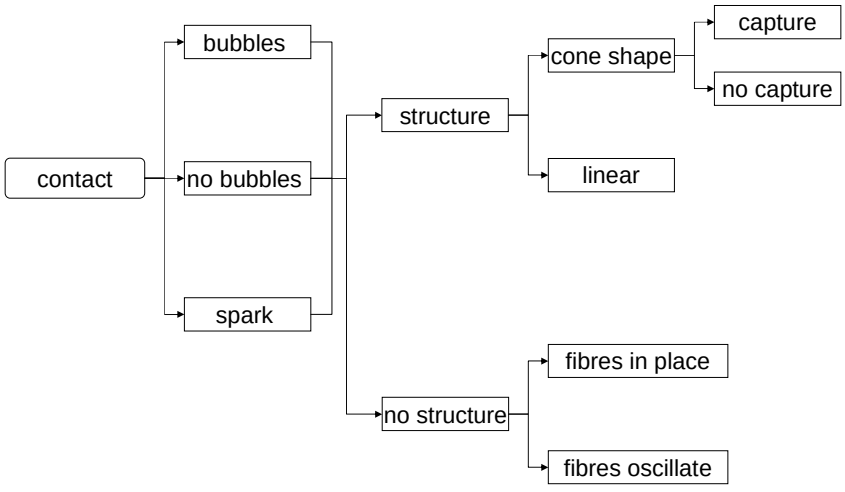

Figure 9. 79: General description of how the process can evolve.

When the needle is moving down, and it is in proximity of the fibres group, the fibres start to orientate, aligning themselves following the field lines. Moreover, they concentrate in the area closer to the needle axis, and try to move toward the tip. Then, continuing to move the needle downward, at a certain point the first fibre reaches the contact with the needle.
In some cases, once the needle reached the contact with the fibre bunch, there was a fluid decomposition with bubble generation.
In the case of PZT fibres, this phenomenon, although it was also observed at lower voltage sometimes, became marked only after the voltage overcame 3kV; this was true at every frequency tested. The size of the bubbles was relatively small (10μm diameter). When the voltage was above 5kV there was a considerable EHD motion that pushed the bubbles far from the needle-fibre contact area.
In the case of carbon fibres the bubbles were generated at every frequency and every voltage we tested. In this case the bubbles dimensions were up to 6-7 times bigger compared to what was observed in the PZT case, but no EHD motion was observed. For a voltage of 7kV also some sparks were visible.
After the contact was established the needle started to rise up. At that point it was eventually possible to observe a fibre structuring (the bunch follows the needle forming a chain-like structure).

In the PZT case, where a DC field was applied, no fibre structuring was achieved. Moreover, on the application of a voltage of 7kV, a massive electrophoretic motion of fibres was observed. Also in AC, a structuring was never observed when the field overcame the 5kV mark. However in that case, for low frequencies (50Hz) the reason for the failure of the structuring was the oscillating behaviour of the fibres. For higher frequencies (1kHz), the structuring failed simply due to a lack of force existing between the needle and the fibres. Conversely, at every frequency, for a voltage below 4kV, a structuring was always observed. The observed structures had two different configurations:

- a “cone-like” structure
- a “pearl-chain” structure

The conical one was always achieved when the frequency overcame 500Hz, while the other appeared for frequencies from 10 to 100Hz. Moreover a “pearl-chain” resulted also after a group of PZT fibres was exposed to a 1kHz signal on which a bias DC signal was superimposed.
In the case of carbon fibres a structuring was always reached, also when a DC signal was applied. The only exceptions were the cases in which a spark occurred, when a voltage of 7kV was applied. In the carbon fibre case, the structuring almost always followed a “pearl-chain” configuration.
The “pearl-chain” configuration was the more suitable one in the case of more conducting particles. For example, the same configuration resulted from a structuring operated on wet PZT fibres.

Once a structuring was generated, when the needle-like upper electrode was lifted up still further, the formed structure started to elongate and became thinner. This is because, the lateral column, being in a region of lower electric field, are always the first ones to disaggregate. However, this does not compromise the fact that a percolating structure of fibres connecting the needle and the bottom electrode can still exist, until when the needle reaches a critical height. At this point two situations were possible:

- The bunch of fibres separated into two parts. A certain amount of fibres dropped, and the another part remained attached to the upper electrode. This was the essential condition for fibre capture. In fact, after separation it was considerably easier to rise up the captured fibres, because they were no longer affected by the electrostatic adhesion with the bottom electrode. Once the separation occurred, the residual bunch was moved up (eventually crossing the boundary between the liquid and the fluid), until the field became so weak that the force exerted by the needle was not sufficient to keep the fibres in place. This distance was h_{max}.

- The adhesion between the needle and the bunch was not strong enough, and therefore, the cohesion force inside the bunch was higher than the pickup force exerted by the needle on the bunch. In that case, above a certain height

the needle detached from the bunch, and the bunch remained compact (sometimes partially structured) and in contact with the bottom electrode. No capture of fibres was possible in this case.

In some cases the field was switched off before reaching h_{max}, to test how the particles were released.
For PZT particles, a release of the particle, after the voltage switch-off did not occur when the voltage was bigger than 3kV, or even at 2kV, when the frequency was bigger than 3kHz. In all these cases of persistent particle capture after the voltage switch-off, a generation of bubbles was observed while the voltage was being applied.
The same principle was followed in the case of carbon fibres. In this case in all experiments bubble generation was observed. Consequently, in all experiments release of the fibres after the switch-off was never observed.

Although, all the considerations outlined above are only qualitative, a series of quantitative considerations was identified after reference to the series of indicators as described above.

The indicator h_{inc} was not dependent on the electric field frequency, but it increased when the voltage increased.
This behaviour is absolutely coherent with the theory. In fact the value of h_{inc} gave indication of the dielectrophoretic electromotive body-force that the upper electrode exerts on the system of fibres. This force depends only on the external field and on the dielectric properties of the material. Considering that the dielectric properties of the material are constant in the frequency range used, it is coherent that the phenomenon was not dependent on the frequency. However, voltage influence is predictable, and its influence was confirmed by the experiments.

The other indicator PUA usually gives an idea of how strong the cohesion between the fibres in a bunch is, with respect to the weight force and the viscous force inside the fluid. Conversely to h_{inc} this indicator was shown to be dependent on the frequency rather than on the voltage. Precisely, PUA increased when the voltage increased up to

5kV (above that no more structuring occurred). Moreover, PUA increased when the frequency increased, reaching a saturation at 1kHz.
This behaviour implies an important consequence. If the interparticle force between the fibres followed an ideal behaviour as described by the dielectric model there would be no dependence on the frequency. At that point it is evident that some effects other than the fibre polarisation are involved in the structuring of piezoelectric fibres.

The last indicator h_{max}, it is particularly important in studying fibre capture efficiency. Giving particular attention to the case where no bubbling has been visible, and consequently a release of the rod after the switch-off was always possible, the higher value of h_{max} was measured when a voltage of 2kV at 1kHz was applied.

A series of experiments on a system characterised by the injection free upper electrodes was conducted to increase the understanding of the interaction between the tip and the fibre. The upper electrodes chosen were:

- a flat metal plate, to check a system in which, besides the absence of injection, no electric field gradient exists.
- an 8mm diameter metallic sphere, to follow how the phenomenon changes when a weak field gradient is introduced
- a sharp needle coated with a thick insulating coating to see what happens in a system characterised by the same high gradient but with no injection occurring.

The first major conclusion was that in all these injection free systems, no fibre capture occurred. This means that the internal cohesion in the bunch was always higher than the adhesion between the upper electrode and the bunch. Two possible reasons for that are:

a) In the case of flat electrode and spherical electrode, the gradient of the electric field was too low. In this case the gradient of the interparticle force induced inside the bunch was so low that it was impossible to find a section in which the condition $F_{up}<F_{down}$ (see section 9.2) was verified.

b) In the third case, even if the gradient was still high, the distance between the needle and the bunch, imposed by the coating, reduced the image attraction between the needle and the fibres, and consequently the capture performance.

The second important result was the dielectrophoretic effect observed in DC. In fact, in this case, even if the chain stability was largely compromised by the intense EP oscillation of the particles, different to what happened with a needle-like upper electrode, a certain chaining effect was observed. This was resulted from the tendency of the fibres to form some columnar agglomerations due to the polarisation forces that at short distances overcome the EP effect.

The third important results was that, defining some structuring performance factor (with an equivalent meanings than PUA), it was confirmed a trend showing a performance increasing from low frequency up to 1kHz.

A further series of evaluations was carried out to also check the influence of other factors playing a role in the structuring process. A list of these conclusions is reported below:

- Needle tip radius: an experiment conducted using a needle, with a tip radius bigger than the usual acupuncture needle, showed that the capture process was less selective; it was impossible to capture a single fibre on the needle tip, only a group of fibres could be captured.

- Fluid viscosity: a silicone oil with a viscosity double that normally utilised was tested. The PUA reduced by 10%; this observation confirmed that the difficulty of achieving a structuring increases with the fluid viscosity.

- Drag speed: an increase of 10 times the drag speed induced almost the same effect as a doubling of the viscosity

- Fluid dielectric constant: an experiment run in Castor oil showed a decrease of the PUA of 25%. This result could be surprising considering that the Castor oil permittivity is almost double than the silicone oil. However, that result becomes meaningful considering that the Castor oil's viscosity is up to 20 times bigger than the one of the silicone oil.

- Fluid conductivity: a series of experiments showed that if the conductivity of the oil increased, as expected, PUA decreases.

- The fibre dimension: the fibres' diameter was varied between 30 and 260μm and no major effects were observed in the structuring phenomenon. An important result has been achieved on some experiments carried out on a batch of PZT powder with grain size varying between 1 and 5μm. In these cases, also when the frequency increased to 1kHz, some instabilities were still visible near the tip. Such instability was not visible during the structuring of bigger fibres.

An experiment carried out in air was particularly interesting. The result was surprising because in air, at 1kV and 10kHz, exactly the same behaviour was observed as in the case of silicone oil at 7kV and 50Hz. This was due to the fact that in air:

- The inception voltage for the corona injection is ten times lower than in a dielectric oil.
- The viscosity of air is negligible compared with the one of the silicone oil.
- The ionic mobility in air is more than a thousand times bigger than in oil, and consequently the injection relaxes above 10kHz

Considering the complete description of the electrostatic capture of the fibres proposed above, a complete description of the phenomenon can be summarised in the chart in figure 9.80.

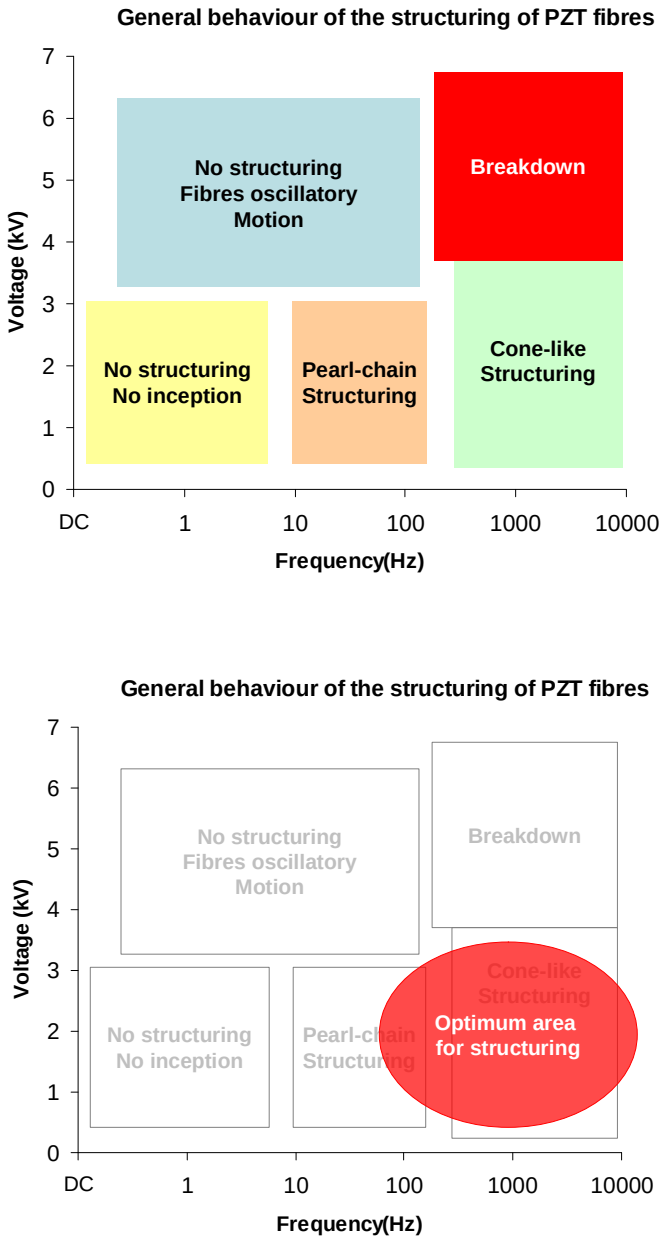

Figure 9. 80: Chart summarising all the behaviours that is possible to visualise exposing a bunch of fibres to the divergent electric field

In DC at low voltages neither structuring nor inception is possible. A structuring can always be achieved in AC but only at low voltage. An increase in the frequency means that the structuring mode moves from a “pearl-chain” to a “cone-like” configuration.

Increasing the voltage, the structuring results more and more difficult to achieve. For lower frequencies the structuring is impossible because the fibres are unstable and affected by an oscillatory motion. At an increased frequency even if the oscillations stop, the structuring is compromised by the occurrence of a breakdown in the gap.

To understand the structuring behaviour described in section 9.2 it is necessary to consider that the phenomenon is controlled by the following factors:

1) The nature of the contact between the upper electrode on the group of fibres (which is related to the magnitude of the force that the upper electrode can exert on the group).
2) The interparticle forces
3) The adhesion of the fibre to the bottom electrode.
4) The gradient in the interparticle force induced by the upper electrode in the bunch of fibres

In an ideal insulating fluid, the force exerted by the needle on the bunch of fibres should be issued only from polarisation forces. However, as the FEM simulation showed, in the conditions employed in our experiments the electric field was too high to still consider the fluid a perfect insulator. In this situation a series of phenomena can then happen:

- An electric field enhanced dissociation with increase of the ohmmic conductivity in the gap; this phenomenon could have, as a consequence, some fluid instabilities due to AC electro-osmosis.
- An injection of homocharge through the needle tip; in this case, if the frequency is low enough, the phenomenon could have, as a consequence, an instability.
- A charging of the fibre by induction, after contact, if the fibre has a certain conductivity.
- A micro-breakdown in the gap, if the current density is too high, with degradation of the fluid, generation of gas bubbles and sometimes electro-polymerisation.

An important consideration arising from this list is that, in any case, there is a transfer of homo-charge between the needle and the fibre, a repulsion is generated and as a consequence, an EP effect arises. Therefore, in the description of the dynamic of the needle-particle force, it is not enough to consider an effect arising only from the polarisation, but it is necessary to consider also an effect due to the EP.

Analysing the interparticle force, it is necessary to consider the same conductivity issues important also in the case of the needle-fibre interaction. In fact a series of FEM simulation of the field in the interparticle gap showed that a failure of the dielectric should be taken into account. In this case the situation is describable with a model like the one proposed by Chen et al. (1991). Nevertheless given that a charge transfer occurs between two insulating particles, an injection contribution would be less likely.
When the field is switched on, an increase in the conductivity in the gap generates a charge transfer between neighbouring fibres and the electric field in the gap decreases. Since then the condition of insulation is re-established, and the interparticle force again becomes dielectrophoretic.
When the particles are conducting, the field is dictated by the ratio between the particle and fluid conductivities (see section 3.4.2). Therefore, if the fluid is an insulator, the field in the gap becomes more intense and in the gap the conductivity starts to rise. Unfortunately, as the particle also conducts, the resulting current become very intense. This high current density induces a fluid degradation higher than in the case of the PZT particle. This is because the size of the bubbles, generated by the degradation of the fluid, was bigger for the carbon fibres than for the PZT ones. Moreover, working with carbon fibres, for high voltages also a generation of sparks was observed. This phenomenon was never observed working on PZT fibres.

At that point, to have a complete picture of the phenomenon, they are still a couple of aspects to focus more in detail:

a) to explain the characteristics of the phenomenon in DC
b) to understand the differences between the two kinds of structures (i.e. pearl-chain and cone-like) it is possible to observe, at lower and higher frequency

The behaviour we observed, in condition of low electric field, when a DC voltage was applied, was essentially due to the charge transferred by the needle to the fibre. Moreover the situation was aggravated by the presence of some injection induced fluid instabilities. This consideration is confirmed by the fact that, in the injection free systems, an electric field structuring was observed also in DC, even if the stability of the columnar structures was strongly conditioned by the EP response.

A substantial characteristic of the two different kinds of structures can be clarified analysing the FEM simulations shown in section 9.3.2., and considering what has been already pointed out in chapter 9.3. When we explained the meaning of the process indicators, we anticipated that the interparticle cohesion force in the "pearl-chain" configuration is always weaker than in the "cone-like" one. Consequently, at that point it becomes important to understand what is the reason responsible for a similar weakening of the interparticle interaction, when the frequency decreased. At least three explanations can be proposed:

1) There is a charge transfer mechanism inside the interparticle gap that is time dependent.
2) There is a transfer of charge from the needle to the bunch of fibres. This charge generates a net charge on the bunch, generating a repulsive force between the particles. This contribution, added to the attractive DEP contribution, reduces the total attractive interparticle force.
3) There is a time dependent instability inside the gap.

Considering the three hypotheses, only the third one seems to be unsuitable. In fact, the frequencies under consideration, even though low, are already too high to allow an injection instability.
The first and the second hypotheses could both be active in the phenomenon.
Considering the first hypothesis, the fact that as the frequency was decreased the structuring factor decreased (even in a parallel plate configuration) gives credence to the hypothesis that some time dependent charge transfer mechanisms have to play a role in

the interparticle interaction. However, this effect alone, can not completely explain the phenomenon of the “pearl-chain” structuring. In fact this particular structuring mode only happened when the upper electrode was an injector. Therefore it is reasonable to assume that the charge transfer between needle tip and fibre bunch also has to play a role. And this role is the one to donate a charge to the fibre group, generating a consequent EP repulsion between the particles. Moreover, in these conditions, a lack in spatial uniformity in the phase factor can occur, all along the chain. This effect, described by Xujing et al. (1997), has been introduced in section 3.3.3.2.

Experimental evidence, further supporting this conclusion, is the difference in the structuring behaviour at 1kHz-2kV whether or not a bias was superimposed on the AC voltage. Another proof is given by the fact that the frequencies, at which, at low voltage, a “pearl-chain” structuring occurred, were the same as those at which, at high voltage, an oscillatory motion of the fibre was observed.

Still considering the charge transfer phenomena between needle tip and fibres, the structuring behaviour showed by a batch of PZT powder was considered particularly important. At 2kV and 1kHz, when normally the motion of the fibres with a 140μm diameter was relaxed, the powder (characterised by particles with a size a couple of orders below the fibres) oscillated in proximity to the tip. This observation supplied a further confirmation of the fact that the charge transfer mechanisms are still active at 1kHz. If the fibre with a 140μm diameter did not oscillate, it was just because its inertia was too high.

Considering all the experimental results and their interpretations, it can be affirmed that the best conditions in which to operate an electric field structuring are in the range of volt magnitudes and frequencies close to 2kV and 1kHz. These conditions minimise the microbreakdown effects, and maximise the strength of the needle-fibre interaction and the interparticle force. However, if the main interest of the structuring process is more oriented to the selectivity, probably at lower frequency, it is possible to find the most interesting experimental conditions and to exploit the characteristics of the pearl-chain structuring effect.

Chapter 10

OVERALL DISCUSSION

This chapter shall offer a summary of all the main experimental results and an overall discussion. All the main results which have emerged during the course of the thesis are here presented in a homogeneous manner.

10.1 SUMMARY OF THE MAIN EXPERIMENTAL RESULTS

The methodology we adopted, to attend the objectives previously declared, can be ordered in five main areas of activity:

1) Design and setup of the experimental process unit
2) Characterisation of the materials employed
3) Electrohydrodynamic characterisation of the needle-plane system without fibres
4) Analysis of the capture of micro-rods operated in a needle-plane system in three main configurations:
    a) a single fibre exposed to a DC electric field
    b) a single fibre exposed to an AC electric field
    c) a group of fibres a single fibre exposed to a DC electric field
5) FEM analysis

The main experimental results can then be listed following the same criteria.

1. Design and setup of the experimental process unit

A process unit for the remote and safe observation of the phenomena has been assembled.

2. Characterisation of the materials employed

The characteristics of fibres and fluids employed in the present study has been measured. In particular, a setup has been especially designed to measure the conductivity and the tribo-charge of the fibres.

3. *Electrohydrodynamic characterisation of the needle-plane system without any fibres*

   The unipolar charge injection through the tip of the needle we used in our experiments was characterised measuring the current with an electrometer. Moreover, also the electrohydrodynamic instabilities consequent to the charge injection, were characterised by PIV (Particle Imagery Velocimetry). This phenomenon is particularly important at low frequency.

4. *a Experimental observation of the behaviour of a single fibre exposed to a DC or a low frequency field (up to 50Hz)*

   In this series of experiments the charge transfer phenomenon was studied in both injection free configuration and non injection free configuration. The charge acquired by a particle through contact with an electrode was measured by analysing the particle motion recorded with the high speed camera. The phenomenon was considered not only with respect to PZT fibres but also conducting particles.

   The charge transfer on particles was analysed also when electrodes were coated with insulating materials. .

   The experiments in DC in a needle-plane configuration showed that it was not possible to capture a PZT rod on a needle tip by applying a DC voltage.

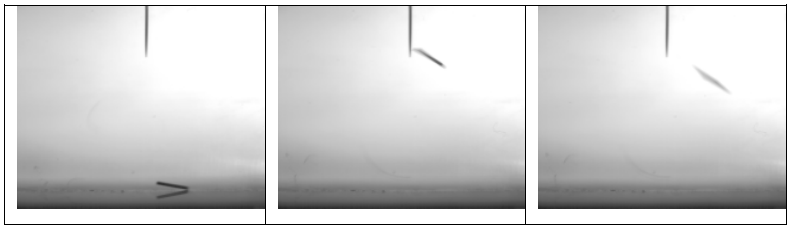

Figure 10. 1: pickup on a single fibre in DC. The fibre is forcefully repulsed (10kV).

Discharge can be avoided, and the fibre can be captured on the tip, through coating the needle tip with a coating thick enough to avoid any tunnelling or breakdown effect through the coating.

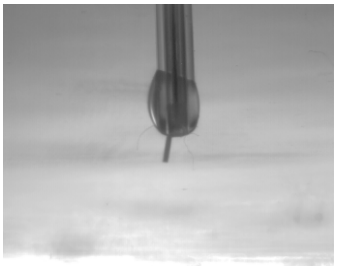

Figure 10. 2: Pickup on a single fibre in DC assisted by an insulator coating (10kV).

4. b Experimental observation of the behaviour of a single fibre exposed to an AC electric field

This set of observations showed the importance of the electrostatic adhesion between the fibre and the bottom electrode in the electrostatic manipulation. A fibre was captured, only when the bottom electrode was coated with a thick insulating layer of PTFE.

A series of experiments was carried out at different voltages. If the voltage was too high, the phenomenon of fluid degradation with generation of impurity occurred, often compromising the fibre pickup. The behaviour at 2kV 1kHz is shown in the figure 10.3.

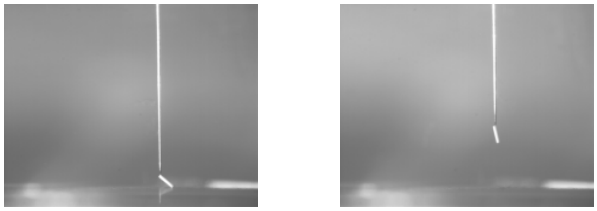

Figure 10. 3: Dielectrophoretic capture of a single fibre in AC (2kV@1kHz)

4. c Experimental observation of the behaviour of a group of fibre exposed to a divergent electric field

This configuration is the most interesting one for the analysis of the electric field structuring technique. The demonstration of its viability is strictly related to the exploitation in industrial applications.

To provide a complete description of the phenomenon, the effect of the following factors on the chaining effect was observed:

- the voltage magnitude
- the voltage frequency
- the voltage wave shape
- the electrode configuration
- the fibre conductivity
- the fluid characteristics
- the drag speed

Studies on a group of fibres, even without coating the bottom electrode, have shown that it is possible to pick up a long chain of fibres by using their mutual polarisation.

As in the case of a single fibre, in the case of a group of fibres, when the field is too high (V>4kV) there is a fluid decomposition, and the fibre dragging is less reliable or impossible. Moreover, also the frequency plays a crucial role. At low voltage (2kV), the following effects are observed

a. DC signal: no pickup exists
b. Lower frequency (i.e. a few tenth of Hz): a “pearl-chain” coherent configuration is created.

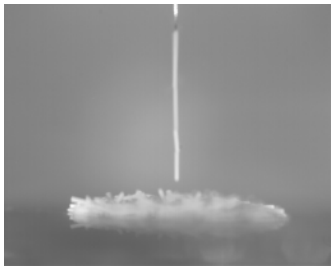

Figure 10. 4: “Pearl-chain” Dielectrophoretic structuring of a group of fibres exposed to an AC field (2kV@50Hz)

c. Higher frequency (i.e. between 0.5 and a few kHz): a “cone-like” structuring is observed

Figure 10. 5: "Cone-like" Dielectrophoretic structuring of a group of fibres exposed to an AC field (2kV@1kHz)

The experiments showed that the structuring phenomenon also depends on the signal wave shape. In particular, the efficiency of the structuring effect decreased considerably if a DC bias was superimposed on the original, zero-averaged alternative.

5. *FEM simulations*

   A series of numerical simulations was used to interpret the main experimental results, with and without fibres and in different configurations. From the simulations, the electric field, the force exerted on the fibres, and, in some cases, the acquired charge were computed.

10.2 OVERALL DISCUSSION OF THE RESULTS

An extensive discussion of the principal results achieved in the present research work was included at the end of each chapter as it became relevant. It is now opportune to discuss about the whole corpus of the experimental work presented in this research. In the course of this discussion the focus of the attention will be on the unity and the consistency of all the results obtained.

First of all, it is appropriate to speak about the properties of the materials, and in particular about the properties of the PZT fibres and the dielectric liquid.
The dielectric constant of the PZT fibres was measured. The measured value of 1800 was very close to that of the bulk material. Conversely the conductivity was one order

of dimension higher than the bulk ceramic; the measured value was $1\text{-}2\times10^{-10}$ S/m. This abnormality is attributed to a thin not-uniform film of moisture always formed on the surface of any body exposed to air. In this condition no relaxation of the fibre polarisability (see sect.2.3.3) phenomenon is expected at ordinary frequency (τ = 100s).

The properties of the fluid were also tested. In particular, the silicone oil showed an ohmic conductivity of around 10^{-12} S/m, except for high values of the electric field, at which a sharp increase of the ohmic conductivity (Onsager's behaviour, see sect.2.4.4) was observed. This increase was caused by electric field enhanced dissociation.
In proximity to a very sharp needle-tip, a region characterised by a highly divergent electric field, a charge injection was also identified. It has been characterised by measuring the current. Moreover, the observation showed that this injection, for voltages above 4kV, was able to induce a fluid instability, with generation of a jet. The fluid instabilities were studied by PIV and were never observed for frequencies above 2Hz. This relaxation frequency for the instability is in complete agreement with the theory (see sect.2.5.3.2), which predicts an incubation time of 0.56s for the instability. Nevertheless, the phenomena of injection were clearly visible in the area surrounding the needle tip up to 50Hz.

A series of experiments was completed by exposing some particles to a DC or a low frequency electric field. The fibres tested were both, insulating PZT fibres and conducting fibres.
Analysis of the charge transfer mechanism between the fibres and the surrounding system was made possible by the study of the motion of the particles when exposed to a uniform electric field. Comparison of the experimental values and the theory, revealed that the values were always considerably lower than expected. However, despite the difference in the charge mechanisms, PZT and conducting particles carried almost the same amount of charge.
Moreover, the importance of the tribocharge was analysed to understand the electrohydrodynamic behaviour of a particle, initially resting on an insulator coated bottom electrode.

A series of experiments was carried out to test the possibility of capturing a fibre applying a DC field in a needle-plane configuration. This was impossible; once the PZT fibre reached the top electrode, it was forcefully repelled far away. This mechanism was due to a charge transfer from the needle-tip. In fact, no repulsion existed when the needle was coated by an insulator, in which case a capture was possible. It is interesting to notice that, after rough estimation of the charge carried by the particle, it was verified that, the amount of charge transferred by the needle to the fibre can be calculated applying the same criteria that were applied in the uniform field case.

Another series of experiments was conducted by exposing a single PZT fibre or a carbon fibre, supported by a metallic plate, to a divergent electric field. The objective was the capture the fibre. To avoid any EP contributions the applied field was alternated. The experiment shows that no capture was possible if the bottom electrode was not coated with an insulating material. This was a consequence of the electrostatic adhesion.
In this case, the attention was particularly focused on the nature of the needle-fibre contact and its effects on the capture force. After the analysis of the results, and a series of FEM simulations, it was clear that the nature of the force relating the needle and the fibre was not only dielectrophoretic, but there was also an electrophoretic contribution. A certain amount of charge was always transferred by the needle tip to the fibre. Interestingly, the value estimated for the charge was absolutely consistent with the value measured in the DC experiment in the system needle-plane.
Furthermore, an important result, in particular related to the possibility of extending the electrostatic micromanipulation to a broader range of materials, was that, a rod capture was possible in the case of a carbon fibre as well.

Another important group of experiments concerned the capture of micro-rods operating a structuring of a group of fibres.
A group of fibres was initially lying on a flat, uncoated, bottom electrode. Through the application of a voltage, on a needle-like upper electrode, which moved up, a structuring of the bunch was induced. As the needle continued to rise up, at a certain point, the bunch separated in two parts and a group of fibres was captured on the tip.

Several experiments were made to understand the dependence of the structuring phenomenon on the fibres, the liquid characteristics, the drag speed, the voltage magnitude and the frequency, and the electrodes geometry.
The experiments show that all the different kinds of structuring configuration which have been observed can fit into one of the two following categories:

- "Pearl-chain", the characteristic structure at lower frequencies
- "Cone-like", the characteristic structure for the higher frequencies

These two different structuring modes have been attributed to some time dependent phenomena of charge transfer between neighbouring fibres and between the needle and the fibre in contact. These charge transfer mechanisms, promoting the acquisition of a net charge by the fibres in the bunch, also generated some EP contribution. These charge transfer phenomena explain why the structuring phenomenon is frequency dependent, even if considering that the time constant of the system is 100s (i.e. its critical frequency is 0.01Hz), no sensitivity to the signal frequency should be expected.

Before concluding, an apparent paradox will be addressed.
As shown by the experiment in chapter 8, no capture of a single fibre is possible, under AC conditions, using a needle-plane configuration, if the bottom electrode is not coated with an insulating material. Conversely, the capture of the rod is possible when the experiment is conducted on a group of fibres, even if no coating exists on the metallic bottom electrode.
But, considering the FEM simulations conducted on a bunch of fibres, it was demonstrated that the adhesion causing a fibre to retain contact with the bottom electrode, even if the fibre is part of a bunch, was always bigger than the interparticle force between such a fibre and its neighbours. Therefore, even in the case of a group of fibres, there is apparently no special reason why the electrostatic adhesion would be overcome.

The explanation to this apparent mismatch lies in the dynamics of the process. When a group of fibres is exposed to a divergent field and structuring occurs, the upper pull

force is never directed against the adhesion force. In fact, the fibres, on the bottom electrode remain in contact with it for the whole duration of the experiment. What happens is that the electric field induces a reorganisation inside the bunch of fibres. This can occur either because the orientation torque, acting on the particles is randomly disposed, or because a rearrangement of the fibres, never acts in the direction in which the interparticle connections is stronger. The particles rotate, slip, and move relative to each other yet always keeping a point of contact. As a result of this process of rearrangement, a structuring is achieved.

Once the structuring has occurred, a certain amount of particles simply acquire a position far enough from the bottom electrode to be more related to the upper needle than to the flat bottom electrode. A separation of the bunch in two parts is then possible, and a pick-up can be achieved.

Considering this mechanism, the process of capturing of fibres carried out on a bunch of fibres, can be appropriately described as an “electric field structuring assisted capture of micro-rods”.

Chapter 11

SUGGESTED FURTHER WORKS

A series of suggested further works aimed at improving the understanding of the phenomenon are listed below:

1) Try to obtain a direct measure of the force exerted by the needle on the fibre. This task could be accomplished using a micro-force sensor.
2) Achieve a nanoscale AFM characterisation of the interparticle force, to analyse the relationship between the nanoscale and the microscale cases.
3) Characterise via PIV the eventual EHD motion during the structuring of the fibres.
4) Analyse in more depth the dependence of the structuring on the drag speed, trying to find the upper limit; this is particularly important regarding the needs of potential industrial partners.
5) Monitor the current during the structuring process in the system, using an electrometer.
6) Study the "fall down" of the fibre after switch off.
7) Introduce to the FEM models the effect of the fluid conductivity on the pickup force.
8) To test the capturing behaviour for other materials: Kevlar, Nylon and glass.

Another series of suggested investigations can be more related to the creation of eventual devices:

1) Analyse the structuring behaviour using an array of needles and try understanding the lower limit of the spacing between the needles.
2) To find the maximum value of drag speed through the holes of the template
3) To attempt the micro-manipulation on a group of fibres immersed in water above the frequency of relaxation of the water conductivity (≈10MHz).

Relatively to the first of the practical application using the setup explained in chapter 1 the viability of the use of a template was also demonstrated in the context of the present research project (Wilson and Capria, 2006) It was demonstrated that to drag a fibre of

PZT through the holes of a template was feasible (see fig.10.6 (a)). The template was an insulating array of holes made by photo-etchable glass (Duguet, 2006). The holes diameters were increased by exposing the template to the etching in HF (see fig.10.6 (b)).

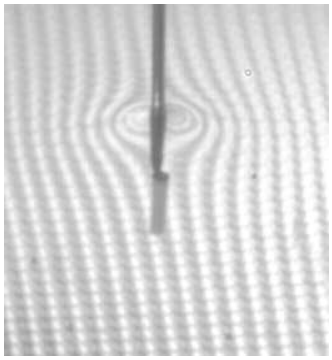
(a)
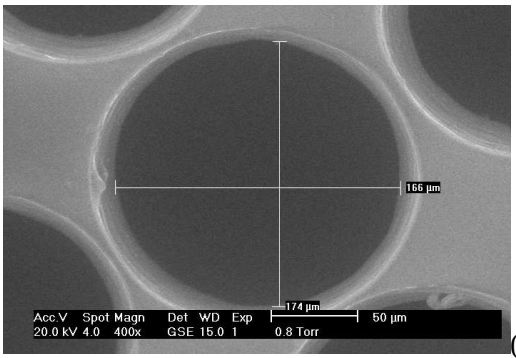

(b)

Figure 11. 1: (a)Detail of a PZT particle captured by a needle tip and dragged through the hole of a glass template (2kV@1kHz) (b)SEM picture of the glass template.

Chapter 12

CONCLUSIONS

Considering the physical mechanisms involved in the phenomenon, the following factors were identified as governing the interactions between needle and fibre, fibre and fibre, and bottom electrode and fibre:

a) Image forces resulting from polarisation of the fibre.
b) Orientation torque, due to an additional effect of the material polarisation
c) Image force due to fixed charge on the fibre, where fixed charge on the fibres can be due to:
    - Charges already on the fibre (e.g. tribocharge)
    - Charges transferred by the needle to the fibre as a consequence of electric field enhanced ohmic conductivity or, eventually, as a consequence of micro-breakdown
    - Charges transferred by unipolar charge injection through the needle tip
d) Viscous forces, eventually enhanced by electrohydrodynamic instabilities in proximity to the needle tip.
e) Phenomena of fluid degradation induced in proximity to the needle tip by the divergent electric field, resulting in gas generation and decomposition product arising from a partial electro-polymerisation of the fluid.

All the results focus on the importance of the charge transfer mechanism. A model for the charge transfer mechanism has been proposed, and it was in good agreement with the experimental results in both cases, with uniform and divergent electric field. Moreover the charge acquired by the PZT particle was practically the same as that which a conducting particle acquired.

The structuring effect of a group of fibres is also sensitive to the phenomenon of charge transfer. Two different kinds of structures were observed. The first one, the so called “pearl-chain” structure, was a structure of fibres extremely coherent and very well aligned, characteristic of the lower frequency (2kV@10-50Hz). The second one, the cone-like structure, was less coherent and was observed at higher frequency (2kV@1kHz). A series of experiments validated by a series of FEM simulations, confirmed in that the “pearl-chain” structuring mode was not only due to a polarisation effect, but also to charge transfer (and consequently to a Coulombian effect). It seems a

reasonable hypothesis that the forces exerted on the fibres result not only from a polarisation effect, but there is also an electrophoretic contribution.

For some particular cases, the tribocharge also plays a fundamental role in the physics of the phenomenon.

One of the most important achievements of the present research project is that a fibre capture has been achieved in three different configurations and consequently the viability of the electrostatic manipulation of micro-rods has been demonstrated (see section 10.1).
In the DC, the main problem to solve was that of capturing a single fibre while preventing the charge transfer through the tip. For that, to make the capture possible, an insulating coating on the needle was necessary.
In the AC case, the main problem was to deal with the huge electrostatic adhesion at the bottom electrode which prevents particle lift. This problem was bypassed through coating the bottom electrode with an insulator or enabling the capture of a bunch of fibres.

References

Adamec, V. (1972), "Electrical properties of an epoxy resin during and after cure", *Journal of Polymer Science: Part A-1,* vol. 10, pp. 1277–1295.

Adamec, V. and Calderwood, J. H. (1989), "Electrode polarization in polymeric dielectrics", *Electrical Insulation, IEEE Transactions on [see also Dielectrics and Electrical Insulation, IEEE Transactions on],* vol. 24, no. 2, pp. 205-214.

Adamiak, K. and Atten, P. (2004), "Simulation of corona discharge in point–plane configuration", *Journal of Electrostatics,* vol. 61, no. 2, pp. 85-98.

Albrecht, H. E., Borys, M., Damaschke, N. and Tropea, C. (2003), *Laser Doppler and Phase Doppler Measurement Techniques,* 1st ed, Springer, Berlin.

Amato, I. and Montanaro, L. (2000), *Lezioni dal corso di scienza e tecnologia dei materiali ceramici / I ceramici ingegneristici,* Ed. Cortina, Torino.

Anderson, R. A. (1991), "Effects of finite conductivity in electrorheological fluids", .

Arp, P. A. and Mason, S. G. (1977), "The kinetics of flowing dispersions. VIII. Doublets of rigid spheres (theoretical)", *J.Colloid Interface Sci,* vol. 61, pp. 21-43.

Asano, K., Anno, K. and Higashiyama, Y. (1997a), "The behavior of charged conducting particles in electric fields", *Industry Applications, IEEE Transactions on,* vol. 33, no. 3, pp. 679-686.

Asano, K., Sato, K., Yatsuzuka, K. and Higashiyama, Y. (1997b), "Rotational motion of a dielectric particle immersed in slightly conductive dielectric liquid", *Electrical Insulation and Dielectric Phenomena, 1997.IEEE 1997 Annual Report., Conference on,* vol. 2.

Asano, K., Choi, C., Kamiya, M. and Yatsuzuka, K. (2000a), "The behavior of a spherical particle under non-uniform electric field in silicone oil", *Electrical Insulation and Dielectric Phenomena, 2000 Annual Report Conference on,* vol. 1.

Asano, K., Yatsuzuka, K. and Yamaki, T. (2000b), "DC corona discharge of a metal filament particle within parallel-plate electrodes", *Industry Applications, IEEE Transactions on,* vol. 36, no. 1, pp. 87-92.

Asano, K., Hishinuma, R. and Yatsuzuka, K. (2002), "Bipolar DC Corona Discharge From a Floating Filamentary Metal Particle", *IEEE Transactions on Industry Applications*, vol. 38, no. 1, pp. 57.

Atten, P. (1996a), "Electrohydrodynamic instability and motion induced by injected space charge in insulating liquids", *IEEE Transactions on Dielectrics and Electrical Insulation*, vol. 3, no. 1, pp. 1-17.

Atten, P. (1996b), "On the use of an ionic pump in a convector heater", *Industry Applications, IEEE Transactions on*, vol. 32, no. 1, pp. 80-89.

Atten, P. and Honda, T. (1982), "The electroviscous effect and its explanation. I-The electrohydrodynamic origin; study under unipolar dc injection", *J.Electrostatics*, vol. 11, pp. 225-245.

Atten, P., Foulc, J. N., Felici, N. J. and Bossis, G. (1993), "A Large Scale Test of a Conduction Model of the Electrorheological Effect", *IEEE*, , pp. 1785-1791.

Atten, P., Foulc, J. N. and Felici, N. J. (1994), "A conduction model of the electrorheological effect", *Int.J.Mod.Phys.B*, vol. 8, no. 20-21, pp. 2731-2745.

Atten, P., Mairaison, B. and Zahn, M. (1997a), "Electrohydrodynamic Plumes in Point-plane Geometry", *IEEE Transactions on Dielectrics and Electrical Insulation*, vol. 4, no. 6, pp. 710-718.

Atten, P., Boissy, C. and Foulc, J. N. (1997b), "Role of conduction in electrorheological fluids: from interaction between particles to structuration of suspensions", *Journal of Electrostatics*, vol. 40, pp. 3-12.

Atten, P., Adamiak, K. and Atrazhev, V. (2002), "Electric corona discharge simulation in the hyperbolic point-ground plane configuration", *Electrical Insulation and Dielectric Phenomena, 2002 Annual Report Conference on*, , pp. 109-112.

Atten, P., Adamiak, K., Khaddour, B., Coulomb, J. L. and et de Matériaux, L.E. (2004), "Simulation of corona discharge in configurations with a sharp electrode", J*ournal of optoelectronics and advanced materials*, vol. 6, pp. 1023-1028.

Atten, P., Coulomb, J. L. and Khaddour, B. (2005), "Modeling of electrical field modified by injected space charge", *Magnetics, IEEE Transactions on*, vol. 41, no. 5, pp. 1436-1439.

Bamji, S. S., Bulinski, A. T. and Prasad, K. M. (1993), "Electric field calculations with the boundary element method", *Electrical Insulation, IEEE Transactions on [see also Dielectrics and Electrical Insulation, IEEE Transactions on]*, vol. 28, no. 3, pp. 420-424.

Batina, J., Noël, F., Lachaud, S., Peyrous, R. and Loiseau, J. F. (2001), "Hydrodynamical simulation of the electric wind in a cylindrical vessel with positive point-to-plane device", *J.Phys.D: Appl.Phys*, vol. 34, pp. 1510-1524.

Birlasekaran, S. and Darveniza, M. (1972), "Observations due to particle movement in transformer oil", *Proceedings of the Fourth ICDL Conference*, Dublin, pp. 120.

Birlasekaran, S. (1991), "The measurement of charge on single particles in transformer oil", *Electrical Insulation, IEEE Transactions on [see also Dielectrics and Electrical Insulation, IEEE Transactions on]*, vol. 26, no. 6, pp. 1094-1103.

Blackwood, K. M., Block, H., Rattray, P., Tsangaris, G. and Vorobiev, D. N. (1994), "The polarization, structuring and rheology of ER fluids", *Electrorheological Fluids (ed.Tao, R.et al.), Singapore: World Scientific*, vol. 3.

Block, H., Kelly, J. P., Qin, A. and Watson, T. (1990), "Materials and mechanisms in electrorheology", *Langmuir*, vol. 6, no. 1, pp. 6-14.

Block, H. (1999), A dielectric study of Order in Electric Field Aligned Dispersions and its Application to Electrorheology, EPSRC Report GR/K15947.

Boissy, C., Foulc, J. N. and Atten, P. (1994), "Influence of the electric field frequency on the electrorheological fluids properties", in Tao, R. and Roy, G.D. (ed.), *Proceedings of the 4th International Conference on Electrorheological fluids*, Vol. 1, Feldkirch, Austria, World Scientific, Singapore, pp. 453.

Boissy, C., Atten, P. and Foulc, J. N. (1995), "Les fluides électrorhéologiques: rôle de la conductivité des différents constituants", *J.Phys.III France*, vol. 5, pp. 677-688.

Boissy, C., Atten, P. and Foulc, J. N. (1996), "The conduction model of electrorheological effect revisited", *Int.J.Mod.Phys.B*, vol. 10, pp. 2991-3000.

Boukamp, B. A., Pham, M. T. N., Blank, D. H. A. and Bouwmeester, H. J. M. (2004), "Ionic and electronic conductivity in lead–zirconate–titanate (PZT)", *Solid State Ionics*, vol. 170, no. 3-4, pp. 239-254.

Bowen, L. J., Gentilman, R. L., Pham, H. T., Fiore, D. F. and French, K. W. (1993), "Injection molded fine-scale piezoelectric composite transducers", *Ultrasonics Symposium 1993 Proceedings,* Vol. 1, Baltimore, MD, USA, IEEE, pp. 499.

Bowen, C. P., Shrout, T. R., Newnham, R. H. and Randall, C. A. (1994), "A Study of the Frequency Dependence of the Dielectrophoretic Effect in Thermoset Polymers", *J. Mater. Res.,* vol. 9, no. 3, pp. 781-788.

Briere, G. and Gaspard, F. (1968), "Electric conduction in nitrobenzene", *Chem Phys Letter,* vol. 1, no. 13, pp. 706-708.

Capria, E. and Wilson, S. A. (2006a), "Electrostatic manipulation of piezoelectric rods: a new way to fabricate micro-scale array composites" *Proceedings of the 6th International Conference on Materials for Microelectronics & Nanoengineering*, Cranfield, UK

Capria, E. and Wilson, S. A. (2006b), "Corona Enhanced Electrowetting and Dielectrophoresis in a Dielectric Fluid", *Proceedings of the 8th International Conference on Properties and Application of Dielectric Materials*, Sanur, Indonesia

Castellanos, A. (ed.) (1998), *Electrohydrodynamics,* 1st ed, Springer Wein, New York.

Chakrabarti, A. K., van Heeswijk, R. G. and Srivastava, K. D. (1989), "Free particle-initiated 60 Hz breakdown at a spacer surface in agas-insulated bus", *Electrical Insulation, IEEE Transactions on [see also Dielectrics and Electrical Insulation, IEEE Transactions on],* vol. 24, no. 4, pp. 549-560.

Chaumet, P. C. and Dufour, J. P. (1998), "Electric potential and field between two different spheres", *Journal of Electrostatics,* vol. 43, no. 2, pp. 145-159.

Chen, Y., Sprecher, A. F. and Conrad, H. (1991), "Electrostatic particle–particle interactions in electrorheological fluids", *J. Appl. Phys,* vol. 70, pp. 6796–803.

Cheng, H. and Torquato, S. (1997), "Electric-field fluctuations in random dielectric composites", *Physical Review B,* vol. 56, no. 13, pp. 8060-8068.

Cheung, V. G., Morley, M., Aguilar, F., Massimi, A., Kucherlapati, R. and Childs, G. (1999), "Making and reading microarrays", *Nature genetics,* vol. 21, no. 1 Suppl, pp. 15-19.

Choi, C., Yatsuzuka, K. and Asano, K. (1999), "Motion of a conductive particle in viscous fluid simulatingliquefied plastic waste", *Industry Applications Conference, 1999.Thirty-Fourth IAS Annual Meeting.Conference Record of the 1999 IEEE,* vol. 3.

Choi, C., Yatsuzuka, K. and Asano, K. (2000), "The behavior of spherical particle under uniform electric field in silicone oil", *Electrical Insulation and Dielectric Phenomena, 2000 Annual Report Conference on,* vol. 1.

Choi, C., Yatsuzuka, K. and Asano, K. (2001), "Dynamic Motion of a Conductive Particle in Viscous Fluid Under DC Electric Field", *IEEE Transactions on Industry Applications,* vol. 37, no. 3, pp. 785.

Choi, C., Yatsuzuka, K. and Asano, K. (2002), "Trapped and transverse motion of a charged particle within tilted electrodes in silicone oil", *Electrical Insulation and Dielectric Phenomena, 2002 Annual Report Conference on,* , pp. 188-191.

Clercx, H. J. and Bossis, G. (1993), "Many-body electrostatic interactions in electrorheological fluids", P*hysical review e.statistical physics, plasmas, fluids, and related interdisciplinary topics,* vol. 48, no. 4, pp. 2721-2738.

Clift, R., Grace, J. R. and Weber, M. E. (1978), *Bubbles, drops, and particles,* 1st ed, Academic Press, San Diego, Calif.

Coelhot, R. and Debeaus, J. (1971), "Properties of the tip-plane configuration", *J.Phys.D:'Appl.Phys,* vol. 4.

Coulson, C. A. (1948), *Electricity,* 1st ed, Oliver and Boyd, Edinburgh.

Cross, J. A. (1987), "Electrostatics: Principles, Problems and Applications", *Problems and Applications, Adam Hilger, Bristol,* , pp. 81.

Dakin T.W, Hugues J. (1968), *Annual Report Conf. on Electrical Insulators and Dielectric Phenomena,* Washington DC, USA, pp. 68.

Dascalescu, L., Tobazeon, R. and Atten, P. (1995), "Behaviour of conducting particles in corona-dominated electric fields", *J. Physics D: Applied Physics,* , no. 28, pp. 1611-1618.

Dascalescu, L., Mihailescu, M. and Tobazeon, R. (1996), "Modelling of conductive particle behaviour in insulating fluids affected by DC electric fields", *Industry*

Applications Conference, 1996.Thirty-First IAS Annual Meeting, IAS'96., Conference Record of the 1996 IEEE, vol. 3.

Dascalescu, L., Rafiroiu, D., Samuila, A. and Tobazeon, R. (1998), "Charging of insulating spheres on the surface of an electrode affected by monopolar ions", *Industry Applications, IEEE Transactions on,* vol. 34, no. 1, pp. 35-42.

Davis, L. C. (1992a), "Finite-element analysis of particle-particle forces in electrorheological fluids", *Applied Physics Letters,* vol. 60, no. 3, pp. 319-321.

Davis, L. C. (1992b), "Polarization forces and conductivity effects in electrorheological fluids", *Journal of Applied Physics,* vol. 72, no. 4, pp. 1334-1340.

Davis, L. C. and Ginder, J. M. (1995), "Electrostatic forces in electrorheological fluids *Progress in Electrorheology*", , pp. 107–114.

Davis, M. H. (1969), "Electrostatic Field and Force on a Dielectric Sphere near a Conducting Plane—A Note on the Application of Electrostatic Theory to Water Droplets", *American Journal of Physics,* vol. 37, pp. 26.

Day, D. R., Lewis, T. J., Lee, H. L. and Senturia, S. D. (1985), "The role of boundary layer capacitance at blocking electrodes in the interpretation of dielectric cure data in adhesives", *J.Adhesion,* vol. 18, pp. 73-90.

Dechev, N., Cleghorn, W. and Mills, J. K. (2004), "Microassembly of 3-D microstructures using a compliant, passive microgripper", *Microelectromechanical Systems, Journal of,* vol. 13, no. 2, pp. 176-189.

Delon, J. F. (1966), "Théorie de la séparation électrostatique à l'aide de l'effet corona", *Annales des Mines,* vol. 3, pp. 37-50.

De Marchi, A. and Lo Presti L. (1993), *Incertezze di misura*, 1st ed., CLUT, Torino.

Dietz, P. W. and Melcher, J. R. (1978), "Interparticle Electrical Forces in Packed and Fluidized Beds", *Industrial & Engineering Chemistry Fundamentals,* vol. 17, no. 1, pp. 28-32.

Duguet, S. (2007), *Micro assembly of piezoelectric array composites by dielectrophoresis* (unpublished MSc thesis), Cranfield University, Cranfield (UK).

Durand, E. (1966), *Electrostatique. Tome I,* 1st ed., Masson et Cie, Paris.

Einstein, A. (1906), "Eine neue Bestimmung der Molekuldimensionen", *Ann. Physik*, vol. 19, pp. 289-306.

Faraday, M. (1838), "Experimental Researches in Electricity. Eleventh Series", *Philosophical Transactions of the Royal Society of London*, vol. 128, pp. 1-40.

Farral, G. A. and Hudda, G. (1980), "The movement of elongated metal particles under high-voltage stress in vacuum", *Journal of Applied Physics*, vol. 51, no. 9, pp. 4706–17.

Farzaneh, M. and Teisseyre, Y. (1988), "Mechanical vibration of HV conductors induced by corona: roles of the space charge and ionic wind", *Power Delivery, IEEE Transactions on*, vol. 3, no. 3, pp. 1122-1130.

Feddema, J. T., Xavier, P. and Brown, R. (2001), "Micro-assembly planning with van der Waals force", *Journal of Micromechatronics*, vol. 1, no. 2, pp. 139-153.

Felici, N. J. (1966), "Forces et charges de petits objets en contact avec une électrode affectée d'un champ électrique", *Rev.Gen.Electr*, vol. 75, pp. 1145-1160.

Felici, N. J. (1971), "D. C. Conduction in liquid dielectrics-A survey of recent progress(Part I)", *Direct Current*, vol. 2, no. 3, pp. 90-99.

Felici, N. J., Foulc, J. N. and Atten, P. (1994), "A conduction model of electro-rheological effect", in Tao, R. and Roy, G.D. (ed.), *Proc. 4th Int. Conf. Electrorheological Fluids ed R Tao and G D Roy (Singapore: World Scientific) pp 139-52*, Feldkirch, Austria, World Scientific, Singapore, pp. 139.

Felsenthal, P. and Vonnegut, B. (1967), "Enhanced charge transfer in dielectric fluids containing conducting particles", *British Journal of Applied Physics*, vol. 18, no. 12, pp. 1801-1806.

Feng, J. Q. (2000), "Electrostatic interaction between two charged dielectric spheres in contact", *Physical Review. E, Statistical Physics, Plasmas, Fluids, and Related Interdisciplinary Topics*, vol. 62, no. 2 Pt B, pp. 2891-2897.

Foll, H. (2006), *Electronic materials*, University of Kiel, Kiel, Germany.

Fukumoto, M. and Ohyama, R. (2003), "Image analysis of gas-phase EHD flow field for needle-plane electrode system", *2003 Annual Report Conference on Electrical Insulation and Dielectric Phenomena, Albuquerque, New Mexico*, , pp. 694–697.

Gallagher, T. J. (1975), *Simple Dielectric Liquids: Mobility, Conduction, and Breakdown,* Clarendon Press Oxford.

Gast, A. P. and Zukoski, C. (1989), "Electrorheological fluids as colloidal suspensions", *Advances in Colloid and Interface Science,* vol. 30, no. 3-4, pp. 153-202.

Godin, Y. A. and Zil'bergleit, A. (1986), "Axisymmetric electrostatic problem of a dielectric sphere near a conducting plane", *Sov.Phys.Tech.Phys,* vol. 31, no. 6, pp. 632–637.

Goranovic, G. (2003), *Electrohydrodynamic Aspects of Two-Fluid Microfluidic Systems: Theory and Simulation* (PhD Thesis no. 000699 thesis), Technical University of Denmark, Lyngby.

Gray, D. S., Tan, J. L., Voldman, J. and Chen, C. S. (2004), "Dielectrophoretic registration of living cells to a microelectrode array", *Biosens.Bioelectron,* vol. 19, no. 7, pp. 771–780.

Guillon, O., Thiebaud, F. and Perreux, D. (2002), "Tensile fracture of soft and hard PZT", *International Journal of Fracture,* vol. 117, no. 3, pp. 235-246.

Halsey, T. C. (1992), "Electrorheological Fluids", *Science,* vol. 258, no. 5083, pp. 761.

Happel, J. and Brenner, H. (1965), *Low Reynolds Number Hydrodynamics,* Prentice-Hall.

Harper, W. R. (1967), *Contact and Frictional Electrification,* 1st ed, Clarendon P., Oxford.

Honma, R. and Ohyama, R. (2000), "Experimental study on ionic wind measurement of an electrohydrodynamically induced gas-liquid two-phase flow field by particle image velocimetry", *Annual report of the conference on electrical insulation and dielectric phenomena (CEIDP),* vol. 1, pp. 81-84.

Hooker, M. W. (1998), *Properties of PZT-based Piezoelectric Ceramics Between-150 and 250C°,* National Aeronautics and Space Administration, Langley Research Center; National Technical Information Service, distributor.

House, H. (1957), "High Field Conduction Currents in Hexane", *Proceedings of the Physical Society Section B,* vol. 70, no. 10, pp. 913-927.

Hunt, T. P. and Westervelt, R. M. (2006), "Dielectrophoresis tweezers for single cell manipulation", *Biomedical Microdevices*, vol. 8, no. 3, pp. 227-230.

Hyde, M. (2005), *Personal communication*, Cranfield.

Israelachvili, J. N. (1992), *Intermolecular and surface forces*, 1st ed, Academic Press, London.

Jacobson, S. C., McKnight, T. E. and Ramsey, J. M. (1999), "Microfluidic devices for electrokinetically driven parallel and serial mixing", *Anal.Chem*, vol. 71, no. 20, pp. 4455–4459.

Jonassen, N. (2002), *Electrostatics*, 2nd ed, Kluwer, Denmark.

Jones, T. B. (1985), "Multipole correction in the dielectrophoresis force", *IEEE Transaction on Industry applications*, vol. 4, no. 1A, pp. 930-934.

Jones, T. B. (1995), *Electromechanics of Particles*, Cambridge Univ Press.

Kadaksham, J., Singh, P. and Aubry, N. (2004a), "Dynamics of Electrorheological Suspensions Subjected to Spatially Nonuniform Electric Fields", *Journal of Fluids Engineering*, vol. 126, pp. 170.

Kadaksham, J., Singh, P. and Aubry, N. (2004b), "Manipulation of particles using dielectrophoresis", *Mechanics Research Communications*, vol. 33, pp. 108-122.

Kamiya, K., Honda, H. and Nasu, H. (1990), "Sol-gel Processing of PbTio3 Ceramic Fibers", *Nippon Seramikkusu Kyokai Gakujutsu Ronbunshi*, vol. 98, pp. 759-764.

Karasikov, N. and Ganor, Z. (2000), "A Novel Non-Magnetic Miniature motor for Ultra High Vacuum Applications", *Nanomotion Ltd.*.

Kawamoto, H. and Umezu, S. (2005), "Electrohydrodynamic deformation of water surface in a metal pin to water plate corona discharge system", *Journal of Physics D Applied Physics*, vol. 38, no. 6, pp. 887-894.

Kawamoto, H., Yasuda, H. and Umezu, S. (2006), "Flow distribution and pressure of air due to ionic wind in pin-to-plate corona discharge system", *Journal of Electrostatics*, vol. 64, no. 6, pp. 400-407.

Kazilas, M. C. (2003), *Acquisition and Interpretation of Dielectric Data for Thermoset Cure Monitoring* (PhD thesis), Cranfield University, Cranfield (UK).

Khusid, B. and Acrivos, A. (1995), "Effects of conductivity in electric-field-induced aggregation in electrorheological fluids", P*hysical review e.statistical physics, plasmas, fluids, and related interdisciplinary topics*, vol. 52, no. 2, pp. 1669-1693.

Khusid, B. and Acrivos, A. (1996), "Effects of interparticle electric interactions on dielectrophoresis in colloidal suspensions", P*hysical review e.statistical physics, plasmas, fluids, and related interdisciplinary topics*, vol. 54, no. 5, pp. 5428-5435.

Kim, G. and Shkel, Y. M. (2004), "Polymeric composites tailored by electric field.", *Journal of Materials Research*, vol. 19, no. 4, pp. 1164-1174.

Kim, G. (2005), "Thermo-physical responses of polymeric composites tailored by electric field", *Composites Science and Technology*, vol. 65, no. 11-12, pp. 1728-1735.

Kim, K., Stroud, D., Li, X. and Bergman, D. J. (2005), "Method to calculate electrical forces acting on a sphere in an electrorheological fluid", *Physical review.E, Statistical, nonlinear, and soft matter physics*, vol. 71, no. 3 Pt 1, pp. 031503.

Klass, D. L. and Martinek, T. W. (1967), "Electroviscous fluids", *J.Applied Physics*, vol. 38, pp. 67-74.

Klingenberg, D. J., van Swol, F. and Zukoski, C. F. (1989), "Dynamic simulation of electrorheological suspensions", *Journal of Chemical Physics*, vol. 91, no. 12, pp. 7888-7895.

Krasucki Z. (1968), *Actes du Colloque International N 179 du CNRS*, Grenoble, CNRS, Grenoble, pp. 311.

Lacroix, J., Atten, P. and Hopfinger, E. J. (1975), "Electro-convection in a dielectric liquid layer subjected to unipolar injection", *Journal of Fluid Mechanics Digital Archive*, vol. 69, no. 03, pp. 539-563.

Landau, L.D., Lifshitz, E.M. and Pitaevskii, L. P. (1975), *Course of theoretical physics: Electrodynamics of continuous media (Vol.8)*, 1st ed, Pergamon, New York.

Lebedev, N. N. and Skal'skaya, I. P. (1962), "Forces acting on a conducting sphere in the field of a parallel plane condenser", *Sov.Phys.Tech.Phys*, vol. 7, pp. 268-270.

Levin, P. L., Hansen, A. J., Beatovic, D., Gan, H. and Petragelo, J. H. (1993), *IEEE Trans. Electr. Insul*, vol. 28, pp. 161–167.

Li, J., Zhang, Q., Yang, D. and Tian, J. (2004a), "Fabrication of carbon nanotube field effect transistors by AC dielectrophoresis method", *Carbon(New York, NY)*, vol. 42, no. 11, pp. 2263-2267.

Li, J., Xi, N., Fung, W. K. and Wong, T. S. (2004b), "Nanorobotics and Nanomanipulation", *Encyclopedia of Nanoscience and Nanotechnology, American Scientific Publishers*, vol. 7, no. 15, pp. 351-365.

Love, J. D. (1975), "Dielectric sphere-sphere and sphere-plane problems in electrostatics", *The Quarterly Journal of Mechanics and Applied Mathematics*, vol. 28, no. 4, pp. 449.

Lowell, J. (1984), "Charge accumulation by repeated contacts of metals to insulators", *Journal of Physics D: Applied Physics*, vol. 17, no. 9, pp. 1859-1870.

Lowell, J. (1986a), "Constraints on contact charging of insulators: I. Spatial localization of insulator states.", J.*Phys.D: ApplPphys.*, vol. 19, no. 1, pp. 95-104.

Lowell, J. (1986b), "Constraints on contact charging of insulators: II Energy constraints", *J.Phys.D: Appl.Phys*, vol. 19, pp. 105-113.

Lowell, J. and Truscott, S. (1986c), "Triboelectrification of identical insulators: 11. Theory and further experiments", *J.Phys.D: Appl.Phys*, vol. 19, pp. 1281-1298.

Lowell, J. and Akande, A. R. (1988), "Contact electrification-why is it variable?", *Journal of Physics D.Applied Physics*, vol. 21, pp. 125-137.

Maistros, G. M. and Bucknall, C. B. (1994), "Modeling the dielectric behavior of epoxy resin blends during curing", *Polymer Engineering and Science*, vol. 34, no. 20, pp. 1517-1528.

Malyan, B. and Balachandran, W. (2001), "Sub-micron sized biological particle manipulation and characterisation", *Journal of Electrostatics*, vol. 51, pp. 15-19.

Maxwell, J. C. (1954), *Treatise on Electricity and Magnetism*, Dover Pubns.

Mclean Kenneth, J. (1977), "Cohesion of Precipitation Dust Layer in Electrostatic Precipitators", *J.Air poll.Control Assoc*, vol. 27, no. 11, pp. 1100-1103.

Melcher, J. R. and Taylor, G. I. (1969), "Electrohydrodynamics: A Review of the Role of Interfacial Shear Stresses", *Annual Review of Fluid Mechanics*, vol. 1, no. 1, pp. 111-146.

Miller, D. V., Randall, C. A., Bhalia, A. S., Newnham, R. E. and Adair, J. H. (1993), "Electrorheological properties of of BaTiO3 suspensions", *Ferrroelectrics Letters,* vol. 15, pp. 141–151.

Miller, R. D. and Jones, T. B. (1987), "Frequency dependent Orientation of ellipsoidal Particles in AC electric field", *9th Ann. IEEE-EMBS Conf. Boston,* .

Misono, Y., Furukawa, S., Yosinaga, H., Sugiyama, J. and Negita, K. (2004), "Frequency dependence of electrorheological (ER) effect and its relationship to dielectric and electrical properties in Barium Strontium Titanate", Vol. 1, pp. 1443.

Mooney, M. (1951), "The viscosity of a concentrated suspension of spherical particles", *J.Colloid Sci,* vol. 6, pp. 162-170.

Moore, A. D. (1973), *Electrostatics and its applications,* Wiley.

Morcos, M. M., Zhang, S., Srivastava, K. D. and Gubanski, S. M. (2000), "Dynamics of Metallic Particle Contaminants in GIS with Dielectric-Coated Electrodes", *IEEE Transactions on Power Delivery,* vol. 15, no. 2, pp. 455.

Morgan, H. and Green, N. G. (2003), "AC Electrokinetics: Colloids and Nanoparticles (Herts: Research Studies Press)", .

Moslehi, G. B. and Self, S. (1984), "Electromechanics of precipitated particulate layers.", *IEEE Trans.Indust.Applic.,* vol. 20, no. 6, pp. 1598-1606.

Munson, B. R., Young, D. F. and Okiishi, T. H. (1996), *A Brief Introduction to Fluid Mechanics,* John Wiley & Sons.

Nakajima, Y. and Matsuyama, T. (2002), "Electrostatic field and force calculation for a chain of identical dielectric spheres aligned parallel to uniformly applied electric field", *Journal of Electrostatics,* vol. 55, no. 2, pp. 203-221.

Ohyama, R. and Kaneko, K. (1996), "Experimental flow measurements of electrohydrodynamic convection fields by particle image velocimetry", *Electrical Insulation and Dielectric Phenomena, 1996.IEEE 1996 Annual Report of the Conference on,* vol. 1.

Ohyama, R. and Kaneko, K. (1997), "An experimental study of the optical characterization of AC electrohydrodynamic fields by particle image velocimetry", *Electrical Insulation and Dielectric Phenomena, 1997.IEEE 1997 Annual Report., Conference on,* vol. 2.

Ohyama, R. and Kaneko, K. (1998), "Optical characterization of steady electrohydrodynamic fluid motion induced by surface corona discharge", *Electrical Insulation and Dielectric Phenomena, 1998.Annual Report.Conference on*, vol. 1.

Ohyama, R. K. and Chang, K. J. S. (2003), "Flow visualization and image analysis of gas-phase AC corona discharge induced electrohydrodynamic liquid flow in a stratified fluid", *Dielectrics and Electrical Insulation, IEEE Transactions on [see also Electrical Insulation, IEEE Transactions on]*, vol. 10, no. 1, pp. 57-64.

Pardini, R. S. (1971), "Polychlorinated biphenyls (PCB): effect on mitochondrial enzyme systems", *Bulletin of environmental contamination and toxicology*, vol. 6, no. 6, pp. 539-545.

Pauthenier, M. and Moreau-Hanot, M. (1932), "La charge des particules sphériques dans un champ ionisé", *J.Phys.Radium*, vol. 3, pp. 590–613.

Pauthenier, M. (1956), "Probléme général de la charge acquise par une particule sphérique dans un champ électrique bi-ionisé", *Comptes Rendus*, , pp. 606–1608.

Perez, A. T., Vazquez, P. A. and Castellanos, A. (1995), "Dynamics and linear stability of charged jets in dielectric liquids", *Industry Applications, IEEE Transactions on*, vol. 31, no. 4, pp. 761-767.

Pethig, R., Wang, X. B., Huang, Y. and Burt, J. P. H. (1992), "Positive and negative dielectrophoretic collection of colloidal particles using interdigitated castellated microelectrodes", *Journal of Physics D.Applied Physics*, vol. 25, pp. 881-888.

Pethig, R. (1996), "AC Electrokinetic manipulation of bioparticles", in Coombs, R. R. H. (ed.) and Robinson D. W., *Nanotechnology in Medicine and the Biosciences*, 1st ed, Gordon and Breach Publishers, UK.

Pohl, H. A. (1951), "Some Effects of Nonuniform Fields on Dielectrics", *Journal of Applied Physics*, vol. 29, no. 8, pp. 1182-1188.

Pohl, H. A. (1978), *Dielectrophoresis*, Cambridge University Press, Cambridge.

Prakash, K., Srivastava, K. D. and Morcos, M. M. (1997), "Movement of particles in compressed SF 6 GIS with dielectric coated enclosure", *Dielectrics and Electrical Insulation, IEEE Transactions on [see also Electrical Insulation, IEEE Transactions on]*, vol. 4, no. 3, pp. 344-347.

Radu, I. (1995), "Electric field calculation and the influence of water trees on insulation breakdown in needle–plane geometry", *Journal of Electrostatics,* vol. 60, no. 1, pp. 49-67.

Randall, C. A., Miller, D. V., Adair, J. H. and Bhalia, A. S. (1993), "Processing of electroceramic-polymer composites using the electrorheological effect", *Journal of Materials Research,* vol. 8, no. 4, pp. 899-904.

Randall, C. A., Bowen, C. P., Shrout, T. R., Messing, G. L. and Newnham, R. E. (1994), "Dielectrophoretic Assembly: A Novel Concept in Advanced Composite Fabrication", *Proc. 4th Int. Conf. on Electrorheological Fluids,* , pp. 516-525.

Rattray, P. (1994), *Pulsed Flow and Time-resolved Dielectric Spectroscopy of Electrorheological Fluids.* (PhD Thesis) Cranfield University.

Rhodes, G. M. and Brignell, J. E. (1972), *Proc. 4th Int. Conf. Conduction and Break-down in Dielectric Liquids,* Dublin, Typografia Hiberniae, Dublin, pp. 116-119.

Robinson, K. S. and Jo (1984), "Particle-wall adhesion in electropacked beds.", *IEEE Trans.Indust.Applic.,* vol. 20, no. 6, pp. 1573-1577.

Rougeot, P., Regnier, S. and Chaillet, N. (2005), "Forces analysis for micro-manipulation", *Computational Intelligence in Robotics and Automation, 2005.CIRA 2005.Proceedings.2005 IEEE International Symposium on,* , pp. 105-110.

Rudeforth, D. (2003), *Personal communication*, Cranfield.

Russell, A. (1909), "The Coefficients of Capacity and the Mutual Attractions or Repulsions of Two Electrified Spherical Conductors When Close Together", *Proceedings of the Royal Society of London.Series A, Containing Papers of a Mathematical and Physical Character,* vol. 82, no. 557, pp. 524-531.

Ryo-ichiro, O. and Kiyoji, K. (1997), "An experimental study of The Optical Characterisation of AC Electrohydrodynamic Field by Particle Imagery Velocimetry", *IEEE Annual Report – Conf. on Elec. Insulation and Dielectric phenomena,* , pp. 656-659.

Sacco, E. (1994), *Argomenti di scienza delle costruzioni: Il problema della trave*, Edizioni scientifiche italiane Cassino.

Sanchis, A., Sancho, M., Martinez, G., Sebastian, J. L. and Munoz, S. (2004), "Interparticle forces in electrorheological fluids: effects of polydispersity and shape", *Colloids and Surfaces A: Physicochemical and Engineering Aspects*, vol. 249, no. 1, pp. 119-122.

Sekino, Y., Ohyama, R. and Kaneko, K. (1998), "Measurements of unsteady electrohydrodynamics flow from injectioncharges on free surface by particle image velocimetry", *Electrical Insulation and Dielectric Phenomena, 1998.Annual Report.Conference on*, vol. 1.

Senturia, S. D. and Sheppard Jr, N. F. (1986), "Dielectric analysis of thermoset cure", *Advances in Polymer Science*, vol. 80, no. 1.

Sharbaugh, A. H. and Barker, R. E. (1965), "Ionic impurity conduction in organic liquids" *Process in dielectric liquids*, Grenoble.

Shih, Y. H., Sprecher, A. and Conrad, H. (1994), "Electrostatic Interactions for Particle Arrays in Electrorheological Fluids I:. Calculations", *International Journal of Modern Physics B*, vol. 8, no. 20, pp. 2877–2894.

Sillars, R. W. (1937), "The properties of a dielectric containing semiconducting particles of various shapes", *Journal of Institution of Electrical Engineers*, vol. 80, pp. 378–394.

Smith, D., Pendry, J. B. and Wiltshire, M. C. K. (2004), "Metamaterials and Negative Refractive Index", *Science*, vol. 305, no. 5685, pp. 788-792.

Sternovsky, Z., Horányi, M. and Robertson, S. (2001), "Charging of dust particles on surfaces", *Journal of Vacuum Science & Technology A: Vacuum, Surfaces, and Films*, vol. 19, pp. 2533.

Stratton, J. A. (1941), *Electromagnetic theory*, McGraw-Hill New York.

Studer, V., Pépin, A., Chen, Y. and Ajdari, A. (2002), "Fabrication of microfluidic devices for AC electrokinetic fluid pumping", *Microelectronic Engineering*, vol. 61, pp. 915-920.

Sueda, H. and Kao, K. C. (1980), "Schlieren images observed in electrically stressed dielectric liquids", *Applied Optics*, vol. 19, pp. 2538-2545.

Tang, J., Gao, B., Geng, H., Velev, O. D., Qin, L. C. and Zhou, O. (2003), "Assembly of 1 D nanostructures into sub-micrometer diameter fibrils with controlled and variable length by dielectrophoresis.", *Advanced Materials(FRG)*, vol. 15, no. 16, pp. 1352-1355.

Tao, R., Jiang, Q. and Sim, H. K. (1995), "Finite-element analysis of electrostatic interactions in electrorheological fluids", P*hysical review E. Statistical physics, plasmas, fluids, and related interdisciplinary topics*, vol. 52, no. 3, pp. 2727-2735.

Tay, B. Y. and Evans, J. R. G. (2003), "Solid freeform fabrication of ceramics.", *International Materials Reviews*, vol. 48, no. 6, pp. 341-370.

Techaumnat, B., Eua-arporn, B. and Takuma, T. (2004), "Electric field and dielectrophoretic force on a dielectric particle chain in a parallel-plate electrode system", *Journal of Physics D Applied Physics*, vol. 37, no. 23, pp. 3337-3346.

Terris, B. D., Stern, J. E., Rugar, D. and Mamin, H. J. (1989), "Contact electrification using force microscopy", P*hysical review letters*, vol. 63, no. 24, pp. 2669-2672.

Tilmatine, A., Flazi, S., Medles, K., Ramdani, Y. and Dascalescu, L. (2004), "Separation electrostatique: complement des procedes mecaniques de recyclage des dechets industriels", *Journal of Electrostatics*, vol. 61, pp. 21-30.

Timoshenko, S. P., Young, D. H. and Weaver, W. (1990), *Vibration Problems in Engineering*, John Wiley & Sons Inc.

Tobazeon, R. (1984), "Electrohydrodynamic Instabilities and Electroconvection in the Transient and ac Regime of Unipolar Injection in Insulating Liquids: A Review", *J.Electrostatics*, vol. 15, pp. 359-384.

Tobazeon, R. (1996), "Electrohydrodynamic behaviour of single spherical or cylindrical conducting particles in an insulating liquid subjected to a uniform DC field", *Journal of Physics D.Applied Physics*, vol. 29, no. 10, pp. 2595-2608.

Tombs, T. N. and Jones, T. B. (1993), "Effect of moisture on the dielectrophoretic spectra of glasspheres", *Industry Applications, IEEE Transactions on*, vol. 29, no. 2, pp. 281-285.

Trau, M., Sankaran, S., Saville, D. A. and Aksay, I. A. (1995), "Electric-field-induced pattern formation in colloidal dispersions", *Nature*, vol. 374, no. 6521, pp. 437-439.

Tsuchida, N. and Ueda, M. (1980), "Ionic behaviours in silicone oil", *J.Phys.D: Appl.Phys*, vol. 13, pp. 1681-1687.

Uchino, K. (1997), "Piezoelectric actuators and ultrasonic motors(Book)", *Dordrecht, Netherlands: Kluwer Academic Publishers, 1997.*

Ueha, S. and Tomikawa, Y. (1993), *Ultrasonic motors: theory and applications*, Clarendon Press.

Von Hippel, A. R. (1995), *Dielectrics and Waves*, Artech House, Boston.

Wang, Z., Shen, R., Niu, X., Lu, K. and Wen, W. (2003), "Frequency dependence of a field-induced force between two high dielectric spheres in various fluid media", *Journal of Applied Physics*, vol. 94, no. 12, pp. 7832-7834.

Wang, Z., Shen, R., Niu, X., Sun, G., Lu, K., Hou, B. and Wen, W. (2005), "Dielectric dependence of field-induced interspherical force", *Journal of Physics D Applied Physics*, vol. 38, no. 8, pp. 1325-1329.

Washizu, M. and Jones, T. B. (1996), "Dielectrophoretic interaction of two spherical particles calculated by equivalent multipole-moment method", *Industry Applications, IEEE Transactions on*, vol. 32, no. 2, pp. 233-242.

Watson, A. (1998), "A survey of conduction phenomena in liquid dielectrics", in Castellanos, A. (ed.) *Electrohydrodynamics*, 1st ed, Springer Wein, New York.

Whatmore, R. W. (1986), "Pyroelectric devices and materials", *Reports on Progress in Physics*, vol. 49, pp. 1335-1386.

White, F. M. (1991), *Viscous Fluid Flow*, 2nd ed, McGraw-Hill Inc., Singapore.

Wilson, S. A. (1999), *Electric field Structuring of Piezoelectric composite materials* (PhD Thesis), Cranfield.

Wilson, S.A., (2003), *Personal communication*, Cranfield.

Wilson, S. A., Maistros, G. M. and Whatmore, R. W. (2005), "Structure modification of 0–3 piezoelectric ceramic/polymer composites through dielectrophoresis", *Journal of Physics D Applied Physics*, vol. 38, no. 2, pp. 175-182.

Wilson, S. A. and Capria, E. (2006), ”Assembly of PZT fibre array composites by dielectrophoresis”, *Proceedings of the IEE Seminar on MEMS Sensors and Actuators*, pp237, London, UK

Winslow, W. M. (1949), "Induced Fibrillation of Suspensions", *Journal of Applied Physics*, vol. 20, pp. 1137.

Wu, C. W. and Conrad, H. (1996), "A modified conduction model for the electrorheological effect", *Journal of Physics D.Applied Physics*, vol. 29, no. 12, pp. 3147-3153.

Wu, C. W. and Conrad, H. (1997), "Dielectric and conduction effects in non-Ohmic electrorheological fluids", *Physical Review E*, vol. 56, no. 5, pp. 5789-5797.

Xu, Y. (1991), *Ferroelectric materials and their applications*, 1st ed, North-Holland, New York, NY.

Xujing, W., Wang, X. B. and Gascoyne, P. R. C. (1997), "General expressions for dielectrophoretic force and electrorotational torque derived using the Maxwell stress tensor method", *Journal of Electrostatics*, vol. 39, no. 4, pp. 277-295.

Yatsuzuka, K., Ahn, Y. S. and Asano, K. (1995), "Electrostatic motion of polymer particles in silicon fluid", *Industry Applications Conference, 1995, Thirtieth IAS Annual Meeting, IAS'95., Conference Record of the 1995 IEEE*, vol. 2, pp. 1223.

Yatsuzuka, K., Choi, C. and Asano, K. (1999), "On the charge of a moving particle within parallel electrodes in viscous fluid", *Industry Applications Conference, 1999, Thirty-Fourth IAS Annual Meeting.Conference Record of the 1999 IEEE*, vol. 3.

Zhakin, A. (1998), "Conduction models in dielectric liquids", in Castellanos, A. (ed.) *Electrohydrodynamics*, 1st ed, Springer Wien, New York.

Zheng, L., Brody, J. P. and Burke, P. J. (2004), "Electronic manipulation of DNA, proteins, and nanoparticles for potential circuit assembly", *Biosensors & bioelectronics*, vol. 20, no. 3, pp. 606-619.

Zukoski, C. F. (1993), "Material Properties and the Electrorheological Response", *Annual Review of Materials Science*, vol. 23, no. 1, pp. 45-78.

Appendix A

Design of the motion system

In this appendix we inserted the designs of the 4 support made to permit the assembly of the motion system. All the part was designed using Solid Edge, a 3D CAD system available in the Computer Centre of the University.

Appendix B

Nanoscale AFM investigations

Using the AFM (Atomic Force Microscopy), it is possible to trace a chart of the force exerted by a substrate on a probe. This mode is called the Force-Distance mode. Using this method with a conductive, very sensitive, probe it should be possible to map the field of the electric forces generated by a dielectric particle on the surrounding medium. The potential description and the surface charge on the particle could be derived from the results.
To test the potential application of this technique we measured the interaction between a silicon tip and a PT particle (10 μm of diameter) and we compared the results with the interaction in a region without any particles. The charts below (fig.A1 and A2) show the results.

Discussion of the results and conclusion

We tried to quantify the surface charge on the particle using the AFM.
An interaction between the tip and the particle was observed. Unfortunately, we can suppose the existence of another charge distribution on the silicon tip, but without further information.
The repulsive force that we are measuring is probably the result of the repulsion between the charges induced on both bodies. It became therefore very difficult to extrapolate any data about the charge present on the particle. We can only say that if a surface charge exists on the particle, we could measure it. But, to do so, a more accurate measure should be done grounding the tip.

We need to use the AFM Force-Distance measuring to calculate the effective surface charge on the filler.
However, the application of this technique to measure the interaction between two particles in a chain-like structure under the action of the electric field could be investigated.

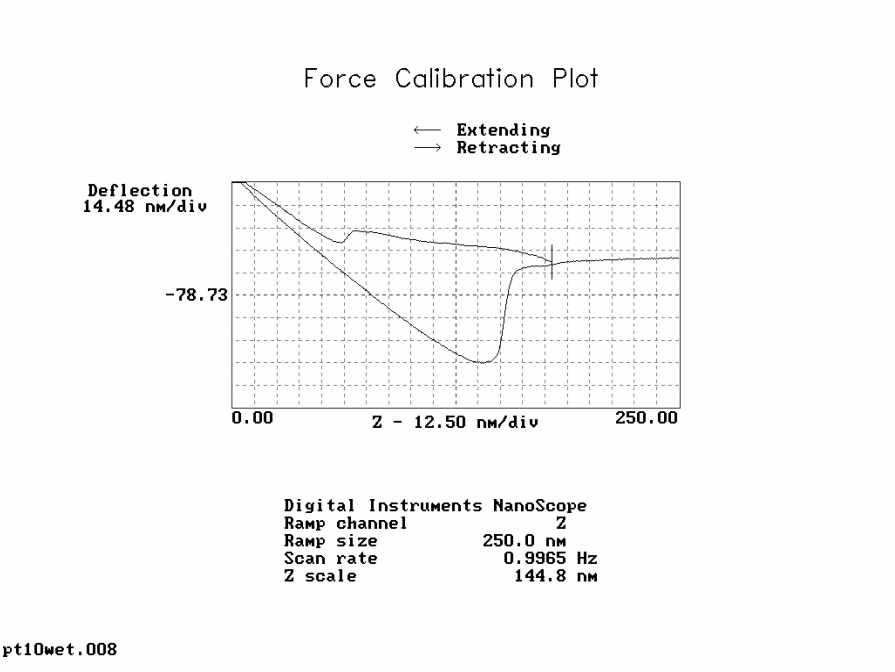

Figure A. 1. Force-Distance plot of a PT monocristalline 10 micron particle immersed in Fluorinert FD40 Fixed on Polished Copper using Black Wax

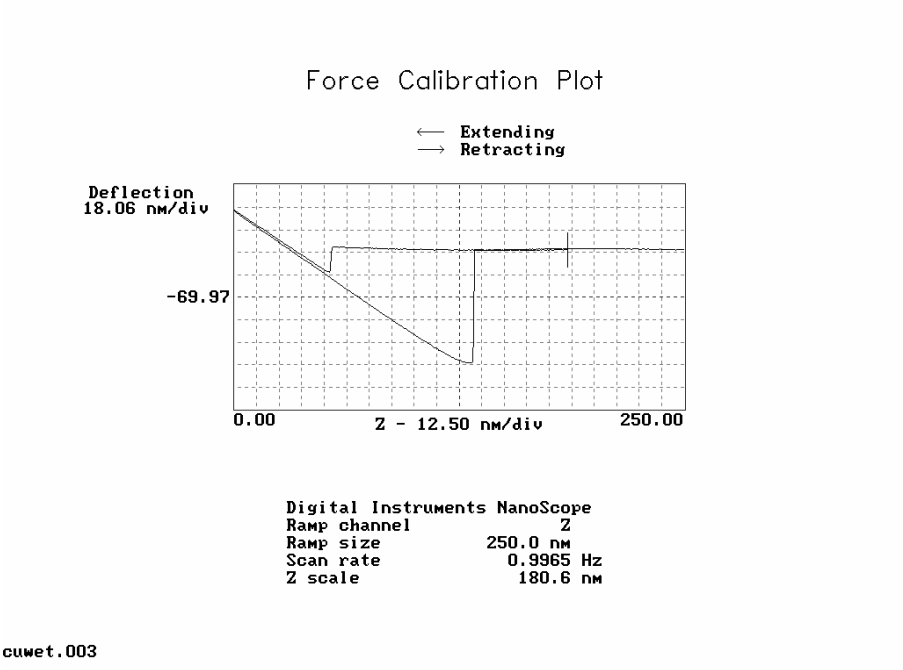

Figure A. 2. Force-Distance plot of a sample area immersed in Fluorinert FD40 without any particles

Appendix C

Dielectric spectra of PZT fibres achieved via interdigitated electrode in different configurations

This appendix collects the results of a series of measurement conducted on various sample of fibres in air, in IPA and in silicone oil with an interdigitated electrode. Though these curves are not used to extrapolate the values of permittivity, they can suggest a lot of information about the behaviour in frequency of different kinds of fibres, in different surrounding liquids.

Colours legend:

Blue: capacitance of three DRIE etched fibres

Red: capacitance of three DRIE normal fibres as supplied

Yellow: capacitance of three coating fibres

Green: Red: capacitance of three DRIE normal fibres as supplied

Pink: capacitance of the support

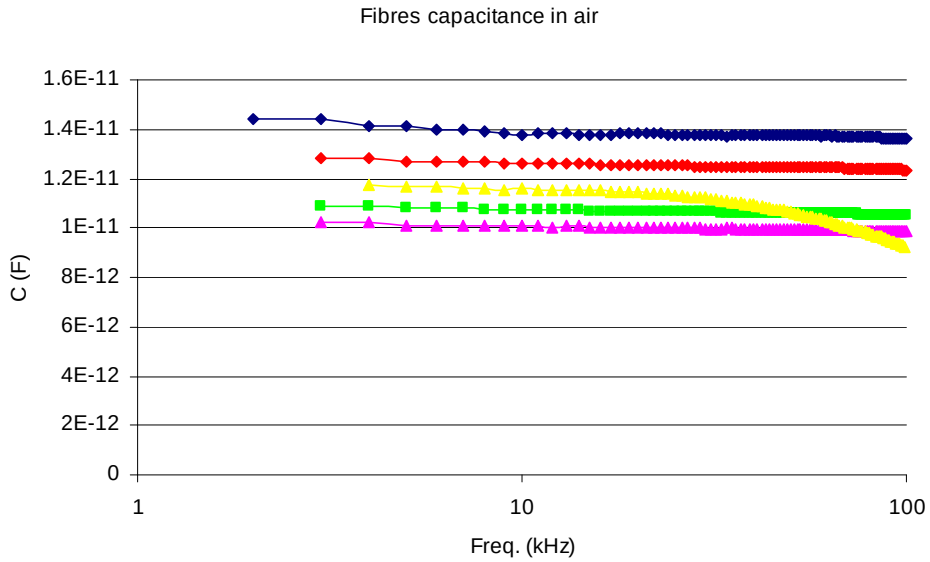

Figure A. 3. Capacitance of a set of fibres in air measured with an interdigitated electrode up to 100 kHz

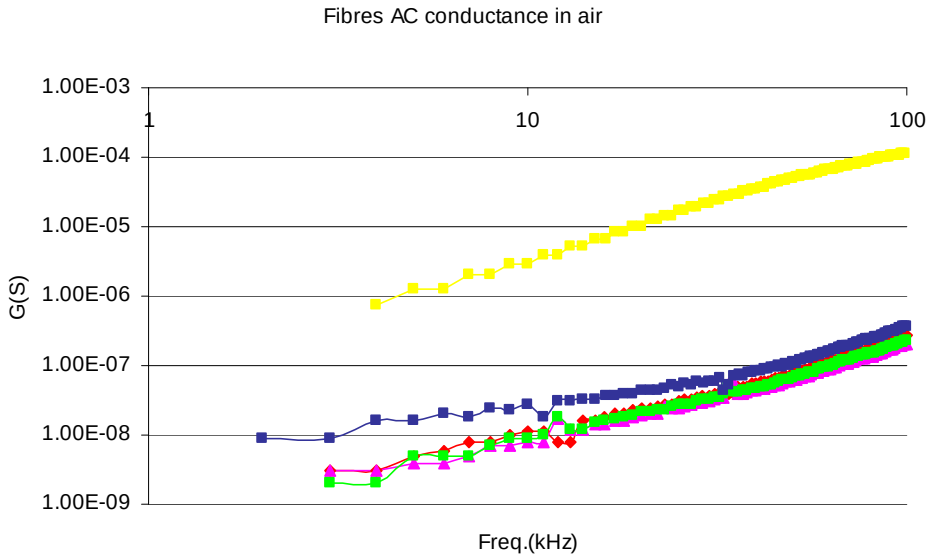

Figure A. 4. AC conductivity of a set of fibres in air measured with an interdigitated electrode up to 100kHz

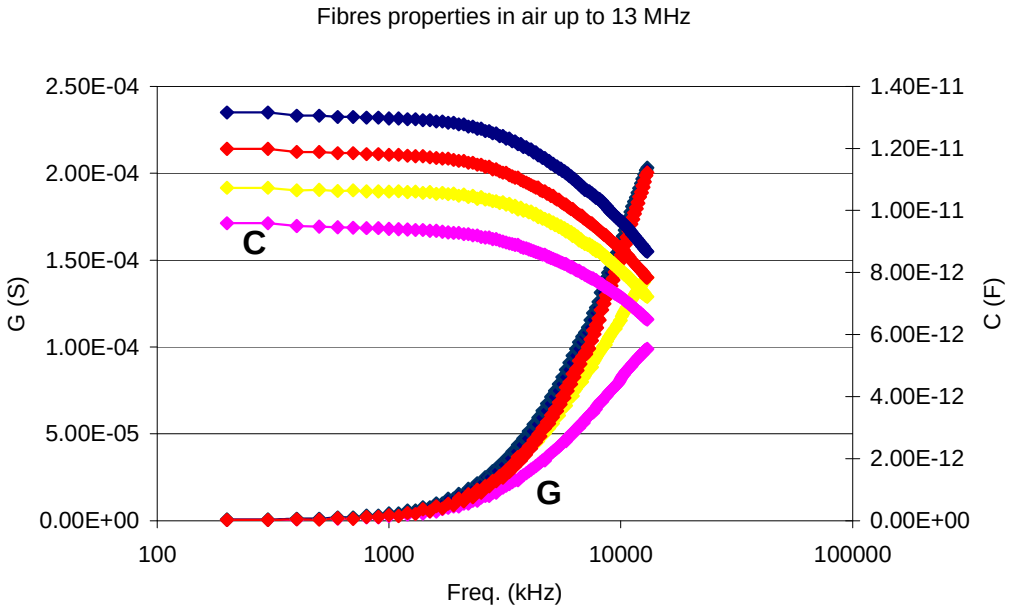

Figure A. 5. Capacitance of a set of fibres in air measured with an interdigitated electrode up to 13 MHz.

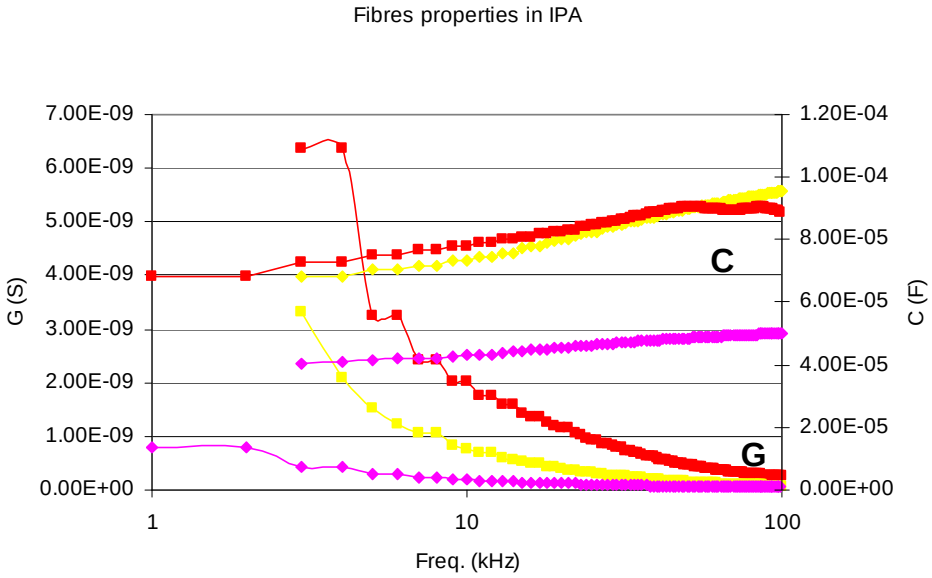

Figure A. 6. Capacitance and AC conductivity of a set of fibres in IPA measured with an interdigitated electrode up to 100 kHz.

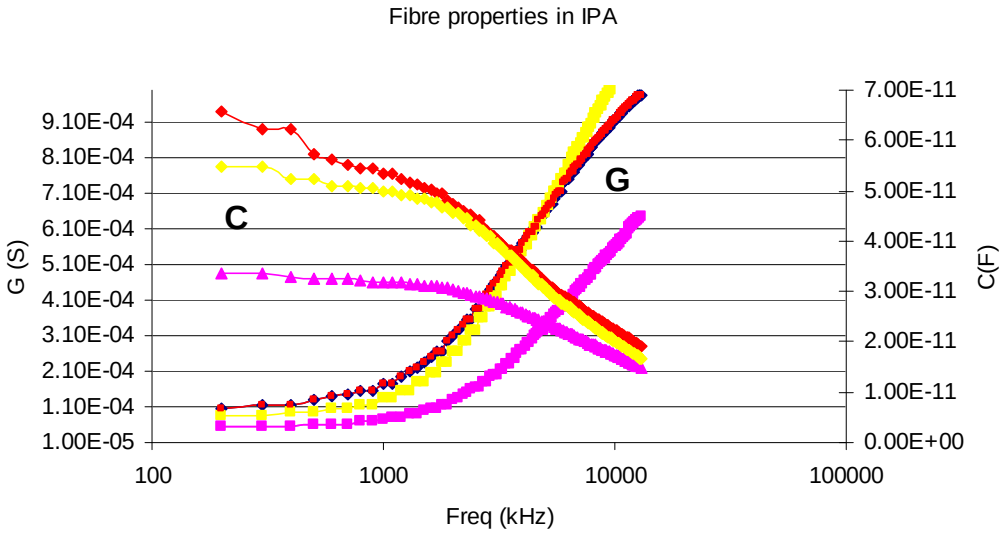

Figure A. 7. AC conductivity of a set of fibres in air measured with an interdigitated electrode up to 13MHz.

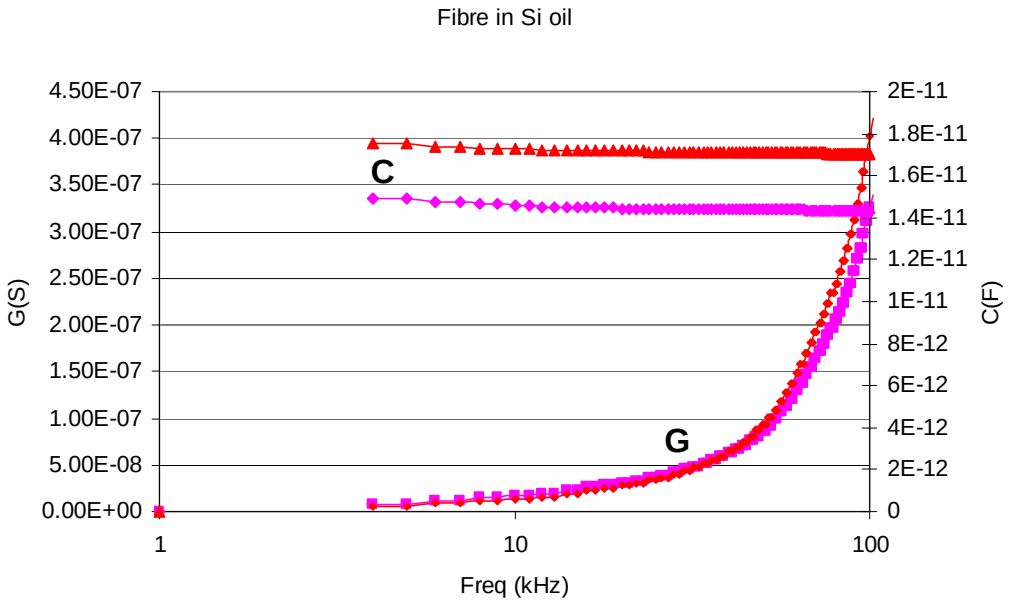

Figure A. 8. Capacitance and AC conductivity of a PZT fibre in silicone oil measured with an interdigitated electrode up to 100 kHz.

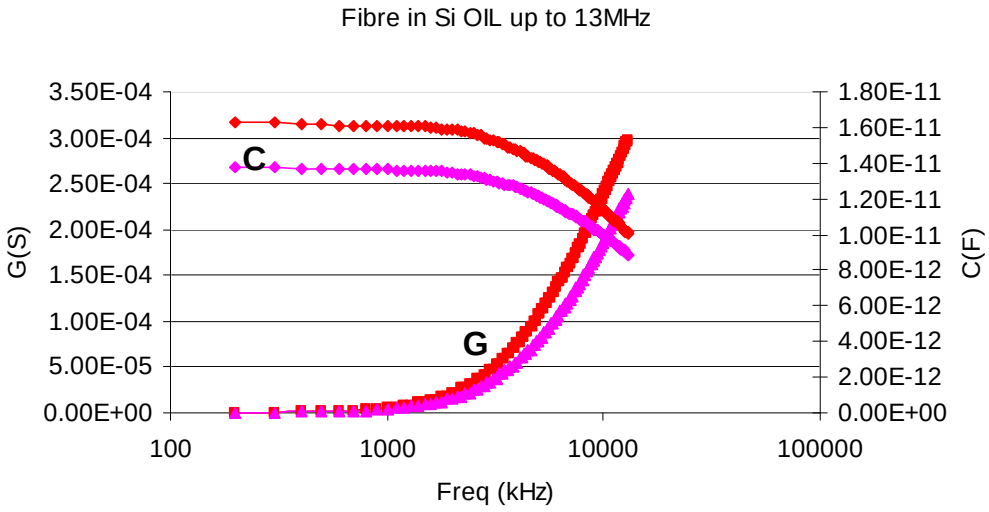

Figure A. 9. Capacitance and AC conductivity of a PZT fibre in silicone oil measured with an interdigitated electrode up to 13 MHz.

Appendix D

Evaluation of the measurement uncertainty

Uncertainty of the density (section 5.2 and 5.3)

The density ρ_m of a piece of fibre has been evaluated by the ratio between mass and volume. Consequently:

$$d\rho_m/\rho_m = dm/m + 2dr/r + dL/L \qquad \text{(A-1)}$$

Considering that the sample we measured was 2cm long, dm/m=4%, dL/L=5%, dr/r=1% (the radius was measured using a microscope), and consequently $d\rho_m/\rho_m$=11%. In the case of liquids, dm/m decreases considerably, because the size of the sample is no more on scale of microns. Nevertheless, the volume measurement is less precise, as we did not use the microscope. As a consequence, an uncertainty around 10% is still reasonable also in the case of liquids.

Uncertainty of the conductivity σ (table 5.1, 5.2 and 5.3)

The conductance G of a dipole is expressed by:

$$G = I / V \qquad \text{(A-2)}$$

The conductivity σ of the material constituting the dipole can be extrapolated from the value of G, knowing the geometry of the body. In the case of a parallel flat capacitor:

$$\sigma = G\, h / S \qquad \text{(A-3)}$$

where S and h are the surface of the electrodes and the distance between them respectively, and:

$$d\sigma/\sigma = dG/G + dS/S + dh/h = dI/I + dV/V + dS/S + dh/h \qquad \text{(A-4)}$$

In the case of the measure of the liquid conductivity (table 5.1), dh/h=50%, dS/S=9%, dI/I=1%, dV/V=0.1% and consequently dσ/σ = 63%. This value of uncertainty is

acceptable considering that these measurements were primarily conducted to estimate the order of dimension of the conductivity.

In the case of the measure of the conductivity of the fibres (table 5.2 and 5.3), the calculation is more complicated because an exact formula for the evaluation of the conductivity is not available, and this was extrapolated via FEM simulations. However, an estimation of the uncertainty is still possible considering the uncertainty on the measurement of the fibre diameter, the electrodes gap and the fibre length. These measurements have been carried out using a microscope, and the uncertainty can be estimated to 1%. Consequently $d\sigma/\sigma = 8\%$.

Uncertainty of the tribo-charge measurement (table 5.4)

a) Bulk value Q:

   Q, measured using the Faraday's pail, has a precision related to the one of the electrometer: 0.4%.

b) Surface charge Q_S:

   Neglecting the charge on the extremity, the surface charge is expressed by:

$$Q_S = Q/4\pi r^2 \qquad \text{(A-5)}$$

   The uncertainty of the radius, measured using the macro lenses of the high speed camera is equal to 7%. Consequently, the uncertainty of the surface charge is:

$$dQ_S/Q_S = dQ/Q + 2\ dr/r = 14.5\% \qquad \text{(A-6)}$$

c) Linear charge Q/L:

   The uncertainty on the linear charge can be calculated considering dL/L = 5% and is equal to 5.4%.

Uncertainty of the particle speed (chapter 6 and 7)

The uncertainty in the measure of a particle speed, carried out by analysing its trajectory, can be written as:

$$du/u = ds/s + dt/t \tag{A-7}$$

where s is the space coordinate and t the time. The time uncertainty can be expressed in absolute value by the duration of a video frame, and at 500fps, dt = 2ms. The expression of the uncertainty, therefore, depends on the value of u, and we have:

$$du/u = (0.16 + 33u)\% \tag{A-8}$$

Considering that the maximum value of speed we measured is ≈ 0.2m/s, $du/u<6.8\%$

Uncertainty of the particle charge (chapter 7)

The particle charge is extrapolated from the particle trajectories using the formula:

$$Q = [(\mathbf{F_W} + \kappa\mathbf{u})\cdot\mathbf{r}]/E_0 \tag{A-9}$$

Consequently:

$$dQ/Q = dF_W/F_W + d\kappa/\kappa + du/u + dE_0/E_0 \tag{A-10}$$

where:

$$\begin{gathered} dF_W/F_W = dL/L + 2dr/r + d\rho_m/\rho_m = 30.4\% \\ d\kappa/\kappa = dF_W/F_W + du/u = 37.2\% \\ du/u < 6.8\% \\ dE_0/E_0 = dV/V + dh/h = 0.18\% \end{gathered} \tag{A-11}$$

and at the end: dQ/Q = 74.6%

$$dQ/Q = 74.6\% \tag{A-12}$$

This value of uncertainty is considerable. However, it gives an estimation of the order of dimension of the particle charge, which is sometimes enough to make some evaluations. Moreover, it is important to consider that when the same particle and the same fluid are utilised for a series of experiments characterised by different voltages,

and we are interested to establish an expression to interpolate the results, only the uncertainty derived by the speed and the electric field should be taken into account (De Marchi and Lo Presti, 1993). This is what was considered in the chart in figure 7.10. In figure 7.12 the uncertainty to consider for the interpolation was 37%. In this case, in fact only the fluid remained the same for all the measurements.

Uncertainty of the fibre linear charge (section 5.3.4)

In section 5.3.4, we extrapolated the linear charge on a fibre from its deflection when exposed to an electric field E_0. The value of Q/L was extrapolated using the expression:

$$Q/L = \Delta y/\{E_0 L^2[\chi_z/(2G_y A) + L^2/(8\, Y_x I_y)]\} \quad \text{(A-13)}$$

Considering that the contribution due to the shear effect is negligible in respect to that due to the bending, the uncertainty of Q/L can be calculated with:

$$d(Q/L)/(Q/L) = d\Delta y/\Delta y + dE_0/E_0 + dY_x/Y_x + 4dL/L + dI_y/I_y \quad \text{(A-14)}$$

where, considering (5-9):

$$dI_y/I_y = 4d\phi/\phi \quad \text{(A-15)}$$

By evaluating each partial contribution, it is possible to calculate the final uncertainty. The deflection uncertainty is expressed by an absolute contribution that can be translated in a relative value equal to maximum ±18%. The field uncertainty has been calculated above and is equal to ±0.2%. Considering that the densification of the PZT is between 90% and 100%, the Young's module uncertainty can be considered equal to ±5% in respect to the value for the 95% of densification. Finally, the uncertainty of the diameter can be considered equal to 1%, because the diameter has been measured using the microscope, and the uncertainty of the length is always 5%.
The final uncertainty of the linear charge is 47%, a good value, considering the number of variables involved in the extrapolation.

Appendix E

Ancillary effects worthy of further investigation

In the context of the present research project, with the objective of enriching knowledge of the behaviour of a dielectric fluid exposed to a divergent electric field, a series of investigations into heterogeneous fluid systems was carried out. As a result two interesting, original, unreported effects were observed.

The first phenomenon shows an effect that could have an application is a new way to generate picolitre droplets and tiny jets in a multiphase system of dielectric fluids.

An original liquid injection was generated at the interface separating two highly insulating dielectric liquids: silicone oil and a perfluorinated oil. These two oils, which are completely immiscible, once put together in a container, separate into two different layers. The silicone oil occupies the upper layer.
The system was exposed to a DC, highly divergent electric field which was generated between a needle-like electrode and a bottom flat electrode. When the field overcame a certain threshold voltage a series of small picolitre droplets of silicone oil were injected. The droplets size increased if the voltage increased, and at a certain point the droplets were replaced by a continuous jet.

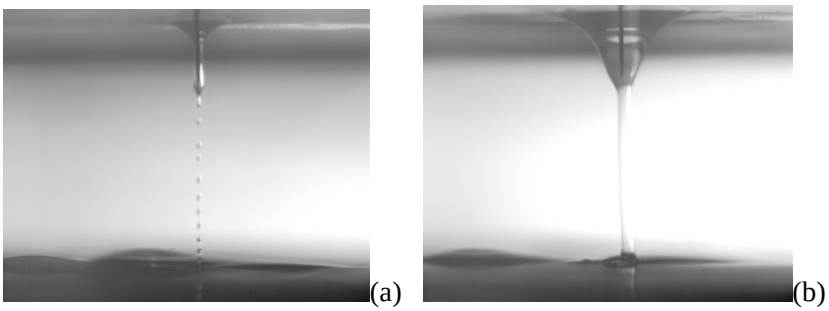

Figure A. 10: Generation of picolitre droplets ((a); 5kV@DC) and fluid jet ((b); 10kV@DC) at the interface between a silicone oil and a perfluorinated oil

The silicone oil – Fluorinert FC40 system was extensively studied. The kinetics of the phenomenon, the dependence of the phenomenon on the voltage magnitude, and on the needle position (with respect to the bottom electrode and to the boundary between the two liquids) were considered.

The relationship between the current and the jet characteristics was established. This relationship was particularly accurate in predicting the droplet charge.

The same phenomenon was also studied in other fluid configurations, with more conducting fluid and with fluid in which some powder was suspended.

The picture 10.8 shows how, with more conduting fluid it is impossible to have a localisation of the jet. The phenomenon is driven by the polarization forces acting on the interface of separation between the two liquids, and it is enhanced by the electrohydrodynamic instability induced by the charge injection through the needle tip.

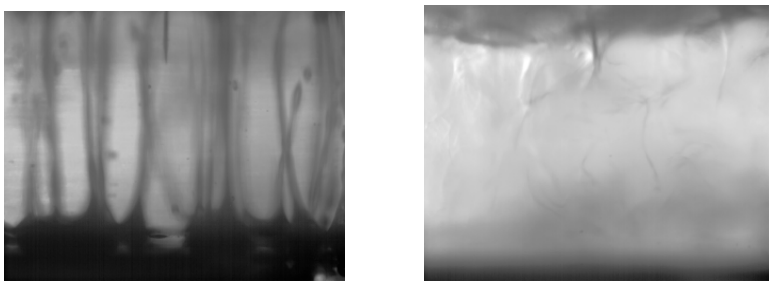

Figure A. 11: Mixing phenomena generated at the interface between a silicone oil and a more conducting dielectric liquid (10kV@DC)

Some other configurations were achievable with more viscous fluids:

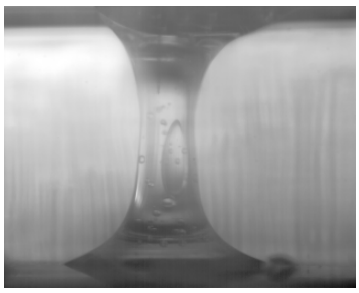

Figure A. 12: Generation of a liquid bridge after creation of a jet from the interface between a silicone oil and Castor oil (10kV@DC)

The same observations were carried out at a frequency of 1kHz. In this case, no jet was observed, but the upper fluid showed a tendency to coat the needle. The thickness of such a coating was directly related to the applied voltage.

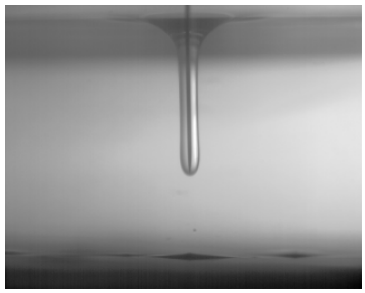

Figure A. 13: Generation of a coating deforming the interface between a silicone oil and a perfluorinated oil (7kV@1kHz)

The second phenomenon to report is a study of the modification of the electrowetting angle exposing the fluid surface to a corona injection.

This experiment objective was to analyse the response to a step voltage of a system which constituted of a needle-like upper electrode partially immersed in dielectric oil, and a bottom flat electrode.

The fluid meniscus at the oil-air interface, in proximity to the needle electrode, rose up when a voltage was applied and dropped down when the voltage was switched off. The phenomenon had characteristic time constants. In the case where the interface was charged by corona spraying, after the voltage was switched off, and the meniscus decayed, a secondary lift of the fluid occurred. At that point the fluid rose to a higher level than it was before, when the field was switched on. This phenomenon is connected to the relaxation of the surface charges and it was only visible when a corona injection existed. Surprisingly, the system reacted in a similar way also when a very low frequency signal was applied. But in this case the fluid rose up to a height twice the height observed in the DC case.

This new phenomenon was called: “corona enhanced electrowetting”.

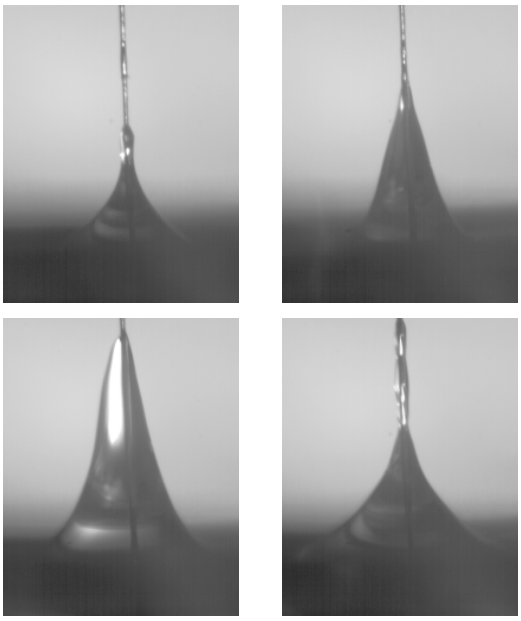

Figure A. 14: Series of pictures describing the Corona Enhanced Eletrowetting as observed applying a signal 10kV@1Hz (Capria and Wilson, 2006b)

In addition to that, many other observations were carried out, considering the response of the fluid in different electrode configurations. The influence of the voltage magnitude, the frequency and the signal waveform on the phenomenon were also considered.